

การสังเคราะห์อนุภาคนาโนพอลิ(สไตรีน-โค-เมทิลเมทาคริเลต)/ซิลิกาและพอลิไอโซพรีนซิลิกา
โดยดิฟเฟอเรนเชียลไมโครอิมัลชันพอลิเมอไรเซชัน

นางสาวอนงค์ คงสินหลาก

วิทยานิพนธ์นี้ เป็นส่วนหนึ่งของการศึกษาตามหลักสูตรปริญญาวิทยาศาสตรดุษฎีบัณฑิต
สาขาวิชาปิโตรเคมี
คณะวิทยาศาสตร์ จุฬาลงกรณ์มหาวิทยาลัย
ปีการศึกษา 2555

ลิขสิทธิ์ของจุฬาลงกรณ์มหาวิทยาลัย
บทคัดย่อและแฟ้มข้อมูลฉบับเต็มของวิทยานิพนธ์ตั้งแต่ปีการศึกษา 2554 ที่ให้บริการในคลังปัญญาจุฬาฯ (CUIR)
เป็นแฟ้มข้อมูลของนิสิตเจ้าของวิทยานิพนธ์ที่ส่งผ่านทางบัณฑิตวิทยาลัย

The abstract and full text of theses from the academic year 2011 in Chulalongkorn University Intellectual Repository (CUIR)
are the thesis authors' files submitted through the Graduate School.

SYNTHESIS OF POLY(STYRENE-CO-METHYL
METHACRYLATE)/SiO₂ AND POLYISOPRENE/SiO₂
NANOPARTICLES VIA DIFFERENTIAL MICROEMULSION
POLYMERIZATION

Miss Anong Kongsinlark

A Dissertation Submitted in Partial Fulfillment of the Requirements
for the Degree of Doctor of Philosophy Program in Petrochemistry

Faculty of Science

Chulalongkorn University

Academic Year 2012

Copyright of Chulalongkorn University

Thesis Title SYNTHESIS OF POLY(STYRENE-CO-METHYL
METHACRYLATE)/SiO₂ AND POLYISOPRENE/SiO₂
NANOPARTICLES VIA DIFFERENTIAL
MICROEMULSION POLYMERIZATION

By Miss Anong Kongsinlark

Field of Study Petrochemistry

Thesis Advisor Professor Pattarapan Prasassarakich, Ph.D.

Thesis Co-advisor Professor Garry L. Rempel, Ph.D.

Accepted by the Faculty of Science, Chulalongkorn University in Partial
Fulfillment of the Requirements for the Doctoral Degree

..... Dean of the Faculty of Science
(Professor Supot Hannongbua, Dr.rer.nat.)

THESIS COMMITTEE

.....Chairman
(Associate Professor Supawan Tantayanon, Ph.D.)

.....Thesis Advisor
(Professor Pattarapan Prasassarakich, Ph.D.)

.....Thesis Co-advisor
(Professor Garry L. Rempel, Ph.D.)

.....Examiner
(Associate Professor Wimonrat Trakarnpruk, Ph.D.)

.....Examiner
(Assistant Professor Napida Hinchiranan, Ph.D.)

.....External Examiner
(Assistant Professor Kitikorn Charmondusit, Ph.D.)

อนงค์ คงสินหลาก: การสังเคราะห์อนุภาคนาโนพอลิ(สไตรีน-โค-เมทิลเมทาคริเลต)/ซิลิกา และพอลิไอโซพรีน/ซิลิกาโดยดิฟเฟอเรนเชียลไมโครอิมัลชันพอลิเมอไรเซชัน (SYNTHESIS OF POLY(STYRENE-CO-METHYL METHACRYLATE)/SiO₂ AND POLYISOPRENE/SiO₂ NANOPARTICLES VIA DIFFERENTIAL MICROEMULSION POLYMERIZATION) อ. ที่ปรึกษาวิทยานิพนธ์หลัก: ศ.ดร.ภัทรพรหม ประศาสน์สารกิจ, อ. ที่ปรึกษาวิทยานิพนธ์ร่วม: Prof. Garry L. Rempel, 175 หน้า.

สังเคราะห์อนุภาคนาโนยางเอทิลีนพรอพิลีนเลเท็กซ์ (EPM) ขนาดอนุภาคเฉลี่ย 47 นาโนเมตร โดยวิธีทางเลือกด้วยพอลิเมอไรเซชันของไอโซพรีนตามด้วยไฮโดรจีเนชัน ยางพอลิเอทิลีนพรอพิลีนร้อยละ 94 ผลิตจากอนุภาคนาโนพอลิไอโซพรีนมีความเสถียรเชิงความร้อนสูงและค่ามอดูลัสสูงเนื่องจากโครงสร้างอิมัลชันของเฮลีนในสายโซ่พอลิเมอไรเซชัน นำเสนอเทคนิคดิฟเฟอเรนเชียลไมโครอิมัลชันพอลิเมอไรเซชันเพื่อใช้สังเคราะห์อนุภาคนาโนพอลิ(สไตรีน-โค-เมทิลเมทาคริเลต)-ซิลิกา และพอลิไอโซพรีน-ซิลิกานาโนคอมพอสิต ได้ออกแบบโครงสร้างคอร์-เชลล์โดยมีอนุภาคนาโนซิลิกาเป็นแกนถูกเคลือบด้วยอนุภาคนาโนพอลิเมอไรเซชันเพื่อให้เกิดการกระจายตัวของอนุภาคที่ดีและลดการรวมตัวกันของอนุภาคซิลิกา สามารถสังเคราะห์อนุภาคนาโนพอลิ(สไตรีน-โค-เมทิลเมทาคริเลต)-ซิลิกาที่มีขนาดอนุภาคเฉลี่ย 40 นาโนเมตรและมีการกระจายตัวแคบ โดยใช้ปริมาณสารลดแรงตึงผิวต่ำมาก (อัตราส่วนสารลดแรงตึงผิวต่อมอนอเมอร์ เท่ากับ 1/57) สามารถสังเคราะห์พอลิไอโซพรีน-ซิลิกานาโนคอมพอสิตขนาดอนุภาค 20-60 นาโนเมตรและประสิทธิภาพการกราฟต์พอลิเมอไรเซชันสูงถึงร้อยละ 78 ได้ใช้วิธีไดอิมิดไฮโดรจีเนชันมาประยุกต์ใช้ในการสังเคราะห์ไฮโดรจีเนตพอลิไอโซพรีน-ซิลิกาซึ่งเป็นนาโนคอมพอสิตชนิดใหม่ โดยระดับไฮโดรจีเนชันสูงสุดคือร้อยละ 98 โดยใช้อัตราส่วนไฮโดรเจนเปอร์ออกไซด์ต่อไฮดราซีนที่ 1.5:1 และไฮโดรจีเนตพอลิไอโซพรีน-ซิลิกานาโนคอมพอสิตแสดงค่าคุณสมบัติหลายตัวสูงสุดที่ 521 องศาเซลเซียส ส่งผลถึงเสถียรภาพเชิงความร้อนที่ดี พอลิไอโซพรีน-ซิลิกาและไฮโดรจีเนตพอลิไอโซพรีน-ซิลิกานาโนคอมพอสิตสามารถใช้เป็นสารตัวเติมชนิดใหม่ในนี้ อยางธรรมชาติซึ่งสามารถเพิ่มสมบัติมอดูลัสการต้านทานแรงดึง การต้านทานการบวมด้วยความร้อน และการต้านทานต่อไอโซน

สาขาวิชา...ปิโตรเคมีและวิทยาศาสตร์พอลิเมอร์...ลายมือชื่อนิสิต.....
ปีการศึกษา...2555.....ลายมือชื่อ อ.ที่ปรึกษาวิทยานิพนธ์หลัก.....
ลายมือชื่อ อ.ที่ปรึกษาวิทยานิพนธ์ร่วม.....

5173876023: MAJOR PETROCHEMISTRY AND POLYMER SCIENCE
 KEYWORDS: DIFFERENTIAL MICROEMULSION POLYMERIZATION/
 DIMIDE HYDROGENATION/ NANOCOMPOSITE/ SILICA/ POLYISOPRENE
 ANONG KONGSINLARK : SYNTHESIS OF POLY(STYRENE-*CO*-METHYL
 METHACRYLATE)/SiO₂ AND POLYISOPRENE/SiO₂ NANOPARTICLES VIA
 DIFFERENTIAL MICROEMULSION POLYMERIZATION. ADVISOR : PROF.
 PATTARAPAN PRASASSARAKICH, Ph.D., CO-ADVISOR : PROF.
 GARRY L. REMPEL, Ph.D., 175 pp.

Nanosized ethylene-propylene rubber (EPM) latex with a particle size of 47 nm was synthesized via an alternative route consisting of isoprene polymerization followed by hydrogenation. EPM yield of 94% produced from nanosized polyisoprene had high thermal stability and high storage modulus due to the saturated carbons domains of the ethylene segments in the polymer chains. Differential microemulsion polymerization was proposed for the synthesis of poly(styrene-*co*-methyl methacrylate) (ST-*co*-MMA)-SiO₂ and polyisoprene (PIP)-SiO₂ nanocomposites. To achieve the monodispersion and reduce nano-SiO₂ aggregation, core-shell morphology was designed, consisting of silica as the nano-core encapsulated by polymer as the nano-shell. Poly(ST-*co*-MMA)-SiO₂ with a particle size of 40 nm having a narrow size distribution could be synthesized using a low surfactant amount (surfactant/monomer weight ratio of 1/57). PIP-SiO₂ with a particle size of 20-60 nm and high polymer grafting efficiency of 78% was obtained. An approach of diimide hydrogenation was applied to synthesize hydrogenated polyisoprene (HPIP)-SiO₂ as new nanocomposite. The highest hydrogenation degree of 98% was achieved using a ratio of hydrogen peroxide to hydrazine at 1.5:1 and HPIP-SiO₂ nanocomposites showed the maximum degradation temperature of 521°C resulting in an excellent thermal stability. PIP-SiO₂ and HPIP-SiO₂ nanocomposites could be used as new nanofiller in natural rubber (NR) latex due to a dramatic improvement in the storage modulus, tensile strength, tensile modulus, and anti-ageing properties and ozone resistance.

Field of Study: Petrochemistry and Polymer Science Student's Signature.....

Academic Year: 2012..... Advisor's Signature.....

Co-advisor's Signature.....

ACKNOWLEDGEMENTS

The author would like to express sincere appreciation and deep thankfulness to her advisor, Prof. Dr. Pattarapan Prasassarakich and co-advisor, Prof. Garry L. Rempel for the helpful discussion, encouraging guidance, supervision and support throughout her research. The author also would like to acknowledge Assoc. Prof. Dr. Supawan Tantayanon, Assoc. Prof. Dr. Wimonrat Trakarnpruk, Asst. Prof. Dr. Napida Hinchiranan and Asst. Prof. Dr. Kitikorn Charmondusit for their participation on the dissertation chairman and members of thesis committee and for their worthy comments and suggestions.

The author gratefully acknowledge the support from the Thailand Research Fund (through the Royal Golden Jubilee Project), Graduate School, Chulalongkorn University, the Natural Sciences and Engineering Research Council of Canada (NSERC), the Thai Government Stimulus Package 2 (TKK2555) under the Project for Establishment of Comprehensive Center for Innovative Food, Health Products and Agriculture and the National Research University Project of CHE and Ratchadaphiseksomphot Endowment Fund (AM1024I).

Many thanks are going to the Program of Petrochemistry and Polymer Science and the Department of Chemical Technology, Faculty of Science, Chulalongkorn University.

Finally, the author wishes to express her deep gratitude to her family for their love, support and encouragement throughout graduate study. Also, special thanks are extended to her friends for friendship, encouragements and cheerful moral support.

CONTENTS

	PAGE
ABSTRACT (THAI).....	iv
ABSTRACT (ENGLISH).....	v
ACKNOWLEDGEMENTS.....	vi
CONTENTS.....	vii
LIST OF TABLES.....	xiii
LIST OF FIGURES.....	xiv
LIST OF ABBREVIATIONS.....	xix
CHAPTER I INTRODUCTION.....	1
1.1 Motivation.....	1
1.2 Miniemulsion Polymerization.....	2
1.3 Microemulsion Polymerization.....	5
1.4 Silica Surface Modification.....	8
1.5 Polymer-Silica Nanocomposites.....	11
1.6 Hydrogenation of Diene-Rubber.....	17
1.6.1 Catalytic Hydrogenation Using Metal Catalysts.....	17
1.6.2 Noncatalytic Hydrogenation Using Diimide Reduction.....	19
1.7 Mechanical Properties and Thermal Stability of Polymer Nanocomposites.....	23
1.8 Objective and Scope of Dissertation.....	25
CHAPTER II EXPERIMENTAL AND CHARACTERIZATION.....	28
2.1 Materials.....	28
2.1.1 Synthesis of Nanosized Ethylene-Propylene Rubber Latex.....	28
2.1.2 Synthesis of Poly(Styrene-co-Methyl Methacrylate)-SiO ₂ Nanocomposites.....	28
2.1.3 Synthesis of Polyisoprene-Silica Nanocomposites.....	29
2.1.4 Synthesis of Hydrogenated Polyisoprene-Silica.....	29

	PAGE
2.1.5 Pre-vulcanization.....	29
2.2 Synthesis of Nanosized Ethylene-Propylene Rubber Latex.....	30
2.2.1 Synthesis of Polyisoprene (PIP) Nanoparticles.....	30
2.2.2 Diimide Hydrogenation for Ethylene-Propylene Rubber Latex Synthesis	30
2.3 Synthesis of Poly(Styrene-co-Methyl Methacrylate)-SiO ₂ Nanocomposites	32
2.3.1 Pretreatment of Nano-SiO ₂ by Acrylic Acid.....	32
2.3.2 Synthesis of Poly(Styrene-co-Methyl Methacrylate)-Silica Nanocomposites	32
2.4 Synthesis of Polyisoprene-Silica Nanocomposites	35
2.4.1 Pretreatment of Nano-SiO ₂ by Organo-Silane Coupling Agents	35
2.4.2 Synthesis of Polyisoprene-Silica Nanocomposites	35
2.5 Synthesis of Hydrogenated Polyisoprene-Silica Nanocomposites	36
2.5.1 Synthesis of Polyisoprene-Silica Nanocomposites	36
2.5.2 Diimide Hydrogenation for Hydrogenated Polyisoprene-Silica Synthesis.....	36
2.6 Preparation of PIP-SiO ₂ filled NR Nanocomposites and Hydrogenated PIP-SiO ₂ filled NR Nanocomposites.....	38
2.7 Characterization	39
2.7.1 Fourier Transform Infrared Spectroscopy.....	39
2.7.2 ¹ H NMR Spectroscopy.....	39
2.7.3 Particle Diameter Measurement.....	39
2.7.4 Thermogravimatic Analysis (TGA).....	40
2.7.5 Morphological Study.....	40
2.8 Determination of Monomer Conversion, Polymer Grafting Efficiency, Silica Encapsulation Efficiency.....	40
2.9 Mechanical Properties of Vulcanized Rubber	42
2.10 Ozone Resistance of Vulcanized Rubber.....	42

	PAGE
CHAPTER III SYNTHESIS OF NANOSIZED ETHYLENE-PROPYLENE	
RUBBER LATEX VIA POLYISOPRENE	
HYDROGENATION.....	43
3.1 Introduction.....	43
3.2 Characterization of Polyisoprene Nanoparticles.....	43
3.3 Characterization of Ethylene-Propylene Rubber (EPM)	
Nanoparticles.....	45
3.4 Diimide Hydrogenation of Nanosized Polyisoprene	49
3.4.1 Effect of Boric Acid Concentration.....	49
3.4.2 Effect of Hydrazine Monohydrate and Hydrogen Peroxide	
Concentration.....	50
3.4.3 Effect of Hydrogen Peroxide to Hydrazine Ratio.....	53
3.4.4 Effect of Reaction Temperature.....	55
3.4.5 Effect of Water Addition.....	56
3.5 Conversion Profile of Nanosized PIP Hydrogenation	57
3.6 Proposed Synthetic Route for Nanosized EPM Synthesis via	
Diimide Hydrogenation.....	60
3.7 Thermal Properties of Nanosized Ethylene-Propylene Rubber.....	61
3.8 Appearance of Nanosized Ethylene-Propylene Rubber Latex.....	63
CHAPTER IV SYNTHESIS OF POLY(STYRENE- <i>CO</i> -METHYL	
METHACRYLATE)-SiO ₂ NANOCOMPOSITES VIA	
DIFFERENTIAL MICROEMULSION	
POLYMERIZATION.....	64
4.1 Introduction	64
4.2 Preliminary Study of Poly(Styrene- <i>co</i> -Methyl Methacrylate)-	
SiO ₂ Nanocomposites.....	65
4.2.1 Effect of Initiator Concentration.....	65
4.2.2 Effect of Surfactant Concentration.....	67
4.2.3 Effect of Monomer/Water Ratio.....	69

	PAGE
4.2.4 Effect of Styrene/Methyl Methacrylate Ratio.....	70
4.2.5 Effect of Silica Loading.....	71
4.3 Characterization of Poly(ST- <i>co</i> -MMA)-SiO ₂ Nanocomposites	76
4.4 Morphology of Poly(ST- <i>co</i> -MMA)-SiO ₂ Nanocomposites.....	78
4.5 Proposed Mechanism for Poly(ST- <i>co</i> -MMA)-SiO ₂ Nanocomposite Synthesis.....	80
 CHAPTER V SYNTHESIS OF POLYISOPRENE-SILICA NANOCOMPOSITES VIA DIFFERENTIAL MICROEMULSION POLYMERIZATION.....	
5.1 Introduction.....	82
5.2 Characterization of Polyisoprene-SiO ₂ Nanocomposites.....	83
5.3 Encapsulation of VTS-SiO ₂ with Polyisoprene.....	85
5.3.1 Influence of Monomer/Water Ratio	85
5.3.2 Influence of Initiator Concentration.....	86
5.3.3 Influence of Surfactant Concentration.....	87
5.3.4 Influence of Silica Loading.....	89
5.4 Particle Size Distribution of PIP-SiO ₂ Nanocomposites	90
5.5 Morphology of PIP-SiO ₂ Nanocomposites	93
5.6 Proposed Mechanism for PIP-SiO ₂ Composite Nanoparticles.....	95
5.7 Thermal Properties of PIP-SiO ₂	96
 CHAPTER VI SYNTHESIS OF HYDROGENATED POLYISOPRENE-SILICA NANOCOMPOSITES VIA DIIMIDE REDUCTION.....	
6.1 Introduction.....	98
6.2 Characterization of PIP-SiO ₂ and HPIP-SiO ₂ Nanocomposites.....	99
6.3 Diimide Hydrogenation for Nanosized HPIP-SiO ₂ Synthesis.....	102
6.3.1 Effect of Hydrazine Monohydrate and Hydrogen Peroxide Concentration.....	102

	PAGE
6.3.3 Effect of Water Addition	105
6.4 Conversion Profile of Nanosized PIP-SiO ₂ Hydrogenation.....	106
6.5 Proposed New Route for Nanosized HPIP-SiO ₂ Synthesis.....	109
6.6 Morphology of HPIP and HPIP-SiO ₂ Nanocomposite.....	111
6.7 Thermal Analysis of HPIP-SiO ₂ Nanocomposites.....	112
CHAPTER VII MECHANICAL PROPERTIES OF RUBBER/SILICA	
NANOCOMPOSITES.....	115
7.1 Introduction.....	115
7.2 Dynamic Mechanical Properties.....	116
7.2.1 Dynamic Mechanical Properties of EPM.....	116
7.2.2 Dynamic Mechanical Properties of NR/PIP-SiO ₂	
Nanocomposite.....	118
7.3 Mechanical Properties of Vulcanized Rubber.....	120
7.3.1 Mechanical Properties of PIP-SiO ₂ Filled NR.....	120
7.3.2 Mechanical Properties of HPIP-SiO ₂ Filled NR.....	125
7.4 Thermal Resistance of NR Nanocomposites.....	128
7.4.1 Thermal Stability of PIP-SiO ₂ Filled NR.....	128
7.4.2 Thermal Stability of HPIP-SiO ₂ Filled NR.....	130
7.5 Surface Morphology of Rubber-Silica Nanocomposites.....	132
7.6 Ozone Resistance of HPIP-SiO ₂ Nanocomposites.....	134
CHAPTER VIII CONCLUSIONS AND RECOMMENDATIONS.....	137
8.1 Conclusions	137
8.2 Recommendations	140
REFERENCES.....	141
APPENDICES.....	160
Appendix A Raw Data of Mechanical Properties of NR/PIP-SiO ₂	161
Appendix B Raw Data of Mechanical Properties of NR/HPIP-SiO ₂	164

	PAGE
Appendix C Raw Data of PIP-SiO ₂ Synthesis.....	167
Appendix D Calculation of Polyisoprene Composition.....	169
Appendix E Calculation of % Hydrogenation.....	170
Appendix F Raw Data of Diimide Hydrogenation of Nanosized Polyisoprene and Polyisoprene-SiO ₂	172
VITA.....	175

LIST OF TABLES

Table	PAGE
1.1 Typical silane coupling agents for silica surface treatment	9
3.1 Effect of hydrazine amount on hydrogenation at the constant [H ₂ O ₂]/[N ₂ H ₄]	54
3.2 Decomposition temperature of rubber samples.....	63
4.1 The formulation for synthesis of poly(ST- <i>co</i> -MMA)-SiO ₂ synthesis and effect of process variables on particle size, conversion, encapsulation efficiency.....	66
4.2 Characterization of nanocomposites at various silica amounts.....	72
4.3 Polymer content and polymer grafting efficiency of composite sample (P-mSi_APS_1).....	73
6.1 Rate constant and activation energy of PIP and PIP-SiO ₂ nanoparticles..	109
6.2 Thermal properties of rubber nanocomposite	114
7.1 Glass transition temperature and decomposition temperature of rubber samples.....	118
7.2 Mechanical properties of NR filled with PIP-SiO ₂ nanocomposites before and after ageing.....	129
7.3 Mechanical properties of NR filled with HPIP-SiO ₂ nanocomposites before and after ageing.....	131

LIST OF FIGURES

Figure	PAGE
1.1 Scheme of the miniemulsion process.....	3
1.2 Comparison between (a) direct and (b) inverse miniemulsion.....	3
1.3 Principle of encapsulation by miniemulsion polymerization.....	4
1.4 Isotropic microemulsion domains in the phase diagram of multicompartment systems.....	6
1.5 The mechanism for surface modification of mesoporous silica.....	10
1.6 Scheme of surface modification for nano-size filler	11
1.7 Different types of polymer nanocomposites. (a) embedding of the filler into the polymer, (b) interpenetrating networks, (c) incorporation of inorganic groups with chemical bonds to the polymer backbone, and (d) dual hybrid polymer.....	12
1.8 Proposed mechanism of differential microemulsion polymerization.....	15
1.9 Different core/shell morphologies of polymer/silica nanocomposites....	16
1.10 Proposed mechanism of diimide reduction.....	21
1.11 Proposed models for the double bonds distribution of hydrogenated SBR latex (a) layer model and (b) uniform model	22
2.1 The schematic diagram of nanosized EPM synthesis	31
2.2 The schematic diagram of poly(ST- <i>co</i> -MMA)-SiO ₂ synthesis	34
2.3 The apparatus of polyisoprene-SiO ₂ synthesis	36
2.4 The schematic diagram of HPIP-SiO ₂ synthesis	37
2.5 Schematic diagram of HF etching method.....	41
3.1 Structure configurations of synthetic polyisoprene nanoparticles.....	44
3.2 ¹ H NMR spectra of (a) PIP, (b) HPIP (78%), (c) HPIP (94%).....	47
3.3 ¹³ C NMR spectra of (a) PIP and (b) 94% EPM.....	48
3.4 Effect of boric acid addition on PIP hydrogenation. Condition: [N ₂ H ₄] = 3 mol/L, [H ₂ O ₂] = 4.5 mol/L, [C=C] = 1 mol/L, [H ₂ O] = 10 mol/L, Temp 70°C, time = 4 h.....	50

Figure	PAGE
3.5 PIP hydrogenation: a) effect of hydrazine concentration on PIP hydrogenation at $[\text{H}_2\text{O}_2] = 4.5 \text{ mol/L}$. b) effect of hydrogen peroxide amount on PIP hydrogenation at $[\text{N}_2\text{H}_4] = 3 \text{ mol/L}$. Condition: $[\text{H}_3\text{BO}_3] = 0.15 \text{ mol/L}$, $[\text{C}=\text{C}] = 1 \text{ mol/L}$, $[\text{H}_2\text{O}] = 10 \text{ mol/L}$, $T = 70^\circ\text{C}$, time = 4 h.....	52
3.6 Effect of hydrogen peroxide to hydrazine ratio on PIP hydrogenation. Condition: $[\text{N}_2\text{H}_4] = 3 \text{ mol/L}$, $[\text{H}_3\text{BO}_3] = 0.15 \text{ mol/L}$, $[\text{C}=\text{C}] = 1 \text{ mol/L}$, $[\text{H}_2\text{O}] = 10 \text{ mol/L}$, $T = 70^\circ\text{C}$, time = 4 h.....	54
3.7 Effect of reaction temperature on PIP hydrogenation. Condition: $[\text{N}_2\text{H}_4] = 5 \text{ mol/L}$, $[\text{H}_2\text{O}_2] = 7.5 \text{ mol/L}$, $[\text{H}_3\text{BO}_3] = 0.15 \text{ mol/L}$, $[\text{C}=\text{C}] = 1 \text{ mol/L}$, $[\text{H}_2\text{O}] = 10 \text{ mol/L}$, time = 4 h.....	55
3.8 Effect of water addition on PIP hydrogenation. Condition: $[\text{N}_2\text{H}_4] = 5 \text{ mol/L}$, $[\text{H}_2\text{O}_2] = 7.5 \text{ mol/L}$, $[\text{C}=\text{C}] = 1 \text{ mol/L}$, $[\text{H}_3\text{BO}_3] = 0.15 \text{ mol/L}$, $T = 70^\circ\text{C}$, time = 4 h.....	56
3.9 (a) Conversion profile, (b) First order in \ln plot of PIP hydrogenation. Condition: $[\text{N}_2\text{H}_4] = 5 \text{ mol/L}$, $[\text{H}_2\text{O}_2] = 7.5 \text{ mol/L}$, $[\text{C}=\text{C}] = 1 \text{ mol/L}$, $[\text{H}_3\text{BO}_3] = 0.15 \text{ mol/L}$, $[\text{H}_2\text{O}] = 10 \text{ mol/L}$, $T = 70^\circ\text{C}$	59
3.10 Proposed synthetic route for nanosized EPM synthesis by diimide hydrogenation of PIP.....	61
3.11 Thermograms of (a) nanosized PIP, (b) HPIP (57 %), (c) HPIP (78%), (d) HPIP (94%).....	62
3.12 The appearance of rubber latex samples and particle size distribution: (a) nanosized PIP, (b) nanosized EPM at 40% hydrogenation and (c) nanosized EPM at 94% hydrogenation	63
4.1 Particle size and conversion at various initiator amounts. Condition: ST/MMA ratio = 1.5/1, surfactant amount = 1.75%, modified silica loading = 10%, monomer/water = 0.2.....	67
4.2 Dependence of particle size and conversion on SDS concentration. Condition: ST/MMA ratio = 1.5/1, APS amount = 1% based on monomer weight, modified silica loading = 10% based on monomer	

Figure	PAGE
weight, monomer/water = 0.2.....	68
4.3 Conversion and silica encapsulation efficiency at various monomer to water ratio. Condition: ST/MMA ratio = 1.5/1, surfactant amount = 1.75%, initiator amount = 1%, modified silica loading = 10% based on monomer weight.....	69
4.4 Dependence of particle size and grafting efficiency on ST/MMA ratio. Condition: SDS amount = 1.75%, APS amount = 1%, modified-SiO ₂ loading = 10% based on monomer weight, monomer/water = 0.2.....	71
4.5 Thermogravimetric analysis curve of composite sample, P-mSi_APS_1	73
4.6 Particle size distributions of composite samples (a) P-mSi_APS_1, (b) P-untreated-Si_APS_1 and (c) P-Si_APS_1 (Physical Mixing).....	75
4.7 Appearance of composite latex (a) P-Si_APS_1 (Physical Mixing), (b) P-mSi_APS_1.....	75
4.8 FTIR spectrum of modified silica at high AA amount (m-Si 1).....	76
4.9 FTIR spectrum of P-mSi_APS_1 after separation of the free latex particles.....	77
4.10 ¹ H NMR spectrum of composite sample, P-mSi_APS_1, in CDCl ₃	78
4.11 TEM micrographs of (a) untreated-SiO ₂ , (b) P-mSi_APS_1, (c) P-mSi_APS_1 at higher magnification.....	79
4.12 The proposed model for formation mechanism of nanosized-SiO ₂ encapsulated by poly(ST-co-MMA) with core/shell morphology.....	81
5.1 FTIR spectra of (a) MPS-SiO ₂ , (b) VTS-SiO ₂ , (c) PIP-VTS-SiO ₂	84
5.2 Effect of monomer to water ratio (M/H ₂ O) on PIP-SiO ₂ ; (▲) Particle diameter, (◆) %Conversion, (■) %GE. Condition: SPS = 1 %wt, SDS = 3 %wt, VTS-SiO ₂ = 10 %wt based on monomer.....	86
5.3 Effect of initiator concentration on PIP-SiO ₂ ; (▲) Particle diameter, (◆) %Conversion, (■) %GE. Condition: M/H ₂ O = 0.3, SDS = 3 %wt, VTS-SiO ₂ = 10 %wt based on monomer.....	87
5.4 Effect of SDS concentration on PIP-SiO ₂ ; (▲) Particle diameter, (◆) %Conversion, (■) %GE. Condition: M/H ₂ O = 0.3, SPS = 1 %wt, VTS-SiO ₂ = 10 %wt based on monomer.....	88

Figure	PAGE
5.5 Effect of silica loading on PIP-SiO ₂ ; (▲) Particle diameter, (■) %Si encapsulation, (◆) %Conversion. Condition: M/H ₂ O = 0.3, SPS = 1 %wt, SDS = 3 %wt based on monomer.....	90
5.6 Particle size distribution of samples (a) PIP, (b) PIP/untreated SiO ₂ (10 %wt) and (c) PIP-VTS-SiO ₂ (10 %wt).....	92
5.7 Appearance of (a) PIP/untreated SiO ₂ and (b) PIP-VTS-SiO ₂	93
5.8 TEM micrographs of (a) PIP/untreated SiO ₂ , (b) PIP-VTS-SiO ₂ , (c) PIP-MPS-SiO ₂	94
5.9 The proposed formation mechanism of nanosize-SiO ₂ encapsulated by nanosized PIP with core/shell morphology.....	96
5.10 Thermograms of (a) nanosized PIP, (b) PIP-VTS-SiO ₂ (10 %wt), (c) PIP-VTS-SiO ₂ (15 %wt,) (d) PIP-VTS-SiO ₂ (20 %wt), (e) PIP-untreated SiO ₂ (10 %wt).....	97
6.1 FTIR spectra of (a) VTS-SiO ₂ and (b) PIP-VTS-SiO ₂	100
6.2 ¹ H NMR spectra of (a) PIP-SiO ₂ , (b) HPIP-SiO ₂ (98% HD).....	101
6.3 Hydrogenation of PIP-SiO ₂ : a) effect of [N ₂ H ₄] at [H ₂ O ₂] = 4.5 mol/L. b) effect of [H ₂ O ₂] at [N ₂ H ₄] = 3 mol/L. Condition: [H ₃ BO ₃] = 0.15 mol/L, [C=C] = 1 mol/L, [H ₂ O] = 10 mol/L, T = 70°C, time = 4 h. ● %HD, ◆ Particle size.....	103
6.4 Effect of boric acid addition on PIP-SiO ₂ hydrogenation. Condition: [N ₂ H ₄] = 3 mol/L, [H ₂ O ₂] = 4.5 mol/L, [C=C] = 1 mol/L, [H ₂ O] = 10 mol/L, Temp 70°C, time = 4 h. ● %HD, ◆ Particle size.....	104
6.5 Effect of water addition on PIP-SiO ₂ hydrogenation. Condition: [N ₂ H ₄] = 5 mol/L, [H ₂ O ₂] = 7.5 mol/L, [C=C] = 1 mol/L, [H ₃ BO ₃] = 0.15 mol/L, T = 70°C, time = 4 h. ● %HD, ◆ Particle size.....	105
6.6 Conversion profiles of (a) HPIP-SiO ₂ , (b) HPIP without SiO ₂ and First order in ln plot of (c) HPIP-SiO ₂ , (d) PIP without SiO ₂ . Condition: [N ₂ H ₄] = 5 mol/L, [H ₂ O ₂] = 7.5 mol/L, [C=C] = 1 mol/L, [H ₃ BO ₃] = 0.15 mol/L, [H ₂ O] = 10 mol/L. ◆ = 50°C, ■ = 60°C, ▲ = 70°C.....	108
6.7 Proposed mechanism for synthesis of HPIP-SiO ₂ nanocomposite.....	110

Figure	PAGE
6.8 TEM micrographs of (a) PIP, (b) PIP at 64 %HD, (c) PIP at 94 %HD, (d) HPIP-SiO ₂ , (e) HPIP-SiO ₂ at 64% HD and (f) HPIP-SiO ₂ (98% HD)...	112
6.9 Thermograms of (a) nanosized PIP, (b) PIP-SiO ₂ , (c) HPIP-SiO ₂ (64% HD) and (d) HPIP-SiO ₂ (98% HD).....	114
7.1 Temperature dependence of (a) storage modulus (E') and (b) loss tangent ($\tan \delta$) for PIP and HPIP.....	117
7.2 Temperature dependence of (a) storage modulus (E') and (b) loss tangent ($\tan \delta$) for NR and its composites.....	120
7.3 Stress-strain curves of (i) PIP-VTS-SiO ₂ filled NR before ageing; (a) NR, (b) 95:5 of NR:PIP-SiO ₂ , (c) 90:10 of NR:PIP-SiO ₂ , (d) 80:20 of NR:PIP-SiO ₂ , (e) 70:30 of NR:PIP-SiO ₂ and (ii) PIP-VTS-SiO ₂ filled NR after ageing.....	122
7.4 Stress-strain curves of (i) PIP-MPS-SiO ₂ filled NR before ageing; (a) NR, (b) 95:5 of NR:PIP-SiO ₂ , (c) 90:10 of NR:PIP-SiO ₂ , (d) 80:20 of NR:PIP-SiO ₂ , (e) 70:30 of NR:PIP-SiO ₂ and (ii) PIP-MPS-SiO ₂ filled NR after ageing.....	124
7.5 Stress-strain curves of (i) vulcanized NR nanocomposite before ageing; (a) NR, (b) 80:20 of NR:PIP-VTS-SiO ₂ , (c) 80:20 of NR:HPIP-SiO ₂ (64%HD) (d) 90:10 of NR:HPIP-SiO ₂ , (e) 80:20 of NR:HPIP-SiO ₂ , (f) 70:30 of NR:PIP-SiO ₂ , (g) 60:40 of NR:HPIP-SiO ₂ and (ii) vulcanized NR nanocomposite after.....	126
7.6 SEM micrographs of samples before and after ageing (x 1000). (a) NR, (b) aged NR, (c) NR filled with untreated SiO ₂ , (d) aged NR filled with untreated SiO ₂ , (e) NR filled with PIP-VTS-SiO ₂ , (f) aged NR filled with PIP-VTS-SiO ₂ , (g) NR filled with PIP-MPS-SiO ₂ , (h) aged NR filled with PIP-MPS-SiO ₂	133
7.7 Surface of NR filled with HPIP-SiO ₂ at various blend ratios after ozone exposure for 72 h: (a) 100/0, (b) 80/20, (c) 70/30, (d) 60/40.....	136

LIST OF ABBREVIATIONS

ASTM	: American Society for Testing and Materials
AA	: Acrylic acid
VTM	: Vinyl Trimethoxy Silane
MPS	: 3-Methylacryloxypropyl Trimethoxy Silane
PIP	: Polyisoprene
HPIP	: Hydrogenated Polyisoprene
EPM	: Ethylene-Propylene Rubber
EPDM	: Ethylene-Propylene Diene Monomer
DRC	: Dry Rubber Content
GE	: Grafting Efficiency
HD	: Hydrogenation Degree
ISO	: International Standardization for Organization
NBR	: Acrylonitrile-Butadiene Rubber
BR	: Polybutadiene Rubber
SBR	: Styrene-Butadiene Rubber
ST	: Styrene
MMA	: Methyl Methacrylate
NMR	: Nuclear Magnetic Resonance Spectrometer
NRL	: Natural Rubber Latex
OsO ₄	: Osmium Tetraoxide
SPS	: Sodium Persulfate
SDS	: Sodium Dodecylsulfate
ZnO	: Zinc Oxide
ZDEC	: Zincdiethyl Dithiocarbamate
TEPA	: Tetraethylene Pentamine
T_g	: Glass Transition Temperature
TGA	: Thermal Gravimetric Analysis
T_{id}	: Initial Decomposition Temperature
T_{max}	: Maximum Decomposition Temperature

CHAPTER I

INTRODUCTION

1.1 Motivation

Polymer nanocomposites are novel materials consisting of an inorganic component as a reinforcing filler and an organic component as the polymer system. The research field of polymer nanocomposites is of tremendous interest and is beneficial to many different industries. Nanosilica, one of the most common inorganic systems, has many functional properties including effective reinforcement for the rubber and plastic industry. Hence, polymer/silica nanocomposites have grown to being the focus of a great deal of academic and industrial research. These materials combine the advantageous properties of a polymer species such as elasticity, processibility, flexibility and then dispersed silica provides high thermal stability and reinforcement. However, these remarkable properties could not be fulfilled due to the poor dispersion, the inferior compatibility and the lower stability of the filler in the polymer matrix. The drawbacks of hybrid nanoparticles are due to the difference of polarity between the filler and polymer. The filler has the highest polarity at its surface resulting in a strong aggregation tendency. On the other hand, the polymer is less polar resulting in a decrease in mechanical, chemical and thermal properties. Since silica particles with hydrophilic surfaces easily adhere to each other through hydrogen bonding and form irregular agglomerates, this hydrophilic surface does not possess good compatibility with the polymer. Therefore, mechanical mixing/dispersion methods such as high speed shearing or milling are not effective to break down the agglomeration because the electrostatic forces holding the particles together are stronger than the shear force created by the velocity gradient.

Consequently, the development of new polymer/silica nanocomposites to achieve the homogeneity of the silica nanoparticle in the nanosized polymer as well as a good colloidal stability via an alternative synthetic route is a challenge. A new direction in this area is to synthesize nanosized rubber and rubber nanocomposites in

latex form via a green process which avoids the obvious problems; such as, high pressure hydrogen equipment, high cost of a noble metal catalyst, and environmental problems which may result from the use of toxic organic solvents.

1.2 Miniemulsion Polymerization

The synthesis and application of polymers via miniemulsion polymerization have gained popularity in both the academia and industry. Miniemulsion polymerization was first investigated by John Ugelstad in 1973 [1]. Miniemulsions are obtained by the combination of a high shear device to break up the monomer droplets into submicron monomer droplets with a water-insoluble or monomer-soluble component. Without a high-shear device, miniemulsion polymerization could revert to macroemulsion polymerization, indicating that the presence of only a costabilizer was not sufficient to cause predominant droplet nucleation [2]. High-shear devices are provided by sonicator or mechanical homogenizer and surfactant is necessary to retard droplet coalescence. The mechanism of miniemulsion polymerization is shown in Figure 1.1. For the first step, small stable droplets ranging in size between 50 and 500 nm are formed by shearing the dispersed phase system, the continuous phase, and surfactant agent. Then, these droplets can propagate during polymerization through small monomer-swollen micelles. Miniemulsion polymerization produces a large droplet surface area in the system and most of the surfactant is adsorbed at the droplet surface to produce very small monomer droplets. Particle nucleation initially occurs via radical entry into the monomer droplets by using either oil-soluble or water-soluble initiators. The important key is that the reaction proceeds by polymerization of the monomer in these small droplets [3].

Landfester and coworkers [4] studied the preparation of polystyrene nanoparticles via miniemulsion polymerization using the cationic surfactants of cetyltrimethyl ammonium bromide (CTAB) and cetyltrimethyl ammonium tartrate (CTAT). It was reported that these surfactants could produce particles of similar size to those produced when using anionic surfactants at the same levels.

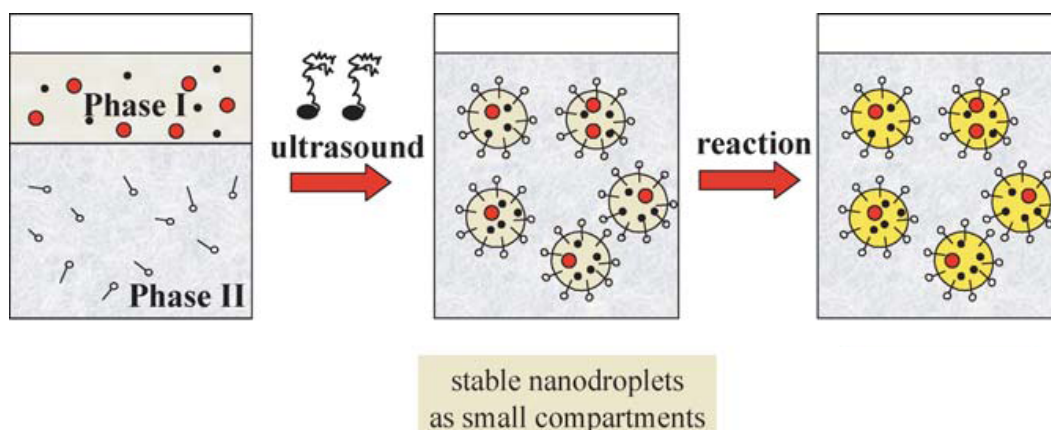


Figure 1.1 Scheme of the miniemulsion process [3].

For direct miniemulsions (oil-in-water), the droplet size also changed rapidly through the the sonication process [5]. When homogenization begins, the polydispersity of the droplet was still high and the miniemulsion reaches a steady state. For inverse miniemulsions (water-in-oil), the concept of emulsion stabilization is different in which the reaction medium is insoluble in the continuous oil phase, so-called lipophobe [6] as shown in Figure 1.2. Due to a change of the continuous phase from hydrophilic to hydrophobic in the inverse miniemulsion, the surface coverage of the droplet with surfactant was incomplete, and empty micelles were absent. The particle size decreased with increasing surfactant amount, and these relations depend on the amount of hydrophobe [7].

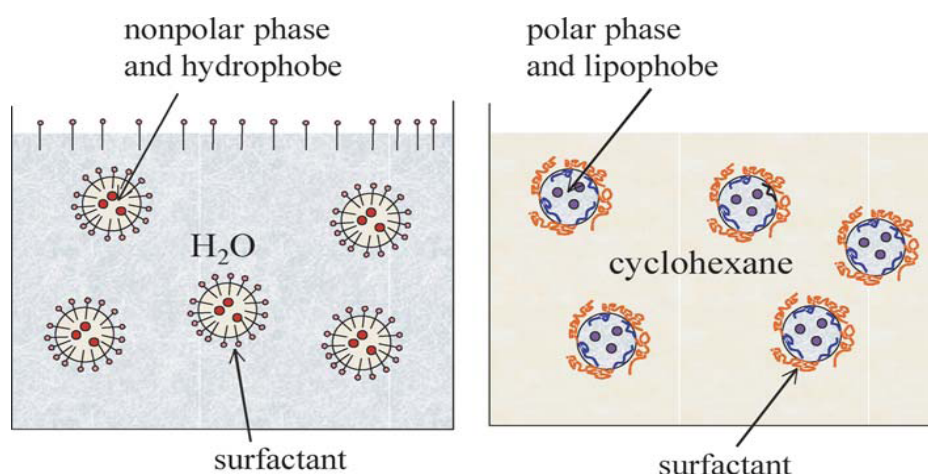


Figure 1.2 Comparison between (a) direct and (b) inverse miniemulsion [6].

Miniemulsion polymerization could be applied for synthesizing nanosized polymers of all types of monomers, which were miscible or immiscible with the continuous phase. This enables a variety of polymerization reactions that lead to nanoparticles and hybrid nanoparticle synthesis [8-11].

Li et al. [12] studied the kinetics of conventional emulsion polymerization in comparison with miniemulsion copolymerization of styrene and butadiene using hexadecane as the costabilizer. It was found that the miniemulsion polymerization occurred mainly by nucleation in the small and relatively stable monomer droplets while particle formation occurred within the micelles in conventional emulsion polymerization. The rate of polymerization in miniemulsion polymerization was faster than in the corresponding conventional emulsion system. The homogenization process was important for providing a stable miniemulsion system.

There have been many reports on the preparation of inorganic encapsulation within polymers by miniemulsion polymerization [13-14], Erdem et al. [15-16] studied the encapsulation of TiO₂ particles via miniemulsion polymerization in two steps as shown in Figure 1.3. The TiO₂ was initially dispersed in the monomer by using polybutene-succinimide as stabilizer and the dispersion phase was then dispersed in an aqueous solution to form stable droplets. However, it was found that the incorporation of TiO₂ nanoparticles within the polystyrene droplet was affected by the limits of the droplet size and complete encapsulation of all TiO₂ particles in the colloidal system was not achieved.

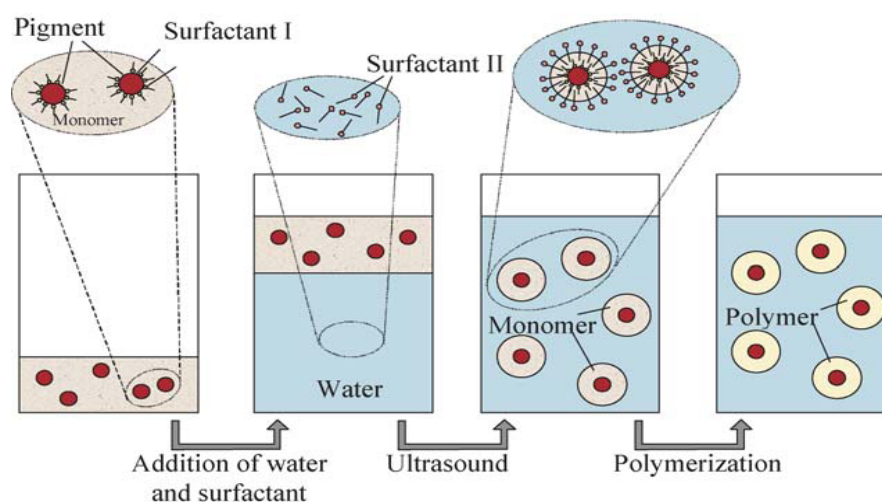


Figure 1.3 Principle of encapsulation by miniemulsion polymerization [16].

Tiarks et al. [17] reported on the encapsulation of silica nanoparticles with polystyrene, poly(butyl acrylate), and poly(methyl methacrylate) by the miniemulsion process. Polymer/silica nanocomposites could be obtained having a raspberry morphology and the overall particle size ranged from 80-120 nm. The particle size of the composites could be controlled by the silica loading. The cationic surfactant of CTAB resulted in an improvement of the silica nanoparticles within the polymer latex [18].

Ali Reza Mahdavian et al. [19] applied miniemulsion polymerization to prepare a nanocomposite latex of nano-alumina (40–47 nm) encapsulated by poly(styrene-*co*-methyl methacrylate) under high-shear ultrasonic irradiation. First, alumina nanoparticles were coated with oleic acid in order to form modified alumina. Then miniemulsion polymerization was performed in the minidroplets including modified alumina, St and MMA for obtaining core/shell nanocomposite particles. The stable poly(St-*co*-MMA)/alumina nanocomposite latexes with high monomer conversion were prepared through miniemulsion polymerization.

1.3 Microemulsion Polymerization

Microemulsion polymerization provides alternative opportunities for producing polymer nanoparticle and polymer nanocomposites due to providing a stable suspension of ultrafine particles in the nanosized range, so-called “microlatexes or nanolatexes”. The concept of microemulsion polymerization appeared in the early 1980s when it was first reported by Stoffer et al. [20]. For miniemulsion polymerization, the monomer droplet size could be sufficiently reduced, the loci of polymerization became the monomer droplets and the particle diameter was in the range of 50 to 500 nm. Based on microemulsion polymerization, the surfactant concentration in a macroemulsion was greatly increased or the monomer concentration was highly reduced resulting in a microemulsion. The particles produced in this system were very small, ranging from 10 to 100 nm.

A microemulsion is defined as being thermodynamically stable, isotropic with optically transparent dispersion of two immiscible liquids composed of oil and water and obtained in a surfactant system consisting both of a single surfactant, a mixture of

surfactants or a mixture of a cosurfactant [21-23]. Microemulsion polymerization, oil in water (o/w) and inverse microemulsion polymerization, water in oil (w/o) have become useful techniques to prepare nanoparticles in latex form and to yield stable polymer with particle size ranging from 10 to 100 nm [24]. A globular oil-in-water or water-in-oil, microemulsion consists of microdroplets surrounded by a surfactant monolayer as shown in Figure 1.4. The small size of the droplets is commonly used as a criterion for the preparation of the microemulsion. The thermodynamic stability of microemulsions arises from the very low interfacial tension of the small droplets. Subsequently, the formation of the microemulsion is a spontaneous process. However, a large amount of surfactant (about 10–15% based on monomer weight) is needed for achieving thermodynamic stability of the microemulsion [25-28].

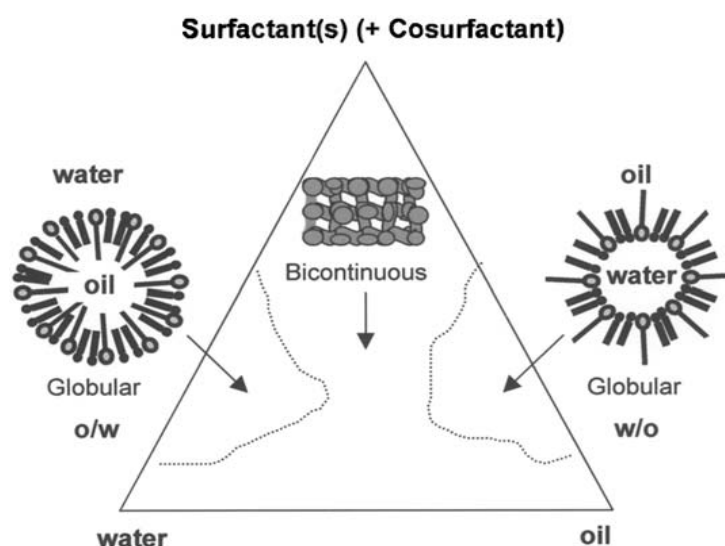


Figure 1.4 Isotropic microemulsion domains in the phase diagram of multicomponent systems [28].

Capek et al. [29] proposed a mechanism for the oil in water microemulsion copolymerization of butyl acrylate and acrylonitrile initiated by ammonium peroxydisulfate in water and dibenzoyl peroxide in oil in the presence of a radical scavenger and water soluble potassium nitrosodisulfonate. The initiation involved a two-step process; the radicals are formed by the decomposition of initiator in the aqueous phase in the first step and then the oligomeric radicals entered the micelles

and initiated the growth of the primary monomer. The production of radicals was initiated in the monomer swollen polymer particles to form radicals in the aqueous phase and propagated the growth of the polymer chains in both the aqueous phase and the monomer-swollen micelles. The nucleation of monomer swollen micelles resulted in the formation of colloidal primary particles and stable polymer particles.

Gan et al. [30] studied the polymerization of styrene in stable o/w microemulsions using a cationic surfactant of cetyltrimethyl ammonium bromide (CTAB) and a glycol type cosurfactant initiated by water-soluble potassium persulphate to produce microlatex. Final latexes with high molecular weight ($5-10 \times 10^6$) and small particle diameter (20-40 nm) were achieved.

Many investigations have been carried out on the polymerization of globular o/w or w/o microemulsions through free-radical polymerization of styrene, methyl methacrylate, methacrylic acid [31-33]. The microemulsion polymerization was achieved by using a cationic surfactant, CTAB [34] or cetyltrimethyl ammonium chloride (CTAC) [35], and microemulsions were prepared using a surfactant of sodium dodecyl sulfate (SDS) [36] and a mixture of cosurfactant of SDS with pentanol [37-38]. However, the monomer content that could be incorporated was low and usually lower than the surfactant amount used.

These polymerized o/w microemulsions were applied for producing small latex diameter of poly(methyl methacrylate) and poly(hexyl methacrylate) (30-50 nm), [39-40] and high molecular weight polystyrene (10^5-10^6) [41]. The polymerization of styrene has also been successfully carried out in o/w microemulsions stabilized by dodecyltrimethyl ammonium bromide without using a cosurfactant [42-43].

Sanghvi et al. [44] reported that stable and transparent poly(styrene-acrylonitrile) latexes were produced by the copolymerization of styrene with acrylonitrile in a ternary o/w microemulsion containing SDS as an anionic surfactant. The average particle size was found to be 15-20 nm. The anionic nature of the free radicals and oligomeric free radicals generated due to potassium persulfate (KPS) and the solubility of acrylonitrile in water experience more resistance from the SDS molecules compared with OH radicals generated from H_2O_2 /ascorbic acid. The kinetics of the copolymerization was studied at different temperatures using different

concentrations of KPS and H₂O₂/ascorbic acid. As a result the rate of polymerization showed a higher dependency on initiator concentration for the KPS system.

A major difference between emulsion and microemulsion arises from the amount of surfactant needed to stabilize the reaction systems. This surfactant concentration is much larger for a microemulsion (10-50% of the monomer weight), as compared with conventional emulsion polymerization. However, high solid content and low surfactant concentration are desirable for industrial applications. This is a drawback that considerably limits the potential uses of microemulsion polymerization. On comparison with conventional emulsion polymerization, microemulsion polymerization of a non-polar monomer could produce polymer latex particles with small particle diameters of less than 50 nm, whereas particles obtained from conventional emulsion polymerization were large being greater than 400 nm in diameter. For all the above microemulsion polymerization processes, high surfactant concentration was required to form a stable polymer latex which is an obvious drawback in comparison with those particles obtained from conventional emulsion polymerization. High surfactant levels and low polymer contents restrict the application of microemulsion latexes in industry. To minimize the surfactant amount and maximize polymer content, alternative methods have been developed.

1.4 Silica Surface Modification

One of the important applications of silica is the use of it as a filler in polymer matrices for reinforcement. Nano-silica has more prominent reinforcing effect over commercial micro-silica due to its high surface area which leads to better dispersion capability in a polymer material. However, silica nanoparticles have a tendency to form agglomerates due to high polarity and surface energy through hydrogen bonding. This phenomenon of strong filler-filler interactions is not favorable for effective reinforcement. This problem could be resolved by surface modification of the silica nanoparticles.

The strategy for modification or functionalization of silica particles depends on the specific structure of their surface and specific surface area. The hydroxyl group on the silica surface was used as capping groups and reacted with a carboxyl group

through hydrolysis and polycondensation using various silane groups to form siloxane linkage Si-O-Si bond [45-47]. Amine and oxysilane are two other popular functional groups that are used for surface modification of nanoparticles due to the protection of the nanoparticles from aggregation or agglomeration [48]. The modifiers or coupling agents should have dual functional groups, one for surface binding and the other for initiating the designed chemical reactions [49]. Electrostatic interactions [50-51] and other types of Van der Waals interactions [52] are the main driving forces in preliminary silica surface modification. However, both these types of interaction are physical in nature which tends to be weak compared to chemical reactions.

Among these strategies, silane coupling agents provide a popular approach to produce functionalized silica; this process is based on two main reactions of hydrolysis followed by polycondensation. Some typical silane coupling agents used for surface functionalization of silica particles are presented in Table 1.1 and the mechanism for surface modification of mesoporous silica is shown in Figure 1.5 [53].

Table 1.1 Typical silane coupling agents for silica surface treatment [53]

Name	Structure
3-aminopropyltriethoxysilane	$\text{H}_2\text{N}(\text{CH}_2)_3\text{Si}(\text{OC}_2\text{H}_5)_3$
3-aminopropyltrimethoxysilane	$\text{H}_2\text{N}(\text{CH}_2)_3\text{Si}(\text{OCH}_3)_3$
Vinyltriethoxysilane	$\text{CH}_2=\text{CHSi}(\text{OC}_2\text{H}_5)_3$
Vinyltrimethoxysilane	$\text{CH}_2=\text{CHSi}(\text{OCH}_3)_3$
3-isocyanatopropyltriethoxysilane	$\text{OCN}(\text{CH}_2)_3\text{Si}(\text{OC}_2\text{H}_5)_3$
methacryloxymethyltriethoxysilane	$\text{CH}_2=\text{C}(\text{CH}_3)\text{COO}(\text{CH}_2)_3\text{Si}(\text{OC}_2\text{H}_5)_3$
3-methacryloxypropyltrimethoxysilane	$\text{CH}_2=\text{C}(\text{CH}_3)\text{COO}(\text{CH}_2)_3\text{Si}(\text{OCH}_3)_3$
mercaptopropyl triethoxysilane	$\text{SH}(\text{CH}_2)_3\text{Si}(\text{OC}_2\text{H}_5)_3$
methyltriethoxysilane	$\text{CH}_3\text{Si}(\text{OC}_2\text{H}_5)_3$
phenyltrimethoxysilane	$\text{PhSi}(\text{OCH}_3)_3$
bis(triethoxysilylpropyl)tetrasulfane	$(\text{C}_2\text{H}_5\text{O})_3\text{Si}(\text{CH}_2)_3\text{S}_4(\text{CH}_2)_3\text{Si}(\text{OC}_2\text{H}_5)_3$
3-glycidoxypropyltrimethoxysilane	$\text{CH}_2(\text{O})\text{CHCH}_2\text{O}(\text{CH}_2)_3\text{Si}(\text{OCH}_3)_3$
dimethyldichlorosilane	$(\text{CH}_3)_2\text{SiCl}_2$

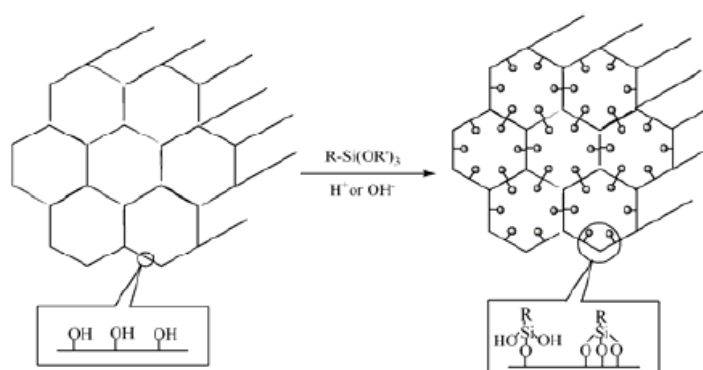


Figure 1.5 The mechanism for surface modification of mesoporous silica [53].

For silica treatment, homogeneous base catalysts such as ammonia solution or sodium hydroxide and acid catalysts such as hydrochloric acid or nitric acid are necessary for the hydrolysis and condensation. The hydrolysis leads to the formation of silanol and removes the leaving group during the first step. These silanol groups would crosslink during polycondensations to form oligomers which further condense catalytically through OH interactions on their surfaces. When the hydroxyl group exists on the silica surface, many chemical reactions target interactions with this group [54-56]. (3-mercaptopropyl) trimethoxysilane (MPS) are the agents most often used for silica modification [57-59]. Polyethylene glycol (PEG) [60], vinyl [61], phenyl [62] and amino [63-64] are the most common functional groups at the end of these agents.

Therefore, chemical treatment of the nanoparticle surface is necessary to achieve better compatibility and dispersion of the filler in the polymer latex. This treatment leads to bonding between the coupling agent and the silica surface to remove the surface silanol groups and to change the hydrophilic surface into a hydrophobic surface. As shown in Figure 1.6, the ideal result of surface treatment is to reduce the filler–filler interaction and to achieve homogeneity of the nano-size silica in the polymer [65].

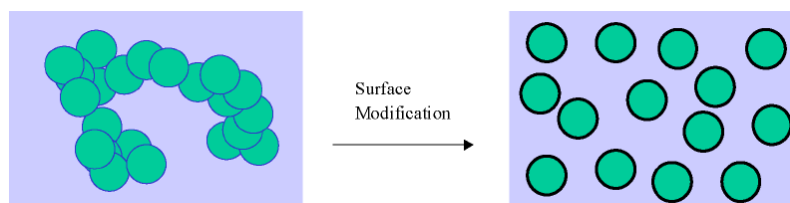


Figure 1.6 Scheme of surface modification for nano-size filler [65].

1.5 Polymer-Silica Nanocomposites

Physical blending of the silica particles with the polymer is the simplest method to prepare polymer/silica composites. The mixing can be classified by melt blending and solution blending. Melt blending was done by mixing the silica with the polymer above the glass-transition temperature (T_g) of the polymers or above the melting point [66]. Perez et al. [67] reported that the addition of silica into styrene-butadiene rubber (SBR) by melt blending to prepare SBR/silica nanocomposites resulted in increasing the T_g and thermal resistance while the modulus and tensile strength slightly increased due to the adhesion of the filler in rubber nanocomposites. For solution blending, silica and polymer were mixed in an organic solvent and the polymer nanocomposites were obtained after removal of the solvent. This method can provide a good molecular level of mixing, and can overcome the limitation of melt mixing. Many polymers undergo good mixing with silica using this method [68-71]; however, solution blending has drawbacks as high amounts of solvent are required and the solvent must be removed after processing.

The preparation of polymer/silica nanocomposites by direct mixing led to physisorption, which is a relatively weak interaction and it was sensitive to temperature and chemical reagents resulting in easy desorption. Hence, many chemical methods have been applied to produce polymer/silica nanocomposites providing strong covalent bonds with functional groups.

An incorporation of inorganic fillers in organic polymers has several ways to form the different interactions. The strong interaction such as covalent bond, coordination, and ionic bond or weak interaction such as van-der-Waals force, hydrogen bonding, hydrophilic-hydrophobic interaction could occur between the two

components depending on the different methods. (Figure 1.7) [72]. However, strong interaction and chemisorption between two different phases are preferred.

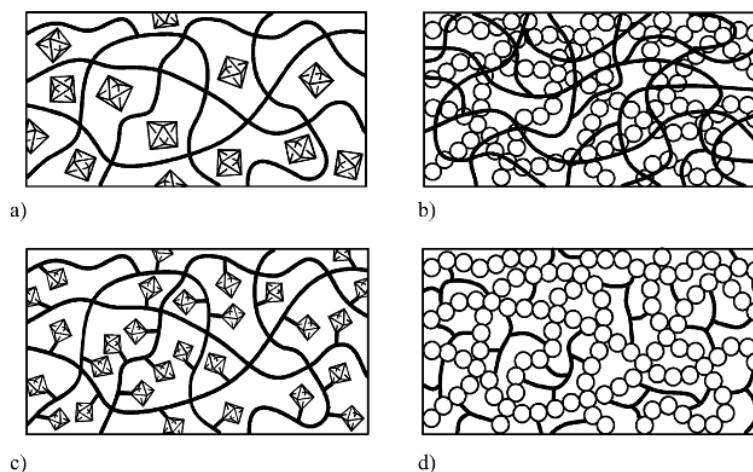


Figure 1.7 Different types of polymer nanocomposites. (a) embedding of the filler into the polymer, (b) interpenetrating networks, (c) incorporation of inorganic groups with chemical bonds to the polymer backbone, and (d) dual hybrid polymer [72].

Polymerization methods have been developed in order to provide many advantages, such as ease of processing and good performance of the final products [73]. Further, polymerization can produce good dispersion of silica in the polymer matrix and increase the strong interaction between the polymers and the nanofillers. In 1998, Moller et al. [74] studied the synthesis of poly(methyl methacrylate)/silica composites by solution polymerization initiated with benzoyl peroxide through radical chain polymerization, implying strong interaction and chemical bonding between the polymers and fillers as confirmed by FTIR spectroscopy and SEM.

Some previous work has been reported on heterophase polymerization techniques to prepare polymer/silica nanocomposites by using dispersion [75-77], suspension-dispersion [78-80], and emulsion polymerization [81-85]. Bourgeat-Lami et al. [86] studied polystyrene encapsulation of silica particles using dispersion

polymerization and a nanocomposite particle size of 0.2-0.5 μm was obtained. The polymer encapsulation of small silica particles, using dispersion polymerization of styrene was performed in aqueous ethanol medium with poly(*N*-vinyl pyrrolidone) (PVP) as stabilizer. Zhu et al. [87] studied the preparation of poly(styrene-butylacrylate-acrylic acid)-graft-silica (PSBA-g-silica) hybrid nanoparticles by suspension-dispersion polymerization to improve the present unsatisfactory UV-shielding and water resistance properties. Later, core-shell poly(methyl methacrylate) (PMMA)-SiO₂ nanoparticles were synthesized using suspension-dispersion-polymerization and these nanoparticles were used as a filler in a poly(vinyl chloride) (PVC) matrix, resulting in the increased tensile strength, elongation at break and heat resistance of PVC [88].

Alternatively, emulsion polymerization provides an effective way of synthesizing polymer/silica nanoparticles. Ding et al. [89] reported the preparation of monodispersed polystyrene/SiO₂ composite particles with a core-shell structure by in situ emulsion polymerization of styrene (ST) on the surface of silica nanoparticles modified with oleic acid since the C=C bonds of oleic acid were adsorbed by the silanol groups at the surface of nanosized silica to induce the coating. Later, Mahdavian et al. [90] reported that the preparation of poly(ST-MMA)/SiO₂ composites via emulsion polymerization was accomplished by modification of nano-SiO₂ with oleic acid and composites of particle size in the range of 90-200 nm with high silica encapsulation efficiency of 87.2% were obtained. Reculosa et al. [91] reported the preparation of polystyrene/silica nanocomposites with the raspberry like morphology through emulsion polymerization using the adsorption of a poly(ethylene glycol) methacrylate derivative. Hence, emulsion polymerization is commonly used in the production of polymer particles with very small size. This method can control the reaction rate, particle size and morphology effectively [92].

Recently, modified emulsion polymerization has been developed to obtain particles of smaller size by using microemulsion or miniemulsion polymerization. Qi et al. [93] studied the preparation of poly(methyl methacrylate-*co*-butyl acrylate)-graft-silica using miniemulsion polymerization to obtain particles smaller than 100 nm at a surfactant level of 20 % based on the monomer weight. The miniemulsion is a relatively stable oil-in-water dispersion, which is typically obtained by shearing a

system containing monomer(s), water, surfactant and a costabilizer. The monomer droplets have a diameter in the range of 50 to 500 nm. Xu et al. [94] reported that the PMMA/SiO₂ nanocomposite particles could be prepared through microemulsion polymerization by using silica particles coated with 3-(trimethoxysilyl) propylmethacrylate (MSMA). This technique can produce particles smaller than 100 nm, however the surfactant amount used is about 40 % based on monomer weight.

However both microemulsion and miniemulsion polymerization required a high amount of surfactant. The surfactants are not only expensive but also have significantly negative impact on the physical properties of the polymers. Moreover, the concentration of such surfactant molecules in solution needs to be tuned carefully because latex formation in free micelles in the emulsion can be observed at higher concentrations of surfactant. These molecules are usually only weakly bonded to the surface and can therefore be desorbed easily [95].

Since it is desirable to reduce the surfactant amount and also achieve nanosized particles, a differential microemulsion polymerization method was proposed. Differential microemulsion polymerization has been developed in which the monomer feed was provided continuously as very small droplets and slowly added to the polymerization system under mild agitation. Compared with conventional emulsion polymerization, the differential microemulsion polymerization requires an extremely low surfactant concentration and is controllable in providing PMMA nanoparticles of less than 20 nm at a surfactant concentration of 5% based on monomer weight, which is difficult to be realized by conventional methods [96].

Norakankorn et al. [97] studied differential microemulsion polymerization applied to synthesize nanosized poly(methyl methacrylate) using an oil soluble initiator as azobisisobutyronitrile (AIBN). These particles of less than 50 nm were produced by using 5g/L surfactant concentration. He et al [98] proposed a mathematical model for the differential microemulsion polymerization of PMMA. In the reaction system as illustrated in Figure 1.8, the initiator decomposes in the water phase to form primary radicals. Some of the primary radicals could attack monomers to form polymer radicals. These polymer radicals propagated in the water phase reaching a critical chain length and precipitated to form polymer particles (homogeneous nucleation) or entered into monomer-swollen micelles to generate

polymer particles (heterogeneous nucleation). The radicals in the water phase also could be terminated by combination or disproportion or be captured by either active (polymer particles having free radicals in them) or dead polymer particles.

Differential microemulsion polymerization has many advantages for the production of nanosized polymer latex particles of less than 50 nm with high monomer conversion and high polymer content by using an extremely low surfactant concentration and is normally performed using an environmental friendly process due to the absence of organic solvents under mild conditions.

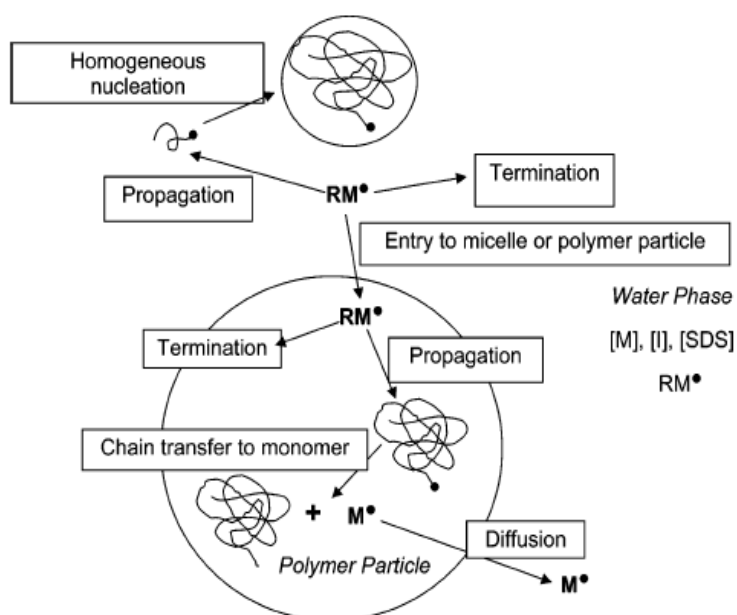


Figure 1.8 Proposed mechanism of differential microemulsion polymerization [98].

Encapsulation of silica nanoparticles by a polymer layer, so-called core-shell particles, can be carried out by an emulsion polymerization process. Polymerization could not occur at the surface of unmodified silica particles due to the absence of functional groups on the surface. Hence, surface modification of silica pretreatment becomes necessary followed by polymerization on the functionalized-silica. The surface-active molecules could prevent agglomeration and provide compatibilization of the filler into the polymer matrix. Depending on the reaction conditions and type of

silica particle, different products were obtained in which particles were encapsulated in a polymer shell through only single shell particles or several cores. However, pure polymer latex particles so called “free polymer or ungrafted polymer” can also be formed in the emulsion (Figure 1.9). Therefore, the surfactant concentration needs to be controlled carefully since free polymer formation in micelles can be observed at higher surfactant concentrations.

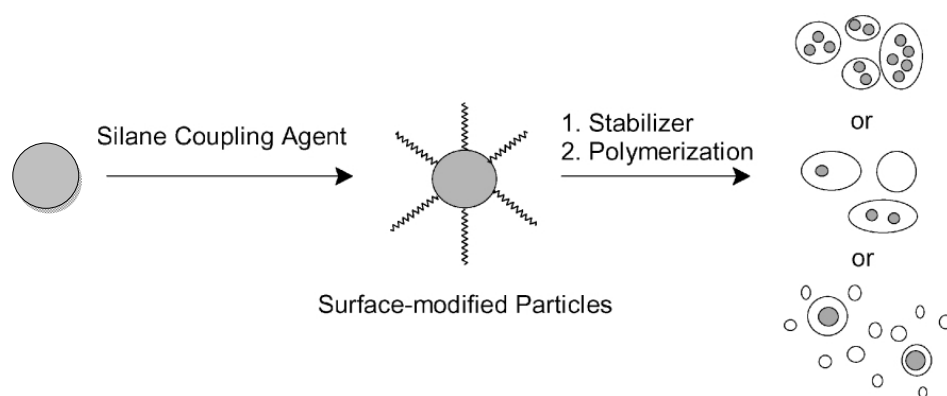


Figure 1.9 Different core/shell morphologies of polymer/silica nanocomposites [95].

Besides polymerization, a self-assembly technique is a commonly used strategy in the synthesis of polymer/silica nanocomposites with good stability. Self-assembly is a method capable of making one, two and three dimensional structures of nanomaterials [99-100]. The major interaction for self-assembly includes electrostatic interactions, surface tension, and hydrophobic interactions [101]. The thickness of the shells can be adjusted by depositing oppositely charged reactants as polyelectrolyte through predominantly electrostatic interactions [102]. Moreover surface self-assembly can also be used for the formation of capsules from core-shell structures using templating methods [103]. The most commonly used polyelectrolyte pairs include poly(styrene sulfonate) (PSS) and poly(diallyldimethylammonium chloride) (PDADMAC) [104] PSS and poly(allylamine hydrochloride) (PAH) [105-106], PSS and poly(diallyldimethyl-ammonium) (PDDA) or poly(pyrrole) and poly(N-methylpyrrole) [107].

1.6 Hydrogenation of Diene-Rubber

Generally, diene-based rubber is widely utilized for industrial purposes. These rubbers have carbon-carbon double bonds in their polymer chain which are advantageous for vulcanization. However, the residual unsaturated carbons present a disadvantage for weather resistance, oxidation, high temperature and ozone resistance. Hydrogenation is a reaction in which the addition of hydrogen to double or triple bonds are replaced by saturated hydrocarbon bonds. Hydrogenation of diene-based rubbers is very useful for improving the thermal and oxidative stability as well as mechanical properties of hydrogenated polymers. The hydrogenation of the carbon-carbon double bonds in diene-based rubber is an important process to obtain the hydrogenated rubber which is more resistant than the unsaturated polymer under the aggressive environments for outdoor application while maintaining their elastomeric property. The hydrogenation of diene-based rubber could be achieved by both catalytic process and noncatalytic hydrogenation.

1.6.1 Catalytic Hydrogenation Using Metal Catalysts

The process involved dissolution of the diene rubber in an organic solvent in contact with hydrogen in the presence of a hydrogenation catalyst. Homogeneous and heterogeneous catalysts have been developed for providing the hydrogenated rubber [108-110]. A soluble catalyst complex in an organic solvent under hydrogen pressure is needed for homogeneous hydrogenation while insoluble transition metal catalysts are used for heterogeneous hydrogenation to promote hydrogen addition to the unsaturated carbon-carbon double bonds. Heterogeneous catalysts such as Pd/Al₂O₃ and Pd/BaSO₄ were used to catalyze the hydrogenation of polybutadiene rubber [111-112]; it was found that low double bond conversion (<40%) was observed at high catalyst concentration.

Homogeneous catalysts have been reported to increase the rate of hydrogenation. High degrees of hydrogenation ($\geq 97\%$) of *cis*-1,4-polyisoprene was achieved with a Ru(CH=CH(Ph))Cl(CO)(PCy₃)₂ concentration of 200 μ M and 180°C in monochlorobenzene [113]. For the hydrogenation of natural rubber (NR) using

$\text{Ru}(\text{CH}=\text{CH}(\text{Ph}))\text{Cl}(\text{CO})(\text{PCy}_3)_2$, a degree of hydrogenation of 99% was obtained and an activation energy of 26 kJ/mol was reported. The hydrogenation of NR led to an increase in the thermal stability of HNR without affecting its T_g [114].

Hinchiranan et al. [115] studied the hydrogenation of natural rubber by using the homogeneous catalyst $\text{OsHCl}(\text{CO})(\text{O}_2)(\text{PCy}_3)_2$ for producing an alternating ethylene-propylene copolymer. The kinetic results showed that the hydrogenation rate was a first-order shifted to zero-order depending on hydrogen pressure at lower to moderate hydrogen pressure which then decreased toward an inverse behavior at pressures higher than 41.4 bar. The apparent activation energy was 122.76 kJ/mol. Later, Mahittikul et al. [116] studied the use of $\text{OsHClCO}(\text{O}_2)(\text{PCy}_3)_2$ as an effective catalyst for hydrogenation of NRL in chlorobenzene; however, impurities in NRL such as protein and lipolipids reduce the catalytic activity. However, the presence of a sulfonic acid in the hydrogenation process could prevent the poisoning of the osmium catalyst by impurities.

Catalytic hydrogenation is a potentially a useful method for the hydrogenation of acrylonitrile-butadiene rubber in the presence of Wilkinson's catalyst under mild conditions. The process is selective to terminal or internal double bonds in rubber backbone without any hydrogenation of the nitrile groups [117]. Moreover, the Wilkinson's catalyst could be used for hydrogenation of chloroprene rubber. The hydrogenated chloroprene rubber exhibited the improvement in properties such as oxidative resistance, thermal degradation resistance and oil resistance [118].

Wei et al. [119] reported on a new approach for hydrogenation of acrylonitrile-butadiene rubber by direct hydrogenation in latex form using $\text{RhCl}(\text{PPh}_3)_3$ as a homogeneous catalyst. A degree of hydrogenation of greater than 95% was achieved in the absence of any organic solvent. Although the reaction rate for the direct hydrogenation of the NBR latex was slower than for an organic solution, this process did not show any problems of cross-linking in the resulting product and can hydrogenate only the carbon-carbon double bonds.

Escobar Barrios et al. [120] studied the hydrogenation of styrene-butadiene rubber (SBR) by using cyclohexane and n-butyllithium as the solvent and catalyst promoter, respectively. The dissolved SBR in cyclohexane was homogeneously hydrogenated using a Ziegler-Natta catalyst, prepared from nickel acetylacetonate and

n-butyllithium. A Ziegler-Natta catalyst demonstrated an increase in selectivity towards the saturation of the 1,2- vinyl double bonds, as compared with the 1,4-trans double bonds.

From literature reviews, catalytic hydrogenation of rubber such as natural rubber [121-122], nitrile-butadiene rubber [123], styrene-butadiene rubber and polyisoprene rubber [124-128] has proven to be a successful process for providing hydrogenated rubber.

1.6.2 Noncatalytic Hydrogenation Using Diimide Reduction

From previous work, the hydrogenation of rubber required hydrogen gas, organic solvent, and a metal catalyst; therefore, an alternative way of diimide reduction was developed [129]. The numerous sources of diimide mentioned below were discovered through the uncatalysed hydrogenation of olefins.

1. Hydrazine yields diimide according to Eq. (1.1) in the presence of oxidizing agents such as atmospheric oxygen, mercuric oxide, hexacyanoferrate(III) [130], N,N-dichlorotoluenesulfonamide [131] and peroxides [132].



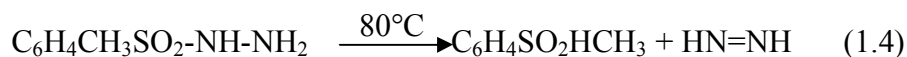
2. Decomposition of azodicarboxylate in accordance with Eq. (1.2) to produce diimide and carbon dioxide, this reaction proceeds especially readily in the presence of acid [132].



3. High thermal cleavage of arenesulfonyl hydrazide [133] in accordance with Eq. (1.3)



4. Thermolysis of p-toluenesulfonyl hydrazide (TSH) [134] as Eq. (1.4)



The source for releasing diimide as active species from the redox reaction of hydrazine hydrate (N_2H_4) with hydrogen peroxide (H_2O_2) as strong oxidizing agent is energetically favorable due to the production of final product in latex form and the absence of any organic solvent [135]. Furthermore, this technique could be operated without high hydrogen pressure equipment. The reaction for diimide hydrogenation is illustrated in accordance with Eqs. (1.5) and (1.6) while the side reactions of diimide decomposition and diimide disproportionation are presented in Eqs. (1.7) and (1.8), respectively.



The production of diimide as Eq. (1.5) possibly occurs at the interface of the rubber particles and the bulk aqueous phase whereas a competitive reaction before the diffusion of diimide into the rubber particles may appear not only at the interface but also in the aqueous phase. The radical source for gel formation and the crosslinking process is observed according to Eq. (1.8) [136]. A mechanism for diimide hydrogenation of nitrile rubber catalyzed by cupric ion is proposed in Figure 1.10. The anionic surfactant can produce a soap particle interface and is useful for the diffusion of the diimide molecule from the interface to the rubber phase resulting in high hydrogenation efficiency for hydrogenation of diene-based rubber [137].

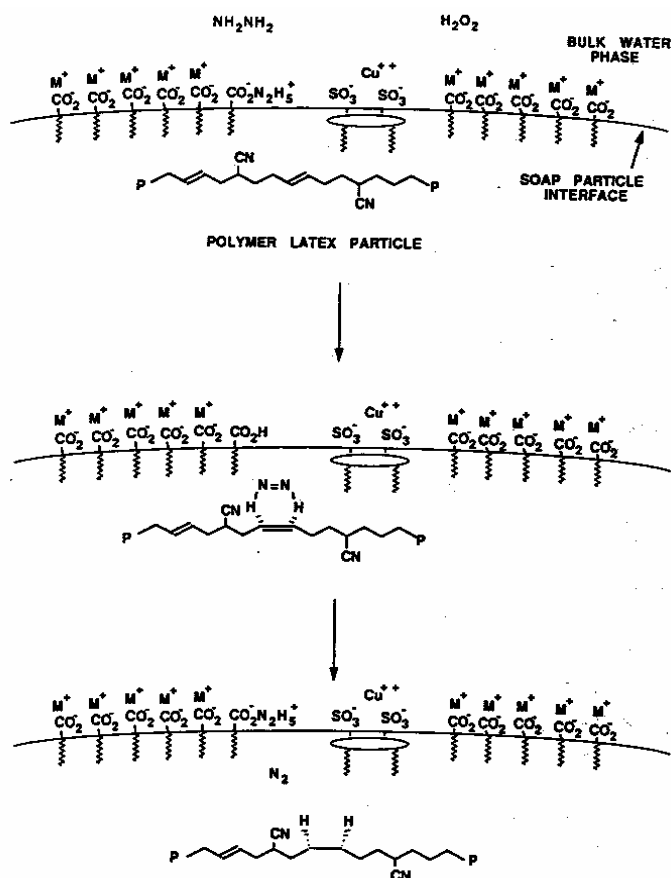


Figure 1.10 Proposed mechanism of diimide reduction [137].

The two models of diimide hydrogenation of SBR were proposed for the understanding of double bonds distribution as shown in (Figure 1.11). He et al. [138] compared the hydrogenation of SBR latex with different particle sizes, SBR latex with a diameter of 230 nm showed that a low hydrogenation level of 42%. On the other hand, a high hydrogenation degree of 91% was obtained for SBR latex with a small diameter of 50 nm. A further result resulted in a “Layer model” for hydrogenation of the latex [139]. The hydrogenation was initiated at the outer layer of the rubber particles and the diimide reduction was then propagated in the inner layer to attach with carbon-carbon double bonds deep inside the particle. The mobility of the diimide species was retarded for the attachment within the core rubber particles. Therefore, a layer model could be proposed for hydrogenation of diene rubber comparable with the uniform model.

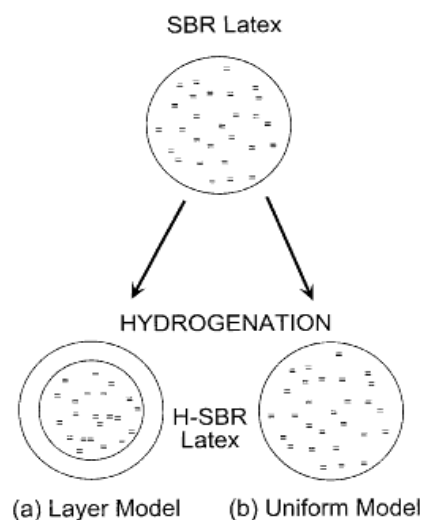


Figure 1.11 Proposed models for the double bonds distribution of hydrogenated SBR latex (a) layer model and (b) uniform model [138].

Diimide reduction has been applied for the hydrogenation of carbon-carbon double bonds within acrylonitrile-butadiene rubber (NBR) with a hydrogenation degree of 81% [139], carboxylated styrene butadiene rubber (XSBR) with a hydrogenation degree of 80 % [140] and natural rubber latex (NR) with a hydrogenation degree of 67% [141]. However, a low degree of hydrogenation of natural rubber was obtained due to the larger size of the rubber particles (0.2-2 μm).

Simma et al. [142] reported on the diimide hydrogenation of skim natural rubber latex (SNRL) in a system of hydrazine/hydrogen peroxide using cupric ion as catalyst. A result provided a degree of hydrogenation of 64.5% at a hydrazine: hydrogen peroxide of 1.6:1 and a low copper sulfate concentration of 49.5 mM. The apparent activation energy of the catalytic and non-catalytic hydrogenation of SNRL over the range of 60–80 $^{\circ}\text{C}$ was found to be 9.5 and 21.1 kJ/mol, respectively. The SHNR/NR vulcanizate exhibited the highest retention of mechanical properties after ageing and a high resistance to surface cracking caused by ozone.

Xie et al. [143] reported on the hydrogenation of NBR latex via diimide reduction to produce HNBR by reduction of the gel content of the hydrogenation product to 15% while maintaining a high hydrogenation degree. The hydrogenated product exhibited good oil resistance, excellent thermo-oxidative resistance and good

mechanical properties. The retention after thermal ageing in tensile strength and ultimate elongation was 98% and 96%, respectively.

Lin et al. [144] investigated the hydrogenation of NBR latex via utilization of diimide. It was found that the use of boric acid as a promoter could produce a hydrogenation efficiency of nearly 100% and the hydrogenation efficiency by using the catalysts of copper ion, silver ion or ferrous ion were lower than that of boric acid. Crosslinking was also related to the side reactions of diimide in the organic phase. Radical scavengers are not efficient to suppress the gel formation.

1.7 Mechanical Properties and Thermal Stability of Polymer Nanocomposites

Polymer properties such as mechanical and thermal properties are important in indicating the use of a specific polymer in various applications. The mechanical behavior of a polymer can be characterized by its stress–strain properties. Generally, polymer products require both reinforcement and thermal stability to extend the usage period of the products. In order to improve the mechanical properties of a polymer, the incorporation of a filler in the polymer matrix to prepare polymer composites were reported. Mammeri et al [145] reported on an improvement of mechanical properties of hybrid thin films by adding nanosilica encapsulation with PMMA.

Rubber is a high molecular weight polymeric material, with high elongation and excellent resilience possessing low tensile strength and modulus and poor creep characteristics leading to the limits for rubber applications. Silica is one of the reinforcing substances currently used, so fillers as silica are frequently added to polymers in order to improve the mechanical properties of the composites. The use of silica particles, instead of carbon black, has proven to be of interest for rubber reinforcement [146]. Gauthier et al. [147] studied silica-filled styrene–butadiene rubber (SBR) by varying filler content and surface treatment of silica. It was found that the use of coupling agents that promote covalent bond between rubber and fillers reduced the amplitude of the non-linear phenomenon resulting in improved tensile strength of the rubber. Chuayjuljit et al. [148] reported that polystyrene (PS)-encapsulated nanosilica was used as a filler in the NR nanocomposite. The properties

of NR in tensile strength and modulus at 300% strain were found to be increased by the incorporation of PS-encapsulated nanosilica at 9 parts per hundred rubber (phr).

Liu et al. [149] studied the properties of styrene–butadiene rubber (SBR) filled with nanosilica powder prepared by solution polymerization which was modified by three silane coupling agents of 3-methacryloxypropyl trimethoxy silane (MEMO), [3-(2-aminoethyl)aminopropyl] trimethoxy silane (AMMO), and bis[3-(triethoxysilyl)propyl] disulfide (TESPD). This result reported that SBR filled with silica powder modified by MEMO exhibited better filler dispersion and mechanical properties in tensile strength, modulus at 300%, hardness and tear strength as compared with unfilled SBR and SBR filled with unmodified silica powder.

Thammathadanukul et al. [150] compared rubber/silica reinforcement using different organo-silane coupling agents to prepare styrene–butadiene/silica composite and styrene-*co*-isoprene/silica rubber composite. The results showed that the surface modification of silica processes highly increased the compound cure rate and also increased tensile strength, tear strength, abrasion resistance and compression set of the cured compound. Later, Pongprayoon et al. [151] reported that the mechanical properties of natural rubber reinforced with silica modified by admicellar polymerization were superior to those reinforced with unmodified silica or silica modified by thermal admicellar polymerization. For preparation of NR/silica via admicellar polymerization, cetyltrimethyl ammonium bromide (CTAB) proved to be the most effective surfactant.

Many types of rubber, such as natural rubber (NR), butadiene rubber (BR), acrylonitrile butadiene rubber (NBR) and styrene butadiene rubber (SBR) have unsaturated carbon–carbon double bonds in the chemical structure. These double bonds present a disadvantage for high thermal heating and can enter easily into additional reaction with ozone resulting in degradation of the rubber. Since thermal resistance of rubber would be improved, the filler having high thermal stability could be used for providing the desirable properties. The thermal ageing resistance of the rubber vulcanizates was greatly improved by the presence of silica filler resulting to high resistance to heat degradation [152].

Park et al [153] compared the rubber/silica composites treated by silane coupling agents, γ -aminopropyl triethoxysilane (APS), γ -chloropropyl

trimethoxysilane (CPS), and γ -methacryloxypropyl trimethoxysilane (MPS). The modification of organic functional groups on silica surfaces resulted in an increase in the crosslink density of the composites, resulting in increasing the final thermal stability of the final product. The results further showed that the rubber filled with silica treated by MPS had the superior thermal stability and improved crosslink density. Therefore, treatment of silica particles could be utilized to develop effective fillers for rubber industry. Previous works reported on incorporation of silica in polychloroprene rubber [154-157] natural rubber [158-161], styrene butadiene rubber [162-163] and carboxylated styrene butadiene rubber [164] for improving the thermal stability of rubber composites have been presented.

1.8 Objective and Scope of Dissertation

Polymer/silica nanoparticles have shown great potential for future applications. However, silica particles have amounts of hydroxyl groups on their surface resulting in the strong filler-filler interaction through hydrogen bonding. This phenomenon cannot be broken down by the shear forces during physical mixing and also lead to a decrease in mechanical and thermal properties. In this work, the good dispersion, superior compatibility, and high stability of nano-silica into nanosized polymer matrix are targeted. Therefore, the nanocomposites are designed as a core/shell morphology containing a silica core covered by a polymeric shell to enhance a new class of polymer/silica nanocomposites as well as an environmentally friendly process with high encapsulation efficiency are desired. A novel technique of differential microemulsion polymerization is applied for nanosized polymer/silica synthesis due to the advantages of producing nanosized polymer in latex form in the absence of organic solvents and at extremely low surfactant concentration. For rubber applications, the preparation of rubber/SiO₂ nanocomposite with excellent elastomeric properties and good reinforcement properties has been explored in demand for industrial production. However, diene-based rubber consisting of carbon-carbon double bonds have many drawbacks under aggressive environment such as poor heat resistance and less oxidative stability due to the presence of unsaturated bonds in their polymer backbones leading to the limits of rubber application.

One approach is to carry out the hydrogenation of rubber nanocomposites in aqueous latex form and carbon bonds are replaced by saturated carbon resulting in high thermal stability. Hydrogenated rubber is produced by diimide hydrogenation; moreover, the dissolution and separation of solvents from rubbers would be omitted and this process is favorable rather than in the solution hydrogenation process. An optimized process would be available from this research work. Preparation of polymer/silica nanocomposites without the use of organic solvents has been investigated in this work.

Chapter I, the subjects of miniemulsion polymerization and microemulsion polymerization were reviewed. The different techniques for the synthesis of polymer/silica nanocomposites with historical and tutorial approaches were described. The fundamentals of catalytic and noncatalytic hydrogenation of diene-based rubber and the overview of principal concepts of nanocomposites for different applications were also described.

Chapter II, the experimental procedures for the preparation of polymer-silica nanocomposites with good dispersion and high efficiency were revealed. The novel methods for the synthesis of nanosized rubber with high conversion as well as hydrogenated rubber nanocomposites with high hydrogenation degree were presented. The various techniques were applied for characterization of nanocomposites and nanosized rubber product.

Chapter III, the alternative route for the synthesis of nanosized ethylene-propylene rubber latex by isoprene polymerization followed by diimide reduction was developed. The influences of process variables on polyisoprene hydrogenation were discussed and the kinetics of the polyisoprene hydrogenation at different particle size was also studied. The thermal stability of ethylene-propylene rubber was investigated.

Chapter IV, the synthesis of poly(styrene-*co*-methyl methacrylate)-SiO₂ nanocomposite was carried out for the preliminary study and the effects of process

variables on encapsulation were analyzed. The dispersion of two different phases between nanosilica and nanosized polymer was clarified.

Chapter V, the utilization of differential microemulsion polymerization to perform the silica encapsulation with polyisoprene and the proposed mechanism of polyisoprene-SiO₂ formation was reported. The process variables on particle size, monomer conversion and grafting efficiency were studied. Morphology and thermal properties of polyisoprene/silica nanocomposites were also investigated.

Chapter VI, the preparation of new nanocomposites of hydrogenated polyisoprene-silica was reported. The polyisoprene-SiO₂ nanocomposites were hydrogenated by diimide reduction using hydrazine and hydrogen peroxide with boric acid as promoter. The effect of process parameters on hydrogenation level was investigated and the thermal stability of hydrogenated polyisoprene-silica was reported. The kinetics and activation energy of diimide hydrogenation as well as a reasonable mechanism of hydrogenated polyisoprene-silica were also reported.

Chapter VII, the mechanical properties, thermal resistance by ageing and ozone resistance of rubber nanocomposites were studied for utilization in rubber application. The nanocomposites of polyisoprene-silica/NR and hydrogenated polyisoprene-silica/NR were prepared. A discussion of stress-strain behavior and surface morphology was included in order to compare the improved properties of polyisoprene nanocomposite with unfilled natural rubber.

Chapter VIII, the summarization of results and the recommendations for future work was highlighted.

CHAPTER II

EXPERIMENTAL AND CHARACTERIZATION

2.1 Materials

2.1.1 Synthesis of Nanosized Ethylene-Propylene Rubber Latex

Isoprene (IP) (Aldrich), sodium persulfate (SPS) (Sigma), sodium dodecyl sulphonate (SDS) (Fisher Scientific), sodium bicarbonate (NaHCO_3) (Aldrich) were used as received for nanosized polyisoprene synthesis. Hydrazine hydrate (Aldrich), boric acid (Aldrich), and hydrogen peroxide (30% aqueous solution, VWR Scientific) were used as received for the diimide hydrogenation. Reagent grade methyl ethyl ketone (MEK) was obtained from Fisher Scientific for rubber precipitation and d-chloroform (99.9%) was purchased from Aldrich Chemical for NMR analysis. De-ionized water was used in all experiments.

2.1.2 Synthesis of Poly(Styrene-*co*-Methyl Methacrylate)-SiO₂ Nanocomposites

Styrene (ST) (Aldrich, AR) was washed with 5 %wt aqueous sodium hydroxide to remove the inhibitor, dried over anhydrous magnesium sulfate and stored at 0°C. Methyl methacrylate (MMA) from (Aldrich, AR) was purified by washing, drying, and then distillation under reduced pressure before use. Acrylic acid (AA) (Aldrich), ammonium persulfate (APS) (Ajax), hydrochloric acid (35% HCl, Mallinkrodt), sodium dodecyl sulphonate (SDS) (Fisher Scientific), ammonia solution (25% NaOH, BDH), sodium bicarbonate (Aldrich) and methanol (Fisher) were used as received. Commercial nano-SiO₂ (Aerosil 200) with average particle size of 12 nm was supplied from Degussa.

2.1.3 Synthesis of Polyisoprene-Silica Nanocomposites

Nano-SiO₂ (Aerosil 200) with an average particle size of 12 nm was supplied by Degussa (Thailand). The 3-methylacryloxypropyl trimethoxy silane (MPS, Sigma) and vinyl trimethoxysilane (VTS, Sigma) were used as coupling agents. An ammonia solution (25% NH₄OH, BDH) was used as catalyst for silica surface modification. Isoprene monomer (IP, Aldrich), sodium dodecyl sulphate (SDS, Fisher Scientific), sodium persulfate (SPS, Aldrich) and sodium bicarbonate (NaHCO₃, VWR) were used for synthesis of the polyisoprene-SiO₂ emulsion. The methanol (MeOH, Fisher Scientific) and methyl ethyl ketone (MEK, Fisher Scientific) were used for the modified silica precipitation and the rubber coagulation, respectively. De-ionized water was also used in all experiments.

2.1.4 Synthesis of Hydrogenated Polyisoprene-Silica Nanocomposites

Nano-SiO₂ (Aerosil 200) with an average particle size of 12 nm was supplied by Degussa (Thailand). Vinyl trimethoxysilane (VTS, Sigma) were used as coupling agents and ammonia solution (25% NH₄OH, BDH) as catalyst for silica surface modification. Isoprene monomer (IP, Aldrich), sodium dodecyl sulphate (SDS, Fisher Scientific), sodium persulfate (SPS, Aldrich) and sodium bicarbonate (NaHCO₃, VWR) were used for synthesis of the polyisoprene-SiO₂ emulsion. Hydrazine hydrate (Aldrich), boric acid (Aldrich), and hydrogen peroxide (30% aqueous solution, VWR Scientific) were used as received for diimide hydrogenation and d-chloroform (99.9%, Aldrich) was used for NMR analysis. The methanol (MeOH, Fisher Scientific) for the modified silica precipitation and methyl ethyl ketone (MEK, Fisher Scientific) for rubber coagulation were used as received. De-ionized water was also used in all experiments.

2.1.5 Pre-Vulcanization

Nanosized polyisoprene-SiO₂ and nanosized hydrogenated polyisoprene-SiO₂ were used as nanofiller in rubber film pre-vulcanization. For the preparation of

prevulcanized NR nanocomposites, high ammonia natural rubber latex (NRL) comprised almost of cis-polyisoprene with 60% dry rubber content, sulfur as a vulcanizing agent, zinc oxide (ZnO) and zincdiethyl dithiocarbamate (ZDEC) as vulcanization accelerators were obtained from the Rubber Research Institute of Thailand.

2.2 Synthesis of Nanosized Ethylene-Propylene Rubber Latex

2.2.1 Synthesis of Polyisoprene (PIP) Nanoparticles

Polyisoprene (PIP) nanoparticles were synthesized by differential microemulsion polymerization. The differential microemulsion polymerization of isoprene was carried out in a 250-mL Parr reactor. 0.2 g SPS initiator, 0.6 g SDS and 0.7 g sodium bicarbonate were dissolved in de-ionized water (70 mL) and charged into the reactor. The solution was stirred at 300 rpm under a nitrogen atmosphere. Then the mixture was heated to the desired reaction temperature of 75 °C and then condensed isoprene monomer (20 g) was fed via small dropwise addition continuously using a peristaltic pump at a feeding rate of 0.8 mL/min. After the addition of the monomer was completed, the reaction system was held at a constant temperature (75°C) and stirring rate (300 rpm) for 18 h.

2.2.2 Diimide Hydrogenation for Ethylene-Propylene Rubber Latex Synthesis

Polyisoprene latex was used as the starting reactant for diimide hydrogenation. The hydrogenation of nanosized polyisoprene latex in the presence of a hydrazine/hydrogen peroxide system was conducted in a 250 mL glass reactor equipped with a temperature controlled oil bath, reflux condenser, a nitrogen gas inlet and a feeding tube. The de-ionized water was added into the polyisoprene latex and charged into the glass reactor. Then hydrazine hydrate and dissolved boric acid were dropped into the latex. Then nitrogen gas was charged for degassing the reaction system before heating up to the reaction temperature.

Subsequently, the mixture was heated up to the desired temperature and hydrogen peroxide was added dropwise using a peristaltic pump at a feeding rate of 0.4 mL/min at a constant temperature. When the addition of hydrogen peroxide was completed, the reaction was left to proceed for 4 h under a constant stirring rate. The synthetic EPM latex thus produced was then precipitated using methyl ethyl ketone to form the coagulated rubber. The schematic diagram of EPM synthesis is shown in Figure 2.1.

The influence of process variables on PIP hydrogenation was studied by varying hydrazine concentration (0.5-6 M), hydrogen peroxide concentration (0.5-6 M), amount of boric acid addition (0.02-0.15 M), ratio of hydrogen peroxide to hydrazine (0.5-2), water concentration (7-40 M) and reaction temperature (40-80 °C).

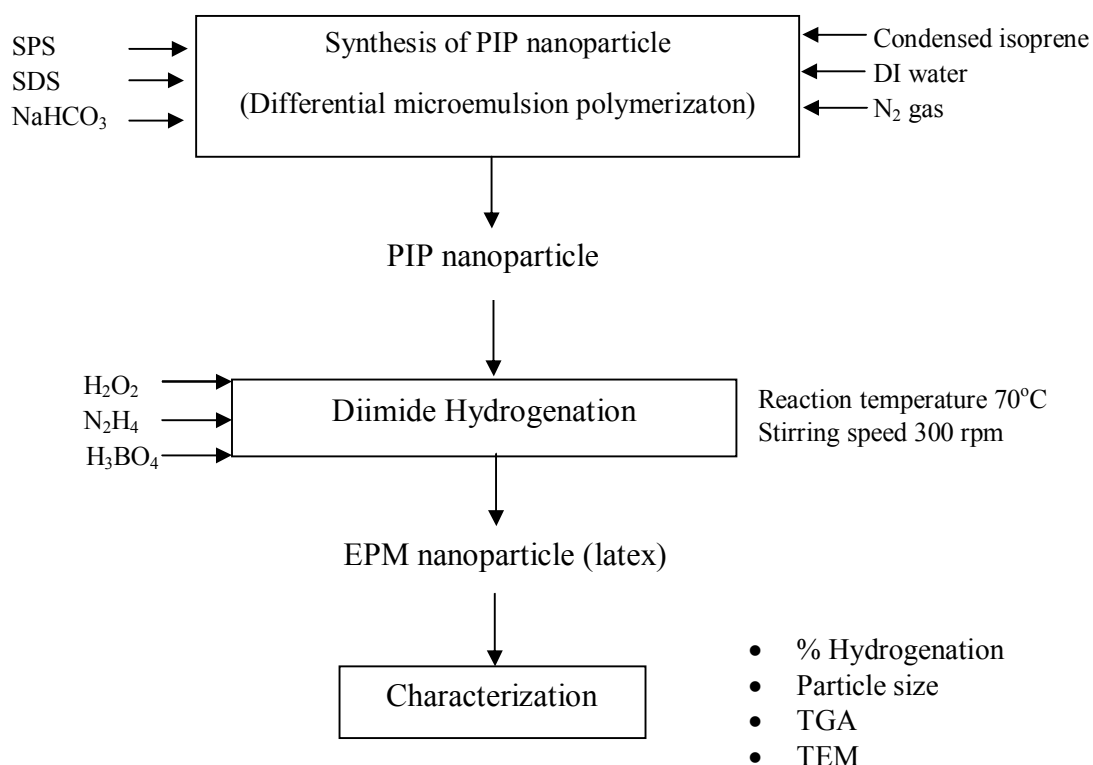


Figure 2.1 The schematic diagram of nanosized EPM synthesis.

2.3 Synthesis of Poly(Styrene-*co*-Methyl Methacrylate)-SiO₂ Nanocomposites

2.3.1 Pretreatment of Nano-SiO₂ by Acrylic Acid

5 g of nanosilica was initially dispersed in 90 mL of distilled water with the aid of an ultrasound bath for 3 h. Then, 1.5 g of acrylic acid (AA) was added into the dispersion which was vigorously stirred for 90 min at room temperature. Then, 4 mL of 25 wt% aqueous ammonia solution was added into the solution and the agitation was continued overnight. Then the dispersion was neutralized with 30 wt% aqueous HCl solution. The mixture was dried for 48 h at 55 °C to obtain modified-SiO₂. The excess amount of acrylic acid on silica particles was removed using a centrifugation/redispersion cycle. Free AA was separated from grafted AA onto silica surface in 1/1 ethanol/water (v/v) solution. The original precipitates containing free silica, free AA, and grafted AA onto silica surface were centrifuged at 10,000 rpm for 20 min. The supernatant solution (denoted as a serum) was carefully separated from the residue. The settled modified silica was washed with ethanol/water solution, again separated from the serum by centrifugation. The operation was repeated until a constant weight of residue was obtained. This procedure was necessary to ensure the complete extraction of unreacted AA from the coated AA onto the silica surface. Finally, the resulting precipitates were dried in oven at 55 °C for 48 h to produce the modified nano-SiO₂ (m-SiO₂) powders.

2.3.2 Synthesis of Poly(Styrene-*co*-Methyl Methacrylate)-Silica Nanocomposites

For differential microemulsion polymerization, styrene and methyl methacrylate monomers were polymerized in a 500 mL four necked round bottomed glass reactor equipped with a reflux condenser, a thermometer, a peristaltic pump and a magnetic stirrer under nitrogen atmosphere to prevent probable inhibition. The process to obtain nanocomposite latex was as follows: typically, 0.5 g modified nano-SiO₂ powder was dispersed into 4 mL of distilled water with the aid of an ultrasound bath for 1 h just before use. The ammonium persulfate initiator (APS) was dissolved

in distilled water, then a small amount of NaHCO_3 and surfactant (SDS) was added and the solution was transferred into the glass reactor. The reaction vessel was charged with the modified nano- SiO_2 suspension. The suspension was stirred at 300 rpm and heated up to 75°C . Then, the mixture of ST and MMA was fed dropwise into reactor by using a peristaltic pump at the feed rate of 0.23 mL/min. When the addition of the monomers was completed, the solution was stirred for an additional 4 h. Then, the system was cooled down to room temperature.

The composite latex was precipitated with excess methanol to produce the coagulated solid then the precipitated solid and was dried at 50°C overnight. The surfactant and initiator were removed by washing with a sufficient amount of warm distilled water and methanol. Then the precipitated solids were extracted using acetone in a Soxhlet apparatus to remove the free polymer (ungrafting polymer) and dried to a constant weight. The schematic diagram of poly(ST-*co*-MMA)- SiO_2 synthesis is shown in Figure 2.2.

The univariate experiments were utilized to investigate the effect of parameters on particle size, monomer conversion, polymer grafting efficiency, and silica encapsulation efficiency. The influences of initiator concentration over the range of 1-4 %wt surfactant concentration over the range of 0.5-5 %wt, the ratio of monomer to water over the range of 0.1-0.4 and styrene-to-methyl methacrylate ratio range of 0.5-4 were also studied.

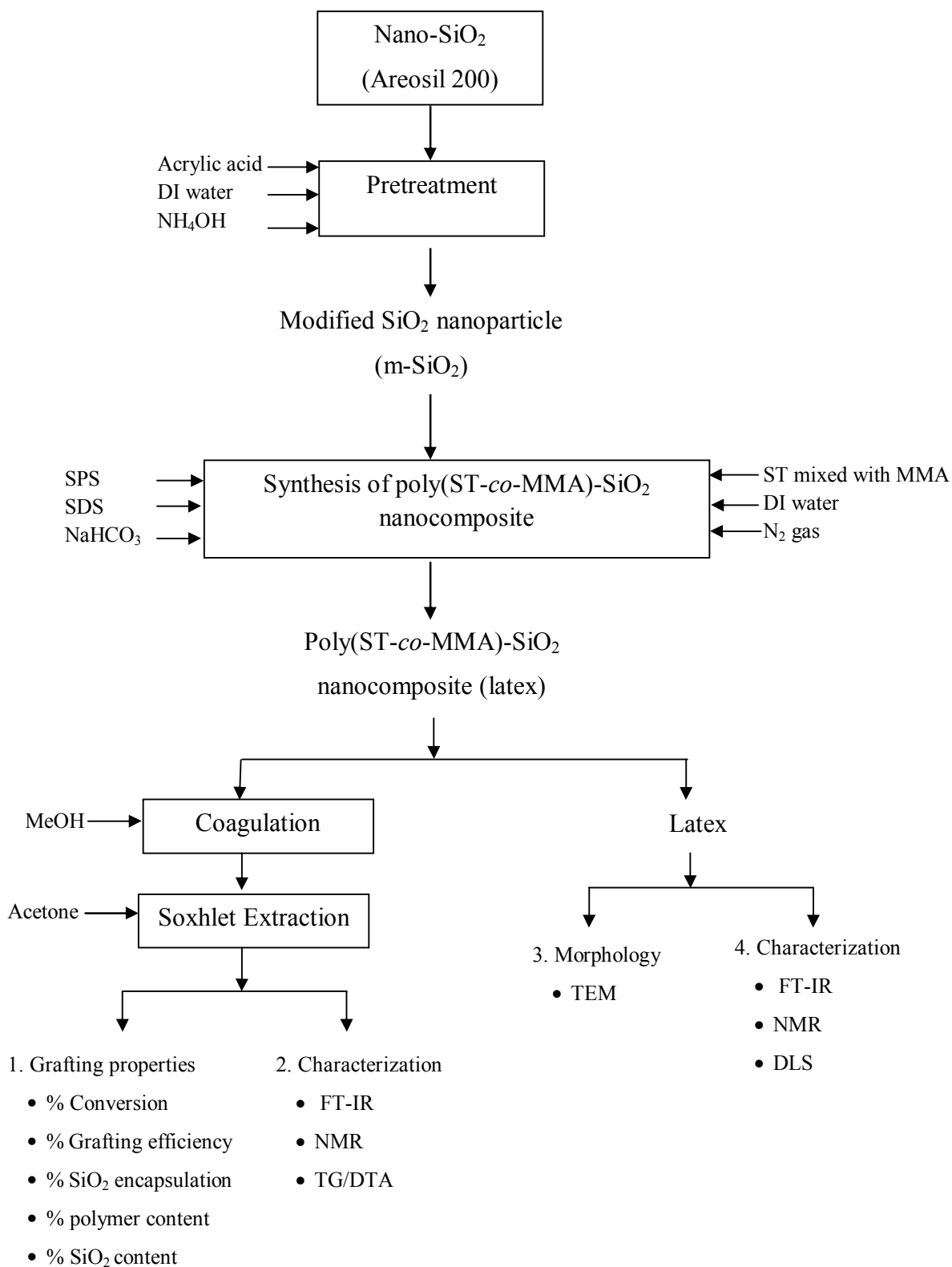


Figure 2.2 The schematic diagram of poly(ST-co-MMA)-SiO₂ synthesis.

2.4 Synthesis of Polyisoprene-Silica Nanocomposites

2.4.1 Pretreatment of Nano-SiO₂ by Organo-Silane Coupling Agents

10 g of nanosilica was initially dispersed in 300 mL of de-ionized water with stirring at 450 rpm for 30 min. Then, 0.3 g of the coupling agent (MPS, VTS) was added dropwise into the dispersion and the pH of the solution was then adjusted to around 10 with the addition of 25 %wt aqueous ammonia solution. The dispersion was stirred for 30 min at room temperature, and then heated up to a reaction temperature of 80°C with continuous stirring overnight. Afterwards, the suspension was dried at 90°C for 24 h to obtain a modified-SiO₂. A Soxhlet extraction was used to remove coupling agents which were not effectively bonded on the silica surface. Finally, the nano-SiO₂ powders (MPS-SiO₂, VTS-SiO₂) produced was dried in an oven at 55 °C for 48 h.

2.4.2 Synthesis of Polyisoprene-Silica Nanocomposites

Nanosized PIP-SiO₂ particles were prepared in a 250 mL Parr reactor equipped with a thermocouple, a feeding tube, a coolant, and a magnetic stirrer under a nitrogen atmosphere and the apparatus is shown in Figure 2.3. Modified nano-SiO₂ (VTS-SiO₂) was dispersed in de-ionized water with the aid of an ultrasonic bath for 1 h. Then, SPS initiator, SDS surfactant and NaHCO₃ buffer solution was dissolved in distilled water. Then, the solution and the modified nano-SiO₂ was charged into the Parr reactor and stirred at 300 rpm for 45 min. After degassing, the solution was heated up to the reaction temperature. For differential microemulsion polymerization, the condensed isoprene was slowly fed dropwise into the reactor using a peristaltic pump at a feed rate of 0.4 mL/min. When the addition of the monomers was complete, the solution was stirred at a specific temperature for an additional 18 h. Then, the system was cooled down to room temperature.

For precipitation of rubber-SiO₂ nanocomposite the composite latex was precipitated with an excess of methyl ethyl ketone to produce the coagulated rubber. The coagulated rubber was dried at 50°C overnight. Furthermore, the coagulated

rubber composite was then extracted using petroleum ether in a Soxhlet apparatus to remove the free polymer (ungrafted polyisoprene) and then dried to a constant weight.

The influence of initiator and surfactant concentration, monomer/water ratio and silica loading on particle size, monomer conversion as well as encapsulation efficiency was also investigated. The influences of initiator concentration over the range of 0.5-5 %wt surfactant concentration over the range of 0.5-10 %wt, monomer to water ratio range of 0.1-0.5 and silica loading range of 2.5-20 % were also studied.

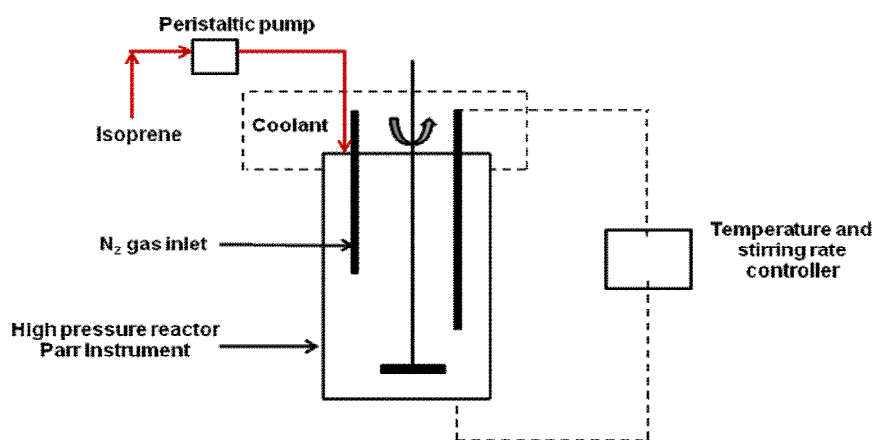


Figure 2.3 The apparatus of polyisoprene-SiO₂ synthesis.

2.5 Synthesis of Hydrogenated Polyisoprene-Silica Nanocomposites

2.5.1 Synthesis of Polyisoprene-Silica Nanocomposites

The pretreatment of nano-SiO₂ was carried out similarly to the procedure mentioned in section 2.4.1. The synthesis of nanosized PIP-SiO₂ particles via differential microemulsion polymerization was carried out similarly to the procedure mentioned in section 2.4.2.

2.5.2 Diimide Hydrogenation for Hydrogenated Polyisoprene-Silica Synthesis

The hydrogenation of PIP-SiO₂ (VTS-SiO₂ at 10 %wt) latex was carried out similar to the procedure mentioned in section 2.2.2. The schematic diagram of HPIP-

SiO₂ synthesis is shown in Figure 2.4. In this section, the process variables of hydrazine concentration (0.5-6 M), hydrogen peroxide concentration (0.5-5 M), amount of boric acid addition (0.02-0.15) and water concentration (5-40 M) on PIP-SiO₂ hydrogenation was investigated.

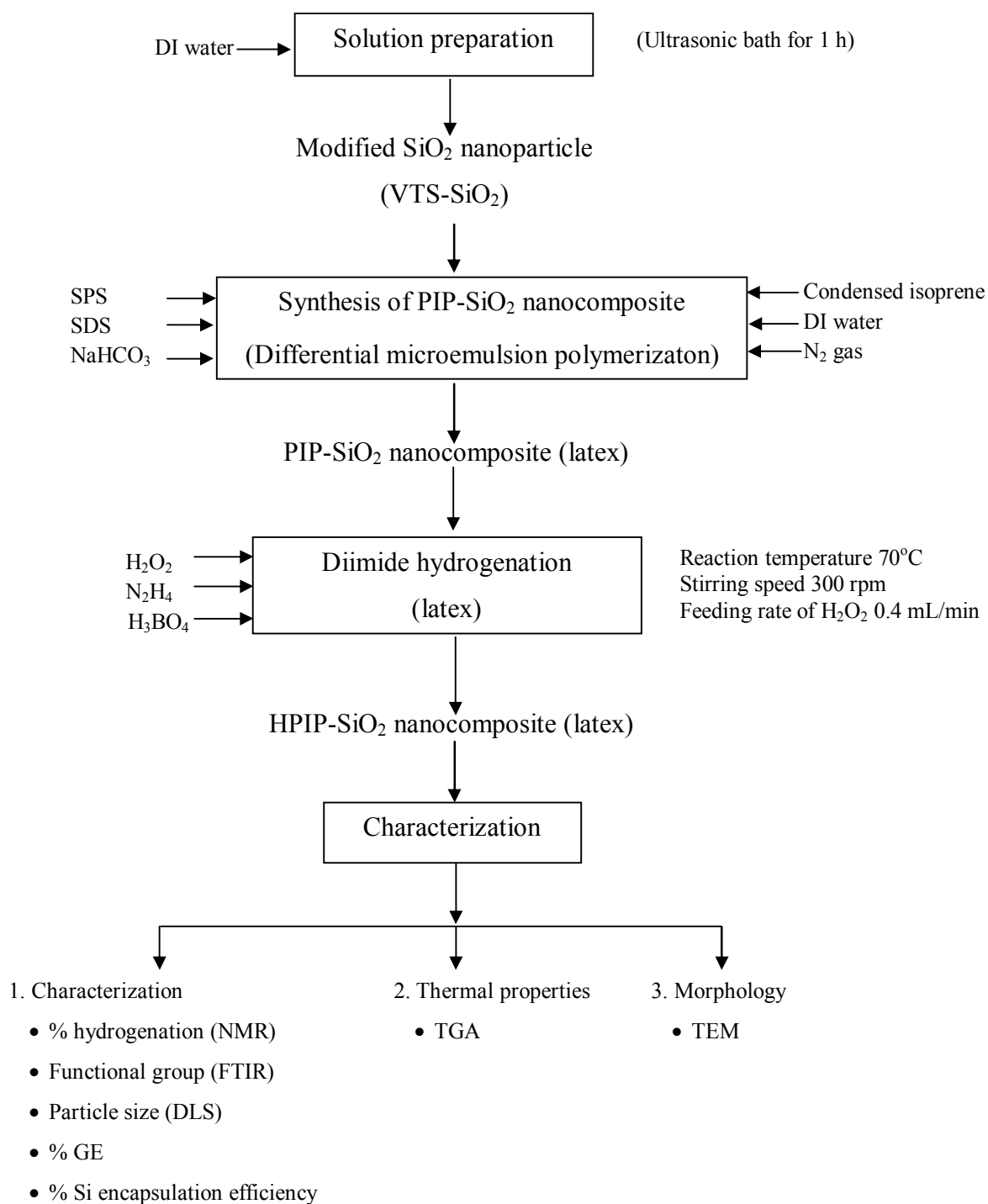


Figure 2.4 The schematic diagram of HPIP-SiO₂ synthesis.

2.6 Preparation of PIP-SiO₂ Filled NR Nanocomposites and Hydrogenated PIP-SiO₂ Filled NR Nanocomposites

i) Preparation of PIP-SiO₂ Filled NR Nanocomposites

For the preparation of prevulcanized PIP-SiO₂ filled NR nanocomposite, natural rubber latex (NRL) with a total solid content of 60% was selected to blend with PIP-VTS-SiO₂ or PIP-MPS-SiO₂. The lattices of PIP-VTS-SiO₂ and PIP-MPS-SiO₂ were dropped into NRL at various weight ratios (NR: PIP-VTS-SiO₂ and NR: PIP-MPS-SiO₂ = 100:0, 95:5, 90:10, 80:20, 70:30) under a stirring rate of 450 rpm for 30 min to form a good dispersion of NR/PIP-SiO₂ composite. Then, sulfur (1.5 phr) as vulcanizing agent, ZDEC (1 phr) and ZnO (2 phr) as accelerators were added into the mixture and the temperature was raised to 60°C with constant stirring at 300 rpm for 2 h. Then, the NR nanocomposite latex was cooled to room temperature and cast on a raised glass plate having a dimension of 13 cm × 13 cm × 3 mm. The cast sheet was dried at 70°C for 5 h. For thermal ageing of composites, tensile specimens were aged at 100°C for 24 h in an air circulating ageing oven and the mechanical properties of the samples before and after ageing were measured to estimate the ageing resistance.

ii) Preparation of Hydrogenated PIP-SiO₂ Filled NR Nanocomposites

The preparation of prevulcanized HPIP-SiO₂ filled NR nanocomposite was carried out similarly to the procedure mentioned in section 2.6 i).

2.7 Characterization

2.7.1 Fourier Transform Infrared Spectroscopy

Modified-silica, PIP-SiO₂ and HPIP-SiO₂ were characterized using Fourier transform infrared spectroscopy (Bruker 3000X spectrometer). Before measurement, all samples were purified via soxhlet extraction to remove the unreacted coupling

agent and ungrafted polyisoprene, the grafted PIP-SiO₂ samples were ground with dried KBr powder and compressed into a pellet.

2.7.2 ¹H NMR Spectroscopy

For hydrogenated polyisoprene (HPIP) and HPIP-SiO₂, the actual final degree of hydrogenation and polyisoprene conversion was examined by proton nuclear magnetic resonance spectroscopy (¹H NMR, Advanced 500 MHz spectrometer, Bruker). The structure identification of ethylene-propylene rubber (EPM) was interpreted from ¹³C NMR spectroscopy. All samples were dissolved in CDCl₃ at room temperature and the spectra were recorded on a Advance Bruker 300 MHz spectrometer. The composition of copolymer (ST/MMA) in composite samples was quantified for chemical structure and end group analysis, the sample was dissolved in CDCl₃ and analyzed by ¹H NMR spectroscopy.

2.7.3 Particle Diameter Measurement

For the determination of particle size, the number-average diameter (D_n) and particle size distribution of ethylene-propylene rubber (EPM), poly(styrene-*co*-methyl methacrylate)-silica, polyisoprene-SiO₂ and hydrogenated PIP-SiO₂ were measured using a dynamic light scattering technique (Malvern Instrument, USA).

2.7.4 Thermogravimetric Analysis (TGA)

The amount of silica content in the poly(styrene-*co*-methyl methacrylate)-silica was determined using thermogravimetric/differential thermal analysis (TG/DTA) on a Perkin-Elmer Pyris Diamond instrument. The samples were placed into a platinum pan and the temperature was raised under a nitrogen atmosphere from room temperature to 700 °C at a constant heating rate of 10°C/min. The nitrogen gas flow rate was 50 mL/min. For thermal analysis, the initial decomposition temperature (T_{id}) was determined from the intersection of two tangents at the onset of the decomposition temperature. Another important thermal characteristic is the

temperature at the maximum rate of weight loss (T_{\max}) which was determined from the peak maxima of the derivative of TG curves. A sample weight of 10 mg was placed on a platinum pan and the temperature was raised from room temperature to 800°C under a nitrogen atmosphere at a flow rate of 50 mL/min and the heating rate for all experiments was 10°C/min.

2.7.5 Morphological Study

The morphology of PIP-SiO₂ nanoparticle was examined by a transmission electron microscope (TEM) (JEOL, 80 kV). The samples diluted 20 times were stained with OsO₄ and dropped on a copper grid.

2.8 Determination of Monomer Conversion, Polymer Grafting Efficiency, Silica Encapsulation Efficiency

The monomer conversion was determined by a gravimetric method and calculated using Eq. (2.1):

$$\text{Conversion (\%)} = (M_0 - M_1) / M_2 \times 100\% \quad (2.1)$$

where M_0 is the mass of the resulting composite particles, M_1 is the mass of the charged SiO₂ particles, and M_2 is the mass of the charged monomer.

The polymer grafting efficiency (%GE) was calculated using Eq. (2.2):

$$\text{Grafting efficiency} = \frac{\text{Amount of polymer in the composite sample} \times 100}{\text{Total amount of polymer formed}} \quad (2.2)$$

The silica encapsulation efficiency was measured by an acid etching method as shown in Figure 2.5. The free silica particles were separated from the PIP-SiO₂ latex by HF etching. Trial experiments were conducted in which a HF solution was added to bare silica particles, PIP and PIP-SiO₂ latex. After HF etching, it was found that all of the bare silica particles were consumed whereas the weight of PIP particles

remained constant and the PIP-SiO₂ only lost the weight of the free silica particles and the incompletely encapsulated SiO₂. Therefore, completely encapsulated SiO₂ was not extracted by HF etching. The weight percent of residue (encapsulated SiO₂) was measured gravimetrically.

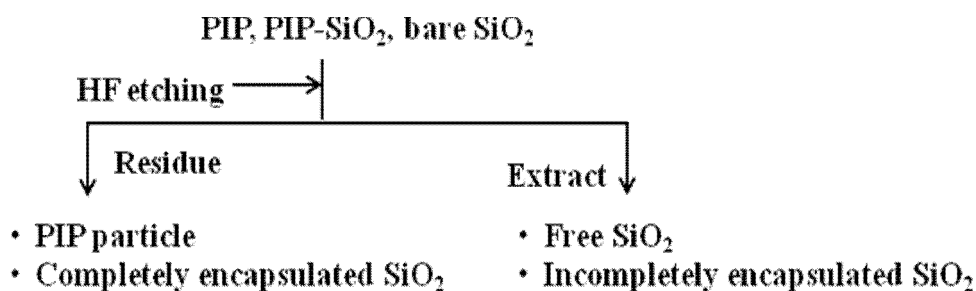


Figure 2.5 Schematic diagram of HF etching method.

The solid content of EPM was measured gravimetrically and calculated according to Eq. (2.3).

$$\% \text{ Dry rubber content (DRC)} = (M_1/M_2) \times 100 \quad (2.3)$$

where, M₁= mass of dry coagulated rubber (g), M₂= mass of the latex sample (g)

2.9 Mechanical Properties of EPM and Vulcanized Rubber

Dynamic mechanical thermal analysis of PIP-SiO₂ and NR filled with PIP-SiO₂ nanocomposites was performed using a dynamic mechanical thermal analyzer (DMA, METTLER). NR nanocomposites were measured with a strain of 70 μm peak to peak displacements over the temperature range of -70°C to 60°C at a frequency of 10 Hz and the heating rate was 5°C/min. The storage modulus and the loss tangent (tan δ) curve dependence on temperature was observed.

Mechanical properties in terms of tensile strength, %elongation at break and modulus were measured by a Universal Testing Machine (LLOYD model LR5K),

according to the ASTM-412 method at 500 mm/min of the cross-head speed. All samples were cut into dumbbell-type specimens using a Wallance die cutter. The data points were averaged from three measurements of the four specimens, and stress-strain curves were also recorded.

2.10 Ozone Resistance of Vulcanized Rubber

Ozone resistance of HPIP-SiO₂ filled NR was studied using an ozone test chamber (HAMPDEN, Northampton, England) at 40 °C according to ISO 1431-1:2004. The ozone concentration used was 50 parts per hundred million (pphm). Before exposure to ozone, all rubber specimens were stretched by 20% extension for 48 h in the absence of light under an ozone-free atmosphere. Photographs were taken using a CCTV camera to investigate the cracks on a rubber surface.

CHAPTER III

SYNTHESIS OF NANOSIZED ETHYLENE-PROPYLENE RUBBER LATEX VIA POLYISOPRENE HYDROGENATION

3.1 Introduction

Generally, the synthesis of ethylene-propylene rubber (EPM) requires gaseous monomer equipment, organic solvent with solvent recovery, and a metal catalyst. Hence, an alternative method is proposed for the synthesis of EPM nanoparticles by hydrogenation of nanosized polyisoprene in the absence of any organic solvent, pressurized gas equipment and a metal catalyst, thus providing a “new green process”. The method of diimide hydrogenation of carbon-carbon double bonds in a latex system was employed and diimide generated from the reaction between hydrazine and hydrogen peroxide could be used to release hydrogen from diimide for the hydrogenation. In this work, nanosized ethylene-*co*-propylene rubber latex was synthesized via diimide hydrogenation of synthetic polyisoprene nanoparticles. First, the polyisoprene nanoparticles were synthesized by differential microemulsion polymerization, and the nanosized polyisoprene obtained was then hydrogenated by diimide reduction in a aqueous system using hydrazine reacted with hydrogen peroxide and boric acid as promoter. Diimide hydrogenation is normally performed via an environmental friendly process due to the absence of organic solvents and metal catalyst. The influences of process variables on polyisoprene hydrogenation and the thermal properties of ethylene-propylene rubber were investigated.

3.2 Characterization of Polyisoprene Nanoparticles

The polyisoprene nanoparticles synthesized via differential microemulsion polymerization had an average particle size of 42 nm with a narrow size distribution of polydispersity index (PDI) equal to 0.02. The configurations of

polyisoprene were in four structures of the isoprene unit, 1,4-*cis*, 1,4-*trans*, 1,2-vinyl and 3,4-polyisoprene as shown in Figure 3.1.

The qualitative and quantitative analysis of the functional groups of PIP were identified by ^1H NMR spectroscopy as shown in Figure 3.2 (a). A signal was observed at 5.15 ppm corresponding to olefinic protons of *cis*- and *trans*-1,4 polyisoprene. The methine proton of 1,2-vinyl polyisoprene was identified at 5.7 ppm, whereas the signal in the range of 4.60-4.80 ppm was the characteristic peak of the methylene proton of 3,4 polyisoprene. The ratio of structures was calculated from the integrated peak areas of these signals, therefore, synthetic PIP was composed of 1,4-polyisoprene, 1,2-polyisoprene and 3,4-polyisoprene with an average ratio of 91:3:6. For the aliphatic protons, a high intensity peak at 1.58 and 1.67 ppm was attributed to methyl protons of *cis*-1,4 and *trans*-1,4 polyisoprene, respectively. The appearance of 1,4 addition peaks was calculated resulting in an approximate ratio of *cis*-1,4 to *trans*-1,4 of 80:20. The characteristic peak of the methylene groups for 1,4 addition appeared in the range of 1.95-2.15 ppm, moreover the low intensity peaks at 0.95 ppm and 1.3 ppm could be assigned to methyl protons of 1,2-polyisoprene and 3,4-polyisoprene, respectively.

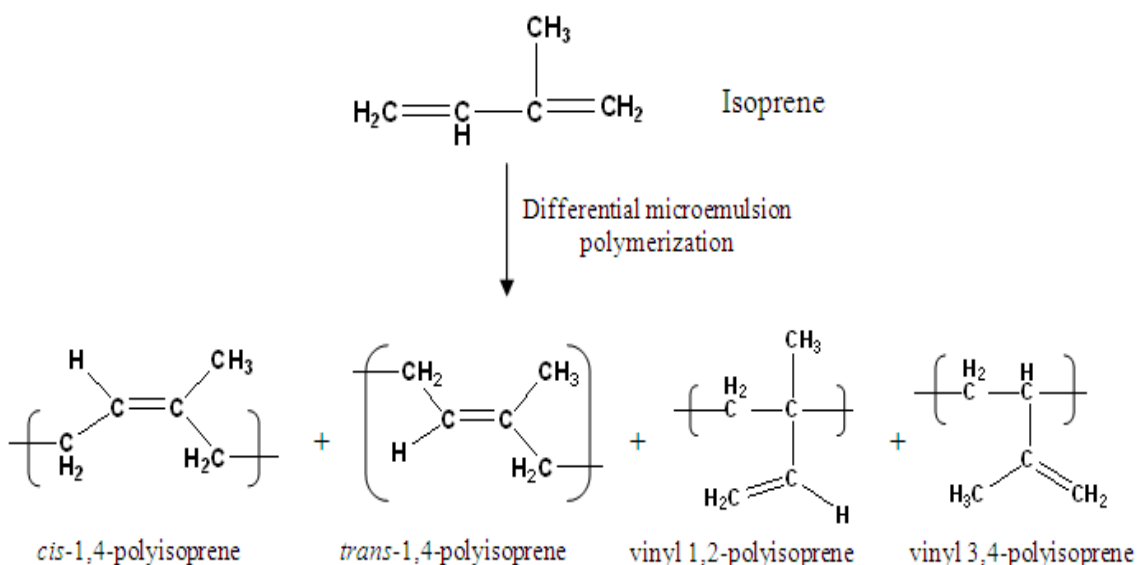


Figure 3.1 Structure configurations of synthetic polyisoprene nanoparticles

3.3 Characterization of Ethylene-Propylene Rubber (EPM) Nanoparticles

The conversion of polyisoprene to ethylene-propylene copolymer was determined in terms of the hydrogenation degree, the increase in hydrogenation degree resulted in an increase in the EPM yield. The hydrogenation degree of hydrogenated polyisoprene (HPIP) was determined using ^1H NMR spectroscopy as shown in Figure 3.2 (b-c). The actual percentage of hydrogenation was calculated from the peak area of the olefinic protons (C=C) and the integrated peak area over the range of 0.8-2.0 ppm. From Figure 3.2 (b), when diimide hydrogenation proceeded to 78% hydrogenation, the signals at 5.7 ppm and 4.7 ppm corresponding to olefinic protons of 1,2-vinyl polyisoprene and 3,4 polyisoprene were greatly decreased. The integrated peak area of *cis*-, *trans*- olefinic protons of 5.15 ppm gradually decreased with the increasing degree of hydrogenation. New peaks appearing at 0.8 ppm attributed to the CH_3 group of saturated carbon and the peak in the range of 1.0-1.3 ppm corresponded to the CH_2 and CH of saturated polyisoprene. When the hydrogenation degree reached 94% as shown in Figure 3.2 (c), the peak at 5.15 ppm belonging to unsaturated carbon shows a very low intensity signal while the peak area of saturated carbon centered at 0.8 -1.3 was sharply increased. The peak area of methylene groups for 1,4 polyisoprene appearing from 1.95 to 2.15 ppm dramatically decreased.

According to the NMR spectra, the double bond conversion of the different structure configurations was also evaluated. The results imply that the vinyl-1,2 polyisoprene is firstly saturated followed by 3,4 polyisoprene and 1,4 polyisoprene as a result of the structure hindrance of the methyl group in the 3,4-polyisoprene which tends to impede the reaction between diimide and the double bond in the coordination step of the diimide hydrogenation cycle. On the other hand, 1,4 addition of *cis*-polyisoprene and *trans*-polyisoprene were hydrogenated at a slower rate due to the steric effect of polyisoprene chain in the *cis*-, *trans*- structures. This indicated that the diimide species could react with the external double bond of the vinyl groups (1,2 and 3,4 polyisoprene) at the end of polymer chain more effectively than the internal double bond (1,4- polyisoprene), resulting in a high degree of hydrogenation. Additionally, it is observed that the reduction of the peak

area at 1.58 ppm (*cis*-1,4 polyisoprene) is higher than the intense signal at 1.67 ppm (*trans*-1,4 polyisoprene), indicating that the structure of the *cis* configuration is hydrogenated to a greater extent than that of the *trans*-1,4 polyisoprene. This selectivity was determined by the ability of saturation of different types of double bonds with diimide. The mechanism of diimide approaching the double bond is believed to occur through a syn-addition, thus steric hindrance significantly affected the coordination and insertion steps for diimide hydrogenation.

Molecular structure confirmation of the polyisoprene and ethylene-propylene rubber at 94% conversion was identified by ^{13}C NMR spectroscopy as shown in Figure 3.3. For the polyisoprene structure (Figure 3.3a), the peaks at 139.3 ppm were attributed to the unsaturated carbon of *cis*-polyisoprene and *trans*-polyisoprene and the signal at 125.7 and 125.9 ppm was attributed to the -CH of the unsaturated carbon of the *cis*- and *trans*-polyisoprene, respectively. The chemical shift of 39.8 and 40.0 ppm corresponded to the -CH₂ of *trans*-polyisoprene while the peak at 26.8 and 28.0 ppm belonged to the -CH₂ of *cis*-polyisoprene. The methyl groups of *cis*- and *trans*-polyisoprene are positioned at 23.4 ppm and the -CH₃ of vinyl-polyisoprene are centered at 17.0 ppm. However, -CH₃ of 3,4-polyisoprene might be observed at 13 ppm. After PIP hydrogenation, the peak in the region of 124-135 ppm corresponding to unsaturated carbon disappeared (Figure 3.3b). Additionally, the new peaks appearing at 19.7, 33.0 and 37.4 ppm were attributed to -CH₃, CH₂ and CH of the propylene unit. The peaks at 33.0 and 24.5 ppm were attributed to CH₂ of the ethylene unit. It is noted that for HPIP at 94% hydrogenation, the structure of an alternating ethylene-propylene copolymer is confirmed by NMR spectroscopy.

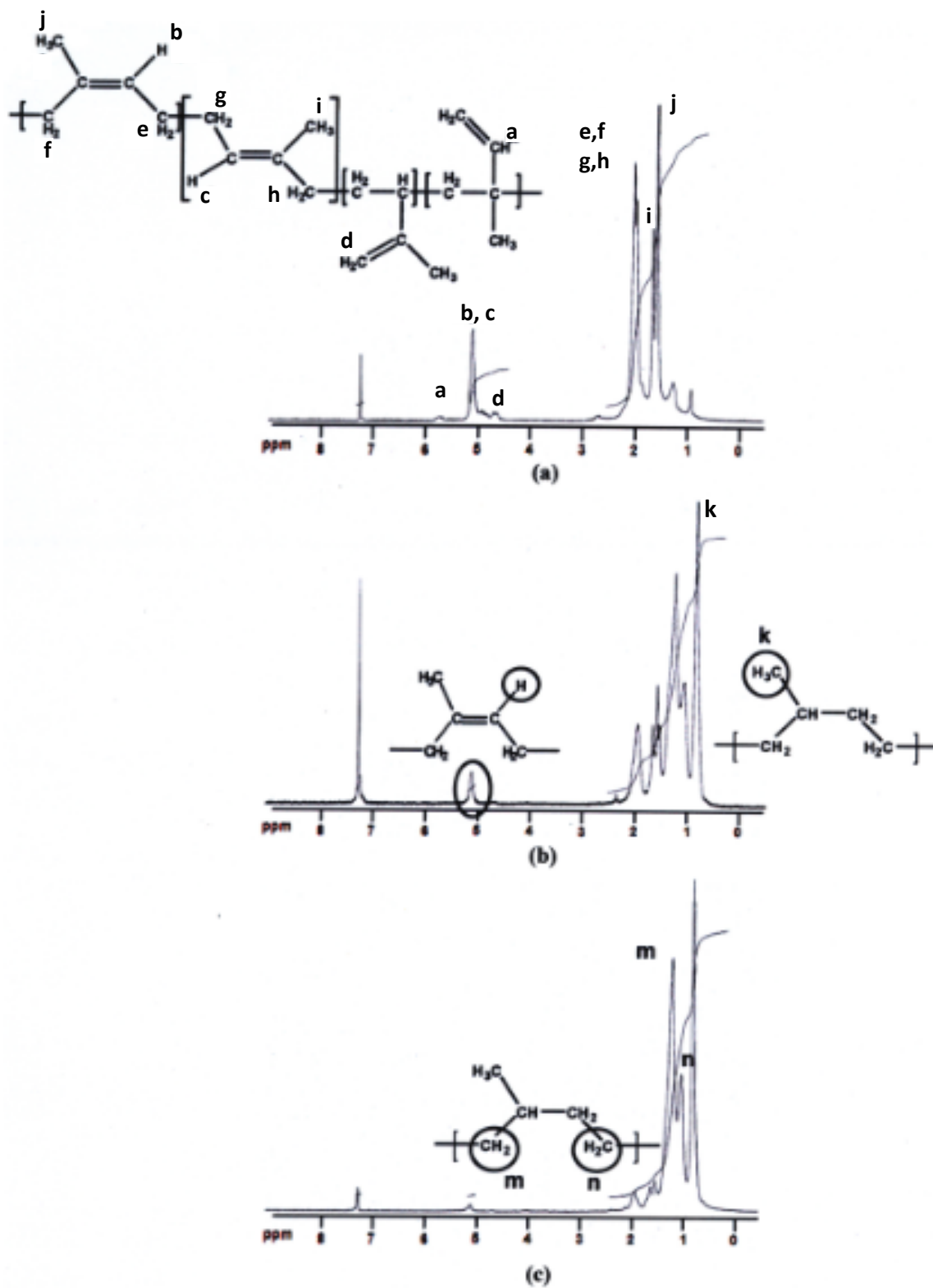


Figure 3.2 ^1H NMR spectra of (a) PIP, (b) HPIP (78%), (c) HPIP (94%).

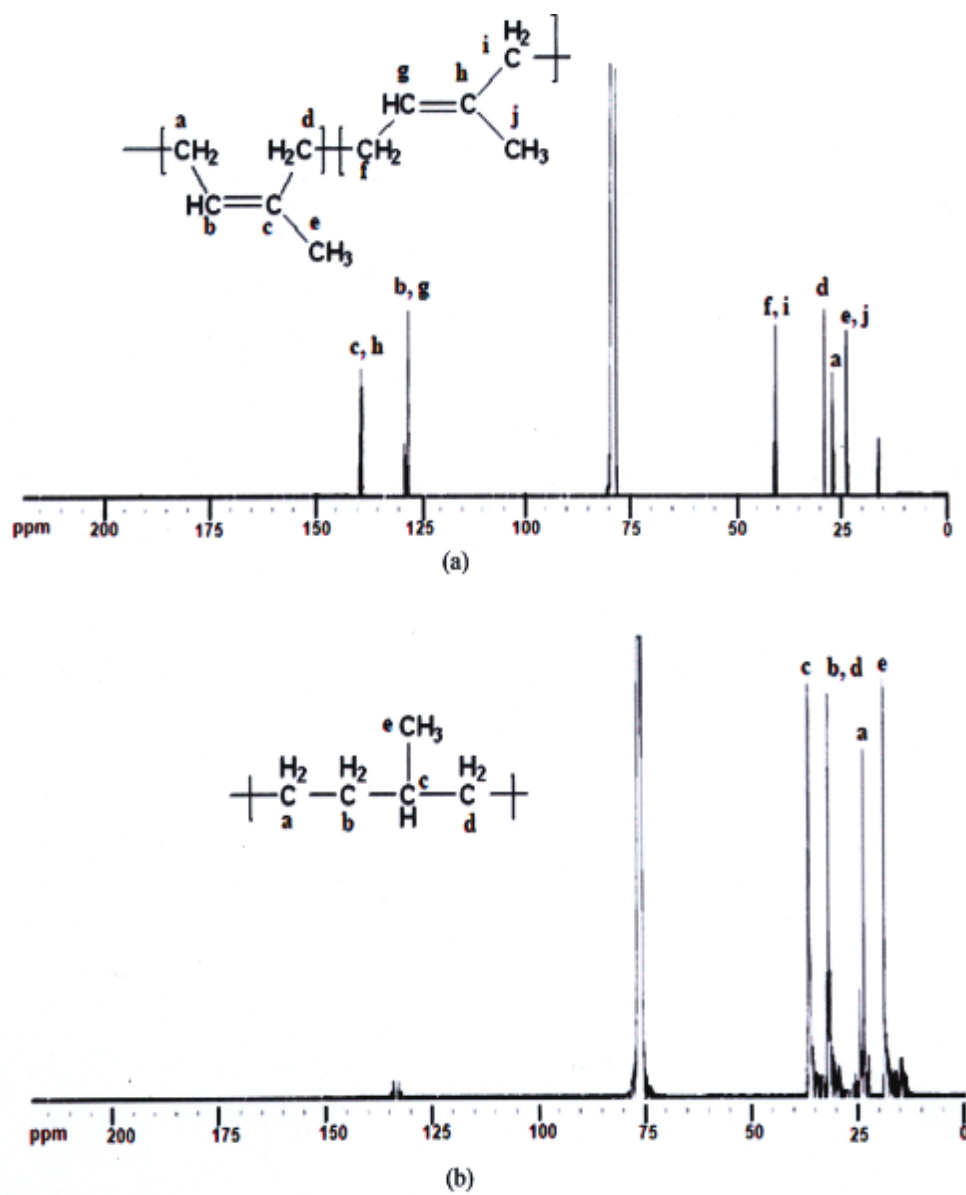


Figure 3.3 ^{13}C NMR spectra of (a) PIP and (b) EPM (94% HD).

3.4 Diimide Hydrogenation of Nanosized Polyisoprene

The influence of process variables on PIP hydrogenation was studied by varying hydrazine concentration, hydrogen peroxide concentration, amount of boric acid addition, ratio of hydrogen peroxide to hydrazine, water content and reaction temperature. The effects of all parameters are discussed in detail below.

3.4.1 Effect of Boric Acid Concentration

Boric acid was added into the hydrogenation system to improve the diimide hydrogenation. The effect of boric acid concentration was studied over the range of 0.02-0.15 mol/L. Figure 3.4 shows that the hydrogenation degree is linearly proportional to the boric acid concentration. This phenomenon illustrated that boric acid could promote hydrogenation with a high selectivity and could reduce the diimide side reactions such as disproportionation and decomposition as presented in Eqs. (3.1) and (3.2), respectively.



Without boric acid addition, the PIP conversion could not reach 60% in 4 h, suggesting that a small amount of boric acid is necessary to accelerate the reaction of hydrogen peroxide dissociation and to induce the diffusion of the diimide active species from the interphase between the water phase and the rubber phase. Lin et al. [144] studied the diimide hydrogenation of nitrile butadiene rubber latex and reported that the efficiency of hydrogenation using copper ion, silver ion and ferrous ion as catalysts was lower than that achieved with boric acid addition.

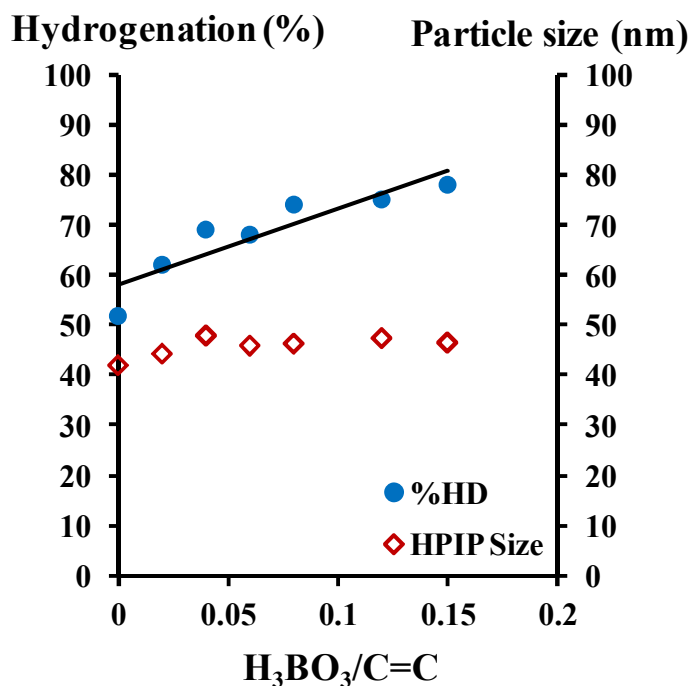
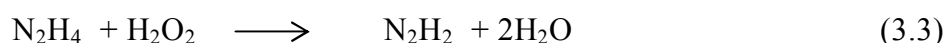


Figure 3.4 Effect of boric acid addition on PIP hydrogenation.
 Condition: $[N_2H_4] = 3 \text{ mol/L}$, $[H_2O_2] = 4.5 \text{ mol/L}$, $[C=C] = 1 \text{ mol/L}$,
 $[H_2O] = 10 \text{ mol/L}$, Temp 70°C , time = 4 h.

3.4.2 Effect of Hydrazine Monohydrate and Hydrogen Peroxide Concentration

Hydrazine was used as source for releasing the diimide species. The dependence of the percentage of hydrogenation (%HD) on hydrazine concentration was studied over the range of 0.5 to 6 mol/L. From Figure 3.5 (a), the degree of hydrogenation is seen to increase with an increase in hydrazine concentration from 0.5 up to 4 mol/L and a maximum PIP conversion of 78% was achieved. This can be explained that with increasing hydrazine concentration, a high amount of diimide molecules are generated in the system through a redox reaction with hydrogen peroxide according to Eq. (3.3). More diimide species would attach to the unsaturated polymer chains resulting in increasing hydrogenation of the carbon

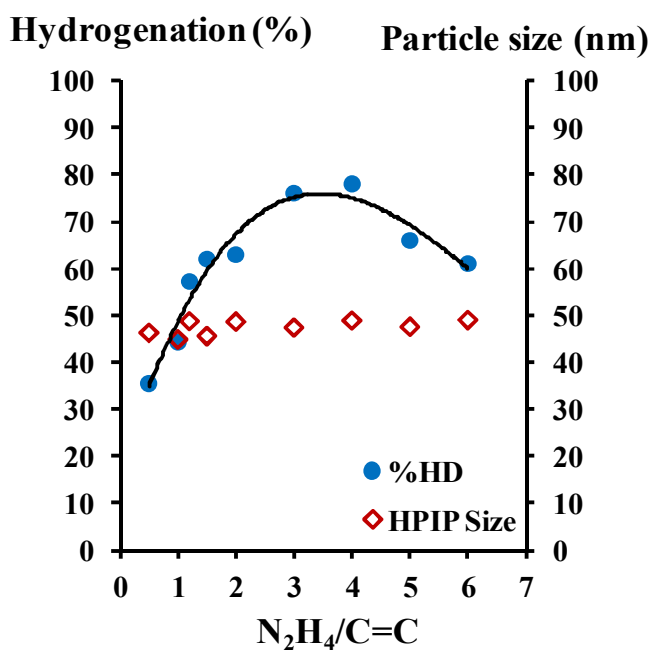
double bonds in the nanosized polyisoprene units, Eq. (3.4). On the other hand, above 4 mol/L of hydrazine, the degree of hydrogenation is suppressed due to the side reaction of the diimide reduction according to Eq. (3.2). Moreover, the particle size slightly increased from 42 nm for PIP to 47 nm for HPIP at 78% hydrogenation.



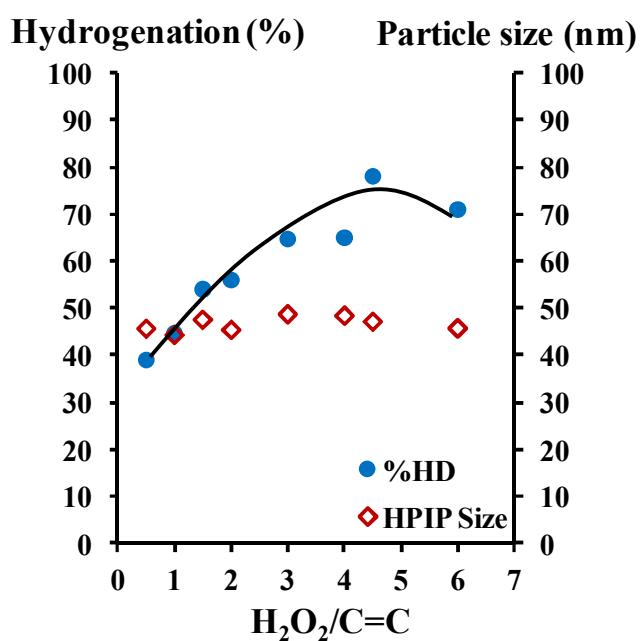
For the redox reaction, hydrogen peroxide was used as a strong oxidizing agent to react with the hydrazine molecule. The effect of hydrogen peroxide concentration on PIP conversion has been studied under a hydrazine concentration of 3 mol/L and boric acid of 0.15 mol/L. The phenomenon of increasing hydrogenation level with increasing hydrogen peroxide concentration is shown in Figure 3.5 (b). It was found that, the percentage of hydrogenation is sharply increased from 40 to 80 % over the studied range of hydrogen peroxide concentration and then decreased, whereas the particle diameter of the hydrogenated product essentially did not change.

Hence, hydrogen peroxide should be provided at a sufficient level for oxidizing the hydrazine molecules to release the diimide species. However, the decreasing hydrogenation degree at a high level of hydrogen peroxide (above 4.5 mol/L hydrogen peroxide) was due to the side reaction of hydrogen peroxide as shown in Eq. (3.5) - Eq. (3.7). Moreover, the high content of hydrogen peroxide in the system possibly tends to cause a crosslinking reaction and forms gel in the rubber latex resulting in a lower hydrogenation efficiency [136], suggesting that an appropriate hydrogen peroxide concentration is important for double bond reduction and to increase the efficiency of the EPM preparation.





(a)



(b)

Figure 3.5 PIP hydrogenation: a) effect of hydrazine concentration on PIP hydrogenation at $[H_2O_2] = 4.5$ mol/L. b) effect of hydrogen peroxide amount on PIP hydrogenation at $[N_2H_4] = 3$ mol/L. Condition: $[H_3BO_3] = 0.15$ mol/L, $[C=C] = 1$ mol/L, $[H_2O] = 10$ mol/L, $T = 70^\circ C$, time = 4 h.

3.4.3 Effect of Hydrogen Peroxide to Hydrazine Ratio

The hydrogen peroxide to hydrazine ratio has a significant effect on the double bond reduction as shown in Figure 3.6. The hydrogenation degree was increased from 50% to 78% with an increasing ratio of hydrogen peroxide to hydrazine from 0.4:1 to 1.5:1, whereafter the hydrogenation degree was suppressed. From Eq. (3.3), the ratio of hydrogen peroxide to hydrazine should be 1:1 based on stoichiometry. However, the maximum PIP conversion was achieved at a ratio of hydrogen peroxide to hydrazine of 1.5:1. It can be implied that hydrogen peroxide could be decomposed easily by reacting with hydrazine or diimide molecule. Therefore, the ratio of hydrogen peroxide to hydrazine needs to be higher than 1:1 to enhance effective diimide production. From previous work, it was found that acrylonitrile butadiene rubber (NBR) [139] and styrene butadiene rubber (SBR) [138] were effectively hydrogenated at a ratio of hydrogen peroxide to hydrazine of 2:1. In this work, the ratio of hydrogen peroxide to hydrazine was 1.5:1 since the diimide active molecule was able to effectively attach with a double bond in an inner portion of nanosized polyisoprene compared with the larger particle size and higher steric hindrance exhibited by NBR and SBR.

On a comparison of the effect of hydrazine concentration (Figure 3.5 a) and hydrogen peroxide concentration (Figure 3.5 b), it is seen that the ratio of hydrogen peroxide to hydrazine was not held constant resulting in a decrease in hydrogenation degree even though hydrazine hydrate concentration was increased. Hence, it is necessary to study the effect of hydrazine concentration on diimide reduction at a constant ratio of hydrogen peroxide to hydrazine of 1.5:1. It was found that the hydrogenation level increased sharply from 66% to 87% with an increase in the hydrazine concentration from 2 mol/L up to 5 mol/L and then slightly increased (Table 3.1). The high hydrogenation degree (87%) was achieved at a concentration of hydrazine and hydrogen peroxide of 5 mol/L and 7.5 mol/L, respectively.

Table 3.1 Effect of hydrazine amount on hydrogenation at the constant $[\text{H}_2\text{O}_2]/[\text{N}_2\text{H}_4]$

PIP particle size = 42 nm.

N_2H_4 (mol)	H_2O_2 (mol)	Degree of hydrogenation (%)	Particle diameter (nm)
2	3	65.9	46.8
3	4.5	78.0	47.4
4	6	83.2	48.2
5	7.5	87.0	47.5
6	9	87.4	49.0

Condition: $[\text{H}_2\text{O}_2]/[\text{N}_2\text{H}_4] = 1.5/1$, $[\text{H}_3\text{BO}_3] = 0.15 \text{ mol/L}$, $[\text{C}=\text{C}] = 1 \text{ mol/L}$, $[\text{H}_2\text{O}] = 10 \text{ mol/L}$, $T = 70^\circ\text{C}$, time = 4 h.

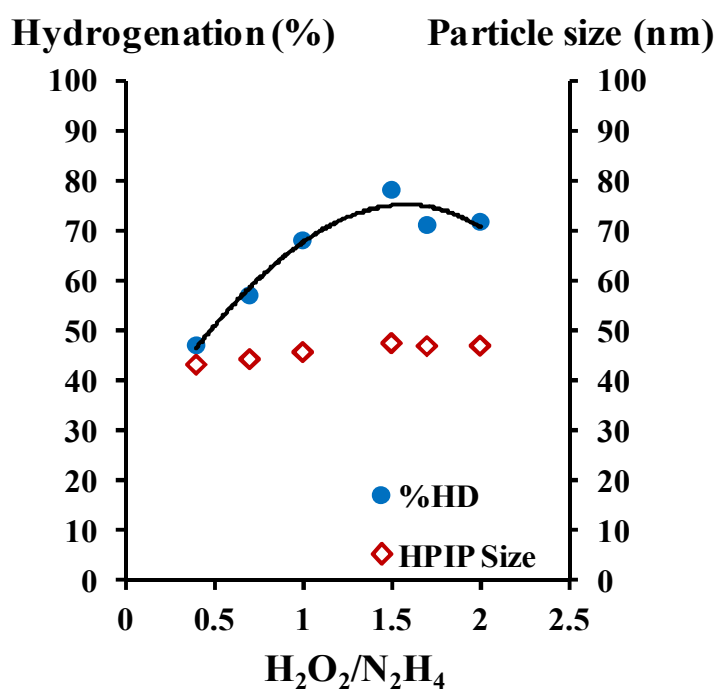


Figure 3.6 Effect of hydrogen peroxide to hydrazine ratio on PIP hydrogenation. Condition: $[\text{N}_2\text{H}_4] = 3 \text{ mol/L}$, $[\text{H}_3\text{BO}_3] = 0.15 \text{ mol/L}$, $[\text{C}=\text{C}] = 1 \text{ mol/L}$, $[\text{H}_2\text{O}] = 10 \text{ mol/L}$, $T = 70^\circ\text{C}$, time = 4 h.

3.4.4 Effect of Reaction Temperature

The effect of reaction temperature was studied over the range of 40-80 °C. From Figure 3.7, the increase in reaction temperature dramatically affected the decrease of the carbon double bonds in the PIP structure. When the reaction temperature was increased from 40 to 80°C, the hydrogenation degree was increased from 40 up to 90%, whereas, the PIP hydrogenation conversion did not reach 70% when the reaction temperature was below 65°C. The high temperature could increase the probability of collision between the starting reactants with the polymer chains and accelerate the diimide mobility to coordinate with the double bonds [139], resulting in a high EPM yield. However, even though high temperature became necessary to obtain a high level of diimide, the particle size was also changed with increasing temperature. For PIP of 42 nm, the particle size was increased from 42 nm to 50 nm for the resulting HPIP with increasing temperature due to the entanglement of the polymer chains induced by the hydrogenation reaction at high temperature. Hence, an optimum reaction temperature of 70°C was preferred and a high EPM yield (87%) and a relative small particle size (47 nm) were achieved.

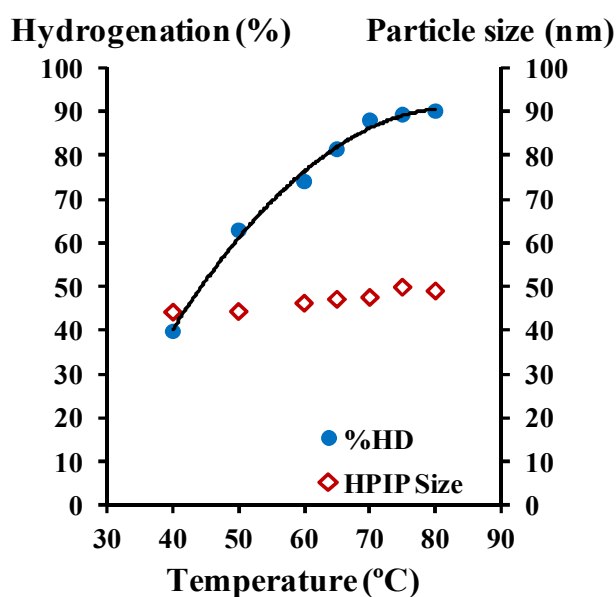


Figure 3.7 Effect of reaction temperature on PIP hydrogenation.

Condition: $[\text{N}_2\text{H}_4] = 5 \text{ mol/L}$, $[\text{H}_2\text{O}_2] = 7.5 \text{ mol/L}$, $[\text{H}_3\text{BO}_3] = 0.15 \text{ mol/L}$, $[\text{C}=\text{C}] = 1 \text{ mol/L}$, $[\text{H}_2\text{O}] = 10 \text{ mol/L}$, time = 4 h.

3.4.5 Effect of Water Addition

De-ionized water was added into the reaction system to reduce the viscosity of the synthetic polyisoprene latex. Figure 3.8 shows that on increasing the water content in the system a linear decrease in the hydrogenation level resulted. The high hydrogenation level of 88% was achieved at a water content of 7 mol/L. Although the presence of water in the system could reduce the viscosity of the latex and increase the attachment between the polymer particles and other substances, the hydrogenation level was decreased at water content above 20 mol/L. Based on dry rubber content (DRC), the water concentration of 5, 7, 10, 20, 40 mol/L is equivalent to 13, 9.5, 6.7, 3, 1.6% DRC, respectively. It can be seen that the hydrogenation degree increased from 66% to 87% with increasing DRC from 1.6% to 6.7% and then decreased to 78% at DRC of 13%. This can be explained that the reaction between hydrazine and hydrogen peroxide occurred in the aqueous phase; thus, the diimide active species was produced in the water phase at high water content and the diimide migration into the rubber phase was limited, and consequently the hydrogenation efficiency was reduced [141].

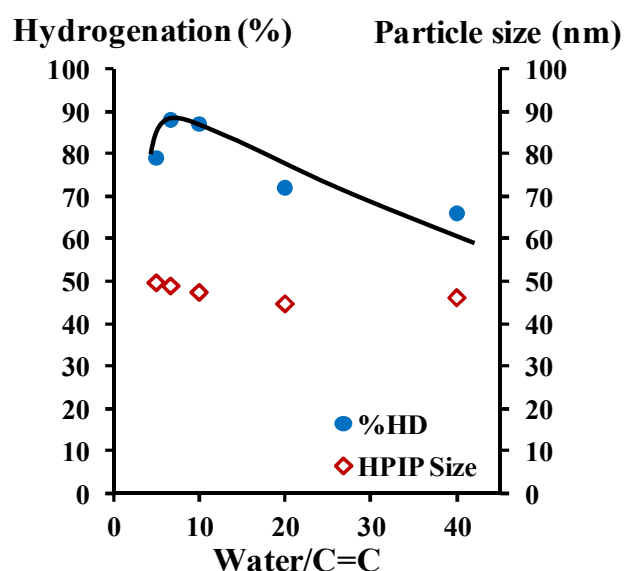


Figure 3.8 Effect of water addition on PIP hydrogenation.

Condition: $[\text{N}_2\text{H}_4] = 5 \text{ mol/L}$, $[\text{H}_2\text{O}_2] = 7.5 \text{ mol/L}$, $[\text{C}=\text{C}] = 1 \text{ mol/L}$, $[\text{H}_3\text{BO}_3] = 0.15 \text{ mol/L}$, $T = 70^\circ\text{C}$, time = 4 h.

3.5 Conversion Profile of Nanosized PIP Hydrogenation

The PIP conversion versus reaction time profile at various particle diameters of PIP was studied over an interval of time from 0 to 5 h (Figure 3.9 a). The double bond conversion was sharply increased with time initially, and then leveled off. It is suggested that diimide is a highly active intermediate species and is consumed toward the surface of the unsaturated rubber particles, so the reduction of the double bonds is observed. For reaction times above 5 h, the PIP conversion remained constant, implying that the mobility of the diimide was retarded in transferring to the carbon double bonds within the particles due to a mass transfer limitation [165]. The dependence on the particle size (30-65 nm), showed that double bond reduction of small particles was higher than that of large size, suggesting that diimide hydrogenation occurred at the outer surface and transferred to the inner particles. Therefore, diimide diffusion was enhanced toward C=C inside smaller particles at a higher rate than that for larger particles resulting in an increase in double bond conversion.

According to the layer model for diimide hydrogenation reported by Lin et al. [166], the double bond reduction was performed from the outer layer and then into the inner particle, so it is suggested that the particles of synthetic PIP should be less than 50 nm in order to achieve a high degree of hydrogenation. This is due to the fact that the high surface area of the polyisoprene nanoparticles can be attached with diimide active species effectively and the diimide molecule can diffuse towards the double bonds inside the particle, resulting in an increase in EPM yield.

The kinetics of hydrogenation of nanosized polyisoprene at various particle sizes was also investigated. From Figure 3.9 (b), the hydrogenation rate exhibits an apparent first-order rate law dependence on the double bond substrate concentration, as described by Eq. (3.8).

The experimental rate law for the reaction could be written as

$$\frac{d[\text{C}=\text{C}]}{dt} = -k' [\text{N}_2\text{H}_2][\text{C}=\text{C}] \quad (3.8)$$

When diimide is a highly active intermediate, a pseudo steady state assumption is made, therefore, the rate of hydrogenation has a first order dependence on double bond concentration

The fractional hydrogenation conversion, x is defined as

$$x = 1 - [C=C]_t / [C=C]_0 \quad (3.9)$$

where $[C=C]_t$ is the double bond concentration at reaction time t and $[C=C]_0$ is the initial double bond concentration

Eqs. (3.8) and (3.9) can further be expressed in term of Eq. (3.10)

$$\ln(1-x) = -k' t \quad (3.10)$$

Plots of $\ln(1-x)$ versus time fit first order kinetics very well, and thus, the rate constant (k') is determined from the slope of these kinetic profiles. It was found that the rate constant for hydrogenation of PIP of 30 nm, 42 nm and 65 nm were 16.0×10^{-5} , 13.0×10^{-5} and 9.9×10^{-5} (s^{-1}), respectively. Previous work reported that the rate constant of NRL [141] and skim natural rubber (SNRL) [142] hydrogenation by using diimide reduction was 5.4×10^{-5} and 5.96×10^{-5} (s^{-1}), respectively. Hence, the higher rate of diimide hydrogenation for PIP nanoparticles was achieved due to the smaller particle size of PIP compared with NRL.

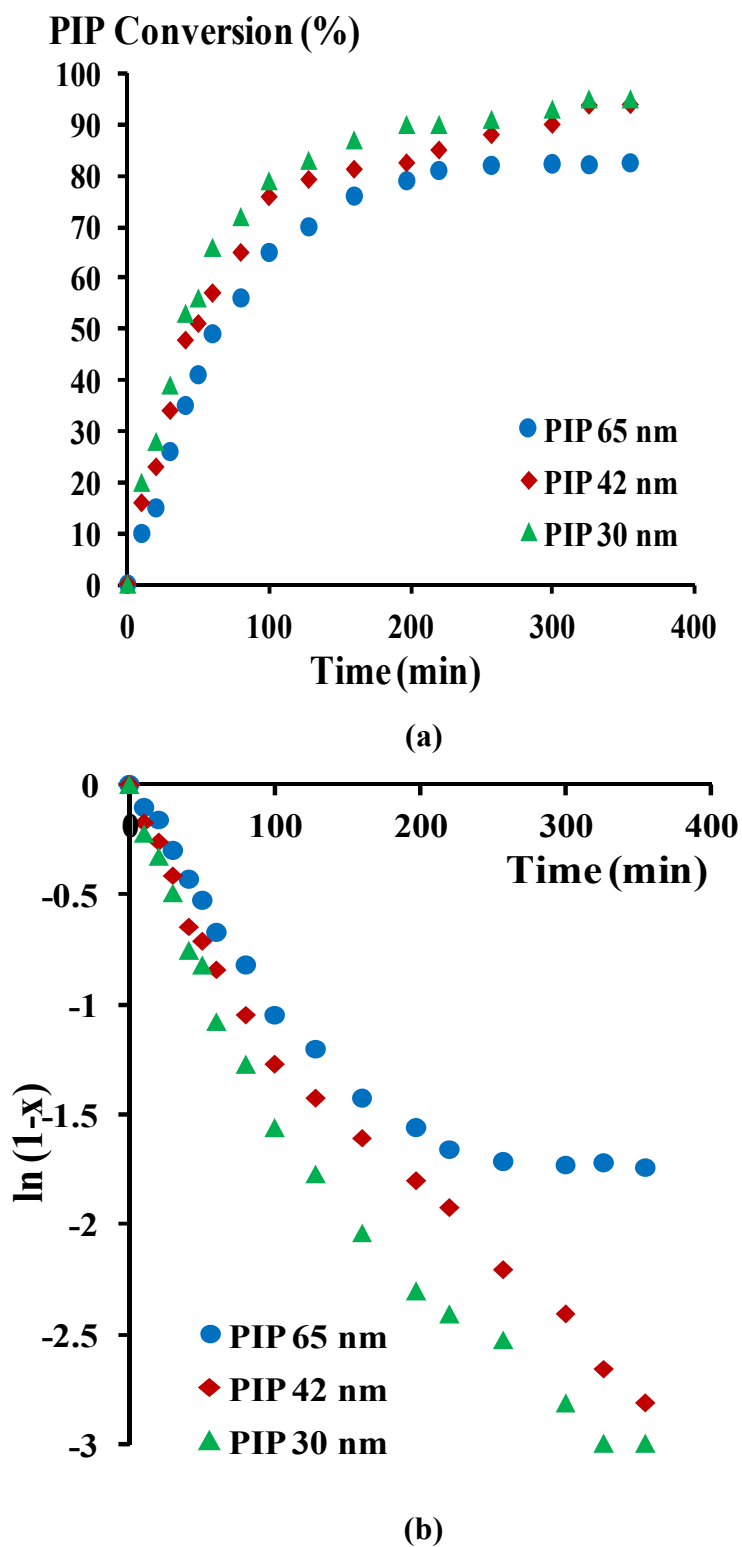


Figure 3.9 (a) Conversion profile, (b) First order in ln plot of PIP hydrogenation. Condition: $[N_2H_4] = 5 \text{ mol/L}$, $[H_2O_2] = 7.5 \text{ mol/L}$, $[C=C] = 1 \text{ mol/L}$, $[H_3BO_3] = 0.15 \text{ mol/L}$, $[H_2O] = 10 \text{ mol/L}$, $T = 70^\circ\text{C}$.

3.6 Proposed Synthetic Route for Nanosized EPM Synthesis via Diimide Hydrogenation

A synthetic route for the synthesis of nanosized ethylene-propylene rubber (EPM) is proposed in Figure 3.10. The preparation of nanosized EPM was synthesized through differential microemulsion polymerization to produce synthetic PIP and then diimide hydrogenation was carried out to produce EPM. Firstly, isoprene monomer is polymerized through a radical chain polymerization mechanism to obtain polyisoprene nanoparticles (Figure 3.10a). For diimide hydrogenation, hydrogen peroxide as a strong oxidizing agent is used to oxidize hydrazine hydrate via a redox system and subsequently the diimide molecule is released at the interphase (Figure 3.10b). This step is accelerated under thermal dissociation of hydrazine which is promoted by boric acid. Then, nanosized particles containing 1,4 polyisoprene (91%) are reacted with the diimide molecule through a coordination process (Figure 3.10c). Indeed, the ability of the unsaturated carbon-carbon bonds to coordinate with the diimide species depends on the structure of configuration of the synthetic polyisoprene. Thus this coordination step would control the configuration of product due to the selectivity between the intermediate diimide molecule and the different double bond structures, suggesting that vinyl polyisoprene is hydrogenated more readily than *cis*-, *trans*- polyisoprene due to steric effects as described in the previous section. After the coordination step, hydrogen is transferred through a hydride shift mechanism toward the olefinic bond to obtain an alkyl complex, and then the alkyl bond is cleaved by a transferred hydride in an insertion step and nitrogen gas is released (Figure 3.10d). Alternatively, the hydrogen atoms for the diimide may transfer to the carbons of double bonds via a four centre intermediate with release of nitrogen. Finally, the nanosized EPM latex is successfully obtained via diimide hydrogenation of polyisoprene nanoparticles.

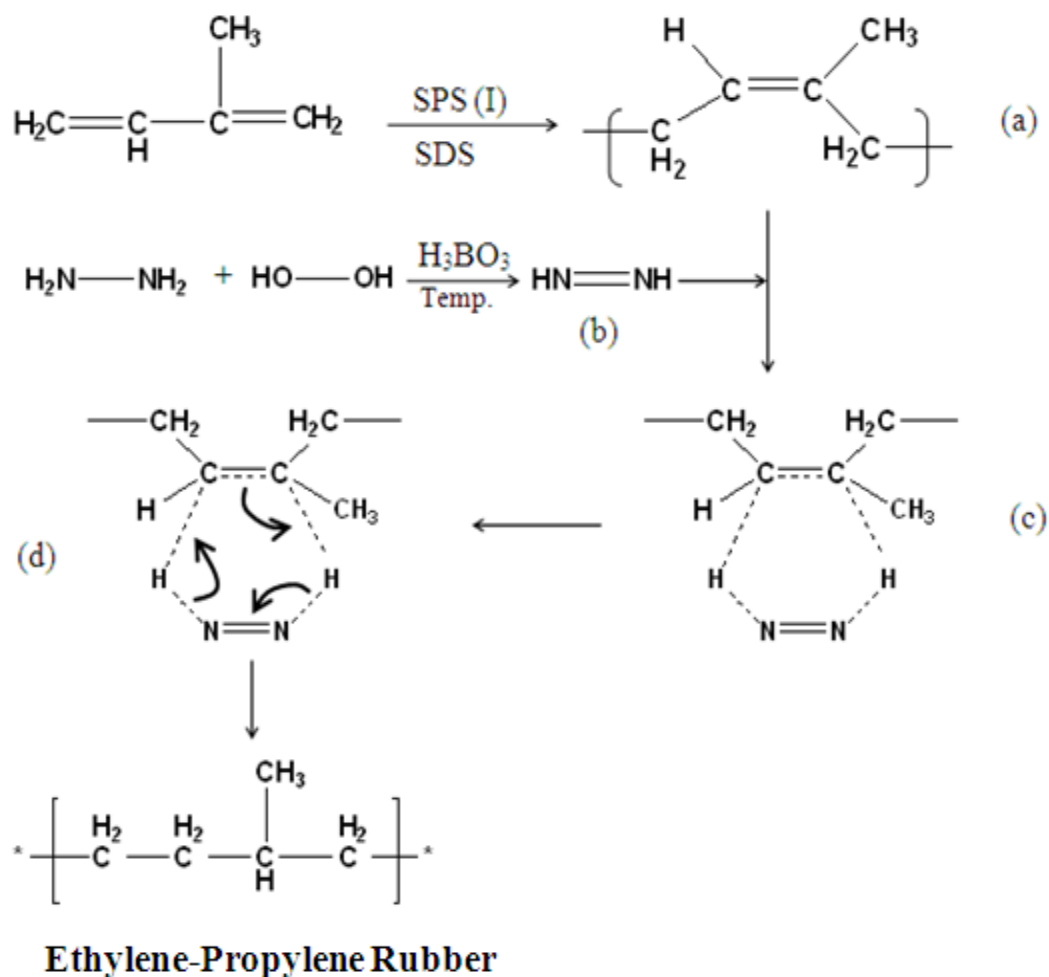


Figure 3.10 Proposed synthetic route for nanosized EPM synthesis by diimide hydrogenation of PIP.

3.7 Thermal Properties of Nanosized Ethylene-Propylene Rubber

Thermal stability of the ethylene-propylene rubber at various hydrogenation levels were investigated using thermogravimetric analysis. From Figure. 3.11, the thermograms of PIP and HPIP show a one-step polymer degradation and provide smooth weight loss curves. The initial decomposition temperature (T_{id}) and the maximum decomposition temperature (T_{max}) are summarized in Table 3.2.

Polyisoprene of 30 nm had a T_{\max} of 425°C while both T_{id} and T_{\max} of all HPIP products are higher than that of PIP. It is noted that the degradation temperature increased with an increasing hydrogenation level. When the extent of hydrogenation increased from 57% to 94%, the maximum decomposition temperature increased from 450°C to 510°C. This implied that thermal stability of nanosized polyisoprene depended on the density of the carbon-carbon double bonds. The sigma bonds are stronger than π bonds because the sigma bonds contain hybridized atomic orbitals. Therefore, hydrogenation involves the breaking of π bonds with a change to sigma bonds resulting in an increase in thermal stability of the hydrogenated polyisoprene nanoparticles. On comparison with commercial ethylene-propylene with an ethylene/propylene ratio of 1:1, the decomposition temperature of nanosized EPM (510°C) was somewhat higher than that of commercial ethylene-propylene rubber (471°C). Therefore, diimide hydrogenation of nanosized polyisoprene rubber leads to a structure of an alternating ethylene-propylene copolymer having improved thermal stability.

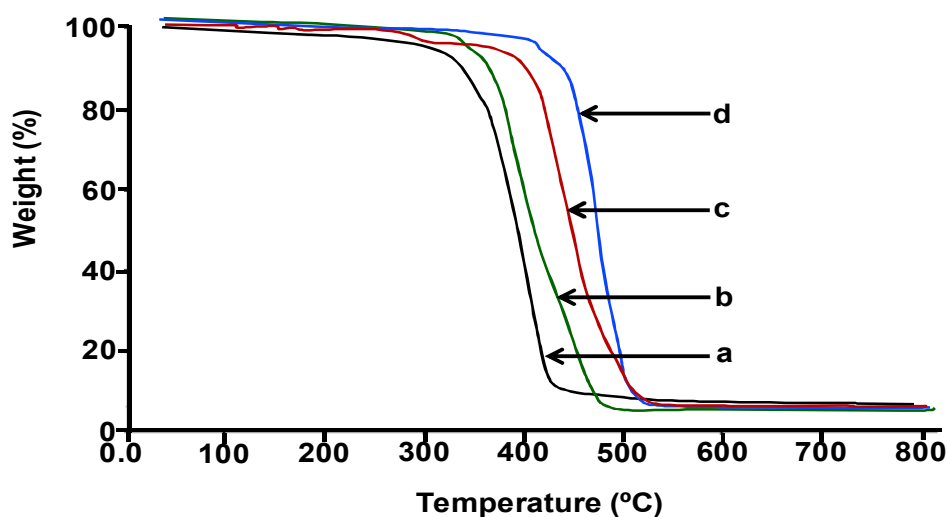


Figure 3.11 Thermograms of (a) nanosized PIP, (b) HPIP (57 %), (c) HPIP (78%), (d) HPIP (94%).

Table 3.2 Decomposition temperature of rubber samples

Rubber	Hydrogenation (%)	T _{id} (°C)	T _{max} (°C)
PIP	-	359.7	425.4
HPIP	57	373.5	450.1
	78	422.6	480.9
	94	447.3	510.1
EPDM ^a	-	452.7	470.7

^aEPDM has an ethylene/propylene ratio of 50/50 and diene content of 9.5%.

3.8 Appearance of Nanosized Ethylene-Propylene Rubber Latex

From Figure 3.12a, the nanosized polyisoprene latex was transparent. All samples of synthetic ethylene-propylene rubber latex (Figure 3.12 b-c) at various hydrogenation levels showed homogeneous dispersion and superior stability of nanoparticles with uniform size distribution.

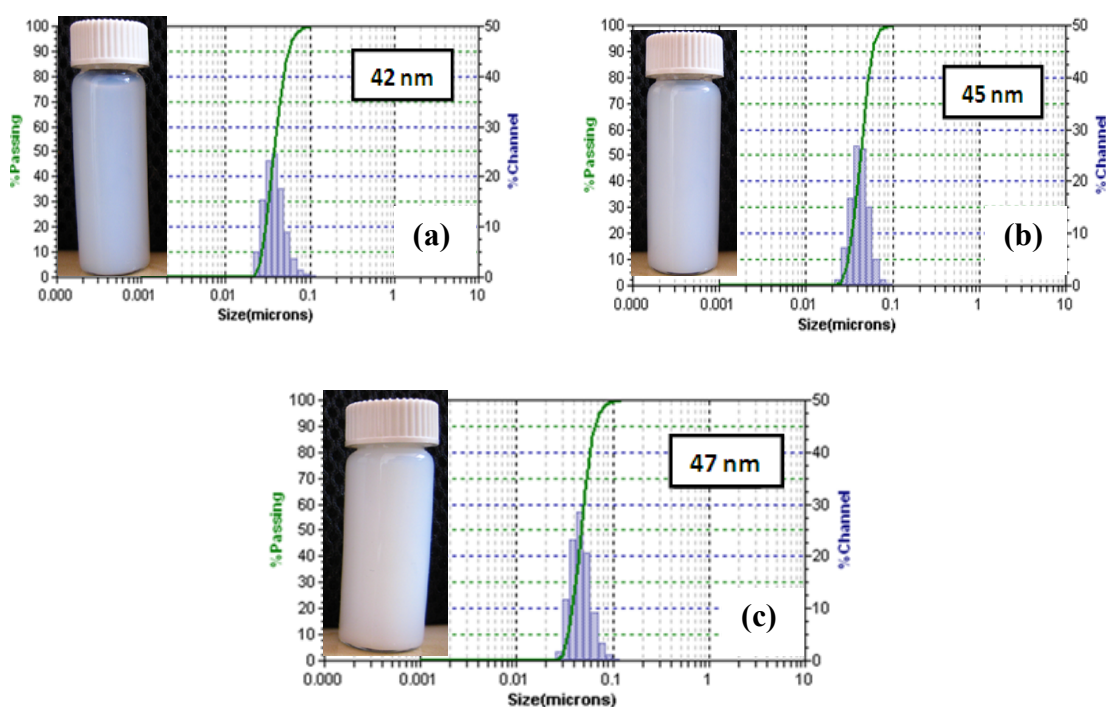


Figure 3.12 The appearance of rubber latex samples and particle size distribution: (a) nanosized PIP, (b) nanosized EPM at 40% hydrogenation and (c) nanosized EPM at 94% hydrogenation.

CHAPTER IV

SYNTHESIS OF POLY(STYRENE-*CO*-METHYL METHACRYLATE)-SiO₂ NANOCOMPOSITES VIA DIFFERENTIAL MICROEMULSION POLYMERIZATION

4.1 Introduction

Both microemulsion and miniemulsion polymerization can provide small particle size of silica encapsulation with polymer; however, these methods required a high amount of surfactant. The surfactants are not only expensive for industrial production but also have a significant negative impact on the physical properties of the resulting polymers. Moreover, the concentration of such surfactant molecules in solution needs to be tuned carefully because a latex formation in the free micelles in the emulsion can be observed at higher concentrations. These molecules are usually only weakly bonded to the surface and can therefore desorb easily. Since, it is desirable to reduce the surfactant amount and also to yield nanosized particles, the differential microemulsion polymerization method has been applied.

The purpose of this work was to prepare a nanocomposite of poly(styrene-*co*-methyl methacrylate)/SiO₂ by a differential microemulsion polymerization method, and to clarify the effects of process variables on encapsulation. To produce modified nanosized silica, the nano-SiO₂ was first pretreated using acrylic acid in which the carboxylic group can be bonded to the silanol groups at the silica surface. The C=C bonds of acrylic acid could be copolymerized with styrene and methyl methacrylate monomer via emulsion polymerization.

4.2 Preliminary Study of Poly(Styrene-*co*-Methyl Methacrylate)-SiO₂ Nanocomposites

Effect of the influence of initiator and surfactant concentration, ST/MMA ratio, monomer/water ratio and silica loading on particle size, as well as silica encapsulation efficiency was also investigated in the preliminary study. The results of the initial study are provided in Table 4.1. From these results, it can be seen that the particle diameter ranges from 29 to 82 nm, conversion from 50 to 75%, polymer content from 12 to 32%, silica content from 68 to 87 %, polymer grafting efficiency from 24 to 67%, and silica encapsulation efficiency from 85 to 95%, depending on the process condition, which will be discussed in detail.

4.2.1 Effect of Initiator Concentration

The amount of initiator has a great influence on particle size. Both particle diameter and %conversion were significantly increased with an increase in initiator level. From Figure 4.1, it can be seen that the particle size was increased from 43 nm to 74 nm with an increasing initiator amount from 1-4% based on monomer weight. At a high initiator concentration, a large amount of free radicals was rapidly reacted with monomers to form oligomeric radicals. Growing oligomer chains were associated with each other resulting in an increase in particle size and conversion. Moreover, the grafting efficiency of polymer onto the silica surface was affected by initiator level as illustrated in Table 4.1. The polymer grafting efficiency decreased from 36.7 % to 18.8 % with increasing initiator amount. It can be considered that the free amount of initiator in the water medium was increased, resulting in a higher free polymer concentration rather than the grafting of the polymer onto the silica surface. The free polymers could form the small aggregates with the grafted silica. Therefore, the increasing initiator amount had a negative impact on particle size (increase) and polymer grafting efficiency (decrease).

Table 4.1 The recipes for the synthesis of poly(ST-*co*-MMA)-SiO₂ and effects of process variables on particle size, conversion, encapsulation efficiency

Sample	SDS (% ^a)	ST/MMA (w/w)	APS (% ^a)	M/H ₂ O (w/w)	Particle size (nm)	Conversion (%)	Polymer Content (%)	Silica Content (%)	Polymer grafting Efficiency (%)	Silica encapsulation Efficiency (%)
P-mSi_APS_1	1.75	1.5/1	1	0.2	43.3	59.7	21.9	78.1	36.7	94.7
P-mSi_APS_2	1.75	1.5/1	2	0.2	57.0	65.2	23.0	77.0	35.3	93.0
P-mSi_APS_3	1.75	1.5/1	3	0.2	64.7	70.5	20.9	79.1	29.6	89.5
P-mSi_APS_4	1.75	1.5/1	4	0.2	73.8	74.3	14.0	86.0	18.8	85.3
P-mSi_SDS_1	0.5	1.5/1	1	0.2	74.8	50.7	12.4	87.6	24.5	90.5
P-mSi_SDS_2	1.0	1.5/1	1	0.2	60.2	54.0	16.7	83.3	30.9	95.5
P-mSi_SDS_3	1.75	1.5/1	1	0.2	43.3	59.7	21.9	78.1	36.7	94.7
P-mSi_SDS_4	3.0	1.5/1	1	0.2	31.7	65.9	22.0	78.0	33.4	93.5
P-mSi_SDS_5	5.0	1.5/1	1	0.2	29.5	66.2	17.0	83.0	25.7	93.9
P-mSi_M/H ₂ O_1	1.75	1.5/1	1	0.1	37.6	75.0	23.9	76.1	31.9	87.4
P-mSi_M/H ₂ O_2	1.75	1.5/1	1	0.2	43.3	59.7	21.9	78.1	36.7	94.7
P-mSi_M/H ₂ O_3	1.75	1.5/1	1	0.3	61.7	54.2	27.6	72.4	50.9	95.0
P-mSi_M/H ₂ O_4	1.75	1.5/1	1	0.4	82.0	50.0	28.0	72.0	56.0	95.6
P-mSi_ST/MMA_1	1.75	0.5/1	1	0.2	30.5	50.0	25.7	74.3	51.4	92.1
P-mSi_ST/MMA_2	1.75	1/1	1	0.2	40.3	52.0	22.8	77.2	43.8	94.1
P-mSi_ST/MMA_3	1.75	1.5/1	1	0.2	43.3	59.7	21.9	78.1	36.7	94.7
P-mSi_ST/MMA_4	1.75	2/1	1	0.2	46.4	59.9	20.6	79.4	34.4	94.1
P-mSi_ST/MMA_5	1.75	3/1	1	0.2	48.9	61.1	19.5	80.5	31.9	93.7
P-mSi_ST/MMA_6	1.75	4/1	1	0.2	50.3	64.6	16.3	83.7	25.2	94.4
Poly(ST/MMA)blank	1.75	1.5/1	1	0.2	31.5	89.0	0	0	0	0

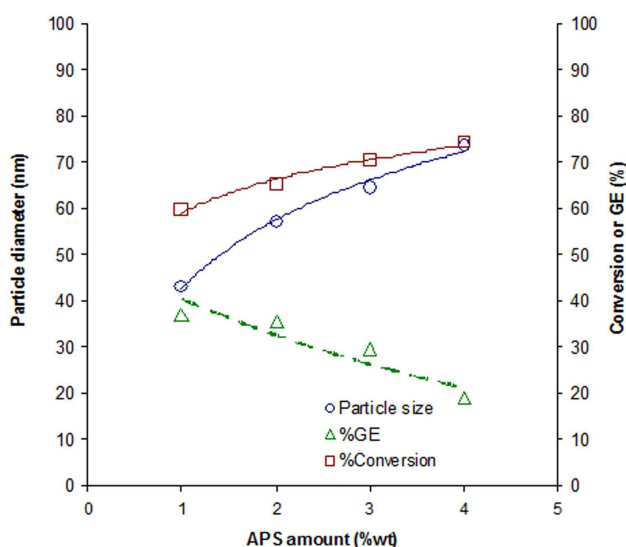


Figure 4.1 Particle size and conversion at various initiator amounts.
 Condition: ST/MMA ratio = 1.5/1, surfactant amount = 1.75%,
 modified silica loading = 10%, monomer/water = 0.2.

4.2.2 Effect of Surfactant Concentration

The influences of surfactant amount on particle size and conversion were investigated. From Figure 4.2, the particle size was decreased from 75 to 29 nm with increasing SDS content from 0.5 to 5% based on monomer weight (surfactant: monomer = 1: 200 and 1: 20). This can be explained in that the initiator decomposed into free radicals in the water phase, then these free radicals firstly attacked monomer in the water phase to form monomer radicals which continued to grow by accepting monomers to produce polymer radicals. These polymer radicals in the small newly formed particles were surrounded by the surfactant to become polymer precursors. Hence, the surfactant amount can be affected to allow the generation of other particle precursors and coverage of the newly formed surfaces. If the amount of surfactant was less than the optimum amount, the number of particle precursors was lower, and therefore, the probability of polymer radicals in the water phase penetrating into the already formed dead particle was higher. That is the main reason that the particle size was the highest when low surfactant amounts were used [96].

Besides the change in the particle size of these composites, monomer conversion increased sharply and reached a maximum conversion around 66% for an SDS amount ranging from 0.5% to 5% i.e., the conversion was increased from 50% to 66%. This indicated that with an increase in the SDS amount, an increase in the monomer diffusion and stability of polymer particles could be realized in the polymerization system. Then, this reaction proceeds in a nucleation mechanism, resulting in a higher conversion [167].

In this research work, the amount of surfactant required (surfactant: monomer = 1: 57) that gave the desirable particle size (smaller than 50 nm) was much lower than those required in the previous work [90-92]. This phenomenon confirms that differential microemulsion polymerization is a novel method for synthesizing composite nanoparticles using an extremely low amount of surfactant. However, for synthesis of poly(ST-*co*-MMA)-SiO₂, maximum conversion was less than 70% compared with the synthesized poly(ST-*co*-MMA) particles without silica (conversion = 89%) because nanosilica particles could possibly decrease or retard the diffusion of monomer in the aqueous phase resulting in a lower conversion.

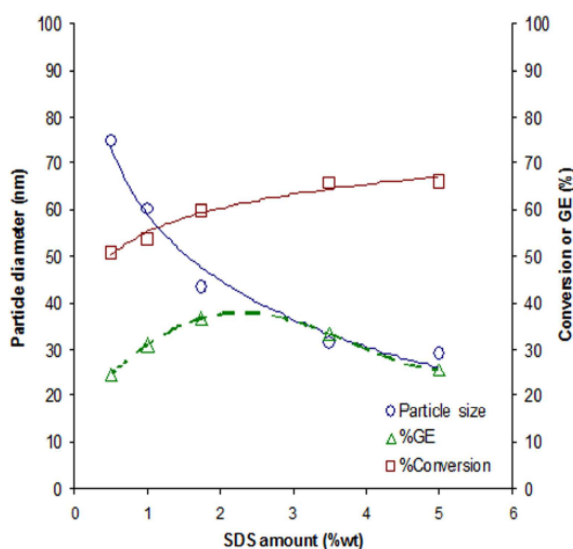


Figure 4.2 Dependence of particle size and conversion on SDS concentration. Condition: ST/MMA ratio = 1.5/1, APS amount = 1% based on monomer weight, modified silica loading = 10% based on monomer weight, monomer/water = 0.2.

4.2.3 Effect of Monomer/Water Ratio

For the effect of monomer/water ratio as shown in Figure 4.3, the increasing water content in the reaction system (low level of monomer/water ratio) caused an increased conversion from 58% to 81%. Therefore, a higher amount of water as reaction medium was necessary for increasing in monomer diffusion and stability of the nanoreactor, resulting in a higher conversion. However, a high level of water enhanced the decrease in silica encapsulation efficiency. Because most silica particles could migrate or transfer from organic phase as monomer phase to aqueous phase, silica encapsulation efficiency was decreased [75]. Furthermore, the particle diameters could be controlled by variation of water content as presented in Table 4.1. The smaller diameters were produced for increasing water amount due to the improvement of stability and dispersion of nanonuclei in polymerization system.

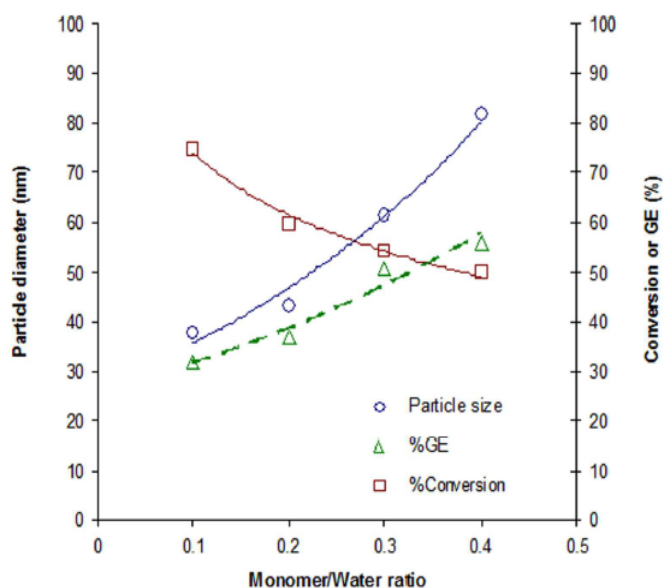


Figure 4.3 Conversion and silica encapsulation efficiency at various monomer to water ratio. Condition: ST/MMA ratio = 1.5/1, surfactant amount = 1.75%, initiator amount = 1%, modified silica loading = 10% based on monomer weight.

4.2.4 Effect of Styrene/Methyl Methacrylate Ratio

From Figure 4.4, the change of particle diameter shows a downward trend with the decrease in ST/MMA ratio or the increase in the MMA feed. The particle size decreased from 50 nm to 30 nm with decreasing ST/MMA ratio from 4:1 to 0.5:1. It is seen that the lower of ST/MMA ratio resulted in the smaller diameter. Due to the hydrophilicity of MMA compared with the hydrophobicity of styrene, the nucleation mechanism likely occurred in the water phase as homogeneous nucleation rather than in the micelles as heterogeneous nucleation [98]. Hence, with increasing MMA feed, smaller nuclei in the system were produced and then a smaller particle size of polymer was formed. This is also attributed to the fact that styrene is more oil-soluble (the solubility = 0.5 wt% in water) than MMA (2 wt% in water) [168]. Therefore, styrene had a stronger tendency to form oil droplets in the aqueous reaction system than MMA, and the presence of these oil droplets caused the reactions to proceed in a similar manner to a conventional emulsion polymerization [96]. This is possibly the reason that the smaller particle size was obtained under a higher MMA feed.

Moreover, at high MMA composition, grafting efficiency increased which implied that more polymers were built up at the silica surface than free polymer formed in the aqueous phase. This is due to the stronger polarity and solubility of the monomer MMA resulting in compatibility between MMA monomer and modified-SiO₂. As a result, the amount of free polymer was reduced but grafting efficiency of polymer on silica surface was increased. Nevertheless, a high ST/MMA ratio of 4/1 enhanced the conversion to as high as 65%, due to the higher monomer reactivity constant of styrene (0.52) than methyl methacrylate (0.46).

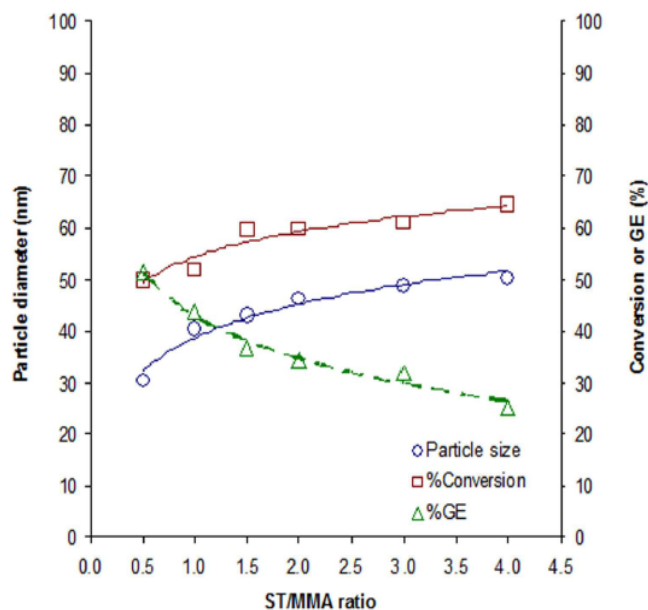


Figure 4.4 Dependence of particle size and grafting efficiency on ST/MMA ratio. Condition: SDS amount = 1.75%, APS amount = 1%, modified-SiO₂ loading = 10% based on monomer weight, monomer/water = 0.2

4.2.5 Effect of Silica Loading

The amounts of silica loading have a significant influence on particle sizes and grafting efficiency of polymer as presented in Table 4.2. When the silica level was increased from 10% to 20% based on monomer weight, the average particle size increased from 43 nm to 70 nm and the size distribution became broader. More aggregation or agglomeration of silica particles were produced for the higher silica loading. On the other hand, at high silica concentration, the grafting efficiency of polymer was sharply increased due to the increase in the total surface area and the interfacial area of silica resulting in an increase in the graft polymerization rate.

Table 4.2 Characterization of nanocomposites at various silica amounts

Sample	m-Si (%wt)	Particle Size (nm)	Size distribution	Conv ^a (%)	Si encap ^b (%)	Polymer content (%)	GE ^c (%)
P-mSi_Si_10	10	43.3	0.27	59.7	94.7	21.9	36.7
P-mSi_Si_15	15	62.8	0.49	49.4	93.0	29.5	59.7
P-mSi_Si_20	20	69.7	0.58	49.0	93.6	32.0	66.7

^a % Conversion

^b % Silica encapsulation efficiency

^c % Grafting efficiency

For polymer content and polymer grafting efficiency, the grafting efficiency of polymer, polymer content and silica content of composite particles were evaluated by the two techniques, an extraction by a Soxhlet apparatus and a thermogravimetric/differential thermogravimetric analysis (TG/DTA). For the extraction method, the free polymer latex was separated from the graft polymer and the amount of polymer in the composite particles was determined gravimetrically as described in the experimental section. For TG/DTA, the thermogram of the composite sample (Figure 4.5), the weight loss over the range of 200-500 °C corresponded to polymer decomposition and the residue weight was attributed to the silica content. Hence, the polymer content and silica content of the composite sample, (P-mSi_APS_1) were 23.2 and 76.8 %, respectively. From Table 4.3, the data obtained by the two techniques are in good agreement and definitely attest the validity of these methods used for the determination of both the grafting efficiency and silica encapsulation of composite particles under these experimental conditions.

Table 4.3 Polymer content and polymer grafting efficiency of composite sample (P-mSi_APS_1)

Method	Polymer content ^a (%)	GE ^b (%)	Silica content (%)
Material balance	21.9	36.7	78.1
Thermogravimetric analysis	23.2	38.9	76.8

^a In weight percent of the composite sample

^b Percent by weight of the total amount of synthesized polymer

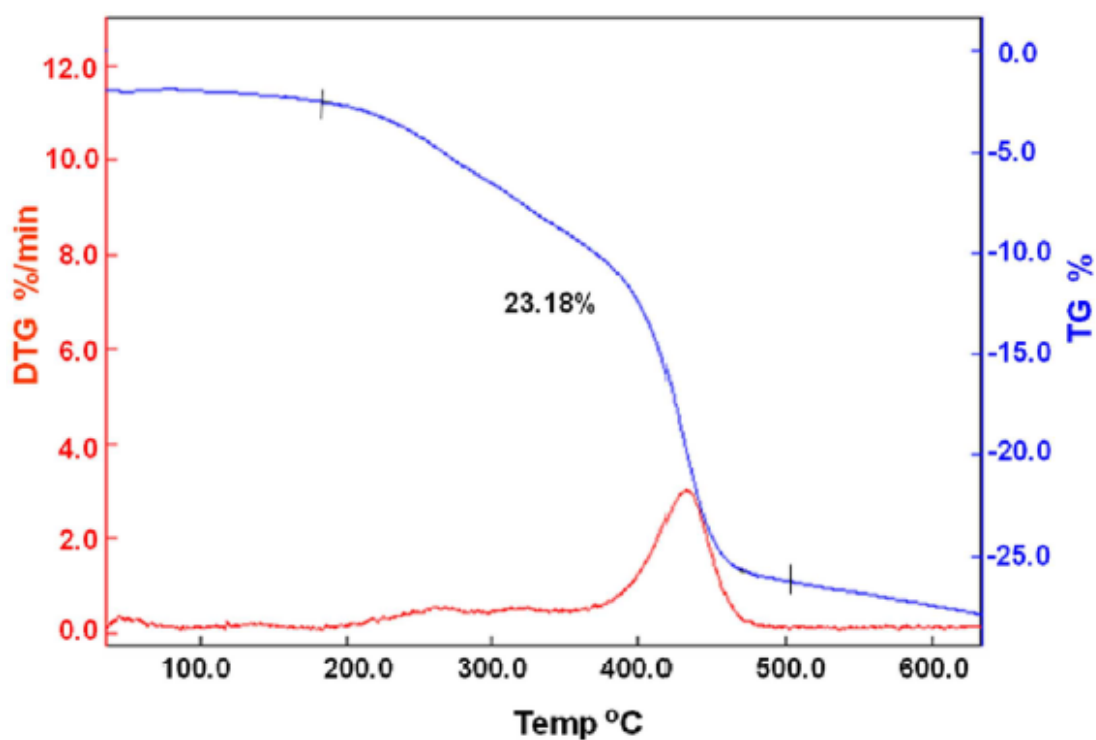


Figure 4.5 Thermogravimetric analysis curve of composite sample, P-mSi_APS_1.

For particle size distribution of poly(ST-*co*-MMA)-SiO₂ nanocomposite, The particle size distribution index was used to identify the dispersion of nano-SiO₂ in polymer matrix. Particle size distribution of poly(ST-*co*-MMA)-modified-SiO₂ (P-mSi_APS_1) compared with poly(ST-*co*-MMA)/unmodified-SiO₂ (P-untreated-Si_APS_1) is shown in Figure 4.6 (a) and Figure 4.6 (b), respectively. For a nanocomposite of SiO₂ pretreated with acrylic acid, a narrow size distribution (0.27) was obtained while a boarder size distribution (0.68) was formed for a composite of untreated SiO₂. It can be noted that the silica surface modification method is required to produce a homogeneous structure rather than an agglomeration structure.

In this work, the pretreatment of the silica surface by acrylic acid could increase the silica dispersion and compatibility between silica and polymer resulting in a uniform size distribution. For comparision, the direct mixing or physical mixing between untreated silica particles and polymer latex was performed. The direct mixing shows the phase separation and also produced the multiple size distribution at 27 nm of poly(ST-*co*-MMA), and 200 nm of agglomerated silica as shown in Figure 4.6 (c). Therefore, the method of differential microemulsion polymerization is a novel technique for synthesizing composite nanoparticles with smaller particle size, narrow size distribution, and homogeneous structure.

The comparison of appearance of poly(ST-*co*-MMA) nanoparticles prepared by differential microemulsion polymerization and by physical mixing is shown in Figure 4.7. The physical mixing between untreated silica particles and polymer latex shows the phase separation due to the precipitation of silica particles at the bottom phase and the dispersion of polymer particles at the top phase. The physical mixing led to the multiple size distribution and the less stability of silica nanoparticles (Figure 4.7 a). A homogeneous dispersion is obtained by differential mocoemulsion polymerization (Figure 4.7 b), indicating that nano-SiO₂ particles have the good dispersion and compatibility with polymer particle resulting to a uniform size distribution and superior stability of nanoparticles.

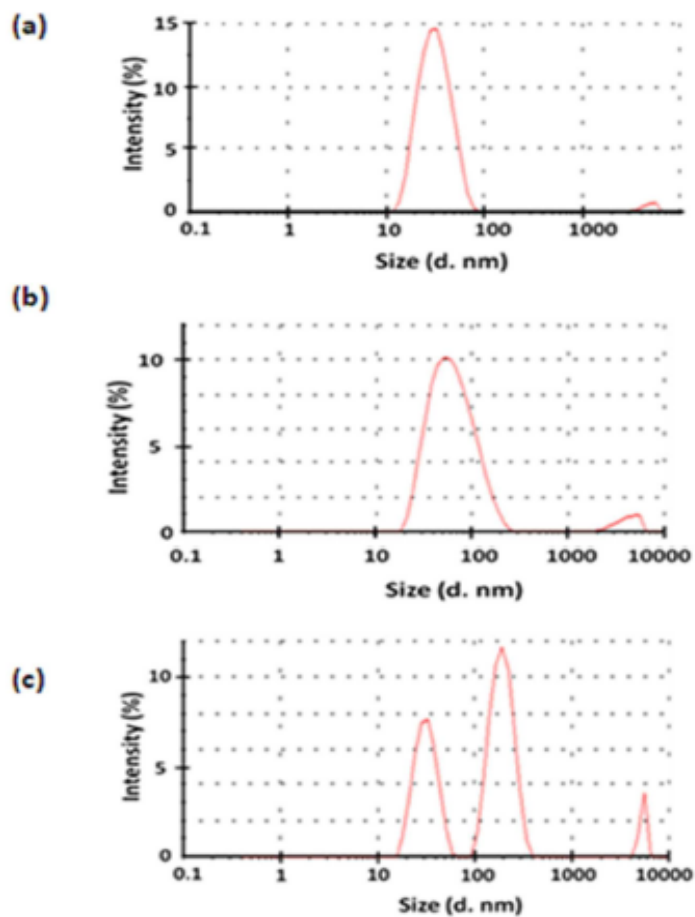


Figure 4.6 Particle size distributions of composite samples (a) P-mSi_APS_1, (b) P-untreated-Si_APS_1 and (c) P-Si_APS_1 (Physical Mixing).

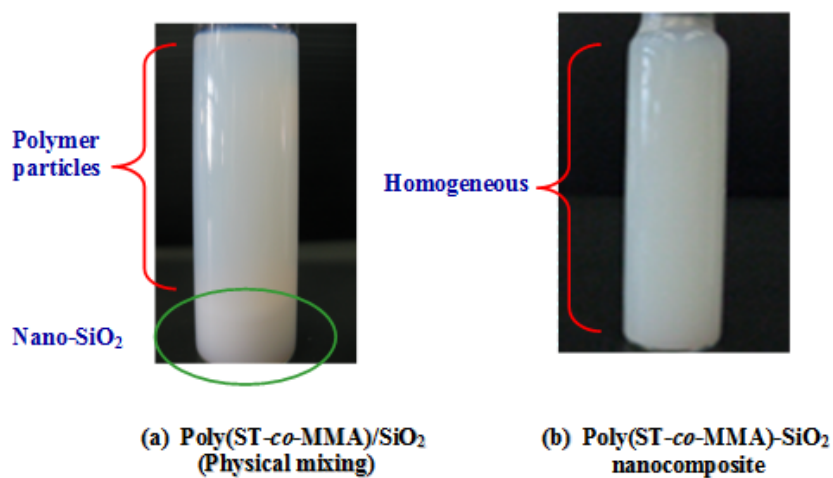


Figure 4.7 Appearance of composite latex (a) P-Si_APS_1 (Physical Mixing), (b) P-mSi_APS_1.

4.3 Characterization of Poly(ST-*co*-MMA)-SiO₂ Nanocomposites

The characterization of the modified-SiO₂ (m-Si 1 and m-Si 2) obtained was performed using FT-IR spectroscopy. From Figure 4.8, the spectrum of treated silica, with high AA content, m-Si 1 shows =CH₂ stretching bands at 3177 cm⁻¹ and the peaks at 3600-3000, 1639, 1548 and 1401 cm⁻¹ corresponding to OH, C=O, C=C stretching and CH₂ bending of AA, respectively. While a very pronounced band appearing at 1105 cm⁻¹, together with two less pronounced bands at 806 and 472 cm⁻¹ correspond to the vibration absorption band of the Si-O-Si groups.

The functional groups of poly(ST-*co*-MMA)/SiO₂ composite particle were also characterized by FT-IR spectroscopy as shown in Figure 4.9. The absorption bands of P-mSi_APS 1 at 1144, 805 and 470 cm⁻¹ correspond to Si-O-Si groups. The peaks at 2936 cm⁻¹ (ν CH₃), 2852 cm⁻¹ (ν CH₂), 1730 cm⁻¹ (ν C=O), 1457 cm⁻¹ (ν CH₂ bending) and 1398 cm⁻¹ (CH₃ bending) relate to methacrylate group of MMA. The bands in 3027 cm⁻¹ (ν CH), 1600 cm⁻¹ (ν C=C) and 700 cm⁻¹ (CH out of plain bending) are attributed to the aromatic group of ST. These results indicate that poly(ST-*co*-MMA) could be grafted onto the silica surface.

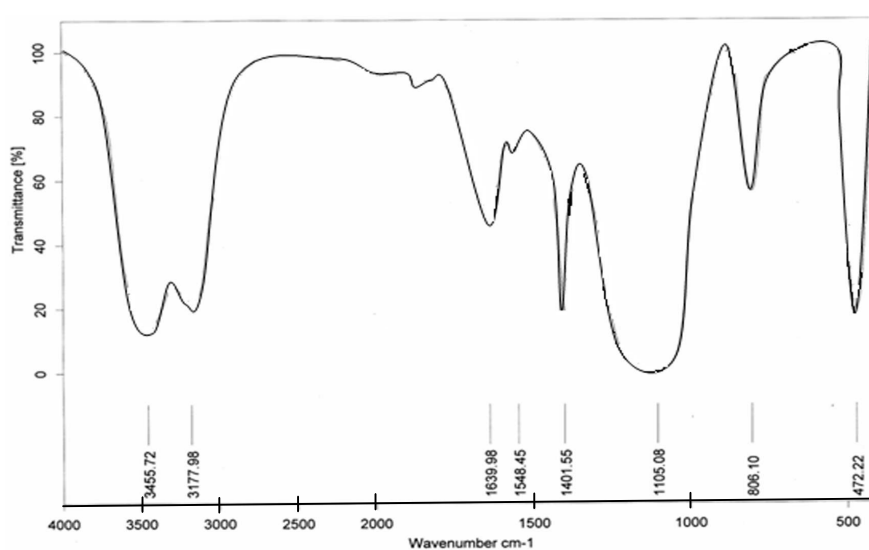


Figure 4.8 FTIR spectrum of modified silica at high AA amount (m-Si 1).

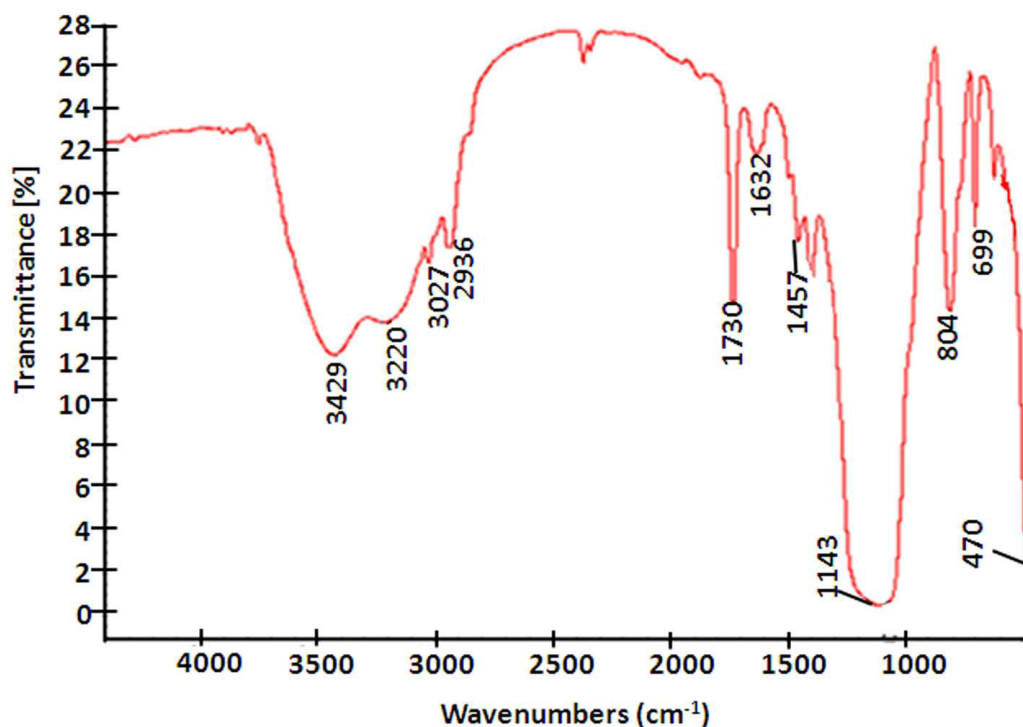


Figure 4.9 FT-IR spectrum of P-mSi_APS_1 after separation of the free latex particles.

Figure 4.10 represents the ¹H NMR spectrum of the poly(ST-co-MMA) extracted from the poly(ST-co-MMA)/SiO₂. Phenyl protons of polystyrene are observed in the range of 7.1-7.4 ppm. Methine protons of PS are found at 1.9 ppm. For PMMA, the peaks at 3.5 and 0.9 ppm are the characteristic peaks of methoxy protons and methyl protons, respectively. Moreover, the peaks in the range of 1.1-1.4 ppm correspond to the methylene protons of both PS and PMMA. Hence, the ratio of ST to MMA in composite particles is determined with the phenyl proton peak area of PS (at 7.1-7.4 ppm) and the methoxy proton peak areas of PMMA (at 3.5 ppm). It could be seen that the ratio of ST/MMA in the composite is 1.47 for P-mSi_APS 1 prepared with a ST/MMA feed ratio of 1.5/1 (Table 4.1).

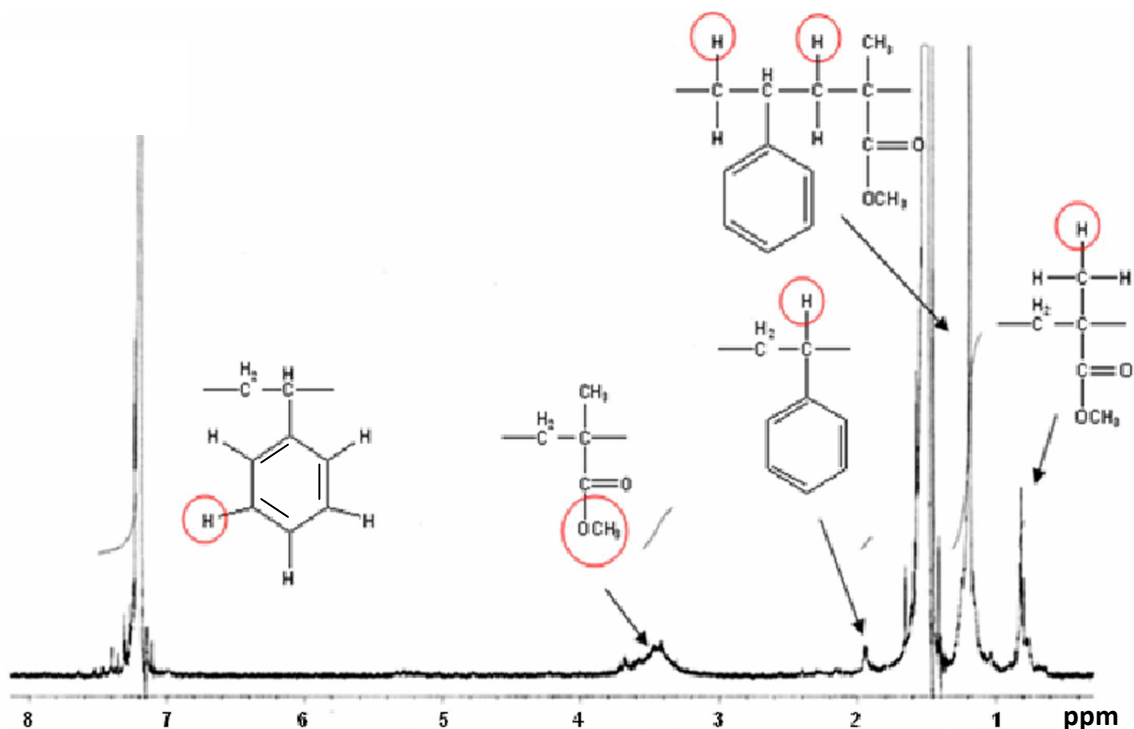


Figure 4.10 ^1H NMR spectrum of composite sample, P-mSi_APS_1, in CDCl_3 .

4.4 Morphology of Poly(ST-co-MMA)- SiO_2 Nanocomposites

TEM micrographs of poly(ST-co-MMA)- SiO_2 composites show dark SiO_2 cores and white polymeric layer shells around each core (Figure 4.11). Figure 4.11 (a) shows that the aggregation phenomenon of silica particles was significant for untreated- SiO_2 . Untreated SiO_2 particles were not able to separate and stabilize each particle due to high polarity on their surface, resulting in the agglomeration structure through hydrogen bonding and free polymer formation. Nevertheless, the regular spheres and a well-dispersed morphology were obtained by using modified- SiO_2 as shown in Figure 4.11 (b). At higher magnification (Figure 4.11 (c)), it can be seen that SiO_2 particles were encapsulated by a polymer shell, indicating that core/shell nanoparticles have been successfully formed under this condition.

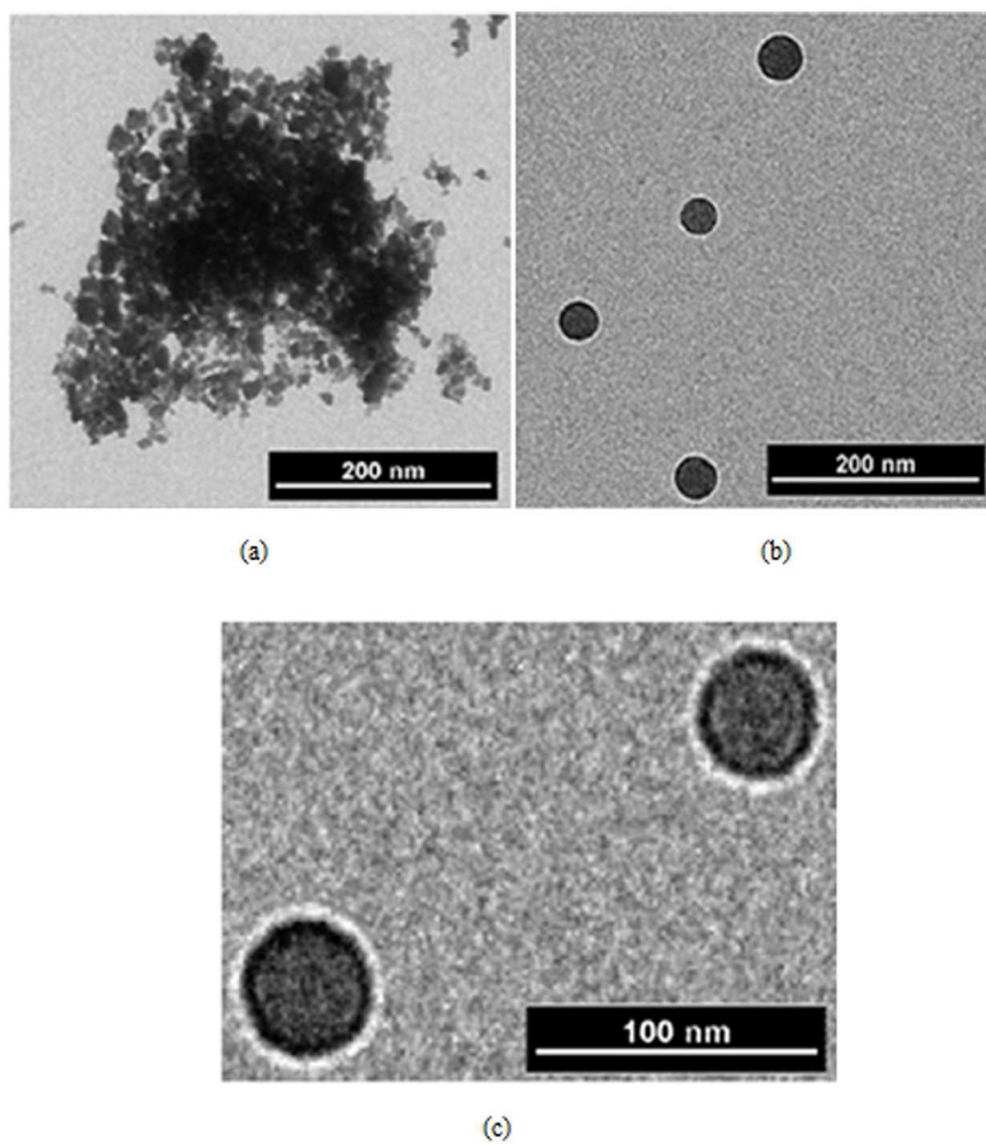


Figure 4.11 TEM micrographs of (a) untreated-SiO₂, (b) P-mSi_APS_1, (c) P-mSi_APS_1 at higher magnification.

4.5 Proposed Mechanism for Poly(ST-*co*-MMA)-SiO₂ Nanocomposites Synthesis

The formation mechanism with controlled morphology of poly(ST-*co*-MMA)/SiO₂ is proposed in Figure 4.12. Firstly, the acrylic acid was bonded to a silica surface through a hydrogen bonding to produce the C=C bonds on their surface. Due to this modification method, the polarity of silica surface was decreased and became amphiphilic characteristic. Then, the hydrophilic initiator (APS) and the surfactant (SDS) could be adsorbed on the silica domains due to its hydrophilic surface. The hydrophobic group of surfactant tended to turn in the oil phase and the hydrophilic group turn towards the aqueous phase as reaction medium (Figure 4.12a). The interface between the oil phase and the aqueous phase could stabilize the colloid particles. The differential microemulsion polymerization consisted of water, water-soluble initiator (APS), surfactants (SDS), nonagglomerated silica and a very small amount of monomer droplet (ST, MMA). The initiator decomposed in water phase to form primary radicals. Some of these radicals could attach both monomers and C=C bonds of acrylic acid to produce polymer radicals on silica surface (b). Therefore, the polymers could graft onto silica surface through the encapsulation reaction to obtain silica core and polymer shell morphology (c). However, some free polymer chains which did not graft would form the nanosized polymer particles.

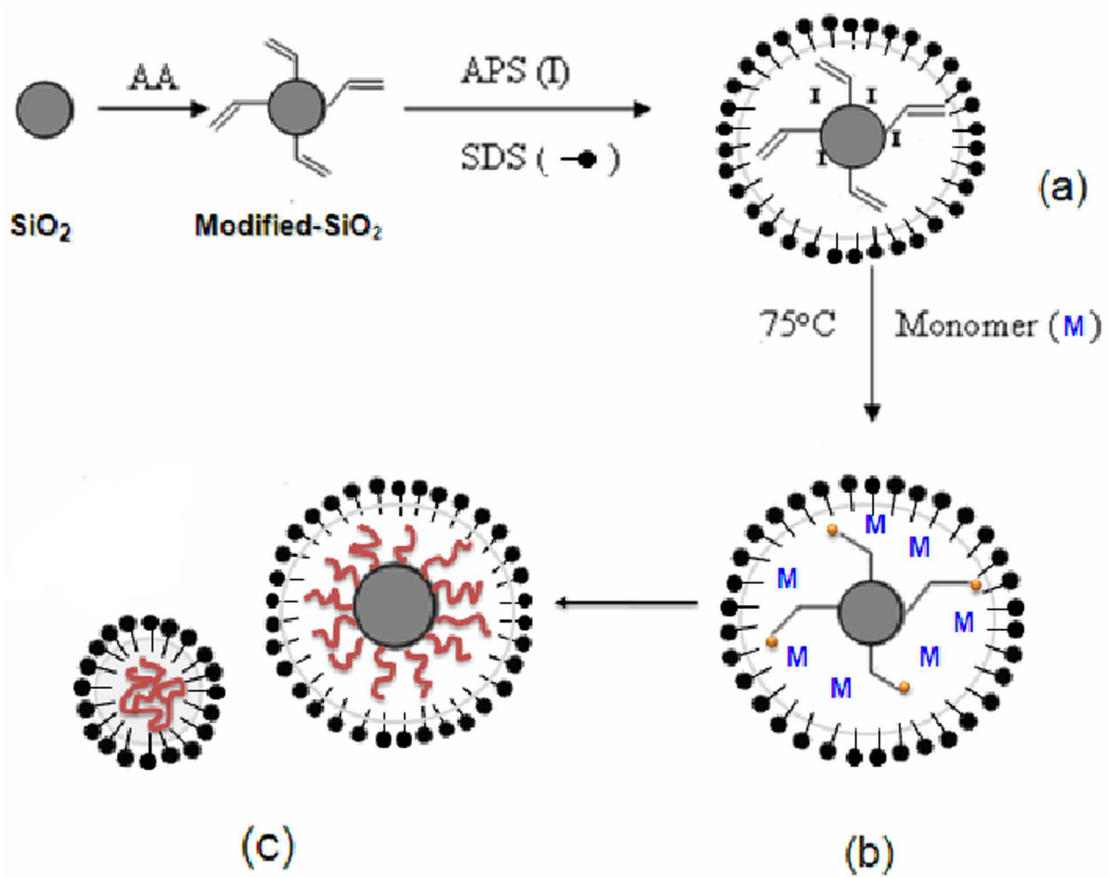


Figure 4.12 The proposed model for formation mechanism of nanosized-SiO₂ encapsulated by poly(ST-co-MMA) with core/shell morphology.

CHAPTER V

SYNTHESIS OF POLYISOPRENE-SILICA NANOCOMPOSITES VIA DIFFERENTIAL MICROEMULSION POLYMERIZATION

5.1 Introduction

Differential microemulsion polymerization is advantageous for the production of nanosized polymer latex with an extremely low surfactant concentration and is normally performed using an environmental friendly process due to the absence of organic solvents and can be performed under mild conditions. For the mechanism of differential microemulsion polymerization, when the reaction was initiated, the system contains initiators, radicals of primary radicals, monomer radicals, and polymer radicals, nonaggregated surfactants, and a very small amount of monomer. The initiator decomposes in the aqueous phase to generate primary radicals and some of the radicals enter into monomer swollen micelles to produce polymer particles. So far, the synthesis of nanosized rubber-SiO₂ by differential microemulsion polymerization has not been reported.

In this research work, the preparation of a monodispersion of nanosized polyisoprene-SiO₂ composite with core/shell morphology was studied. Differential microemulsion polymerization was applied to synthesize the nanocomposites having a uniform particle size distribution. The nano-SiO₂ was pretreated using organo silane coupling agents to produce a siloxane bond at the silica surface and the carbon double bonds at the chain end of the silane coupling agent could be polymerized with the isoprene monomer. The influence of initiator and surfactant concentration, monomer/water ratio and silica loading on particle size, monomer conversion as well as encapsulation efficiency was also investigated.

5.2. Characterization of Polyisoprene-SiO₂ Nanocomposites

From Figure 5.1a, the spectrum of SiO₂-treated with MPS (MPS-SiO₂), the peaks at 2960, 1732 and 1633 cm⁻¹ are attributed to =CH₂, C=O and C=C stretching of the MPS groups, respectively [169, 170]. The peak at 3441 cm⁻¹ is assigned to the surface hydroxyl group (O-H) of silica [65]. While a very broad band appearing at 1111 cm⁻¹, together with two less pronounced bands at 810 and 473 cm⁻¹ correspond to the vibration absorption band of the Si-O-Si groups.

For silica modified with VTS (VTS-SiO₂) (Figure 5.1b), the absorption bands at 1114, 802 and 470 cm⁻¹ correspond to Si-O-Si groups. The peaks at 3443, 3067 and 2962 cm⁻¹ relate to OH, CH and CH₂ stretching of the VTS groups. The bands at 1604 cm⁻¹ (C=C) and 1411 cm⁻¹ (CH out of plane bending) are attributed to the double bonds of VTS. These results indicate that coupling agents could be bonded onto the silica surface. The methoxy groups of silane were firstly hydrolyzed by the water in the aqueous solution to form silanol groups. The added ammonium hydroxide catalyzed the hydrolysis reaction due to a nucleophilic attack at the silicon atom of the silane. The siloxane linkage between the silica surface and the silane agent was then produced through a polycondensation reaction [171].

For the PIP-VTS-SiO₂ composite (Figure 5.1c), new peaks at 2860 and 2972 cm⁻¹ are related to the methyl and methylene stretching of polyisoprene, respectively. Additionally, the low intensity band at 837 cm⁻¹ and medium intensity band at 1674 cm⁻¹ correspond to the CH of trisubstituted olefin and the C=C stretching of polyisoprene, respectively. The methyl deformation bands of polyisoprene were apparent at 1370 and 1490 cm⁻¹ [172]. These results imply that polyisoprene was grafted onto the silica surface.

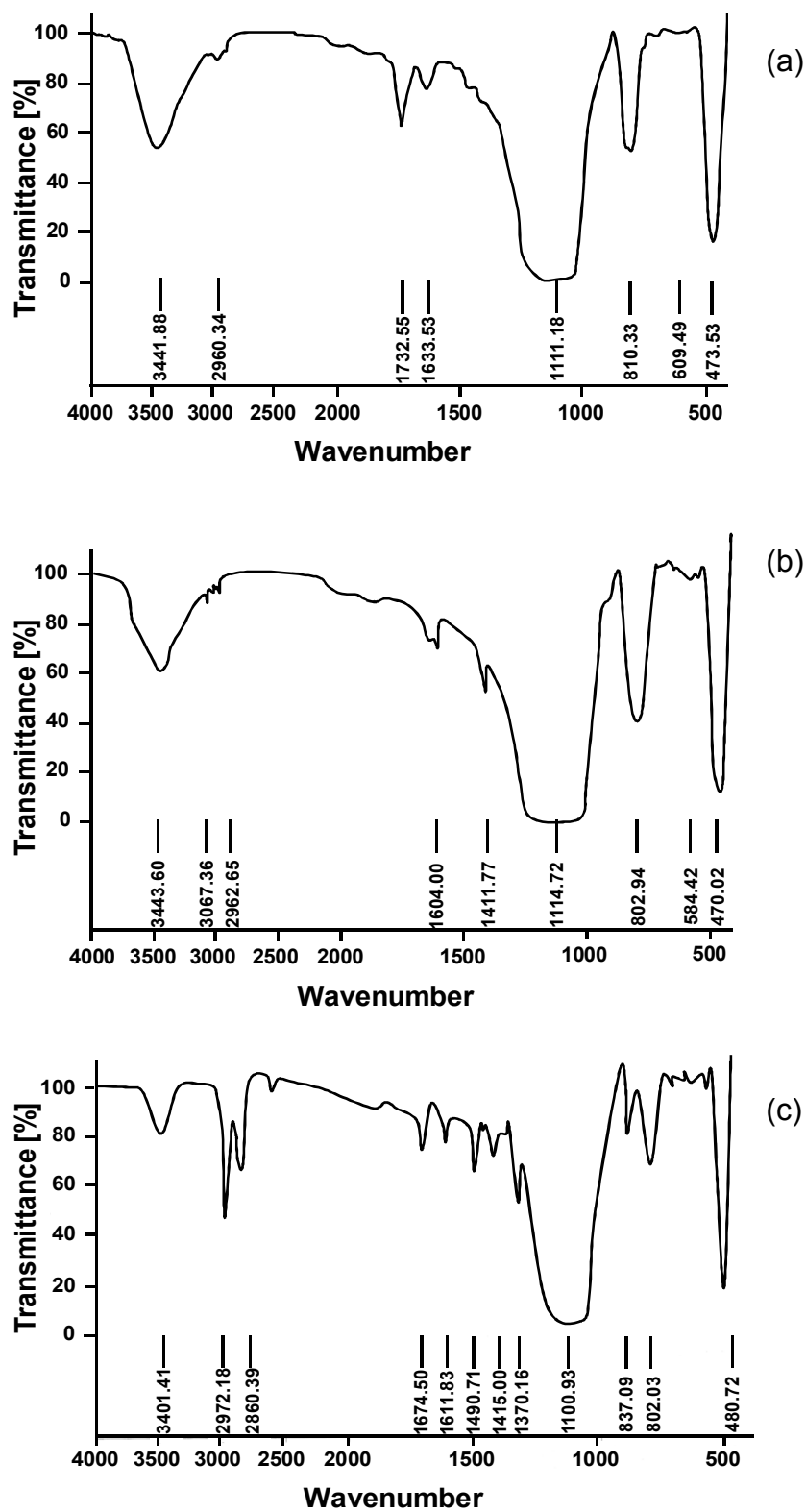


Figure 5.1 FTIR spectra of (a) MPS-SiO₂, (b) VTS-SiO₂, (c) PIP-VTS-SiO₂.

5.3 Encapsulation of VTS-SiO₂ with Polyisoprene

The encapsulation of the nanosized VTS-SiO₂ with PIP was studied under various process parameters such as monomer to water ratio, surfactant concentration, initiator amount and silica loading. The effects of parameters on particle size, polymer grafting efficiency, monomer conversion as well as silica encapsulation efficiency are discussed in detail.

5.3.1 Influence of Monomer/Water Ratio

The monomer to water ratio significantly affected to the encapsulation as shown in Figure 5.2. The particle size of PIP-SiO₂ nanocomposite increased with increasing monomer concentration. The particle diameter was increased from 20 nm to 55 nm when the monomer to water ratio was increased from 0.1 to 0.5. At a high monomer to water ratio, the probability that one particle collided with another particle was higher and thus monomer conversion increased which resulted in a larger particle size than that obtained at low monomer concentration [96]. The monomer conversion and grafting efficiency were increased when increasing the monomer to water ratio from 0.1 to 0.3 and then decreased at a higher ratio. Thus, a high monomer to water ratio above 0.3 caused a negative effect on particle size, conversion and polymer grafting efficiency. However, at the highest monomer to water ratio (0.5), most of the further added monomer molecules had to enter into the existing polymer particles, which was more than that of the newly nucleated particles and the long time needed for monomer diffusion into the particle would decrease the monomer conversion [173]. Thus, the monomer conversion was decreased at high monomer/water ratio. The grafting efficiency (GE) had a similar trend to conversion and the %GE at higher monomer concentration was decreased, due to the fact that the free PIP was more pronounced than grafted PIP [174]. The maximum conversion (87%), grafting efficiency (78%) and small particle size (35 nm) was obtained at a monomer to water ratio of 0.3.

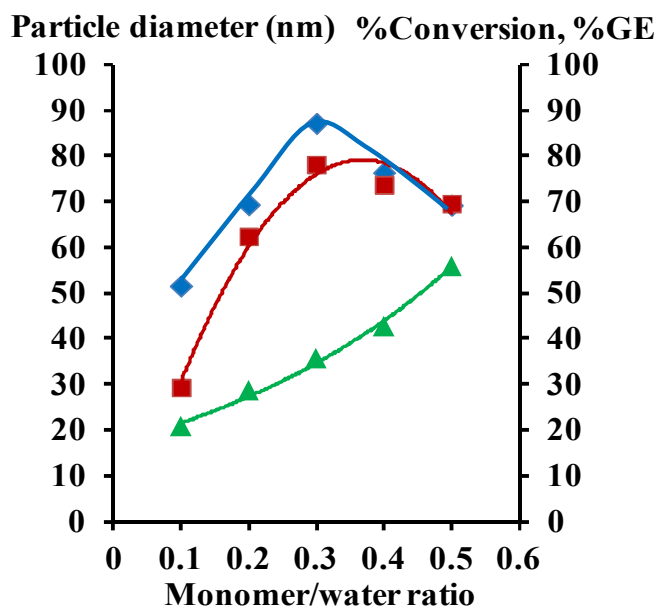


Figure 5.2 Effect of monomer to water ratio (M/H₂O) on PIP-SiO₂; (▲) Particle diameter, (◆) %Conversion, (■) %GE. Condition: SPS = 1 %wt, SDS = 3 %wt, VTS-SiO₂ = 10 %wt based on monomer.

5.3.2 Influence of Initiator Concentration

The effect of initiator concentration on SiO₂ encapsulation with PIP was also studied over the range of 0.5-5 %wt based on monomer. From Figure 5.3, it is seen that the polymer grafting efficiency was dramatically affected by initiator amount. The %GE decreased from 80 to 50% with an increase in initiator concentration from 0.5 to 5 %wt. It can be explained in that, a large amount of oligoradicals are generated in the aqueous phase, but these radicals can enter into the polymer particles to react with the modified silica double bonds. A greater radical entry rate may be the reason for the decrease in the grafting efficiency with the increase in initiator concentration. This phenomenon resulted in a higher free PIP concentration rather than the grafting of PIP onto the silica surface. Although the high initiator amount had a negative effect on the grafting efficiency, the increasing initiator level had a positive effect on the monomer conversion. At high initiator concentration, the initiator decomposed to generate free radicals and the radicals reacted with monomer to produce primary

radicals and then the growing polymer chains increased resulting in an increase in conversion [175]. Therefore, a low initiator concentration is preferred for the preparation of PIP/SiO₂ encapsulation.

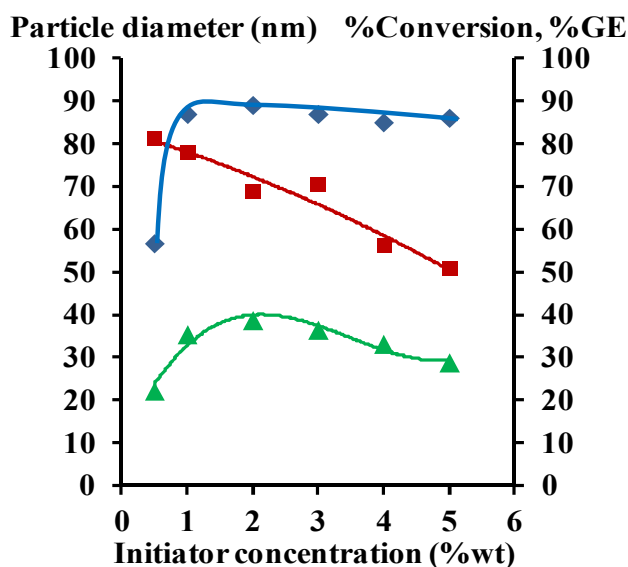


Figure 5.3 Effect of initiator concentration on PIP-SiO₂; (▲) Particle diameter, (◆) %Conversion, (■) %GE. Condition: M/H₂O = 0.3, SDS = 3 %wt, VTS-SiO₂ = 10 %wt based on monomer.

5.3.3 Influence of Surfactant Concentration

SDS was used as an anionic surfactant for encapsulation of nano-SiO₂ with PIP. The amount of surfactant had a great influence on particle size, conversion and polymer grafting efficiency as illustrated in Figure 5.4. Particle size decreased from 50 nm to 20 nm with an increase in the surfactant amount from 0.5 to 10 %wt based on monomer. At a high surfactant level, smaller nuclei in the system were produced and then a smaller particle size of PIP-SiO₂ composite was formed [176]. The conversion was increased from 60 to 90% with an increase in surfactant level from 0.5 to 7% it then leveled off. An increase in the SDS amount increased the number of

monomer-swollen micelles and therefore the number of particles which led to an increase in the polymerization rate and the final conversion. For PIP-SiO₂ encapsulation, polymer grafting efficiency was significantly affected by the surfactant concentration; %GE was increased with increasing SDS, reaching a maximum grafting efficiency of 80% at a SDS amount of 3 %wt and then it decreased. Surfactant could provide the monomer-swollen micelles favoring the diffusion of hydrophobic monomer onto the SiO₂ surface and the stability of PIP-SiO₂ nanocomposite resulted in an increase in grafting efficiency. However, the grafting efficiency decreased at a high surfactant concentration. It is indicated that above the critical micelle concentration (CMC), further addition of surfactant resulted in an increase in micelle concentration while the monomer concentration remained constant in a value close to the CMC; and thus, the formation of ungrafted polyisoprene (free homopolymer) was produced rather than the encapsulation of SiO₂ with PIP [177].

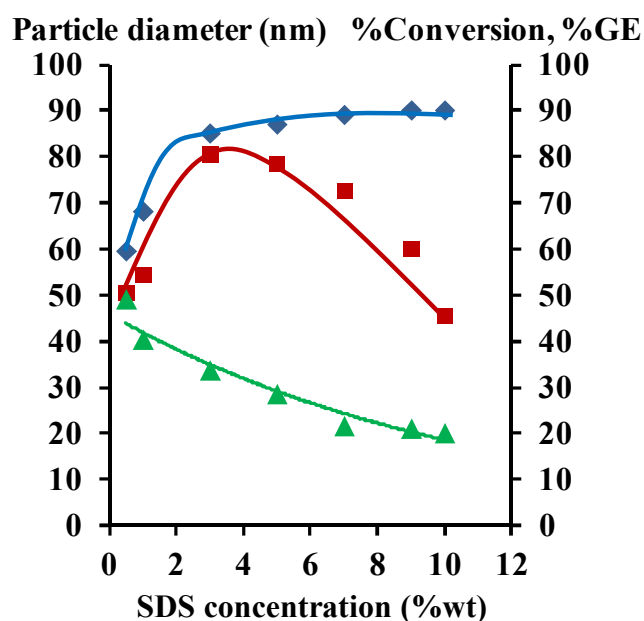


Figure 5.4 Effect of SDS concentration on PIP-SiO₂; (▲) Particle diameter, (◆) %Conversion, (■) %GE. Condition: M/H₂O = 0.3, SPS = 1 %wt, VTS-SiO₂ = 10 %wt based on monomer.

5.3.4 Influence of Silica Loading

The concentration of silica loading had a significant influence on particle size and encapsulation efficiency as shown in Figure 5.5. When the silica level was increased from 5 to 20 %wt based on monomer, the average particle size was linearly increased from 29 nm to 57 nm and the silica encapsulation efficiency and conversion linearly decreased. This implies that at high silica loading, more aggregation of silica particles was produced and SiO₂ particles were not encapsulated, resulting in low encapsulation efficiency and large particle size. It is also probable that, the aggregation of silica particles tended to decrease the number of monomer-swollen micelles and particle stability, and therefore the final conversion was decreased. However, the conversion and silica encapsulation efficiency of PIP-VTS-SiO₂ at 5-20% silica loading were higher than that of PIP/untreated SiO₂ (conversion = 51%, Si encapsulation eff = 22%). Therefore, an appropriate silica loading of 10-15% could be added in the encapsulation for the PIP/SiO₂ nanoparticles with a high conversion (70-80%), small particle size (40 nm), and provided high encapsulation efficiency (75-80%) via this novel method.

Consequently, the optimum condition of PIP-VTS-SiO₂ synthesis was also applied for the synthesis of PIP-MPS-SiO₂ nanoparticles. It was found that at the same condition, the particle size of PIP-MPS-SiO₂ was 40 nm, monomer conversion was 84% and grafting efficiency was 74%. However, the type of silane coupling agents did not seem to have any significant effect on the synthesis of PIP-SiO₂ nanoparticles.

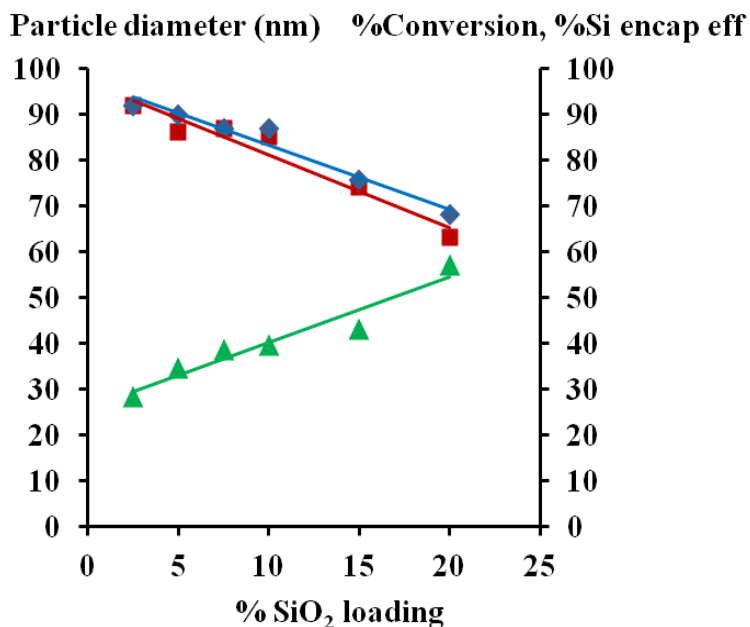


Figure 5.5 Effect of silica loading on PIP-SiO₂; (▲) Particle diameter, (■) %Si encapsulation, (◆) %Conversion. Condition: M/H₂O = 0.3, SPS = 1 %wt, SDS = 3 %wt based on monomer.

5.4 Particle Size Distribution of PIP-SiO₂ Nanocomposites

The particle size distribution characterized by DLS was used to identify the dispersion of nano-SiO₂ in the PIP matrix. For PIP without SiO₂ particles, a particle size of 24 nm and a narrow size distribution of 0.02 were obtained as shown in Figure 5.6 a. For PIP/SiO₂ (untreated SiO₂ of 10 %wt) (Figure 5.6 b), two-phase dispersion of nano-SiO₂ with average particle size of 10 nm and PIP domain with an average particle size of 22 nm was observed. It can be clearly seen that the untreated SiO₂ particles were not able to separate and stabilize due to the high polarity of their surface, resulting in heterogeneity and free polymer formation. Interestingly, the effective dispersion of silica in the PIP latex and an uniform size (average particle diameter of 35 nm) of the composite product were produced for PIP-VTS-SiO₂ (VTS-

SiO₂ of 10 %wt) as illustrated in Figure 5.6 c. The polydispersity index of PIP/unmodified SiO₂ (PDI = 0.16) was higher and the particle size distribution became boarder than that of PIP-VTS-SiO₂ (PDI =0.02). This observation from the size distribution curves provides evidence for an uniform dispersion of PIP-modified SiO₂. Therefore, differential microemulsion polymerization of isoprene on modified SiO₂ could provide PIP-SiO₂ nanoparticles with a narrow size distribution resulting in homogeneous composite latex.

For appearance of PIP-SiO₂ latex, the silica agglomeration and phase separation were observed for PIP/untreated SiO₂ latex due to the precipitation of silica particles at the bottom phase and the dispersion of PIP particles at the top phase (Figure 5.7 a). Nevertheless, PIP/VTS-SiO₂ latex including 10% wt of nano-SiO₂ was kept in a period of time of 1-6 months to investigate the colloidal stability. It was seen that homogeneous and stable colloidal latex were observed during about 6 months and the particle size and size distribution of nanocomposite did not change (Figure 5.7 b). After rubber precipitation, the aggregated silica particles were precipitated onto PIP rubber for PIP/untreated SiO₂; however, the agglomerated silica disappeared for PIP/VTS-SiO₂. This can be explained that the synthesis of PIP/SiO₂ nanoparticles via differential microemulsion polymerization had a high colloidal stability and reduction of silica aggregation.

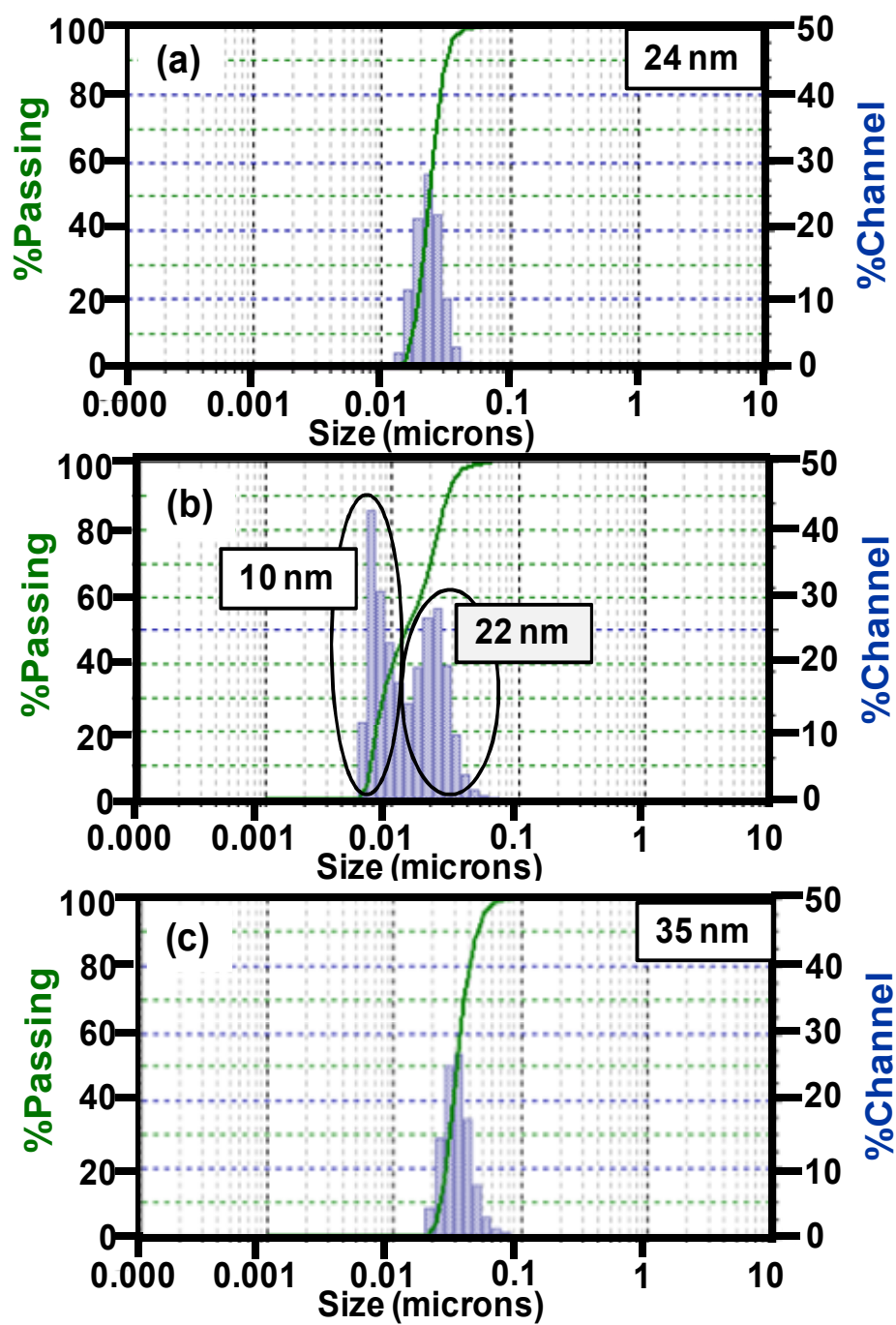


Figure 5.6 Particle size distribution of samples (a) PIP, (b) PIP/untreated SiO₂ (10 %wt) and (c) PIP-VTS-SiO₂ (10 %wt).

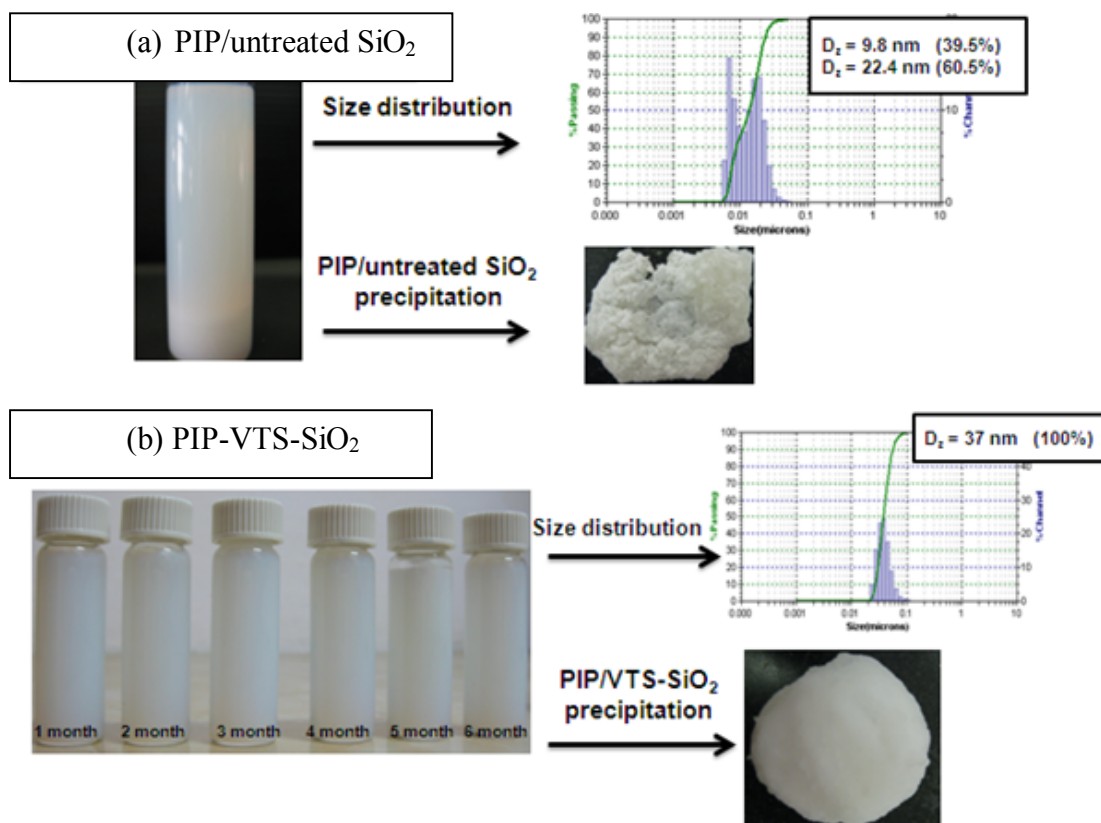


Figure 5.7 Appearance of (a) PIP/untreated SiO₂ and (b) PIP-VTS-SiO₂.

5.5 Morphology of PIP-SiO₂ nanocomposites

Morphology of PIP-SiO₂ nanocomposites characterized by TEM is illustrated in Figure 5.8. For PIP/untreated SiO₂ (at 10 %wt), silica particles as dark domains were aggregated inside the polyisoprene matrix as lighter domains (Figure 5.8a). Free polyisoprene and agglomerated silica appeared; thus a heterogeneous structure of PIP-SiO₂ using untreated SiO₂ was observed due to interface debonding between the silica particle and polyisoprene matrix. For PIP-VTS-SiO₂ (at 10 %wt) (Figure 5.8b) and PIP-MPS-SiO₂ (at 10 %wt) (Figure 5.8c), these morphologies showed the encapsulation of dark SiO₂ cores with white polymeric layer shells around the core. Interestingly, the nanosized SiO₂ particles were well-dispersed inside the polymer latex as regular spheres and no agglomeration morphology of composite particles was

predominantly observed. Therefore, nano-SiO₂ particles were encapsulated with a PIP shell, indicating that core/shell nanoparticles have been successfully produced from a differential microemulsion polymerization. The particle sizes of the composite as seen from the TEM photograph were about 30 nm and 40 nm respectively for PIP-VTS-SiO₂ and PIP-MPS-SiO₂ in good agreement with the DLS characterization.

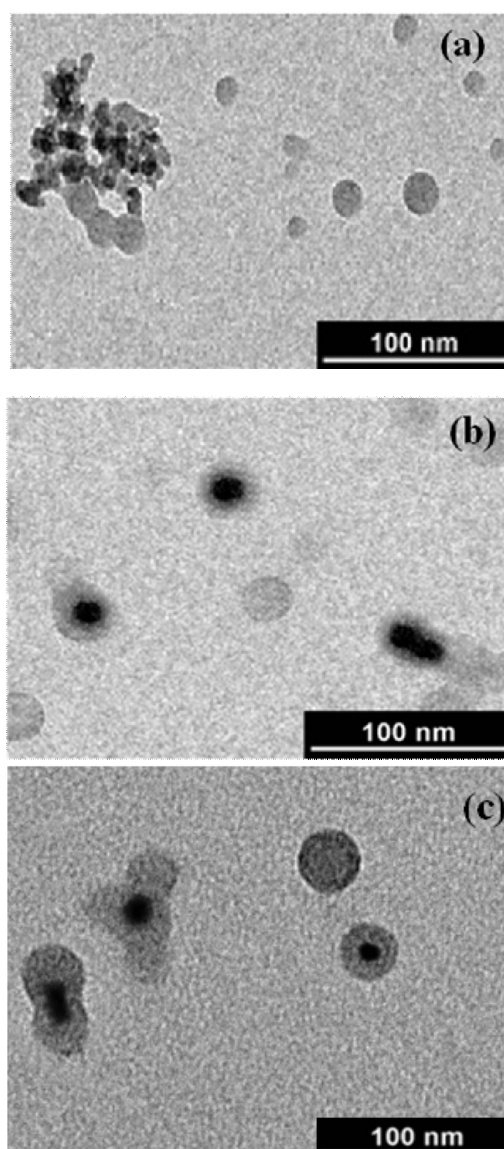


Figure 5.8 TEM micrographs of (a) PIP/untreated SiO₂, (b) PIP-VTS-SiO₂, (c) PIP-MPS-SiO₂.

5.6 Proposed Mechanism for PIP-SiO₂ Composite Nanoparticles

A PIP-SiO₂ formation mechanism with controlled morphology of the core/shell is proposed in Figure 5.9. The silica surface modification using organosilane coupling agents was firstly carried out through hydrolysis and polycondensation to produce the carbon double bonds on the silica surface. For pretreatment, the polarity of the silica surface was decreased (Figure 5.9a). Before polymerization, SPS initiator and SDS surfactant were dispersed in the aqueous silica dispersion. The interface between the oil phase and the aqueous phase could stabilize the colloidal particles by using SDS and the hydrophobic group of the surfactant tended to turn towards the oil phase and the hydrophilic group turned towards the aqueous phase used as the reaction medium (Figure 5.9b). For a differential microemulsion polymerization, the system consisted of water, water-soluble initiator, nonaggregated surfactants, nonagglomerated silica and a very small amount of monomer droplets (isoprene). The initiator decomposed in an aqueous phase to generate free radicals which generated reactive monomer radicals on the silica surface for the initiation stage (Figure 5.9c) and the primary monomer radicals were then polymerized to produce the oligomeric radicals resulting in chain propagation (Figure 5.9d). Therefore, the polymers could graft onto the silica surface through encapsulation to form a silica core and a polymer shell morphology.

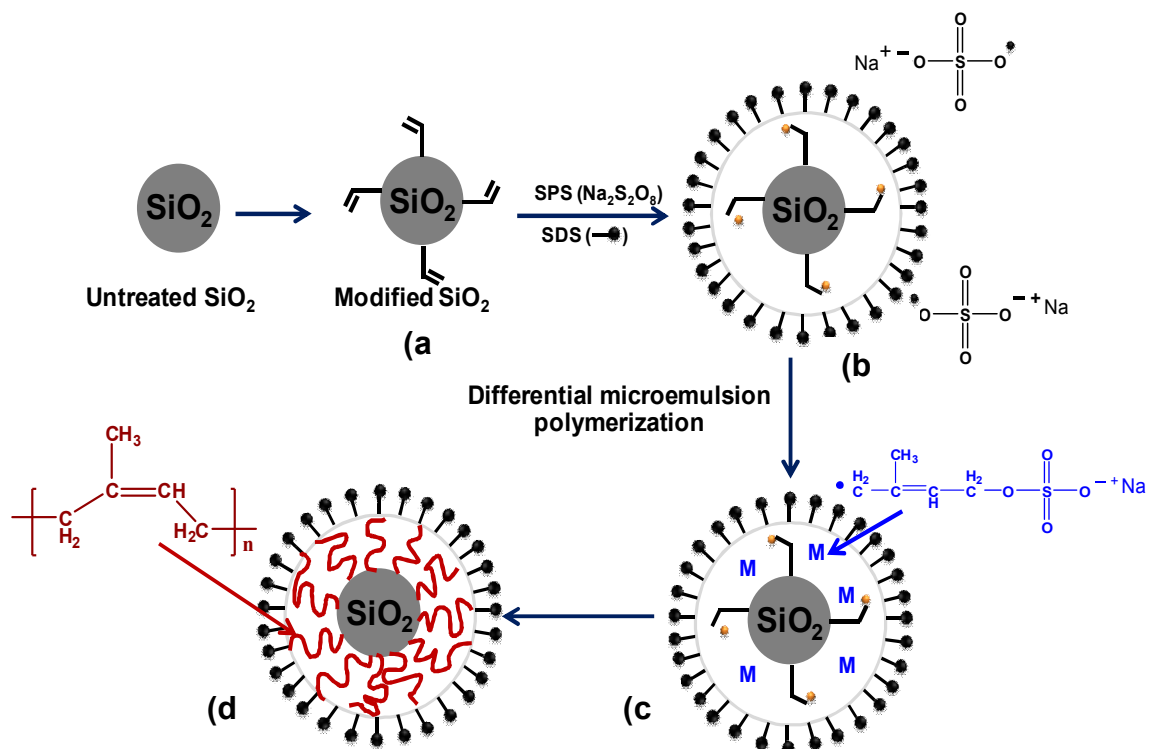


Figure 5.9 The proposed formation mechanism of nanosize-SiO₂ encapsulated by nanosized PIP with core/shell morphology.

5.7 Thermal Properties of PIP-SiO₂

The silica loading affected the decomposition temperature of PIP-SiO₂ nanoparticles as shown in Figure 5.10. The thermograms of PIP and PIP-SiO₂ show a one-step polymer degradation and provide smooth weight loss curves, indicating the good compatibility between PIP and nano-SiO₂. Comparison with PIP-untreated SiO₂, the untreated nano-SiO₂ had a initial weight loss below 100 °C which is related to the elimination of absorbed water from the silica surface [65] and a two-step weight loss at 390 and 430°C was observed due to incompatibility between the silica and the polymer. The SiO₂ content in the PIP/SiO₂ composite increased with increasing silica

loading. From the thermogram, it is seen that the maximum decomposition temperature of PIP filled with VTS-SiO₂ at 0, 10, 15, 20 %wt was 438, 455, 475, and 440°C, respectively. This implies that the nano-SiO₂ could uniformly disperse in the PIP matrix resulting in the high thermal stability of the nanocomposite compared with PIP-untreated SiO₂. However, the decomposition temperature was decreased at high silica loading (20 %wt) due to an agglomeration of nano-SiO₂ in the PIP matrix resulting in a reduction of the thermal resistance. Therefore, the nanosized PIP-SiO₂ at a silica loading of 10-15 %wt led to high thermal stability.

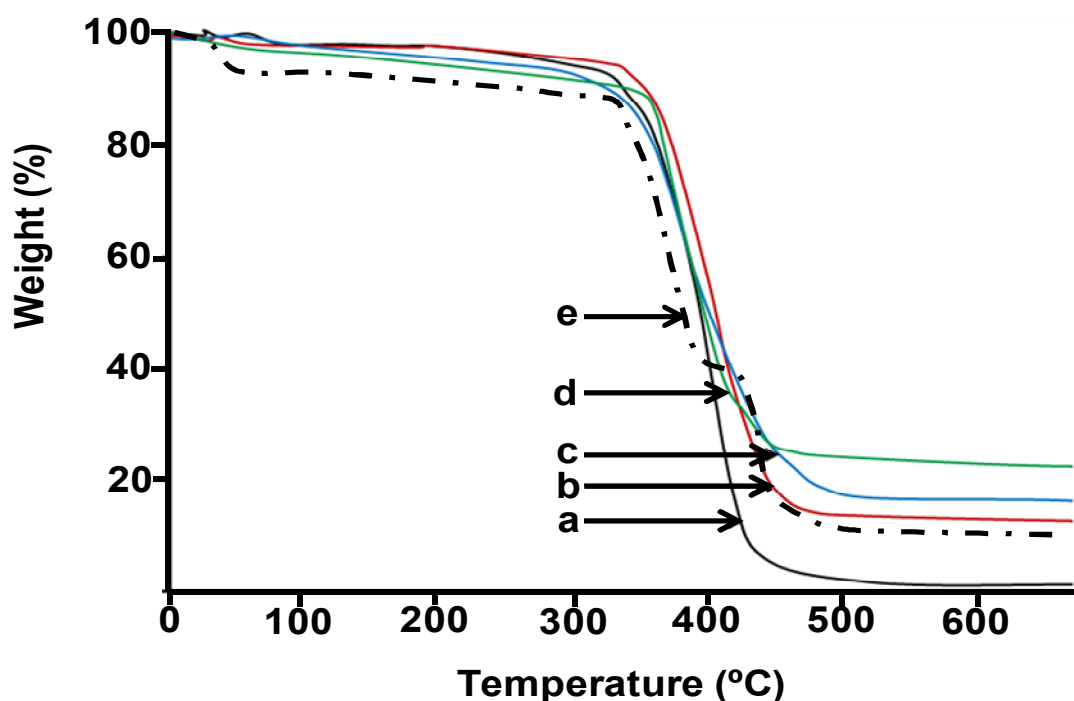


Figure 5.10 Thermograms of (a) nanosized PIP, (b) PIP-VTS-SiO₂ (10 %wt), (c) PIP-VTS-SiO₂ (15 %wt), (d) PIP-VTS-SiO₂ (20 %wt), (e) PIP-untreated SiO₂ (10 %wt).

CHAPTER VI

SYNTHESIS OF HYDROGENATED POLYISOPRENE-SILICA NANOCOMPOSITES VIA DIIMIDE REDUCTION

6.1 Introduction

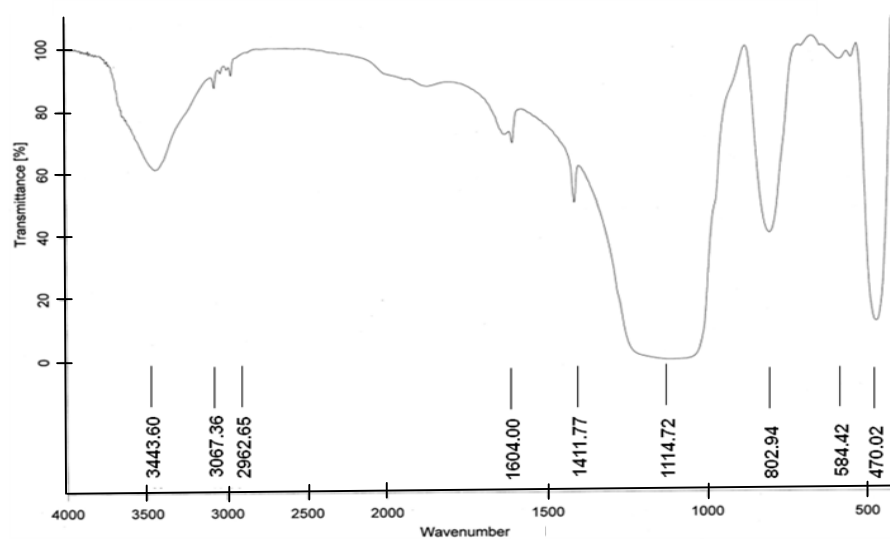
Nanocomposite materials have increasing potential for future applications due to their extraordinary properties based on the combined system of inorganic species with organic polymers. For rubber applications, the preparation of rubber/SiO₂ nanocomposites with elastomeric properties of rubber and reinforcement properties of nanosilica has gained much attention for the industrial production. However, rubber such as polybutadiene rubber and polyisoprene rubber has poor heat resistance due to the presence of carbon-carbon double bonds in their polymer backbones. The carbon double bonds of rubber are sensitive to oxygen, ozone and heat resulting in rubber degradation and the suppression of physical and thermal properties. To improve the thermal properties and oxidative stability of diene rubber, the carbon double bonds can be hydrogenated to the saturated carbon.

In the present work, a new nanocomposite of hydrogenated polyisoprene (HPIP)-SiO₂ was synthesized via diimide reduction. First, PIP-SiO₂ nanoparticles were synthesized by differential microemulsion polymerization of isoprene on silane treated nanosilica, and subsequently hydrogenated by diimide reduction in the presence of hydrazine/hydrogen peroxide using boric acid as promoter. Differential microemulsion polymerization is an advantageous method for the production of monodispersed PIP-SiO₂ nanocomposites using extremely low surfactant concentration and diimide hydrogenation is an environmental friendly process since it is normally performed in the absence of organic solvents and metal catalyst. The influences of process variables on PIP-SiO₂ hydrogenation and the kinetics for diimide hydrogenation were studied. Furthermore, a mechanism for the synthesis of HPIP-SiO₂ nanocomposite is also proposed.

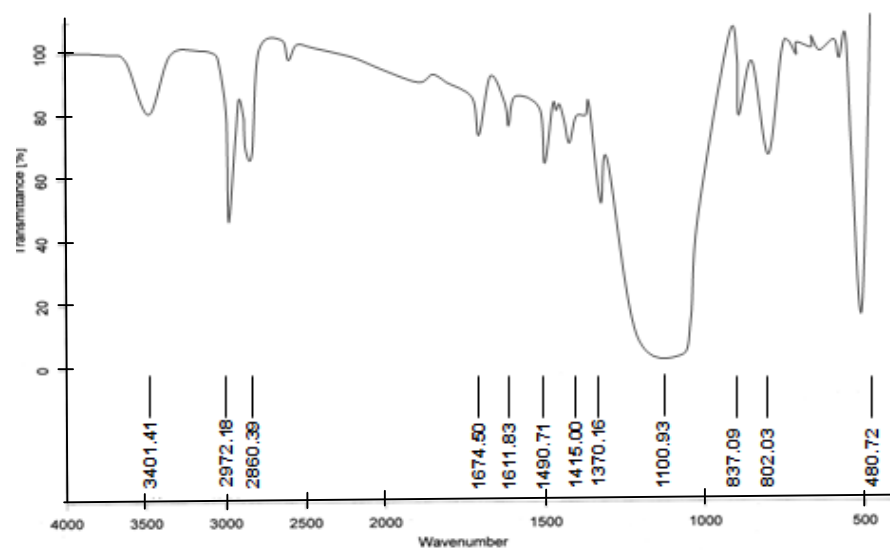
6.2 Characterization of PIP-SiO₂ and HPIP-SiO₂ Nanocomposites

The characterization of VTS-SiO₂ and PIP-SiO₂ by FTIR spectroscopy is shown in Figure 6.1. For VTS-SiO₂, the peaks at 1114, 802 and 470 cm⁻¹ correspond to Si-O-Si groups. The peaks at 3440, 3067 and 2962 cm⁻¹ relate to OH, CH and CH₂ stretching and the bands at 1600 cm⁻¹ (C=C) and 1417 cm⁻¹ (CH out of plane bending) are attributed to the VTS groups². For the PIP-VTS-SiO₂, new peaks at 2860 and 2972 cm⁻¹ are related to the methyl and methylene stretching of PIP, respectively. Additionally, the low intensity band at 837 cm⁻¹ and medium intensity band at 1674 cm⁻¹ correspond to the CH wag of trisubstituted olefin and the C=C stretching of PIP, respectively. These results imply that PIP was grafted onto the silica surface.

The NMR spectra of PIP-SiO₂ and HPIP-SiO₂ are shown in Figure 6.2. For PIP-SiO₂ (VTS-SiO₂ at 10 %wt), signals were observed at 5.09, 1.58 and 1.66 ppm corresponding to olefinic protons, CH₃ of *cis*-1,4 PIP and *trans*-1,4 PIP, respectively. The methylene groups appeared in the range of 1.98-2.15 ppm. For HPIP-SiO₂ (VTS-SiO₂ at 10 %wt), the peak at 5.08 ppm disappeared and new peaks for the saturated carbon centered at 0.8-1.2 ppm were sharply increased. The peak area of methylene groups appearing from 1.93 to 2.11 ppm dramatically decreased. The degree of hydrogenation (HD) calculated from the peak area of the olefinic protons (C=C) and the integrated peak area over the range of 0.8-2.0 ppm was 98%, implying that PIP-SiO₂ was completely hydrogenated under the optimum condition.



(a)



(b)

Figure 6.1 FTIR spectra of (a) VTS-SiO₂ and (b) PIP-VTS-SiO₂.

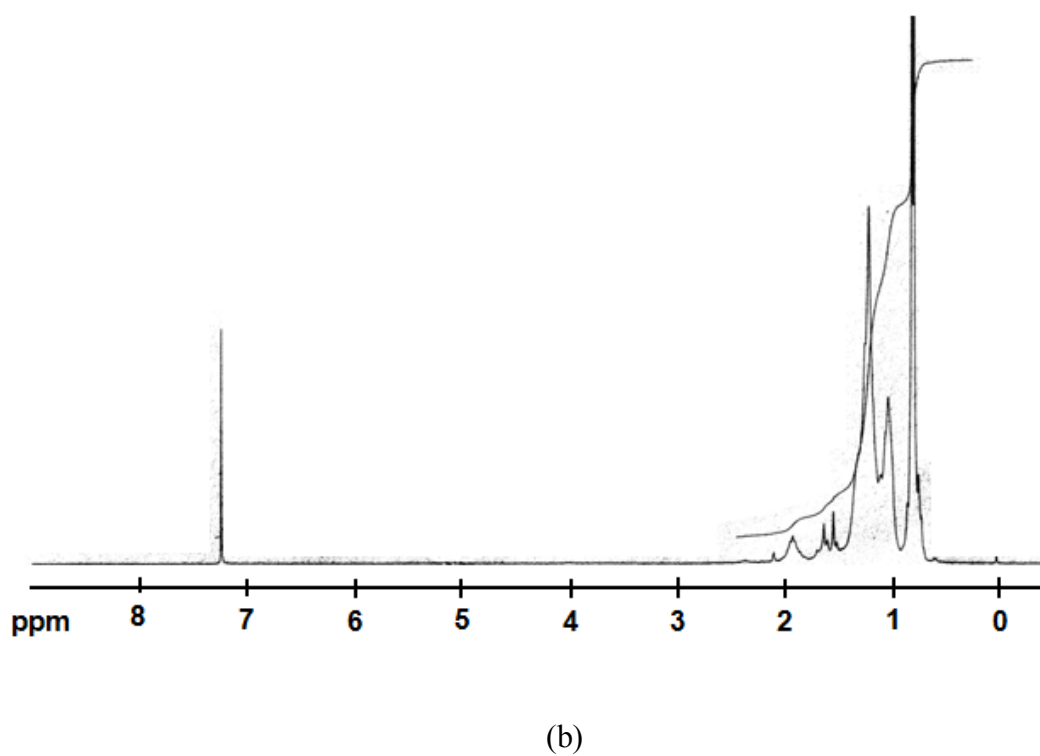
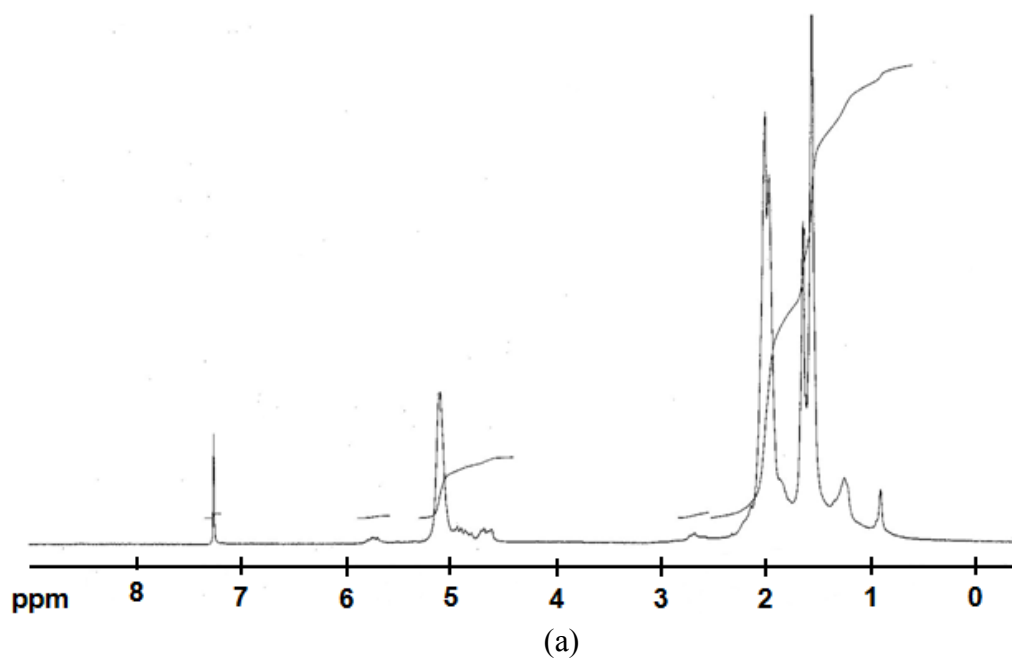


Figure 6.2 ^1H NMR spectra of (a) PIP-SiO₂, (b) HPIP-SiO₂ (98% HD).

6.3 Diimide Hydrogenation for Nanosized HPIP-SiO₂ Synthesis

The nanosized PIP-SiO₂ latex with a particle size of 35 nm and a narrow size distribution (0.02) was obtained by differential microemulsion polymerization. At the optimum condition, monomer to water ratio of 0.3, surfactant concentration of 3 %wt, initiator concentration of 1 %wt and SiO₂ loading of 10 %wt, a high monomer conversion (87%), grafting efficiency (78%), and silica encapsulation (80%) were achieved [178].

In this section, the process variables of hydrazine concentration, hydrogen peroxide concentration, amount of boric acid addition and water content on PIP-SiO₂ hydrogenation was investigated and the effects of all parameters are discussed in detail below.

6.3.1 Effect of Hydrazine Monohydrate and Hydrogen Peroxide Concentration

The influence of hydrazine (N₂H₄) and hydrogen peroxide (H₂O₂) concentration on hydrogenation of PIP-SiO₂ (43 nm) is shown in Figure 6.3. %HD linearly increased from 38 to 96% with an increase in N₂H₄ concentration from 0.5 to 3 mol/L. A large amount of diimide molecules are generated according to Eq. 6.1 and diimide species would attach to the unsaturated PIP chains (Eq. 6.2) resulting in increasing the hydrogenation degree in the nanosized PIP-SiO₂. However, above 5 mol/L of N₂H₄, %HD was suppressed due to the side reaction of diimide decomposition. For the redox reaction, H₂O₂ was used as a strong oxidizing agent to react with the hydrazine molecule for releasing the diimide species. It can be seen that HD is sharply increased from 40 to 96% with an increase in H₂O₂ concentration from 0.5 to 4.5 mol/L. Interestingly, the particle size of HPIP-SiO₂ essentially did not change over the studied range (42-47 nm).



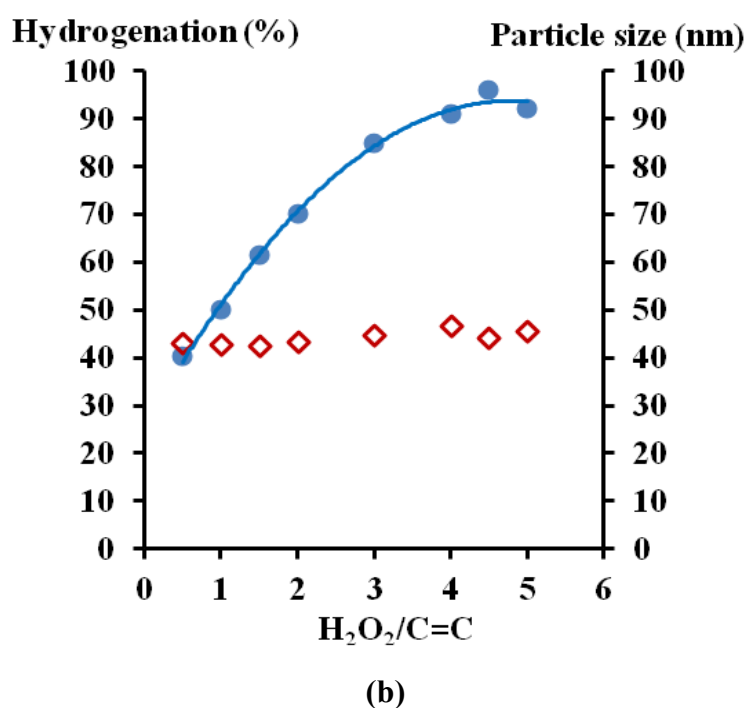
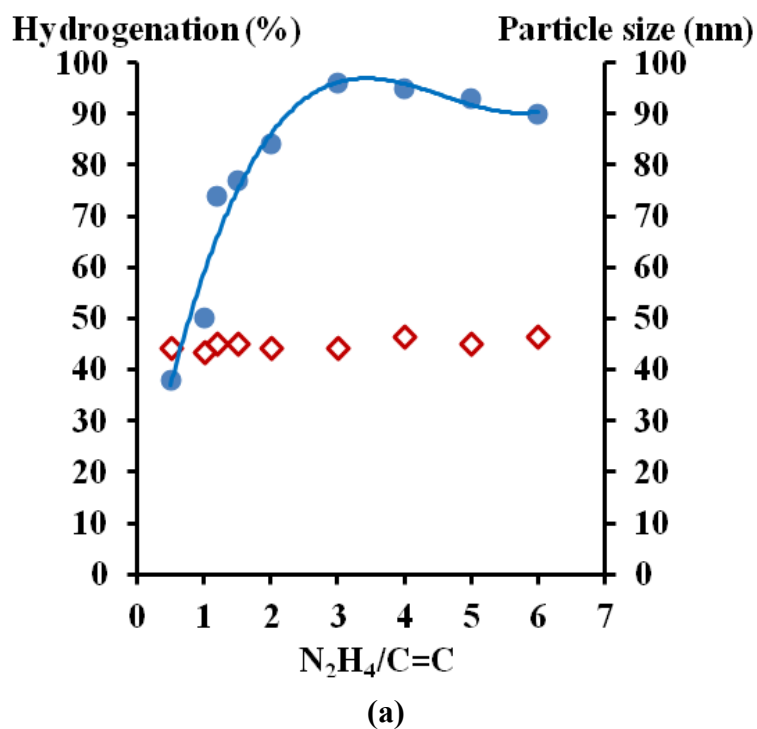


Figure 6.3 Hydrogenation of PIP-SiO₂: a) effect of $[\text{N}_2\text{H}_4]$ at $[\text{H}_2\text{O}_2] = 4.5$ mol/L. b) effect of $[\text{H}_2\text{O}_2]$ at $[\text{N}_2\text{H}_4] = 3$ mol/L. Condition: $[\text{H}_3\text{BO}_3] = 0.15$ mol/L, $[\text{C}=\text{C}] = 1$ mol/L, $[\text{H}_2\text{O}] = 10$ mol/L, $T = 70^\circ\text{C}$, time = 4 h. ● %HD, ◆ Particle size.

6.3.2 Effect of Boric Acid Concentration

Boric acid was added to improve the hydrogenation efficiency. The effect of boric acid concentration was studied over the range of 0.02-0.15 mol/L. Figure 6.4 shows that the hydrogenation degree is linearly proportional to the boric acid concentration. This phenomenon indicated that boric acid could promote hydrogenation with a high selectivity and could reduce the diimide side reactions such as disproportionation and decomposition as presented in Eqs. (6.3) and (6.4).



Without boric acid addition, the PIP conversion could not reach 70% in 4 h, suggesting that a small amount of boric acid is necessary to accelerate the hydrogen peroxide dissociation and to induce the diffusion of the diimide active species from the interphase between the water phase and the rubber phase.

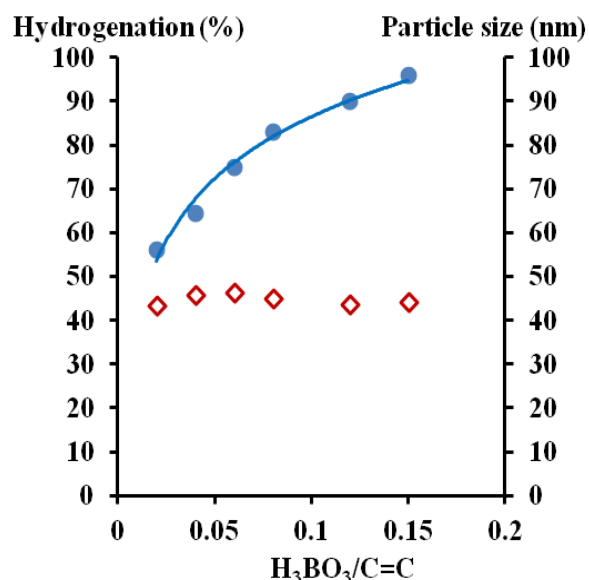


Figure 6.4 Effect of boric acid addition on PIP-SiO₂ hydrogenation. Condition: [N₂H₄] = 3 mol/L, [H₂O₂] = 4.5 mol/L, [C=C] = 1 mol/L, [H₂O] = 10 mol/L, Temp 70°C, time = 4 h. ●%HD, ◇Particle size.

For diimide hydrogenation of nitrile butadiene rubber latex, the hydrogenation efficiency using copper ion, silver ion and ferrous ion as catalysts was lower than that using boric acid addition [166].

6.3.3 Effect of Water Addition

De-ionized water was added into the reaction system to reduce the viscosity of the polyisoprene-SiO₂ latex. From Figure 6.5, increasing the water content in the system resulted a decrease in the hydrogenation level. The highest hydrogenation level of 96% was achieved at a low ratio of water to carbon double bonds (10/1). However, the low amount of water addition could reduce the viscosity of the latex and increase the interaction between the polymer particles and other substances. At high water addition, the reaction between hydrazine and hydrogen peroxide occurred in the aqueous phase; thus, the diimide active species was produced in the water phase and the diimide migration into the rubber phase was limited, and consequently the hydrogenation efficiency was decreased.

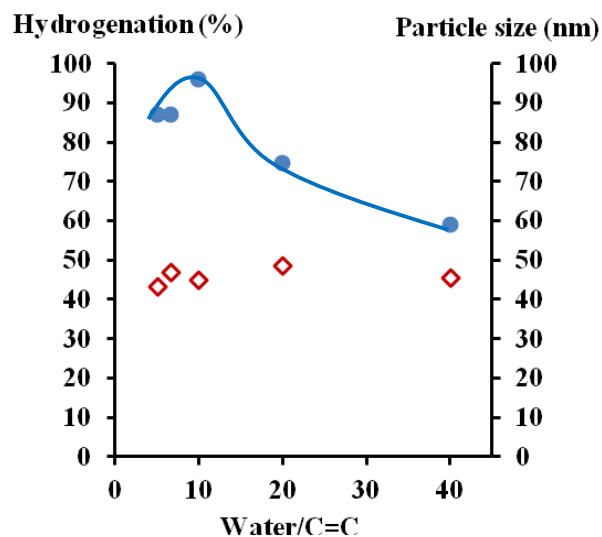


Figure 6.5 Effect of water addition on PIP-SiO₂ hydrogenation. Condition: [N₂H₄] = 5 mol/L, [H₂O₂] = 7.5 mol/L, [C=C] = 1 mol/L, [H₃BO₃] = 0.15 mol/L, T = 70°C, time = 4 h. ● %HD, ◇ Particle size.

6.4 Conversion Profile of Nanosized PIP-SiO₂ Hydrogenation

The PIP conversion versus reaction time profile at various reaction temperatures was studied over an interval of time of 0 to 5 h (Figure 6.6a). The double bond conversion was sharply increased with time initially, and then leveled off. It is suggested that diimide is a highly active intermediate species and is consumed at the surface of the unsaturated rubber particles, so the reduction of the double bonds is observed. For reaction times above 5 h, the PIP-SiO₂ conversion remained constant, implying that the mobility of the diimide was retarded in transferring to the carbon double bonds within the particles due to a mass transfer limitation [165]. Therefore, the highest hydrogenation efficiency of 98% could be obtained for hydrogenation of PIP-SiO₂ (particle size of 43 nm) within 5 h. This is due to the fact that the high surface area of the polyisoprene nanoparticles can interact with the diimide active species effectively and the diimide molecule can diffuse towards the double bonds inside the particle, resulting in an increase in HPIP-SiO₂ product.

The kinetics of diimide hydrogenation of nanosized HPIP-SiO₂ at different reaction temperatures was also investigated. From Figure 6.6b, the hydrogenation rate exhibited an apparent first-order rate law dependence on the double bond substrate concentration, as described by Eq. (6.5).

$$\frac{d[\text{C}=\text{C}]}{dt} = -k' [\text{N}_2\text{H}_2][\text{C}=\text{C}] \quad (6.5)$$

When diimide is a highly active intermediate, a pseudo steady state assumption is made, therefore, the rate of hydrogenation is a first order dependence on double bond concentration.

The fractional hydrogenation conversion, X is defined as

$$X = 1 - [\text{C}=\text{C}]_t / [\text{C}=\text{C}]_0 \quad (6.6)$$

where $[C=C]_t$ is the double bond concentration at reaction time t and $[C=C]_0$ is the initial double bond concentration.

Eqs. (6.5) and (6.6) can further be expressed in term of Eq. (6.7)

$$\ln(1-x) = -k' t \quad (6.7)$$

Plots of $\ln(1-x)$ versus time fit first order kinetics very well, and thus, the rate constant (k') is determined from the slope of these kinetic profiles. It was found that the rate constant for diimide hydrogenation of PIP-SiO₂ (43 nm) at 50, 60 and 70°C was 11.4×10^{-5} , 16.2×10^{-5} and 21.4×10^{-5} (s⁻¹), respectively. Comparison to PIP without SiO₂ (42 nm), the rate constant at 50, 60 and 70°C was 7.4×10^{-5} , 10.7×10^{-5} and 18.3×10^{-5} (s⁻¹), respectively. Thus, it is clearly seen that the rate constants for diimide hydrogenation of PIP-SiO₂ nanoparticles were higher than that of PIP without SiO₂. This indicated that diimide is a highly active intermediate species and is consumed from the surface of the unsaturated PIP particles toward the carbon double bonds core inside; hence, the diimide mobility in the PIP particle without a SiO₂ core was retarded in transferring to the carbon double bonds deep inside the particles due to a mass transfer limitation resulting in a lower kinetic rate constant of PIP hydrogenation than that for core/shell PIP-SiO₂ hydrogenation.

Previous work reported that the rate constant of NRL [141] and skim natural rubber (SNRL) [142] hydrogenation by using diimide reduction was 5.4×10^{-5} and 5.96×10^{-5} (s⁻¹), respectively. Hence, the higher rate of diimide hydrogenation for PIP-SiO₂ nanoparticles was achieved due to the smaller particle size of PIP compared with NRL. From a kinetic study, the rate of PIP-SiO₂ hydrogenation increased with increasing reaction temperature. It can be explained that high temperature could increase the probability of collision between the reactants with the polymer chains and accelerate the diimide mobility to coordinate with the double bonds [139], resulting in a high HPIP-SiO₂ yield. Interesting, high reaction temperature and prolong reaction time were not required for the synthesis of HPIP-SiO₂ nanocomposites, implying that the proposed

synthetic route is a novel technique for the preparation of a new nanocomposite of HPIP-SiO₂ via diimide reduction.

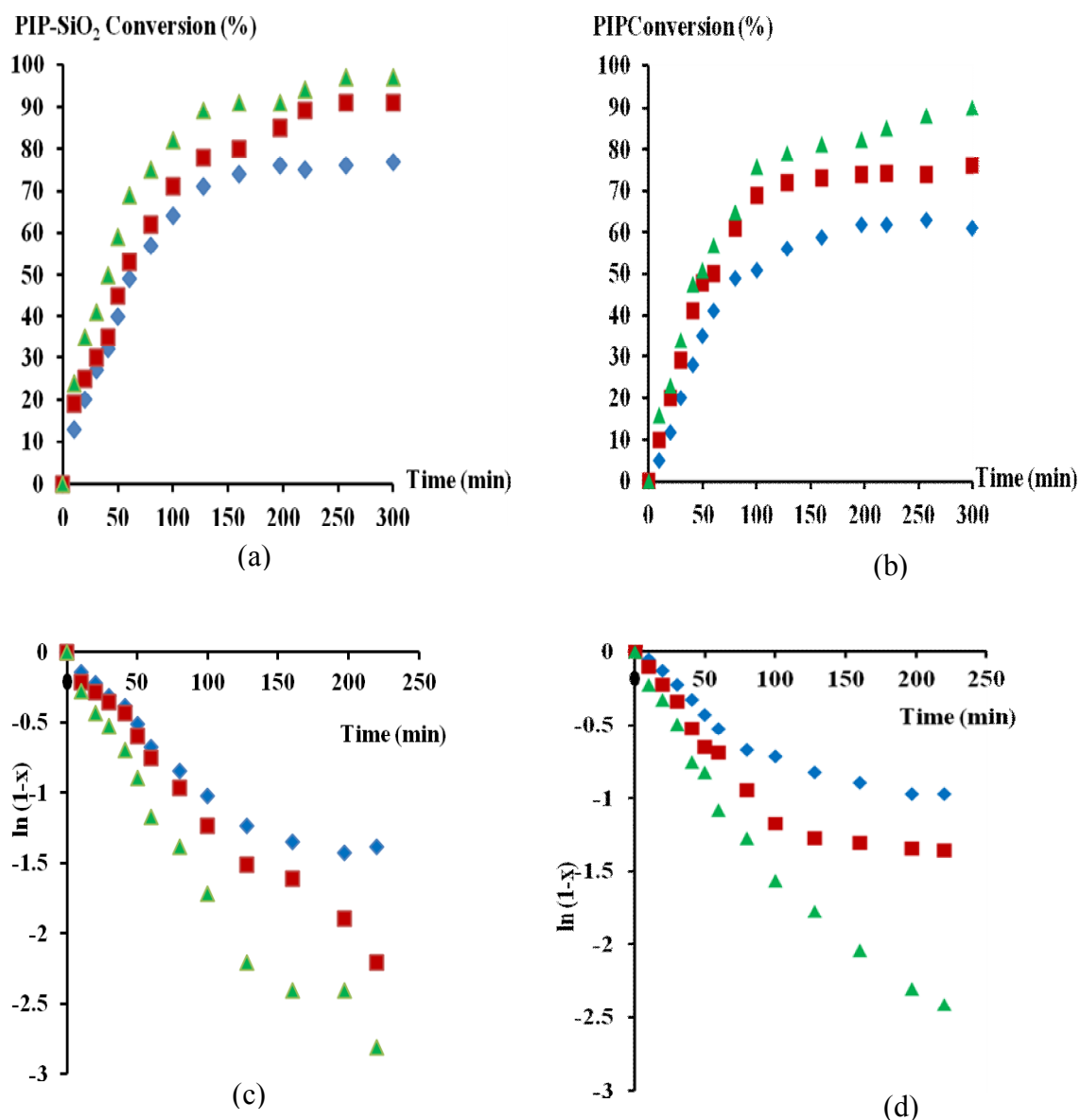


Figure 6.6 Conversion profiles of (a) HPIP-SiO₂, (b) HPIP without SiO₂ and first order in ln plot of (c) HPIP-SiO₂, (d) PIP without SiO₂. Condition: [N₂H₄] = 5 mol/L, [H₂O₂] = 7.5 mol/L, [C=C] = 1 mol/L, [H₃BO₃] = 0.15 mol/L, [H₂O] = 10 mol/L. ◆ = 50°C, ■ = 60°C, ▲ = 70°C.

Rate constants for diimide hydrogenation of PIP and PIP-SiO₂ nanoparticles presented in Table 6.1 are fitted by a linear Arrhenius plot. The apparent activation energy (E_a) calculated from a least squares regression analysis of ln(k') versus 1/T for hydrogenation of PIP and PIP-SiO₂ was 39.8 and 29.1 kJ/mol, respectively over the temperature range of 50 and 70°C. The hydrogenation rate of core/shell PIP-SiO₂ nanoparticle was higher than that of PIP nanoparticle as confirmed by the rate constant and activation energy. From previous work, the activation energy for diimide hydrogenation of NBR catalyzed by a gelatin-cupric ion complex and boric acid was 65.0 and 35.9 kJ/mol, respectively [179].

Table 6.1 Rate constant and activation energy of PIP and PIP-SiO₂ nanoparticles.

Hydrogenation	k' x 10 ⁵ (s ⁻¹)			Activation energy (E _a) (kJ/mol)
	323 K	333 K	343 K	
Nanosized PIP ^a	7.7	10.7	18.3	39.8
Nanosized PIP-SiO ₂ ^a	11.4	16.2	21.4	29.1

^a condition: [N₂H₄] = 5 mol/L, [H₂O₂] = 7.5 mol/L, [C=C] = 1 mol/L, [H₃BO₃] = 0.15 mol/L, [H₂O] = 10 mol/L.

6.5 Proposed New Route for Nanosized HPIP-SiO₂ Synthesis

A synthetic route for a new nanocomposite of HPIP-SiO₂ is proposed in Figure 6.7. Nano-SiO₂ was pretreated using VTS coupling agent through hydrolysis and polycondensation to produce the carbon double bonds on the silica surface. SPS initiator and SDS surfactant were dispersed onto the silica surface due to a hydrophilic effect. The interface between the monomer phase and the aqueous phase could stabilize the colloid particles by using SDS and the hydrophobic group of the surfactant tended to turn towards the monomer phase and the hydrophilic group

turned towards the aqueous phase as the reaction medium (Figure 6.7b). For differential microemulsion polymerization, the system consisted of water, a water-soluble initiator, nonaggregated surfactants, nonagglomerated silica and a very small amount of monomer droplets (isoprene). The initiator decomposed to form primary radicals which generated reactive monomer radicals on the silica surface for the initiation stage and then isoprene was polymerized resulting in chain propagation. Therefore, PIP could graft onto the silica surface with a core/shell morphology. PIP-SiO₂ latex was then hydrogenated by diimide reduction; diimide active species were generated from the redox reaction between hydrazine (N₂H₄) and hydrogen peroxide (H₂O₂). This step was accelerated under thermal dissociation of hydrazine which is promoted by boric acid (H₃BO₃). Then, carbon-carbon double bonds were reacted with the diimide molecule through a coordination process. The hydrogen was transferred through a hydride shift mechanism to produce an alkyl complex, and finally HPIP-SiO₂ was obtained.

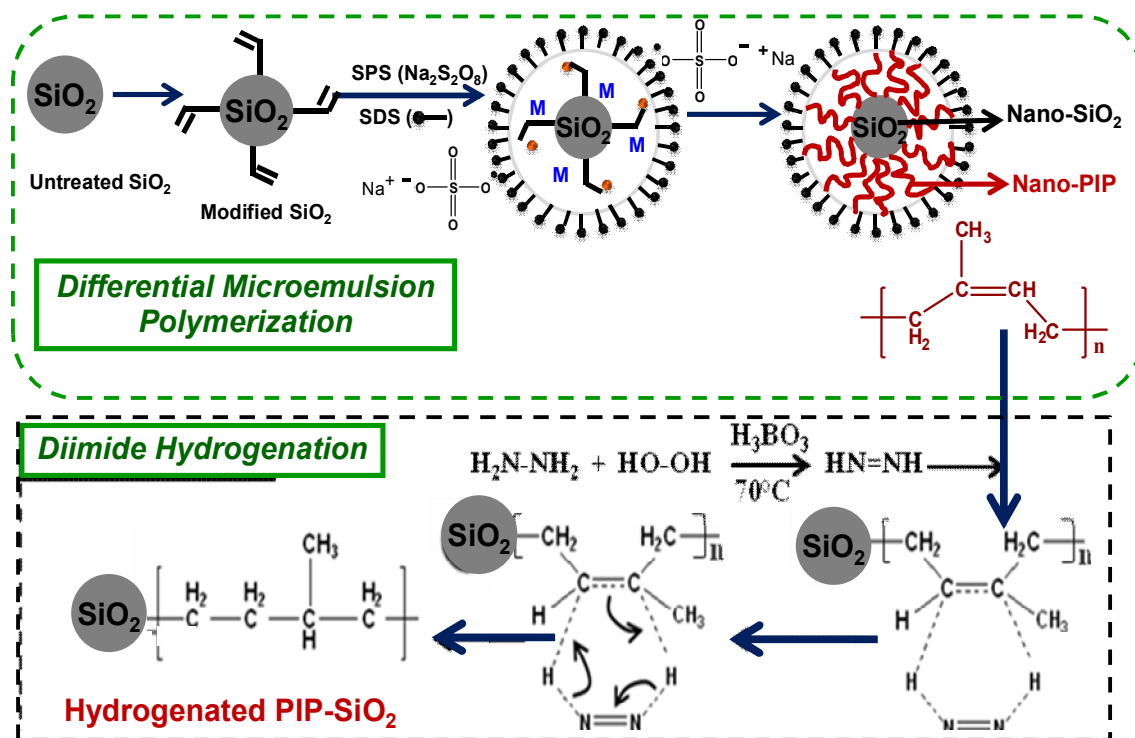


Figure 6.7 Proposed mechanism for synthesis of HPIP-SiO₂ nanocomposite.

6.6 Morphology of HPIP and HPIP-SiO₂ Nanocomposite

Morphologies of HPIP-SiO₂ and HPIP without SiO₂ at different hydrogenation levels are shown in Figure 6.8. It is seen that the polyisoprene nanoparticles with uniform size were spherical with smooth surface, and the average particle size was about 37-42 nm (Figure 6.8a). The surface morphology of all rubber samples was stained with OsO₄ to increase the contrast and gradation of the particles. From Figure 6.8b, when the degree of hydrogenation increased to 64%, the lightly color domain at the outer layer of the nanoparticles appeared, suggesting a core/shell morphology. HPIP at 64 %HD had a shell thickness of about 15-20 nm. This can be explained in that OsO₄ agent could stain only the carbon-carbon double bonds, the dark color domain indicated a high double bond concentration while the lightly color domain indicated a region of low C=C amount. This observation is in good agreement with the layer model for understanding the C=C distribution in the rubber during diimide hydrogenation. For the highest hydrogenation degree in the HPIP latex (Figure 6.8c), the particles showed a lighter color than that of PIP and the core/shell morphology of HPIP at 98 %HD was not observed due to the absence of carbon-carbon double bonds.

Further morphological study is investigated for HPIP-SiO₂ nanocomposites at various degrees of hydrogenation. After being encapsulation with nanosilica, a core/shell structure was clearly observed with a shell thickness of PIP of about 30- 35 nm and a core thickness of silica of about 12-15 nm (Figure 6.8d). A single silica particle was observed due to the thickness of the core close to the size of one silica nanoparticle (12 nm), indicating the monodispersion. At a HPIP-SiO₂ of 64 %HD (Figure 6.8e), the shell of the composite showed a lighter color than that of HPIP-SiO₂. According to the layer model, the rubber particle was hydrogenated from the outer layer to the center of the particle due to the limitation of diimide mobility towards carbon double bonds deep inside the particle. From Figure 6.8f, when the degree of hydrogenation continued to increase to 98%, the composite with a lightly color shell was observed. Furthermore, HPIP at 98 %HD essentially showed core/shell morphology containing the lighter color of a shell than that of HPIP-SiO₂ at 64% HD.

It can be concluded that well-dispersed HPIP-SiO₂ nanocomposites are approximately spherical particles of about 45 nm and the core, SiO₂ nanoparticles, were successfully encapsulated by a shell of hydrogenated polyisoprene rubber.

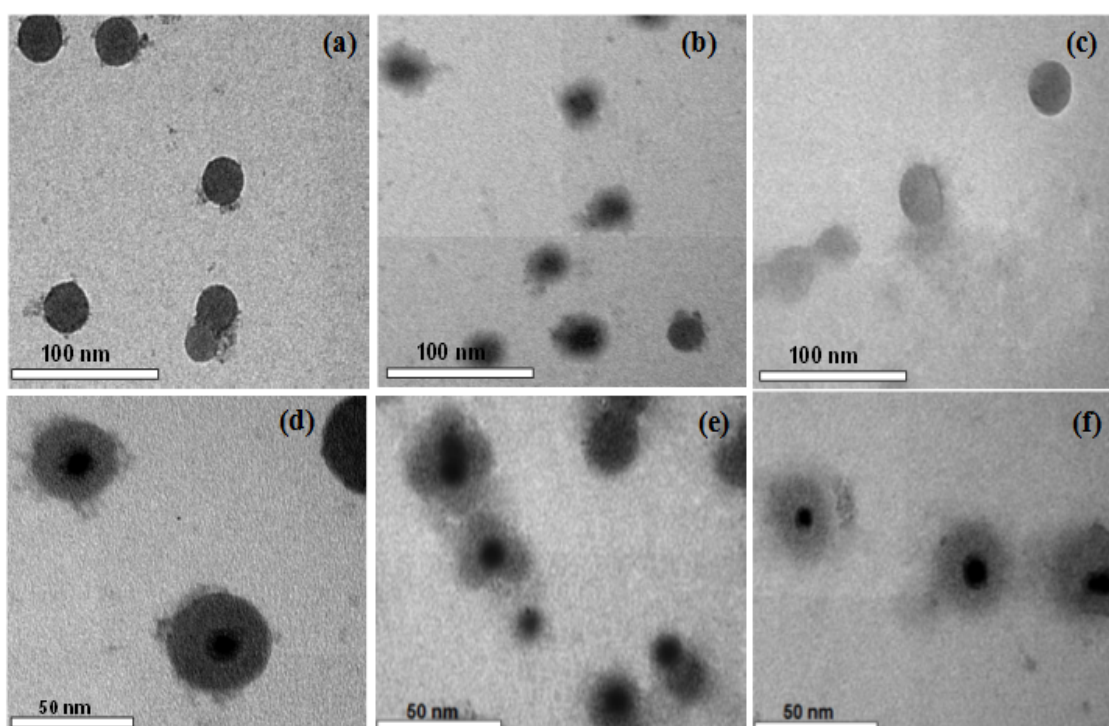


Figure 6.8 TEM micrographs of (a) PIP, (b) PIP at 64 %HD, (c) PIP at 94 %HD, (d) PIP-SiO₂, (e) HPIP-SiO₂ at 64% HD and (f) HPIP-SiO₂ (98% HD).

6.7 Thermal Analysis of HPIP-SiO₂ Nanocomposites

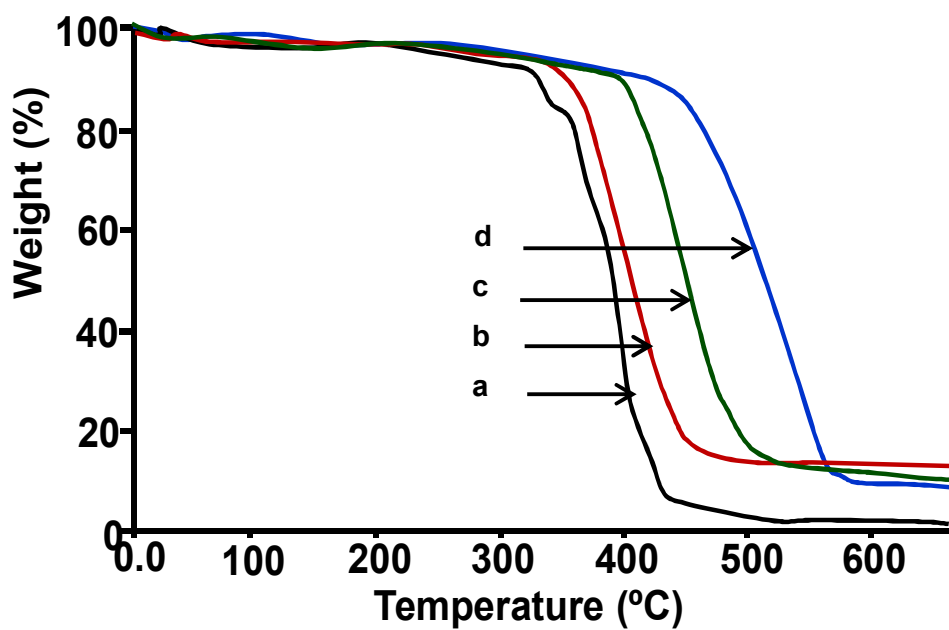
Degradation behavior of the HPIP-SiO₂ nanoparticles at various hydrogenation levels was investigated using thermogravimetric analysis. From Figure 6.9, the thermograms of rubber samples show a one-step polymer

degradation and provide smooth weight loss curves and the detailed data are summarized in Table 6.2. The decomposition of the rubbers PIP and HPIP was observed at temperatures over the range of 350 to 550 °C. On comparison with nanosized PIP, the degradation temperature of modified SiO₂ filled nanosized PIP increased due to the high thermal resistance of the nanofiller and the hindered thermal movement of the polymer molecular chains [180]. With the effect of a high interaction in an organic–inorganic composite, the inorganic phase could restrict the movement of the polymer chains and thus, scission of the chains becomes more difficult and leads to an increase in the decomposition temperature [181]. From these results, it found that T_{id} and T_{max} of PIP-SiO₂ were shifted approximately 19 and 29 °C towards a higher temperature as compared to unfilled PIP.

After diimide hydrogenation, PIP-SiO₂ (0% HD), HPIP-SiO₂ (64%HD) and HPIP-SiO₂ (98%HD) had a decomposition temperature of 416, 483 and 521°C, respectively. It is clearly seen that the degradation temperature is proportional to the hydrogenation level and HPIP-SiO₂ at the highest HD (98%) exhibited the maximum decomposition temperature. As a result, T_{id} and T_{max} of HPIP-SiO₂ at 98% HD were shifted 70 and 105 °C to a higher temperature than that PIP-SiO₂. This implied that thermal stability of nanosized polyisoprene depended on the density of the carbon-carbon double bonds. The sigma bonds are stronger than the π bonds because the sigma bonds contain hybridized atomic orbitals. Therefore, hydrogenation involves the breaking of π bonds with a change to sigma bonds resulting in an increase in thermal stability of HPIP-SiO₂ nanoparticles. It could be concluded that the synthesis of HPIP-SiO₂ nanocomposites shows improved thermal stability and dramatically an increase in heat resistance.

Table 6.2 Thermal properties of rubber nanocomposite

Rubber	Hydrogenation degree (%)	T _{id} (°C)	T _{max} (°C)
Nanosized PIP	-	349.3	387.1
PIP-VTS-SiO ₂	0	368.2	416.2
HPIP-VTS-SiO ₂	64	429.2	483.6
HPIP-VTS-SiO ₂	98	437.9	521.0

**Figure 6.9** Thermograms of (a) nanosized PIP, (b) PIP-SiO₂, (c) HPIP-SiO₂ (64% HD) and (d) HPIP-SiO₂ (98% HD).

CHAPTER VII

MECHANICAL PROPERTIES OF RUBBER/SILICA NANOCOMPOSITES

7.1 Introduction

Natural rubber as a diene polymer is used extensively in many applications and in the manufacturing industry for automobile and airplane rubber components. Due to its high elasticity property and resilience, natural rubber latex can be widely used for applications such as films, coatings, and membranes. However, NR has a drawback in mechanical properties and thermal stability due to the carbon-carbon double bonds present in polyisoprene backbone. Many previous works have reported on the improvement of the mechanical properties of SiO₂ filled NR composites [148-150]. However, difficulties of such an approach for NR/silica composites are due to potential incompatibilities between silica and NR due to the difference of polarity and surface energy, resulting in a phase separation, filler agglomeration and the weakening of mechanical and thermal properties. Admicellar polymerization [182] and radiation induced admicellar polymerization [183] have been used to prepare polyisoprene/silica composites with superior mechanical properties compared with polyisoprene/unmodified SiO₂.

Since it is desirable to achieve high mechanical properties, the SiO₂ encapsulation with polymer and hydrogenation have been developed. This work is divided into 3 parts. 1) For diimide hydrogenation of PIP, the dynamic mechanical analysis of HPIP was studied. 2) For monodispersed PIP-SiO₂ nanocomposites with a uniform particle size distribution used as an effective filler in NRL, the mechanical properties of NR/PIP-SiO₂ nanocomposite were also investigated. 3) For hydrogenated PIP-SiO₂ nanocomposites used as a new nanofiller in NRL, the mechanical properties and thermal stability as well as ozone resistance of NR filled with HPIP-SiO₂ nanocomposite were also investigated.

7.2 Dynamic Mechanical Properties

Dynamic mechanical analysis is a technique to measure the mechanical properties of material as a function of temperature and frequency. The data was reported as modulus and $\tan \delta$ after applying a sinusoidal force. The modulus as an in-phase component and an out of phase component was expressed in term of storage modulus (E') and loss modulus (E''), respectively. The storage modulus is the measure of elastic behavior while $\tan \delta$, which calculated from the ratio of the loss modulus to storage modulus, is a measure of the energy dissipation of material.

7.2.1 Dynamic Mechanical Properties of EPM

The elastic modulus of a rubber and its mechanical damping or energy dissipation characteristics as a function of frequency and temperature can be measured by dynamic mechanical analysis. The storage modulus or elastic modulus is measured from the elastic energy storage of the rubber, indicating the stiffness of materials. From Figure 7.1 (a), it is seen that the storage modulus of PIP and HPIP was decreased with an increase in temperature and rapidly decreased in the transition region due to the mobility and deformation of the polymer chains under the action of an external force. HPIP at 57%, 78% and 94% hydrogenation had a storage modulus of 451 MPa, 486 MPa and 493 MPa, respectively and the storage modulus of all HPIP samples were higher than that of polyisoprene (430 MPa). The improvement of storage modulus properties is due to the domains of poly(ethylene-co-propylene) segments produced from hydrogenation of the isoprene unit. Moreover, when polyisoprene was hydrogenated, the free volume and mobility are decreased by the replacement of the ethylene and propylene units resulting in a stronger effective interaction of the molecular chains and high stiffness of the ethylene-propylene rubber.

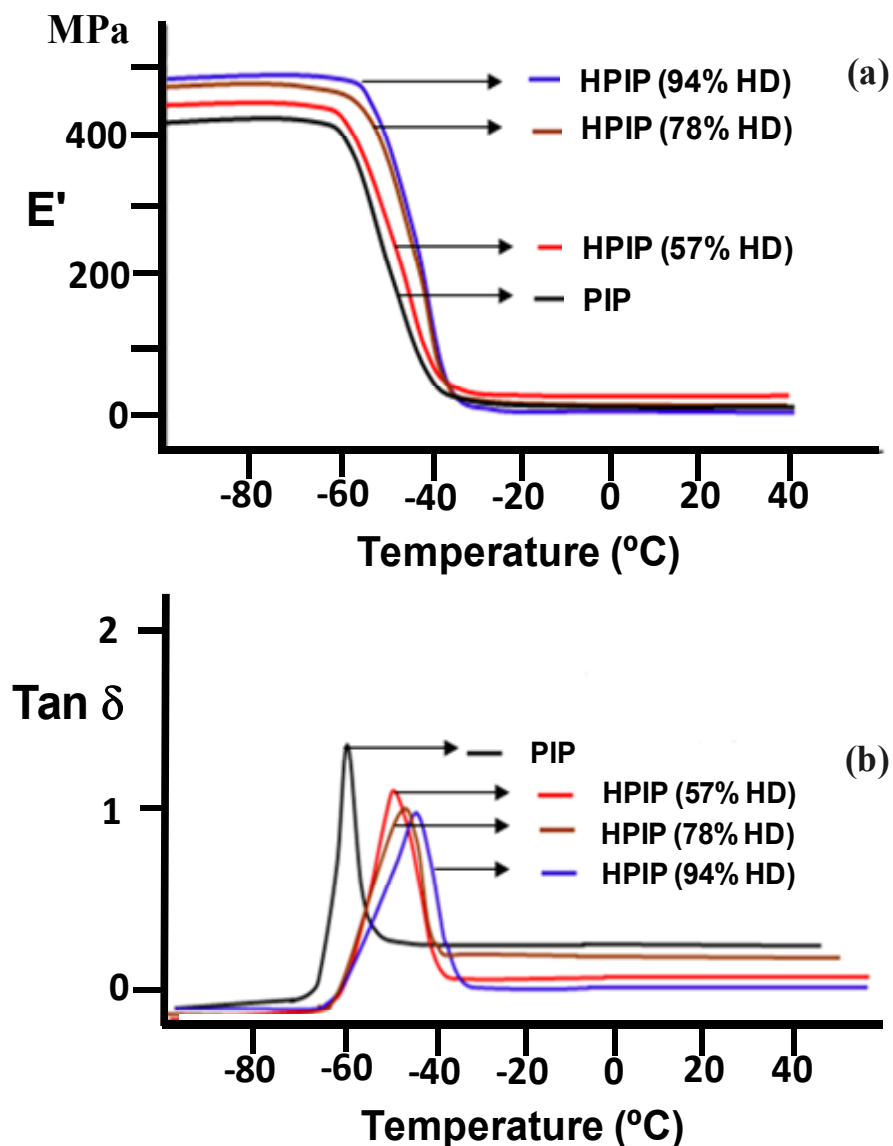


Figure 7.1 Temperature dependence of (a) storage modulus (E') and (b) loss tangent ($\tan \delta$) for PIP and HPIP.

The $\tan \delta$ determined from the ratio of dynamic loss modulus (E'') to storage modulus (E'). From Figure 7.1(b), HPIP at 94% hydrogenation showed a lower $\tan \delta$ than pure polyisoprene which indicated that HPIP had low dynamic loss or low viscous modulus due to a high interaction of the ethylene-propylene segments in the polymer chain.

The glass transition temperature (T_g) could be determined from the center of the peak of the $\tan \delta$ curves and is summarized in Table 7.1. PIP and HPIP had

a single glass transition temperature. The T_g value of HPIP increased over the range of 13-20°C compared with PIP. On hydrogenation, T_g of HPIP gradually increased from -59.9°C to -42.4°C with an increase in hydrogenation level from 0% to 94%. This result was due to the gradual replacement of amorphous segments of polyisoprene by crystalline ethylene segments in the structure of HPIP. A similar shift in T_g from -31°C to -11°C was observed for carboxylated styrene-butadiene rubber at 0% and 80% hydrogenation, respectively [140]. In comparison with ethylene-propylene diene rubber (EPDM), the T_g of 94% EPM nanoparticle is close to EPDM rubber (T_g = 44.6°C).

Table 7.1 Glass transition temperature and decomposition temperature of rubber samples

Rubber	Hydrogenation (%)	T_g (°C)	T_{id} (°C)	T_{max} (°C)
PIP	-	-59.9	359.7	425.4
HPIP	57	-47.9	373.5	450.1
	78	-46.1	422.6	480.9
	94	-42.4	447.3	510.1
EPDM ^a	-	-44.6	452.7	470.7

^aEPDM has an ethylene/propylene ratio of 50/50 and diene content of 9.5%.

7.2.2 Dynamic Mechanical Properties of NR/PIP-SiO₂ Nanocomposite

Dynamic mechanical analysis is a powerful technique for the determination of a rubber modulus as a function of temperature and frequency. For an optimum condition, PIP-VTS-SiO₂ and PIP-MPS-SiO₂ at 10 %wt of SiO₂ loading were selected to blend with NRL due to high monomer conversion and grafting efficiency. Modulus data in the form of the storage modulus (E') of NR, NR filled with 20 %wt of PIP-VTS-SiO₂ and 20 %wt of PIP-MPS-SiO₂ are shown in Figure 7.2a. The E' values of NR and composites exhibited a plateau curve below the glass transition temperature

(T_g) and decreased around the T_g . It is noted that the storage modulus of the unfilled NR (620 MPa) is much lower than that of the PIP-SiO₂ nanocomposite (915 MPa). In comparison with the NR composite, the E' values of NR filled with PIP-VTS-SiO₂ (871MPa) and NR filled with PIP-MPS-SiO₂ (860 MPa) were significantly higher than that of NR filled with 10 %wt untreated SiO₂ (direct mixing) (710 MPa) due to a superior compatibility and a good dispersion of the nanofiller (PIP-SiO₂) within the NR matrix. Therefore, the improvement of the storage modulus could be achieved by the addition of monodispersed PIP-SiO₂ nanocomposite into the NR latex, resulting in the enhancement of strength and stiffness of NR.

The mechanical damping behavior on the temperature dependence for NR filled with 20 %wt of PIP-VTS-SiO₂ and 20 %wt of PIP/MPS-SiO₂ are given in Figure 7.2b. It is clearly seen that the $\tan \delta$ is considerably decreased and the T_g is shifted to a higher temperature with the addition of PIP-SiO₂ into the NR matrix. NR and its composite had a single glass transition temperature and the T_g was -53°C and -48°C for unfilled NR and NR filled with PIP-VTS-SiO₂, respectively. The reduction of $\tan \delta$ which is determined from the ratio of the loss modulus (E'') to storage modulus (E') implies the high storage modulus due to an increase in the homogeneity structure of the composite materials. Nevertheless, the addition of PIP-SiO₂ significantly affected the T_g value due to a lower mobility and flexibility of the polymer chains by the addition of rigid particles.

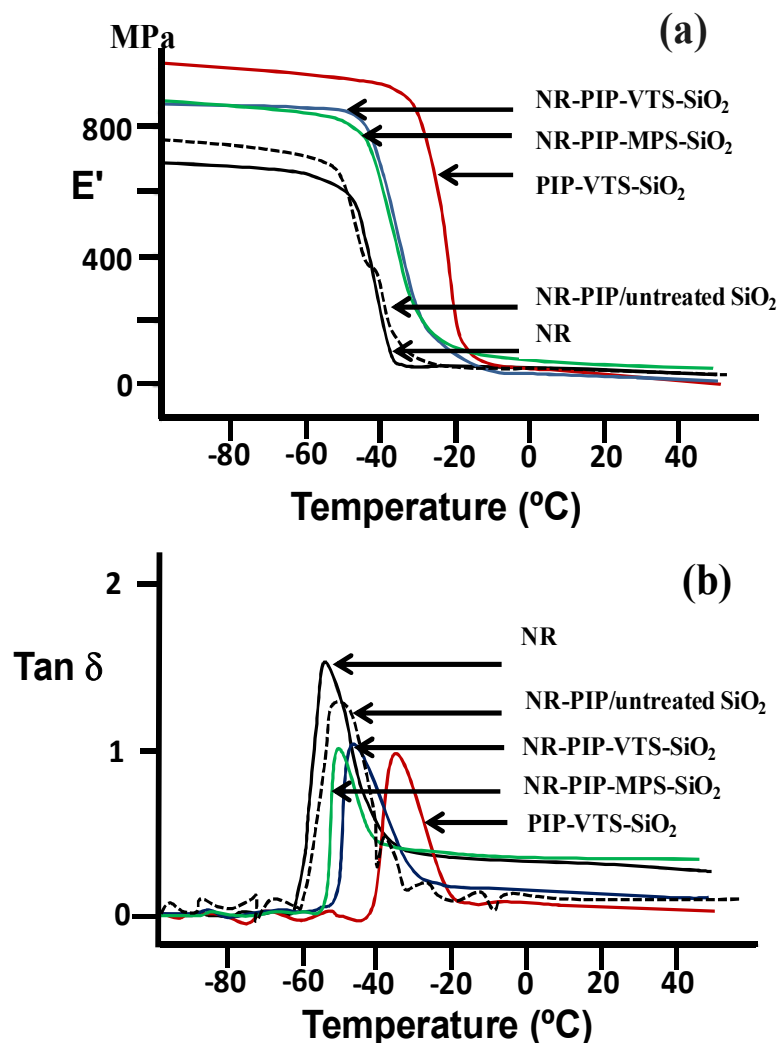


Figure 7.2 Temperature dependence of (a) storage modulus (E') and (b) loss tangent ($\tan \delta$) for NR and its composites.

7.3 Mechanical Properties of Vulcanized Rubber

7.3.1 Mechanical Properties of PIP-SiO₂ Filled NR

For the synthesis of PIP-SiO₂ nanoparticles (Chapter 5), high conversion (87%), high %GE (78%) and narrow size distribution of PIP-SiO₂ were achieved at 10 %wt of VTS-SiO₂ and 10 %wt of MPS-SiO₂ amount. Therefore, PIP-SiO₂ at 10 %wt of SiO₂ loading was selected to blend with NRL for mechanical testing. Mechanical

properties of PIP-SiO₂ filled NR were investigated in terms of tensile strength, modulus, and elongation at break. The influence of the amount of PIP-VTS-SiO₂ and PIP/MPS-SiO₂ on the stress-strain behavior of NR nanocomposites was studied. Figure 7.3a shows the stress-strain curves before aging of unfilled NR and PIP-VTS-SiO₂ filled NR at ratio of NR to PIP-SiO₂ of 95/5, 90/10, 80/20, 70/30 (equivalent to 0.5, 1, 2, and 3% SiO₂ content in all rubbers, respectively). It can be seen that the tensile stress of all PIP-VTS-SiO₂ filled NR were higher than that of unfilled NR, indicating that PIP-VTS-Si filled NR exhibited a reinforcement effect. The tensile stress of NR nanocomposites gradually increased with an increase in PIP-VTS-Si amount from 5 to 20 %wt and then decreased at an amount of 30 %wt. For NR filled with PIP-MPS-SiO₂ nanoparticles as shown in Figure 7.4a, the stress was increased with increasing the PIP-MPS-SiO₂ amount and the lowest tensile stress was observed for unfilled NR. The tensile stress of PIP-MPS-SiO₂ filled NR was slightly lower than that of PIP-VTS-SiO₂ filled NR. However the type of silane coupling agents for silica surface treatment did not show any significant effect on the physical properties of the NR/PIP-SiO₂ nanocomposite.

Another remarkable improvement observed was for the modulus; the modulus at 300% strain was examined. From Table 7.2, a significant increase in the modulus of PIP-VTS-SiO₂ filled NR and PIP-MPS-SiO₂ filled NR was observed. The modulus at 300% strain was found to increase from 3.9 MPa (NR) to 5.7 MPa on increasing the PIP-VTS-SiO₂ amount from 0 to 20 %wt. Moreover, the addition of PIP/MPS-SiO₂ over the range of 5-20% wt also resulted in an increase in modulus at 300% strain. The highest modulus at 300% strain was achieved at a ratio of NR to PIP-MPS-SiO₂ of 80:20. This implied that the improvement in the modulus of NR composites was due to the high interaction between the nanosized filler and the NR matrix [184]. For the elongation at break for unfilled NR and filled NR, it can be seen that unfilled NR exhibited the highest elongation at break (861%). NR rich compounds possessed the highest elongation at break due to NR crystallization which resulted upon stretching [185]. The %elongation at break linearly decreased with an increase in the nanofiller of PIP-VTS-SiO₂ and PIP-MPS-SiO₂ due to the hard and stiff nature of the silica particles. This phenomenon caused strain-reduced crystallization of NR dominating the elongation [186-187].

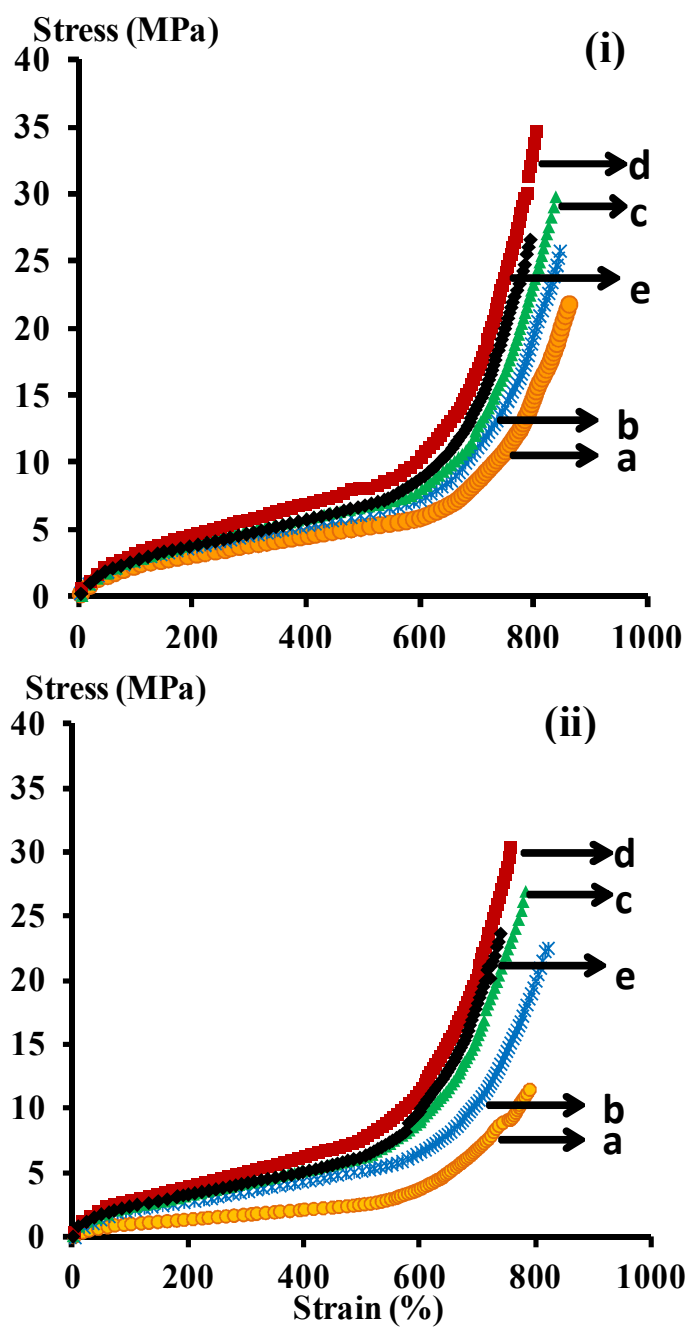


Figure 7.3 Stress-strain curves of (i) PIP-VTS-SiO₂ filled NR before ageing; (a) NR, (b) 95:5 of NR:PIP-SiO₂, (c) 90:10 of NR:PIP-SiO₂, (d) 80:20 of NR:PIP-SiO₂, (e) 70:30 of NR:PIP-SiO₂ and (ii) PIP-VTS-SiO₂ filled NR after ageing.

Tensile strength is an important property of rubber materials since it determines the limit of final stress in rubber applications. The tensile strength of the NR nanocomposite was significantly affected by the addition of PIP-VTS-SiO₂ and PIP-MPS-SiO₂. From Table 7.2, tensile strength is increased from 21.8 MPa (unfilled NR) to 34.6 MPa and modulus at 300% strains is increased from 3.9 MPa (unfilled NR) to 5.7 MPa with an increase in the amount of PIP-VTS-SiO₂ from 0 to 20 %wt. For NR filled with 10 %wt untreated SiO₂ (direct mixing), the tensile strength (28.8 MPa) and modulus at 300% strain (4.6 MPa) were lower than those of NR filled with PIP-VTS-SiO₂ and PIP-MPS-SiO₂. The result indicated that nanosized PIP-SiO₂ could increase the external force resistance resulting in a remarkable enhancement of tensile strength and the incorporation of well-dispersed PIP-SiO₂ nanoparticles into the NR matrix and also led to the reduction of silica agglomeration. Furthermore, it can be explained in that the polyisoprene bonded on the silica surface tended to increase the compatibility within NR due to a major component of *cis*-1,4 polyisoprene in the NR structure. The tensile strength of PIP-MPS-SiO₂ filled NR had the same trend as PIP-VTS-SiO₂ filled NR. The mechanical properties of NR filled with 30% filler loading (PIP-VTS-SiO₂, PIP-MPS-SiO₂) were decreased due to the incompatibility between filler and rubber matrix and SiO₂ aggregation at high filler loading. A similar result was earlier reported for self-assembled natural rubber/silica nanocomposites [186]. The highest tensile strength of 32.1 MPa was achieved by adding PIP-MPS-SiO₂ in the amount of 20 %wt.

In comparison with unfilled NR, the tensile strength of PIP-VTS-SiO₂ filled NR and PIP-MPS-SiO₂ filled NR were at 1.6 and 1.5 fold of the unfilled NR, respectively. The PIP-VTS-SiO₂ and the PIP-MPS-SiO₂ amount of 20 %wt is equivalent to 2% silica content in all rubbers. The tensile strength (34 MPa) and modulus at 300% strain (5.7 MPa) of NR nanocomposites were dramatically improved with an extremely low content of nano-SiO₂ (2 %wt). From the previous work, a maximum tensile strength of 26.1 MPa and a modulus of 3.5 MPa of the NR filled with precipitated silica was obtained at a high silica loading of 30 %wt. [187].

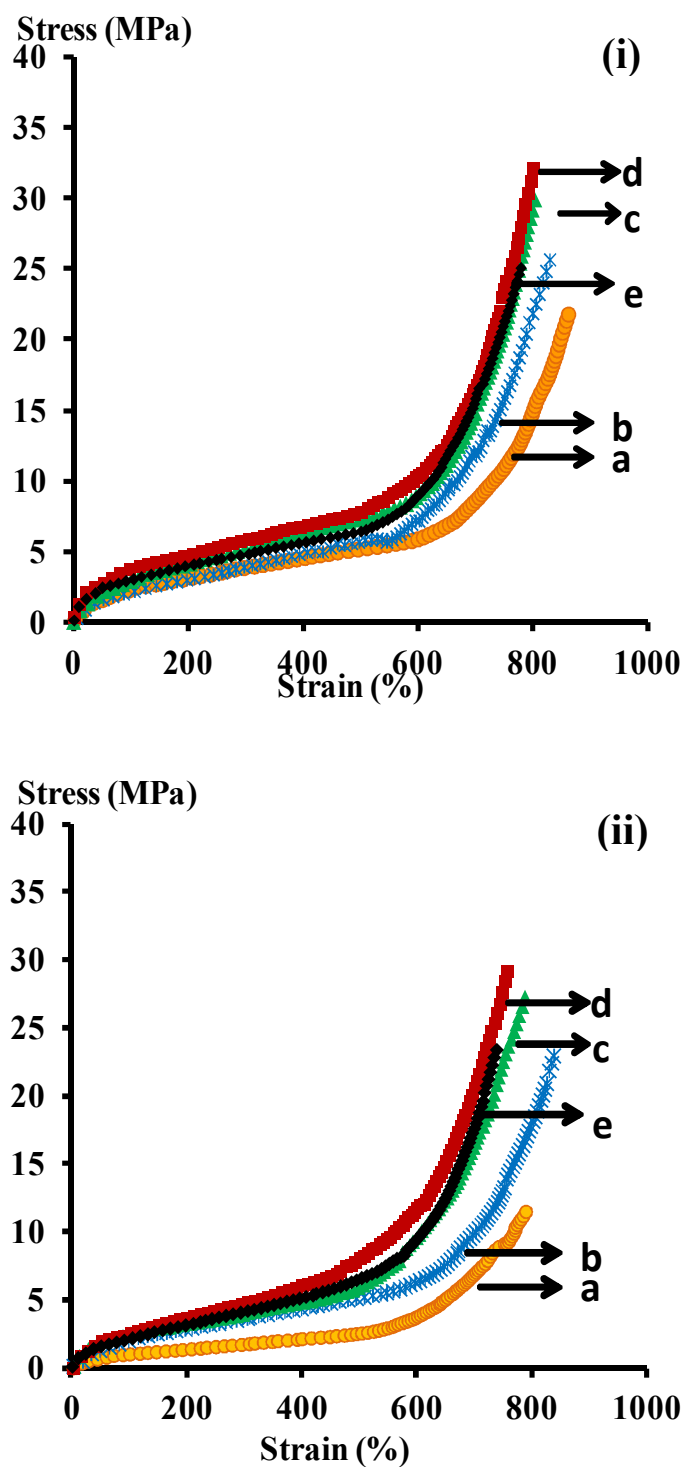


Figure 7.4 Stress-strain curves of (i) PIP-MPS-SiO₂ filled NR before ageing; (a) NR, (b) 95:5 of NR:PIP-SiO₂, (c) 90:10 of NR:PIP-SiO₂, (d) 80:20 of NR:PIP-SiO₂, (e) 70:30 of NR:PIP-SiO₂ and (ii) PIP-MPS-SiO₂ filled NR after ageing.

7.3.2 Mechanical Properties of HPIP-SiO₂ Filled NR

From diimide hydrogenation, HPIP-SiO₂ nanoparticles (47 nm) with high hydrogenation level (98%) were obtained. Therefore, HPIP-SiO₂ latex (HD = 98%) containing 10 %wt of VTS-SiO₂ loading was selected to blend with NRL for mechanical testing. The mechanical properties in tensile strength, modulus and elongation at break, before and after 24 h of thermal ageing have been investigated and the results are summarized in Table 7.3. The stress-strain curves of NR nanocomposites are shown in Figure 7.5. From the stress-strain behavior before thermal aging of unfilled NR, PIP-SiO₂ filled NR (NR/PIP-SiO₂ ratio of 80/20), HPIP-SiO₂ (64%HD) filled NR (NR/HPIP-SiO₂ ratio of 80/20) and HPIP-SiO₂ (98%HD) filled NR (NR/HPIP-SiO₂ ratio of 90/10, 80/20, 70/30, 60/40), the incorporation of nano-SiO₂ in the NR caused an increase in the tensile strength and modulus compared to unfilled NR due to a reinforcement effect of the inorganic filler. However, the improvement in tensile strength by untreated SiO₂ addition required a high silica loading (10 %wt) due to silica agglomeration while the significant increase in mechanical properties was achieved by addition of nanosized PIP-SiO₂ of a very low silica content (2 %wt).

For the HPIP-SiO₂/NR nanocomposite with various amounts of HPIP-SiO₂, the tensile strength of the HPIP-SiO₂/NR blend was higher than that of the PIP-SiO₂/NR blend due to the thermoplastic properties of the ethylene-propylene segments. The stress-strain behavior of the HPIP-SiO₂ filled NR (64% HD) had a similar trend to the PIP-SiO₂ blend. In addition, the HPIP-SiO₂ nanoparticles have a significant influence on the mechanical properties of the NR vulcanizates which could be improved by increasing the HPIP-SiO₂ loading. When a good interfacial adhesion of the PIP-SiO₂ nanocomposite within NR matrix occurs, the nanofiller can act as restriction site for rubber chain mobility, which typically enhances the deformation resistance of material.

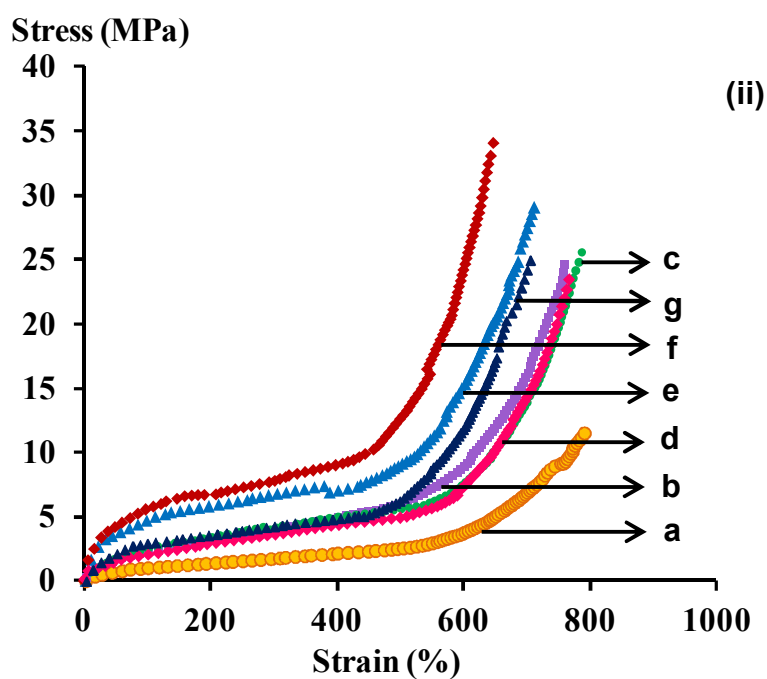
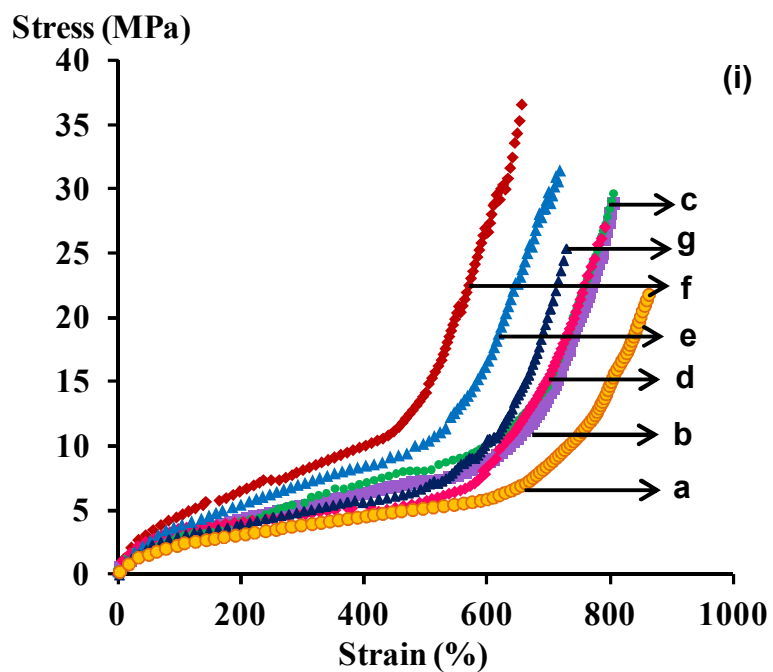


Fig. 7.5 Stress-strain curves of (i) vulcanized NR nanocomposite before ageing; (a) NR, (b) 80:20 of NR:PIP-SiO₂, (c) 80:20 of NR:HPIP-SiO₂ (64%HD) (d) 90:10 of NR:HPIP-SiO₂, (e) 80:20 of NR:HPIP-SiO₂, (f) 70:30 of NR:PIP-SiO₂, (g) 60:40 of NR:HPIP-SiO₂ and (ii) vulcanized NR nanocomposite after ageing.

The tensile strength of the NR nanocomposite was slightly increased by adding untreated SiO₂ while it was dramatically improved by the addition of PIP-SiO₂ and HPIP-SiO₂. From Table 7.3, tensile strength increased from 21.8 MPa (unfilled NR) to 28.9 MPa (PIP-SiO₂). Interestingly, tensile strength of the HPIP-SiO₂/NR blend was higher than that of the PIP-SiO₂/NR blend and increased with HPIP-SiO₂ loading. It can be seen that the highest tensile strength of 36.6 MPa was achieved by adding HPIP-SiO₂ at 30 %wt as equivalent to 3 %wt of SiO₂ content. Thus, the tensile strength of an incorporation of HPIP-SiO₂ to NR ratio at 30/70 increased by 67.4% and 26.7% over that of unfilled NR and a PIP-SiO₂/NR blend, respectively. From previous work, the addition of core-shell structure of PMMA/SiO₂ in NR resulted in a 28% increase in tensile strength as compared to pure NR [188]. It is known that the interface between filler and rubber matrix can transfer stress, which is beneficial for the improvement of the tensile strength of composite materials. However, at high nanofiller loading (40 %wt), the tensile strength and modulus of a HPIP-SiO₂/NR blend decreased due to a decrease in the contact area between the nanoparticles and the rubber matrix resulting in a lack of miscibility in the NR nanocomposites. Hence, the enhanced mechanical properties also depend on not only the HPIP-SiO₂ amount but also the homogeneous dispersion in each loading.

From Table 7.3, the addition of HPIP-SiO₂ over the range of 10-30 %wt also increased the modulus at 300% strain. The highest modulus at 300% strain was achieved at a ratio of NR to HPIP-SiO₂ of 70:30. Therefore, the ethylene-propylene segments that are introduced on the silica surface resulted in adhesion improvement and thermoplastic elasticity of the NR nanocomposite.

Unfilled NR exhibited the highest elongation at break (861%) which indicated that NR rich compounds possessed the highest strain due to NR crystallization which resulted upon stretching [187]. The elongation at break linearly decreased with an increase in PIP-SiO₂ and HPIP-SiO₂ loading due to the rigid and stiff nature of the silica particles. This phenomenon caused strain-reduced crystallization of NR dominating the elongation [184]. The mechanical properties of NR were improved by the addition of nano-SiO₂ into NR due to reinforcing the interaction between nano-SiO₂ and NR matrix and hindering the movement of NR macromolecule chains [188].

7.4 Thermal Resistance of NR Nanocomposites

7.4.1 Thermal Stability of PIP-SiO₂ Filled NR

To investigate the thermal resistance of PIP-SiO₂ filled NR composites, the influence of heat ageing on the mechanical properties of NR filled with PIP-VTS-SiO₂ and PIP-MPS-SiO₂ was studied as shown in Figure 7.3b and Figure 7.4b, respectively. The tensile stress of unfilled NR after heat ageing was greatly decreased over the range of strain studied. This indicated that the NR containing mainly the unsaturated carbon double bonds had poorer properties due to accelerated thermal ageing. On the other hand, the properties of NR filled with PIP-VTS-SiO₂ and PIP-MPS-SiO₂ did not change and retained high stress values after ageing. The percentage retention in tensile strength of unfilled NR (52.8%) was much lower than that of PIP-VTS-SiO₂ filled NR (89.9%) and PIP-MPS-SiO₂ filled NR (90.7%), respectively. This indicated that aged NR exhibited a reduction in NR crystallization and degradation of the polymer chains by high temperature treatment. For NR filled with 10 %wt untreated SiO₂ (direct mixing), the % retention in tensile strength (71.1%) and modulus (50.0%) was lower than those of NR filled with PIP-VTS-SiO₂ and PIP-MPS-SiO₂, indicating a deterioration of properties with accelerated ageing. The low mechanical properties of NR filled with 10 %wt untreated SiO₂ (direct mixing) are due to a poor interaction between SiO₂ and rubber matrix and silica agglomeration. For PIP-modified SiO₂ filled NR, PIP covered onto SiO₂ enhanced the improvement of the interaction between SiO₂ and NR. Similar results were previously observed for PMMA-SiO₂ filled PVC [189].

The modulus at 300% strain after ageing of PIP-VTS-SiO₂ filled NR and PIP-MPS-SiO₂ filled NR remained constant (80-90%) as shown in Table 7.2. The percentage retention in modulus at 300% strain increased from 45 (NR) to 89% when the PIP-SiO₂ amount was increased from 0 to 20 %wt. The lowest modulus retention of unfilled NR also showed poor heat resistance. This can be seen in that the enhancement in ageing resistance was dominated by the addition of well-dispersed PIP-SiO₂ nanoparticles into the rubber matrix. Similarly, the elongation at break of PIP-VTS-SiO₂ filled NR and PIP-MPS-SiO₂ filled NR after ageing linearly decreased

with an increase in nanosized filler amount. The SiO₂ nanoparticles cause a reduction in the flexibility of the NR chain by restriction of the molecular chain slipping along the filler surface. These results clearly demonstrated that the addition of PIP-VTS-SiO₂ and PIP-MPS-SiO₂ could increase the anti-ageing properties of NR products.

Table 7.2 Mechanical properties of NR filled with PIP-SiO₂ nanocomposites before and after ageing

Rubber composite	NR/PIP-SiO ₂ ^a	SiO ₂ content ^b (%wt)	Tensile strength (MPa)		Modulus at 300% strain (MPa)		Elongation at break (%)	
			Before ageing	%Retention ^c	Before ageing	%Retention	Before ageing	%Retention
NR	-	-	21.8 (0.72)	52.8	3.9 (0.21)	45	861 (4.7)	91.6
NR/untreated SiO ₂ ^d	90/10	10	28.8 (2.90)	71.1	4.6 (1.1)	50	799 (21.2)	81.3
NR/PIP-VTS-SiO ₂	95/5	0.5	25.8 (0.66)	87.5	4.6 (0.02)	78.9	845 (12.8)	97.2
	90/10	1	29.7 (0.04)	90.5	4.9 (0.37)	84	839 (5.9)	93.3
	80/20	2	34.6 (0.74)	89.9	5.7 (0.70)	89.1	805 (15.3)	94.3
	70/30	3	29.6 (0.90)	80	4.8 (0.81)	87.9	794 (20.5)	93.4
NR/PIP-MPS-SiO ₂	95/5	0.5	25.7 (0.47)	91.5	4.0 (0.36)	93.1	829 (1.4)	100.9
	90/10	1	29.9 (0.55)	93.4	5.2 (0.09)	75.2	803 (10.6)	98.1
	80/20	2	32.1 (0.81)	90.7	5.7 (0.85)	81.7	801 (19.9)	94.6
	70/30	3	25.0 (0.51)	93.2	4.7 (0.77)	88	780 (22.6)	94.7

Ageing conditions: 100 °C under air atmosphere for 24 h.

^a NR/PIP-SiO₂, ratio of NR to PIP-SiO₂.

^b Silica content based on total rubber.

^c %Retention= (Properties after ageing/Properties before ageing) x 100.

^d direct mixing of untreated SiO₂ with NRL.

7.4.2 Thermal Stability of HPIP-SiO₂ Filled NR

To investigate the thermal degradation resistance of HPIP-SiO₂ filled NR composites, the influence of heat ageing on the mechanical properties of unfilled NR, PIP-SiO₂/NR and HPIP-SiO₂/NR blends were studied. The stress-strain behavior is also illustrated in Figure 7.5b. The tensile stress of unfilled NR after heat ageing was greatly decreased over the range of strain studied due to poor resistance to high temperature of the unsaturated carbon double bonds in the NR chains under accelerated thermal ageing (Table 7.3). Nevertheless, the tensile strength of PIP-SiO₂/NR and HPIP-SiO₂/NR blends did not decrease markedly and showed high retention in mechanical properties as compared to unfilled NR. As expected, the retention in tensile strength of HPIP-SiO₂/NR (85-99%) at all blend ratios was much higher than that of unfilled NR (53%). Thus it can be noted that unfilled NR mainly containing *cis*-1,4 polyisoprene shows polymer chain degradation by high temperature ageing causing poor mechanical properties.

After diimide reduction, the carbon-carbon double bonds were hydrogenated to produce ethylene-propylene domains and no chain scission occurred. Furthermore, good dispersion of nanosized HPIP-SiO₂ within NR is useful for increasing tensile strength retention due to good heat resistance of nano-SiO₂. However, the addition of HPIP-SiO₂ decreased the elongation at break of the NR blend while the unfilled NR had the highest elongation. The decrease in elasticity means that brittleness of samples increase, which implies that the SiO₂ nanoparticles cause a reduction in the flexibility of the NR chain by restriction of the molecular chain slipping along the filler surface [190]. These results clearly demonstrated that nanosized HPIP-SiO₂ could behave as novel nanofillers with high thermal resistance for NR applications.

Table 7.3 Mechanical properties of NR filled with HPIP-SiO₂ nanocomposites before and after ageing

Rubber composite	NR/HPIP-SiO ₂ ^a	SiO ₂ content ^b (%wt)	Tensile strength (MPa)		Modulus at 300% strain (MPa)		Elongation at break (%)	
			Before ageing	%Retention ^c	Before ageing	%Retention	Before ageing	%Retention
NR	-	-	21.8 (0.7)	52.8	3.9 (0.1)	46.4	861 (7.8)	91.7
NR/PIP-VTS-SiO ₂	80/20	2	28.9 (1.9)	85.2	5.3 (0.3)	76.3	805 (14.4)	94.3
NR/HPIP-VTS-SiO ₂ ^d	80/20	2	29.6 (0.6)	86.2	5.6 (0.2)	73.9	805 (17.3)	97.7
NR/HPIP-VTS-SiO ₂ ^e	90/10	1	27.0 (0.9)	86.7	4.6 (0.3)	78.5	791 (5.2)	96.9
	80/20	2	31.4 (1.2)	92.5	7.2 (0.2)	94.8	718 (9.6)	99
	70/30	3	36.6 (0.6)	93.2	8.1 (0.8)	96.1	656 (11.3)	98.6
	60/40	4	25.4 (1.3)	98.3	5.0 (1.1)	85.4	727 (21.8)	96.8

Ageing conditions: 100 °C under air atmosphere for 24 h.

^a NR/HPIP-SiO₂, ratio of NR to HPIP-SiO₂.

^b Silica content based on total rubber.

^c %Retention= (Properties after ageing/Properties before ageing) x 100.

^d HPIP-SiO₂ at degree of hydrogenation 64 %.

^e HPIP-SiO₂ at degree of hydrogenation 98 %.

7.5 Surface Morphology of Rubber-Silica Nanocomposites

The surface morphology of unfilled NR, NR filled with PIP-VTS-SiO₂ at 20 %wt (Si = 2%) and NR filled with PIP-MPS-SiO₂ at 20 %wt (Si = 2%) before and after ageing was characterized by SEM as shown in Figure 7.6. From Figure 7.6a and Figure 7.6b, it is seen that the surface of the unfilled NR after ageing was smooth and exhibited a brittle appearance indicating the deformation failure in the aged NR after high thermal ageing. Hence, the unfilled NR had a lower heat resistance and inferior anti-ageing property. For the addition of nano-SiO₂ into the NR matrix, NR filled with unmodified SiO₂ had SiO₂ aggregates within the NR matrix, and thus phase separation and poor interaction were generated due to an incompatibility between the high polarity of the silanol groups on the silica surface and the nonpolar NR chain (Figure 7.6c). For the addition of PIP-SiO₂ to NR, the surface of the NR nanocomposite exhibited the good compatibility between the nanofiller of PIP-VTS-SiO₂ and the NR matrix (Figure 7.6e). This indicated that the high polarity of the silica surface was completely covered with nonpolar polyisoprene, and therefore the polyisoprene shell could improve the interfacial adhesion with *cis*-1,4 polyisoprene as a major component of NR. Similar results were also observed for PIP-MPS-SiO₂ filled NR (Figure 7.6g). This implied that both PIP-VTS-SiO₂ and PIP-MPS-SiO₂ could increase the interaction and the dispersion of the NR nanocomposite.

For surface morphology of NR composites after heat ageing, the adhesion between the unmodified SiO₂ and NR matrix was lower than that of modified SiO₂ due to aggregation of silica particles (Figure 7.6d). For PIP-VTS-SiO₂ filled NR (Figure 7.6f) and PIP-MPS-SiO₂ filled NR (Figure 7.6h), the nanosilica particles were completely covered within the rubber matrix. This can be explained that silica consists of hydrophilic groups of silanol on its surface while NR is composed of hydrophobic groups of *cis*-1,4 polyisoprene and thus, poor interaction and phase separation occurred. Nevertheless, the modified SiO₂ was strongly embedded with polyisoprene resulting in high interfacial adhesion and good compatibility with the NR matrix. After high thermal ageing, the SiO₂ aggregation and a phase separation was not clearly observed, implying that good miscibility of the filler in the rubber

compound could be achieved through the encapsulation process and that the heat resistance of NR nanocomposites could be dramatically improved.

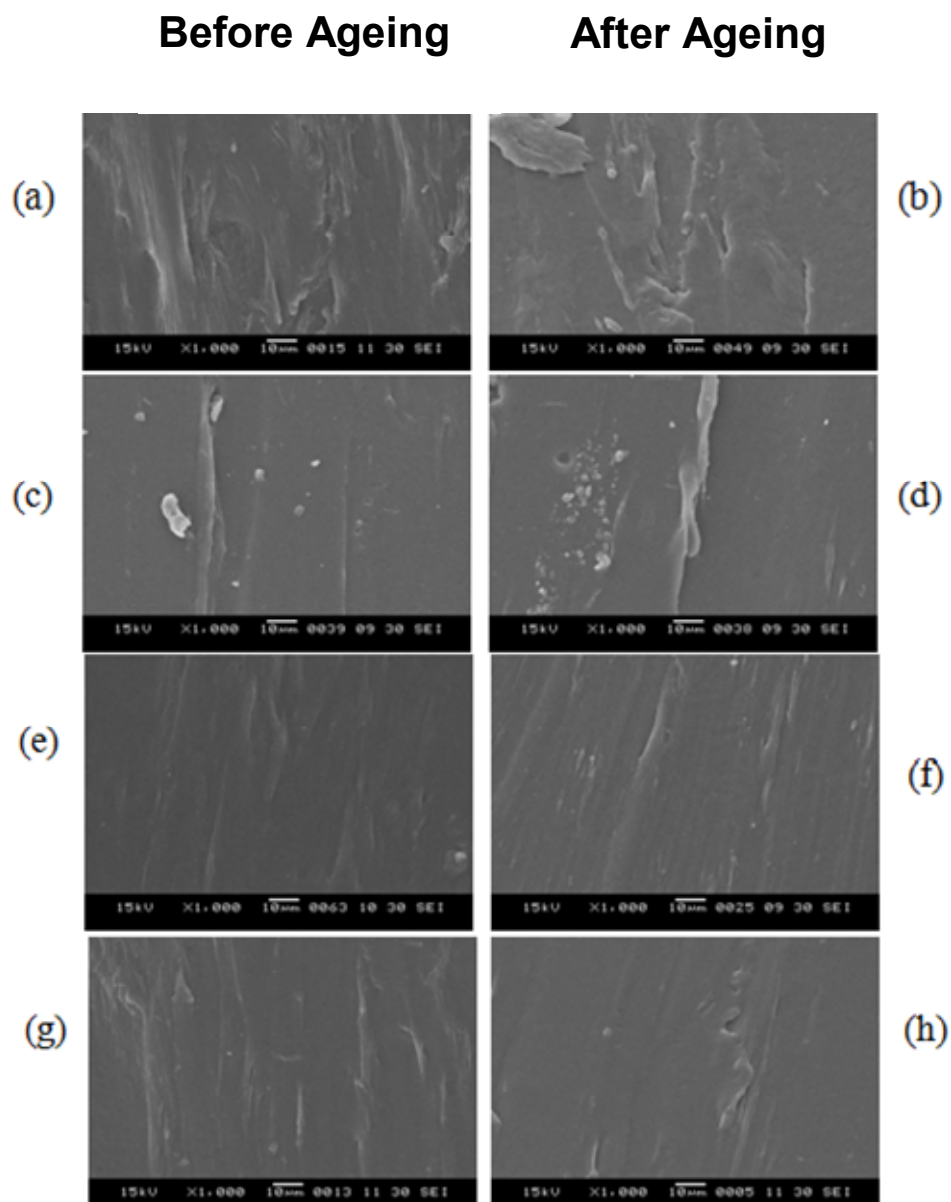


Figure 7.6 SEM micrographs of samples before and after ageing (x 1000). (a) NR, (b) aged NR, (c) NR filled with untreated SiO₂, (d) aged NR filled with untreated SiO₂, (e) NR filled with PIP-VTS-SiO₂, (f) aged NR filled with PIP-VTS-SiO₂, (g) NR filled with PIP-MPS-SiO₂, (h) aged NR filled with PIP-MPS-SiO₂.

7.6 Ozone Resistance of HPIP-SiO₂ Nanocomposites

The degradation of rubbers by ozone is a problem for engineering and outdoor applications. The main chain scission or crosslink scission of rubbers can occur during the ozone ageing. Polyisoprene rubber is highly susceptible to elastomer degradation accelerated by ozone, due to the presence of carbon-carbon double bonds in the main chain. To improve the ozone degradation of the natural rubber, HPIP-SiO₂ could be an effective nano-filler in NR. The effect of HPIP-SiO₂ loading on the ozone resistance of HPIP-SiO₂/NR vulcanizates at various blend ratios is presented in Table 7.4. For the ozone resistance test, samples with 20% strain were exposed to ozonized air of 50 pphm ozone concentration at 40°C. Characteristic cracking in rubber could be clearly observed when a tensile strain was exceeded during exposure.

From Table 7.4, the unfilled NR showed B-5 type cracking after 12 h exposure while the cracks of HPIP-SiO₂/NR at all blend ratios were not observed. After 24h exposure, ozone ageing strongly affected on the surface of unfilled NR (C-3 type) and slightly affected on a HPIP-SiO₂/NR blend at 20/80 ratio (A-3 type). Nevertheless, the surface cracking of HPIP-SiO₂/NR at a ratio of 30/70 and 40/60 was not observed. However, a small degree of cracking (A-2 type) developed on the surface of a HPIP-SiO₂/NR blend after 36 h exposure. This indicated that the interaction of ozone with the unsaturated carbons is the main cause of ozone-induced degradation. Hence, an increase in HPIP-SiO₂ loading could retard the ozonolysis resulting in a reduction of surface cracking by ozone.

Over a prolonged time (48 h), the number of cracks of unfilled NR significantly increased (C-5 type). However, for HPIP-SiO₂/NR blends at ratios of 20/80, 30/70, 40/60 exhibited less cracking of B-5, A-3, A-4, respectively. As a result, the ozone resistance depended on an incorporation of HPIP-SiO₂ loading. It is noted that the cracking trace on the surface of HPIP-SiO₂/NR blend (30/70, 40/60) for 12-24 h was not observed and a low cracking level (B-4, B-5 type) occurred after 72 h exposure. Interestingly, the unfilled NR after 72 h exposure was completely degraded while the HPIP-SiO₂/NR blend at ratio of 40/60 clearly exhibited better ozone resistance. This observation is due to the fact that NR contains almost entirely *cis*-1,4 polyisoprene which is susceptible to degradation by ozone attack because of the

presence of the carbon–carbon double bonds in the backbone structure, which causes macroscopic cracks and numerous cracking on the surface of the rubber specimens. On the other hand, all HPIP-SiO₂/NR blends also showed better resistance towards ozone exposure compared with unfilled NR for 72 h exposure. The presence of HPIP-SiO₂ nanoparticles containing saturated carbon could prevent the growth of cracks in the rubber.

The interaction between rubber and ozone could be identified when stress or elongation was applied to the rubber. Optical photographs of the surfaces of the vulcanized rubbers after ozone exposure for 72 h are shown in Figure 7.7. The photograph of unfilled NR showed macroscopic cracks and numerous horizontal cracking lines on the surface (Figure 7.7a). The appearance of ozone cracking was evident for the degradation of unfilled NR. It is possible that the growth of surface cracks was initiated from the rubber matrix and grew over the critical length resulting in failure.

From Figure 7.7b, the crack density of a HPIP-SiO₂/NR blend (20/80) was lower than that of unfilled NR. The HPIP-SiO₂/NR showed shorter cracks represented by the horizontal lines, indicating that the crack growth through ozonolysis was retarded. It is worthy noting that the ozone resistance of NR at high HPIP-SiO₂ loading (Figure 7.7 c) was much higher than that of the unfilled NR due to the suppression of crack growth. For a HPIP-SiO₂/NR blend (40/60), the cracks generated by ozone exposure were small and discontinuous (Figure 7.7d). It can be concluded that the incorporation of HPIP-SiO₂ in the NR latex provides better ozone resistance.

Table 7.4 Cracking of HPIP-SiO₂ filled NR nanocomposites.

NR/HPIP-SiO ₂	Type of cracking					
	12 h	24 h	36 h	48 h	60 h	72 h
100/0	B-5 ^b	C-3	C-4	C-5	C-5	C-5
80/20	nc ^a	A-3	B-3	B-5	B-5	B-5
70/30	nc	nc	A-2	A-3	A-5	B-5
60/40	nc	nc	A-2	A-4	A-4	B-4

^a The cracking was not appeared on the surface of rubber specimen.

^b Classification of cracking on the surface of rubber specimen.

A: A small number of cracking.

B: A large of number cracking.

C: Numerous cracking.

1. That which cannot be seen with eyes but can be confirmed with 10 times magnifying glass.
2. That which can be confirmed with naked eyes.
3. That which the deep and comparatively long (below 1 mm).
4. That which the deep and long (above 1 mm and below 3 mm).
5. That which about to crack more than 3 mm or about to severe.

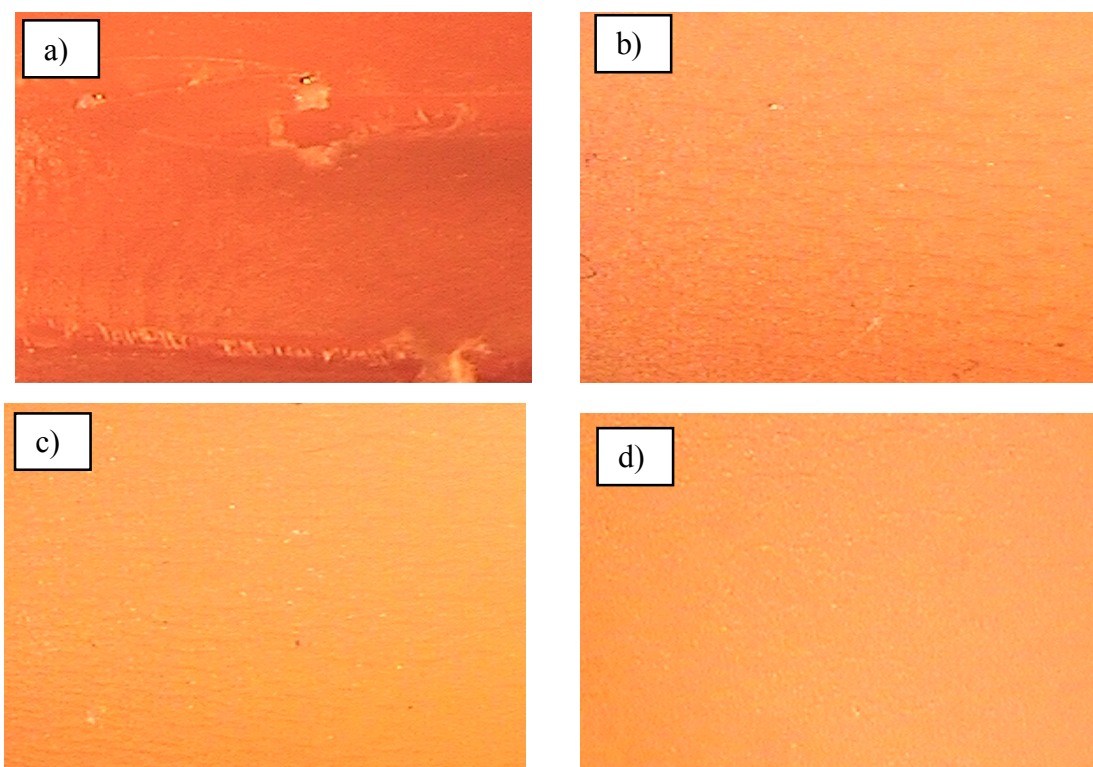


Figure 7.7 Surface of NR filled with HPIP-SiO₂ at various blend ratios after ozone exposure for 72 h: (a) 100/0, (b) 80/20, (c) 70/30, (d) 60/40.

CHAPTER VIII

CONCLUSIONS AND RECOMMENDATIONS

8.1 Conclusions

i) **Synthesis of Nanosized Ethylene-Propylene Rubber Latex via Polyisoprene Hydrogenation**

Ethylene-propylene rubber nanoparticles with a particle size of 47 nm were successfully synthesized from nanosized polyisoprene via diimide hydrogenation in the presence of hydrazine and hydrogen peroxide using boric acid as promotor. The concentration of boric acid exhibited a beneficial effect on the EPM yield whereas, water addition showed an inverse behavior on the hydrogenation level. The highest hydrogenation degree of 94% was achieved at a hydrogen peroxide to hydrazine ratio of 1.5:1, boric acid concentration of 0.15 mol/L and reaction temperature of 70°C. Due to the nanosized PIP, the hydrogenation became more effective for EPM synthesis. This was also confirmed from the hydrogenation rate constant of 30 nm PIP in that it was 1.62 times higher than that of a 65 nm PIP as a result of a mass transfer limitation effect. The 94% EPM product had high thermal stability and provided a maximum decomposition temperature of 510°C. Therefore, the proposed alternative diimide route could prepare EPM nanoparticles in the absence of solvent and metal catalyst and is of importance for production of the improved rubber products.

ii) **Synthesis of Poly(styrene-co-methyl methacrylate)-SiO₂ Nanocomposites via Differential Microemulsion Polymerization**

Poly(ST-co-MMA)-SiO₂ nanoparticles could be successfully produced via a differential microemulsion polymerization by using APS as a hydrophilic initiator and SDS as anionic surfactant. Smaller particle size was achieved by increasing the SDS

amount, MMA feed and water content in the system. Additionally, the polymer grafting efficiency and size distribution were affected by changing the silica loading and ST/MMA ratio. These results showed that the pretreatment of the nano-SiO₂ surface became necessary for producing a good dispersion and interactive bonding of silica with the polymer matrix, as confirmed by the size distribution index and FTIR, respectively. Furthermore, a model for the formation mechanism with core/shell morphology was proposed. The average diameter of the composite particles was 43 nm at a ST/MMA ratio of 1.5/1, and the silica encapsulation efficiency was up to 94%. The monomer conversion was 60% and polymer grafting efficiency was 37% at an extremely low surfactant amount (surfactant/monomer weight ratio of 1/57). Consequently, nanosized particles of poly(ST-co-MMA)/SiO₂ with small size, with narrow distributed particle size of uniform size and good stability could be synthesized using a small amount of surfactant.

iii) Synthesis of Polyisoprene-Silica Nanocomposites via Differential Microemulsion Polymerization

Well-dispersed polyisoprene-SiO₂ with a particle size of 35 nm and with a narrow size distribution was synthesized by a differential microemulsion polymerization technique in an aqueous system. The nano-SiO₂ was initially treated with organo-silane coupling agents of VTS or MPS. Isoprene was then polymerized, and therefore a nano-core (SiO₂) with a nano-shell thin layer (PIP) was completely achieved as confirmed by TEM. From the study of process parameter effects, a high monomer conversion (87%), grafting efficiency (78%), and silica encapsulation (80%) was obtained at optimum reaction conditions at a monomer to water ratio of 0.3, a low surfactant concentration of 3 %wt, an initiator concentration of 1 %wt and a SiO₂ loading of 10 %wt.

iV) Synthesis of Hydrogenated Polyisoprene-Silica Nanocomposites via Diimide Reduction

Novel nanocomposites of nanosized HPIP-SiO₂ (42-48 nm) were successfully synthesized via a new synthetic route of differential microemulsion polymerization followed by diimide hydrogenation. The proposed method is the preparation of HPIP-SiO₂ nanoparticles in the absence of solvent, metal catalyst and hydrogen gas. Diimide species as the active species are generated from the reaction between hydrazine and hydrogen peroxide through a redox system using boric acid as promoter which could hydrogenate effectively the double bonds of the polyisoprene segment. An increase in the concentration of hydrazine, hydrogen peroxide and boric acid had a beneficial effect on the PIP-SiO₂ hydrogenation and the highest HD (98%) was achieved under optimal conditions. Thermal stability of HPIP-SiO₂ nanoparticles was dramatically improved as shown by a maximum degradation temperature of 521°C resulting in excellent thermal stability, demonstrated by a decomposition temperature shift to higher temperature to 134°C compared with unfilled PIP (387°C). Therefore, HPIP-SiO₂ nanoparticles could be used to provide a new novel nanocomposite of PIP for rubber applications.

V) Mechanical Properties of Rubber/SiO₂ Nanocomposites

For EPM synthesis, the EPM product had the highest storage modulus (493 MPa) due to the replacement of the ethylene and propylene units. The improvement of storage modulus was due to the domains of poly(ethylene-co-propylene) segments produced from hydrogenation of the isoprene unit. Furthermore, the tan δ of EPM had a lower value than that of PIP which indicated that EPM had a low dynamic loss modulus and high storage modulus.

For PIP-SiO₂ nanocomposite filled NRL, mechanical properties of tensile strength and modulus of PIP-SiO₂/NR blend were higher than those of unfilled NR and NR/untreated SiO₂, indicating that PIP-SiO₂ filled NR exhibited a reinforcing effect and also led to the reduction of silica agglomeration. Furthermore, the

incorporation of nanosized PIP-SiO₂ in NR clearly showed a positive effect on thermal stability of NR vulcanizates.

For HPIP-SiO₂ filled NR nanocomposite, the mechanical properties in tensile strength and modulus of HPIP-SiO₂/NR blend were dramatically improved as compared to a PIP-SiO₂/NR blend and unfilled NR. The stability of the HPIP-SiO₂/NR nanocomposite after thermal ageing increased, maintaining 93% of its tensile strength and 96% of its modulus. Moreover, an incorporation of HPIP-SiO₂ in NR could retard the ozone-induced degradation resulting in an improvement of ozone resistance at the surface. Therefore, a new nanocomposite of HPIP-SiO₂ could also be potentially used as a novel nanofiller in rubber applications.

8.2 Recommendations

Further research on encapsulation for providing new polymer-silica nanocomposites should be studied as follows:

1. The synthesis of silica nanoparticles encapsulated with ethylene and propylene gas for producing new nanocomposites of EPM-SiO₂ and EPDM-SiO₂ with core/shell morphology should be studied.
2. It is desirable to achieve high thermal stability and good mechanical properties of polybutadiene rubber (PB), thus, the incorporation of nanosilica via differential microemulsion polymerization could be potentially applied to synthesize PB-SiO₂ nanocomposites using modified silica and butadiene as starting materials.
3. Application in natural rubber of PIP-SiO₂ and HPIP-SiO₂ nanocomposites clearly exhibited a dramatic improvement in mechanical properties, thermal stability and ozone resistance. Hence, it is suggested that the use of PIP-SiO₂ and HPIP-SiO₂ filled in PB, SBR, NBR should be further studied to increase their performance under aggressive environments.

REFERENCES

- [1] Ugelstad, J., El-Aasser, M.S., Vanderhoff, J.W. Emulsion polymerization: initiation of polymerization in monomer droplets. *J. Polym. Sci. Pol. Lett.* 11 (1973): 503-513.
- [2] Abismail, B., Canselier, J.P., Wilhelm, A.M., Delmas, H., Gourdon, C. Emulsification by ultrasound: drop size distribution and stability. *Ultrason. Sonochem.* 6 (1999): 75–83.
- [3] Landfester, K. Synthesis of colloidal particles in miniemulsions. *Annu. Rev. Mater. Res.* 36 (2006): 231–279.
- [4] Landfester, K., Bechthold, N., Tiarks, F., Antonietti, M. Miniemulsion polymerization with cationic and nonionic surfactants: a very efficient use of surfactants for heterophase polymerization. *Macromolecules* 32 (1999): 2679-2683
- [5] Fontenot, K., Schork, F.J. Sensitivities of droplet size and stability in monomeric emulsions. *Ind. Eng. Chem. Res.* 32 (1993): 373–385.
- [6] Landfester, K., Bechthold, N., Tiarks, F., Antonietti, M. Formulation and stability mechanisms of polymerizable miniemulsions. *Macromolecules* 32 (1999): 5222–5228.
- [7] Landfester, K. Recent developments in miniemulsions-formation and stability mechanisms. *Macromol. Symp.* 150 (2000): 171–178.
- [8] Fontenot, K., Schork, F.J. Batch polymerization of methyl methacrylate in mini/macroemulsions. *J. Appl. Polym.Sci.* 49 (1993): 633–655.
- [9] Chern, C.S., Chen, T.J., Liou, Y.C. Miniemulsion polymerization of styrene in the presence of a water-insoluble blue dye. *Polymer* 39 (1998): 3767–3777.
- [10] Landfester, K., Bechthold, N., Forster, S., Antonietti, M. Evidence for the preservation of the particle identity in miniemulsion polymerization. *Macromol.Rapid Commun.* 20 (1999): 81–84.
- [11] Reimers, J., Schork, F.J. Miniemulsion copolymerization using waterinsoluble comonomers as cosurfactants. *Polym. React. Eng.* 4 (1996): 135–152.

- [12] Li, D., David Sudol, E., El-Aasser, M.S. Miniemulsion and conventional emulsion copolymerization of styrene and butadiene: a comparative kinetic study. *J. Appl. Polym. Sci.* 101 (2006): 2304–2312.
- [13] Erdem, B., David Sudol, E., Dimonie, V.L., El-Aasser, M.S. Encapsulation of inorganic particles via miniemulsion polymerization. *Macromol. Symp.* 155 (2000): 181–198.
- [14] Erdem, B., David Sudol, E., Dimonie, V.L., El-Aasser, M.S. Encapsulation of inorganic particles via miniemulsion polymerization III: characterization of encapsulation. *J. Polym. Sci. Polym. Chem. Ed.* 38 (2000): 4441–4450.
- [15] Erdem, B., David Sudol, E., Dimonie, V.L., El-Aasser, M.S. Encapsulation of inorganic particles via miniemulsion polymerization I: dispersion of titanium dioxide particles in organic media using OLOA 370 as stabilizer. *J. Polym. Sci. Polym. Chem. Ed.* 38 (2000): 4419–4430.
- [16] Erdem, B., David Sudol, E., Dimonie, V.L., El-Aasser, M.S. Encapsulation of inorganic particles via miniemulsion polymerization II: preparation and characterization of styrene miniemulsion droplets containing TiO₂ particles. *J. Polym. Sci. Polym. Chem. Ed.* 38 (2000): 4431–4440.
- [17] Tiarks, F., Landfester, K., Antonietti, M. Silica nanoparticles as surfactants and fillers for latexes made by miniemulsion polymerization. *Langmuir* 17 (2001): 5775–5780.
- [18] Zhang, S.W., Zhou, S.X., Weng, Y.M., Wu, L.M. Synthesis of SiO₂/polystyrene nanocomposite particles via miniemulsion polymerization. *Langmuir* 21 (2005): 2124–2128.
- [19] Mahdavian, A.R., Sarrafi, Y., Shabankareh, M. Nanocomposite particles with core–shell morphology III: preparation and characterization of nano Al₂O₃–poly(styrene–methyl methacrylate) particles via miniemulsion polymerization *Polym. Bull.* 63 (2009): 329–340.
- [20] Stoffer, J. O., Bone, T. Polymerization in water-in-oil microemulsion systems. *J. Polym. Sci. Polym. Chem. Ed.* 18 (1980) 2641–2648.
- [21] Robb, I.D., Ed. Microemulsions; Plenum Publishers: New York, 1982.

- [22] Prince, L.M., Ed. *Microemulsions: Theory and Practice*; Academic Press: New York, 1977.
- [23] Myers, D., Ed. *Surfactant Science and Technology*, 2nd Ed.; V.C.H. Publishers: New York, 1988.
- [24] Atik, S.S. Thomas, J.K. Polymerized microemulsions. *Am. Chem. SOC.* 103 (1981): 4279-4280.
- [25] Antonietti, M., Lohmann, S. Eisenbach, C.D. Schubert, U.S. Synthesis of metalcomplexing lattices via polymerization in microemulsion. *Macromol. Rapid Commun.* 16 (1995): 283–289.
- [26] Larpent, C., Bernard, E., Richard, J., Vaslin, S. Polymerization in microemulsions with polymerizable cosurfactants: a route to highly functionalized nanoparticles. *Macromolecules* 30 (1997): 354–362.
- [27]. Larpent, C., Bernard, E., Richard, J., Vaslin, S. Synthesis of functionalized nanoparticles via copolymerization in microemulsions and surface reactions. *Reactive Funct. Polym.* 33 (1997): 49–59.
- [28] Larpent, C. Microemulsion polymerization: a way to synthesize well-defined highly functionalized nanoparticles. *J. Colloidal Polym.* (2003).
- [29] Capek, I., Juranicova, V. Barton, J. Effect of stable radicals on the mechanism of microemulsion radical copolymerization of butyl acrylate and acrylonitrile. *Eur. Polym. J.* 35 (1999): 691-698.
- [30] Gan, L.M., Chew, C.H., Lye, I., Imae, T. Microemulsion polymerization of styrene. *Polymer Bull.* 25 (1991): 193-198.
- [31] Larpent, C., Tadros, T.F. Preparation of microlatex dispersions using oil-in-water microemulsions. *Colloid Polym. Sci.* 269 (1991): 1171–1183.
- [32] Amigoni-Gerbier, S., Dessert, S., Gulik-Kryswicki, T., Larpent, C. Ultrafine selective metal-complexing nanoparticles: synthesis by microemulsion copolymerization, binding capacity and ligand accessibility. *Macromolecules* 35 (2002): 1644–1650.
- [33] Larpent, C., Amigoni-Gerbier, S. Synthesis and properties of selective metal complexing nanoparticles. *Macromolecules* 33 (1999): 9071–9073.

- [34] Perez-Luna, V.H., Puig, J.E., Castano, V.M., Rodriguez, B.E., Murthy, A.K., Kaler, E.W. Styrene polymerization in three-component cationic microemulsions. *Langmuir* 6 (1990): 1040–1044.
- [35] Antonietti, M., Basten, B., Lohmann, S. Polymerization in microemulsions—a new approach to ultrafine highly functionalized polymer dispersions. *Macromol. Chem. Phys.* 196 (1995): 441–466.
- [36] Guo, J.S., Sudol, E.D., Vanderhoff, J.W., El-Aasser, M.S. Particle nucleation and monomer partitioning in styrene o/w microemulsion polymerization. *J. Polym. Sci. Polym. Chem.* 30 (1992): 691–702.
- [37] Guo, J.S., Sudol, E.D., Vanderhoff, J.W., El-Aasser, M.S. Modeling of the styrene microemulsion polymerization. *J. Polym. Sci. Polym. Chem.* 30 (1992): 703–712.
- [38] Guo, J.S., Sudol, E.D., Vanderhoff, J.W., Yue, H.J., El-Aasser, M.S. Partitioning behavior and thermodynamic model for styrene o/w microemulsions. *J. Colloid Interf. Sci.* 149 (1992): 184–196.
- [39] Morgan, J.D., Lusvardi, K.M., Kaler, E.W. Kinetics and mechanism of microemulsion polymerization of hexyl methacrylate. *Macromolecules* 30 (1997): 1897–1905.
- [40] Girard, N., Tadros, T.F., Bailey, A.I. Polymerization of oil (styrene and methylmethacrylate)- in-water microemulsions. *Colloid Polym. Sci.* 276 (1998): 999–1009.
- [41] Dreja, M., Tieke, B. Polymerization of styrene in ternary microemulsion using cationic gemini surfactants. *Langmuir* 14 (1998): 800–807.
- [42] Dreja, M., Tieke, B. Polymerization of styrene in ternary microemulsion using gemini surfactants with hydrophilic and hydrophobic spacer groups. *Ber. Bunsenges. Phys. Chem.* 102 (1998): 1705–1709.
- [43] Xu, X., Ge, X., Zhang, Z., Zhang, M. Copolymerization of styrene with acrylates in emulsion and microemulsion. *Polymer* 39 (1998): 5321–5325.
- [44] Sanghvi, P.G., Pokhriyal N.K., Hassan, P.A., Devi, S. Kinetics and mechanism of styrene-acrylonitrile copolymerization in microemulsion. *Polym. Int.* 49 (2000): 1417–1425.

- [45] Wei, L.M., Tang, T., Huang, B.T. Synthesis and characterization of polyethylene/clay–silica nanocomposites: a montmorillonite/silica-hybrid- supported catalyst and *in situ* polymerization. *J. Polym. Sci. Pol. Chem.* 42 (2004): 941-949.
- [46] Hoffmann, F., Cornelius, M., Morell, J., Froba, M. Silica-based mesoporous organic inorganic hybrid materials. *Angew. Chem. Int. Edit.* 45 (2006): 3216-3251.
- [47] Giraldo, L.F., Lopez, B.L., Perez, L., Urrego, S., Sierra, L., Mesa, M. Mesoporous silica applications. *Macromol. Symp.* 258 (2007): 129-141.
- [48] Shen, R., Camargo, P.H.C., Xia, Y., Yang, H. Silane-based poly(ethylene glycol) as a primer for surface modification of nonhydrolytically synthesized nanoparticles using the Stober method. *Langmuir* 24 (2008): 11189-11195.
- [49] LizMarzan, L.M., Giersig, M., Mulvaney, P. Synthesis of nanosized gold-silica core-shell particles. *Langmuir* 12 (1996): 4329-4335.
- [50] De Campos, A. M., Sanchez, A., Gref, R., Calvo, P., Alonso, M. J. The effect of a PEG versus a chitosan coating on the interaction of drug colloidal carriers with the ocular mucosa. *Eur. J. Pharm. Sci.* 20 (2003): 73-81.
- [51] Deng, Z., Chen, W., Wu, L. Novel method to fabricate SiO₂/Ag composite spheres and their catalytic, surface-enhanced Raman scattering properties. *J. Phys. Chem. C* 111 (2007): 11692-11698.
- [52] Ding, J.F., Jiang, J.S. Surface modification of Fe₃O₄ nanoparticles prepared in high temperature organic solution by sodium oleate. *J. Inorg. Mat.* 22 (2007): 859-863.
- [53] Wei, L., Hu, N., Zhang, Y. Synthesis of polymer—mesoporous silica nanocomposites. *Materials* 3 (2010): 4066-4079.
- [54] Darbandi, M., Thomann, R., Nann, T. Hollow silica nanospheres: in situ, semi-in situ, and two-step synthesis. *Chem. Mat.* 19 (2007): 1700-1703.

- [55] Lee, D.C., Mikulec, F.V., Pelaez, J.M., Koo, B., Korgel, B.A. Synthesis and magnetic properties of silica-coated FePt nanocrystals. *J. Phys. Chem. B* 110 (2006): 11160-11166.
- [56] Ge, J.P., Huynh, T., Hu, Y.P., Yin, Y.D. Hierarchical magnetite/silica nanoassemblies as magnetically recoverable catalyst-supports. *Nano Letters* 8 (2008): 931-934.
- [57] Hui, R., Yixin, Q.U., Suhe, Z. Reinforcement of styrene-butadiene rubber with silica modified by silane coupling agents, experimental and theoretical chemistry study. *Chinese J. Chem. Eng.*, 14(2006): 93-98.
- [58] Rao, K.S., El-Hami, K., Kodaki, T., Matsushige, K. Makino, K. A novel method for synthesis of silica nanoparticles, *J. Colloid Interf. Sci.* 289 (2005): 125–131.
- [59] Lopattananon, N., Jitkalong, D., Seadan, M. Hybridized reinforcement of natural rubber with silane-modified short cellulose fibers and silica. *J. Appl. Polym. Sci.* 120 (2011): 3242-3254.
- [60] De Palma, R., Peeters, S., Van Bael, M.J., Van den Rul, H., Bonroy, K., Laureyn, W., Mullens, J., Borghs, G., Maes, G. Silane ligand exchange to make hydrophobic superparamagnetic nanoparticles water-dispersible. *Chemis. Mat.* 19 (2007): 1821-1831.
- [61] Marini, M., Pourabbas, B., Pilati, F., Fabbri, P. Functionally modified core-shell silica nanoparticles by one-pot synthesis. *Colloids Surf. Physicochemical Eng. Asp.* 317 (2008): 473-481.
- [62] Ukaji, E., Furusawa, T., Sato, M., Suzuki, N. The effect of surface modification with silane coupling agent on suppressing the photo-catalytic activity of fine TiO₂ particles as inorganic UV filter. *Appl. Surf. Sci.* 254 (2007): 563-569.
- [63] Kim, D.K., Mikhaylova, M., Zhang, Y., Muhammed, M. Protective coating of superparamagnetic iron oxide nanoparticles. *Chem. Mat.* 15 (2003): 1617-1627.
- [64] Mikhaylova, M., Kim, D. K., Berry, C.C., Zagorodni, A., Toprak, M., Curtis, A.S.G., Muhammed, M. BSA immobilization on amine-functionalized

- superparamagnetic iron oxide nanoparticles. *Chem. Mat.* 16 (2004): 2344-2354.
- [65] Sun, Y., Zhang, Z., Wong, C.P. Study on mono-dispersed nano-size silica by surface modification for underfill applications. *J. Colloid Interf. Sci.* 292 (2005): 436-444.
- [66] Zou, H., Wu, S.S., Shen, J. Polymer/silica nanocomposites: preparation, characterization, properties, and applications. *Chem. Rev.* 108 (2008): 3893-3957.
- [67] Perez, L.D., Giraldo, L.F., Lopez, B.L., Hess, M. Reinforcing of elastomers with mesoporous silica. *Macromol. Symp.* 245 (2006): 628-640.
- [68] Ou, C.P., Hsu, M.C. Preparation and characterization of cyclo olefin copolymer (COC)/silica nanoparticle composites by solution blending. *J. Polym. Res.* 14 (2007): 373-378.
- [69] Kawashima, D., Aihara, T., Kobayashi, Y., Kyotani, Takashi., Tomita, A. Preparation of mesoporous carbon from organic polymer/silica nanocomposite. *Chem. Mater.* 12 (2000): 3397-3401.
- [70] Yang, F., Nelson, G.L. PMMA/silica nanocomposite studies: synthesis and properties. *J. Appl. Polym. Sci.* 91 (2004): 3844-3850.
- [71] Mori, Y., Saito, R. Synthesis of a poly(methyl methacrylate)/silica nanocomposite by soaking of a microphase separated polymer film into a perhydropolysilazane solution. *Polymer* 45 (2004): 95-100
- [72] Judeinstein, P., Sanchez, C. Hybrid organic-inorganic materials: a land of multidisciplinary. *J. Mater. Chem.* 6 (1996): 511-525.
- [73] Zou, H., Wu, S.S., Shen, J. Polymer/silica nanocomposites: preparation, characterization, properties, and applications. *Chem. Rev.* 108 (2008): 3893-3957.
- [74] Moller, K., Bein, T., Fischer, R.X. Entrapment of PMMA polymer strands in micro- and mesoporous materials. *Chem. Mater.* 10 (1998): 1841-1852.
- [75] Percy, M.J., Michailidou, V., Armes, S.P. Synthesis of vinyl polymer-silica colloidal nanocomposites via aqueous dispersion polymerization. *Langmuir* 19 (2003): 2072-2079.

- [76] Schmid, A., Fujii, S., Armes, S.P. Polystyrene-silica nanocomposite particles via alcoholic dispersion polymerization using a cationic azo initiator. *Langmuir* 22 (2006): 4923-4927.
- [77] Stejskal, J., Kratochvíl, P. Polyaniline dispersions: stabilization by colloidal silica particles. *Macromolecules* 29 (1996): 6814-6819.
- [78] Mayes, A.G., Mosbach, K. Molecularly imprinted polymer beads: suspension polymerization using a liquid perfluorocarbon as the dispersing phase. *Anal. Chem.* 68 (1996): 3769-3774.
- [79] Duan, L., Chen, M., Zhou, S., Wu, L. Synthesis and characterization of poly(*N*-isopropylacrylamide)/silica composite microspheres via inverse pickering suspension polymerization. *Langmuir* 25 (2009): 3467-3472.
- [80] Zhu, A., Shi, Z., Cai, A., Zhao F., Liao, T. Synthesis of core-shell PMMA-SiO₂ nanoparticles with suspension-dispersion-polymerization in an aqueous system and its effect on mechanical properties of PVC composites. *Polym. Test.* 27 (2008): 540-547.
- [81] Lee, J., Hong, C.K., Choe, S., Shim, S.E. Synthesis of polystyrene/silica composite particles by soap-free emulsion polymerization using positively charged colloidal silica. *J. Colloid Interf. Sci.* 310 (2007): 112-120.
- [82] Tamai, T., Watanabe, M. Acrylic Polymer/silica hybrids prepared by emulsifier-free emulsion polymerization and the sol-gel process. *J. Polym. Sci.: Part A: Polym. Chem.* 44 (2006): 273-280.
- [83] Zhang, K., Chen, H., Chen, X., Chen, Z., Cui, Z., Yang, Bai. Monodisperse silica-polymer core-shell microspheres via surface grafting and emulsion polymerization. *Macromol. Mater. Eng.* 288 (2003): 380-385
- [84] Chen, M., Wu, L., Zhou, S., You, B. Synthesis of raspberry-like PMMA/SiO₂ nanocomposite particles via a surfactant-free method. *Macromolecules* 37 (2004): 9613-9619.
- [85] Agarwal, G.K., Titman, J.J. Characterization of vinyl polymer/silica colloidal nanocomposites using solid state NMR spectroscopy: probing the

- interaction between the inorganic and organic phases on the molecular level. *J. Phys. Chem. B* 107 (2003): 12497-12502.
- [86] Bourgeat-Lami, E., Lang, J. Encapsulation of inorganic particles by dispersion polymerization in polar media. *J. Colloid Interf. Sci.* 197 (1998): 293-308.
- [87] Zhu, A., Cai, A., Yu, Z., Zhou, W. Film characterization of poly(styrene-butylacrylate-acrylic acid) silica nanocomposite. *J. Colloid Interf. Sci.* 322 (2008): 51-58.
- [88] Zhu, A., Shi, Z., Cai, A., Zhao, F., Liao, T. Synthesis of core-shell PMMA-SiO₂ nanoparticles with suspension-dispersion-polymerization in an aqueous system and its effect on mechanical properties of PVC composites. *Polym. Test.* 27 (2008): 540-547.
- [89] Ding, X., Zhao, J., Liu, Y., Zhang, H., Wang, Z. Silica nanoparticles encapsulated by polystyrene via surface grafting and in situ emulsion polymerization. *J. Mater. Lett.* 58 (2004): 3126-3130.
- [90] Mahdavian, A.L., Ashjari, M., Makoo, A.B. Preparation of poly(styrene-methyl-methacrylate)/SiO₂ composite nanoparticles via emulsion polymerization. An investigation into the compatibilization. *Eur. Polym. J.* 43 (2007): 336-344.
- [91] Reculosa, S., Poncet-Legrand, C., Ravaine, S., Mingotaud, C., Duguet, E., Bourgeat-Lami, E. Syntheses of raspberry-like silica/polystyrene materials. *Chem. Mater.* 14 (2002): 2354-2359.
- [92] Luna-Xavier, J.L., Bourgeat-Lami, E., Guyot, A. The role of initiation in the synthesis of silica/PMMA composite nanoparticles through emulsion polymerization. *Colloid Polym Sci* 279 (2001): 947-958.
- [93] Qi, D.M., Bao, Y.Z., Weng, Z.X., Huang, Z.M. Preparation of polyacrylate/silica nanocomposite particles with high silica encapsulation efficiency via miniemulsion polymerization. *Polymer* 47 (2006): 4622-4629.

- [94] Xu, P., Wang, H., Tong, R., Du, Q., Zhong, W. Preparation and morphology of SiO₂/PMMA nanohybrids by microemulsion polymerization. *Colloid Polym. Sci.* 284 (2006): 755-762.
- [95] Kickelbick, G. Concepts for the incorporation of inorganic building blocks into organic polymers on a nanoscale. *Prog Polym Sci* 28 (2003): 83-114.
- [96] He, G., Pan, Q., Rempel, G.L. Synthesis of poly(methyl methacrylate) Nanosize particles by differential microemulsion polymerization. *Macromol. Rapid Commun.* 24 (2003): 585-588.
- [97] Norakankorn, C., Pan, Q., Rempel, G.L., Kiatkamjornwong, S. Synthesis of poly(methyl methacrylate) nanoparticle initiated by 2,2'-azoisobutyronitrile via differential microemulsion polymerization. *Macromolecular* 28 (2007): 1029-1033.
- [98] He, G., Pan, Q., Rempel, G.L. Modeling of differential microemulsion polymerization for synthesizing nanosized poly(methyl methacrylate) particles. *Ind. Eng. Chem.* 46 (2007): 1682-1689.
- [99] Bergbreiter, D.E. Self-assembled, sub-micrometer diameter semipermeable capsules. *Angewandte Chemie-International Edition* 38 (1999): 2870-2872.
- [100] Ai, H., Jones, S.A., Lvov, Y.M. Biomedical applications of electrostatic layer-by-layer nano-assembly of polymers, enzymes, and nanoparticles. *Cell Biochem. Biophys.* 39 (2003): 23-43.
- [101] Caruso, F., Spasova, M., Saigueirino-Maceira, V., Liz-Marzan, L.M. Multilayer assemblies of silica-encapsulated gold nanoparticles on decomposable colloid templates. *Advan. Mater.* 13 (2001): 1090-1094.
- [102] Decher, G. Fuzzy nanoassemblies: toward layered polymeric multicomposites. *Science* 277 (1997): 1232-1237.
- [103] Wang, Y., Angelatos, A.S., Caruso, F. Template synthesis of nanostructured materials via layer-by-layer assembly. *Chem. Mater.* 20 (2008): 848-858.

- [104] Caruso, F., Mohwald, H. Preparation and characterization of ordered nanoparticle and polymer composite multilayers on colloids. *Langmuir* 15 (1999): 8276-8281.
- [105] Caruso, F., Donath, E., Mohwald, H. Influence of polyelectrolyte multilayer coatings on Forster resonance energy transfer between 6-carboxyfluorescein and rhodamine B-labeled particles in aqueous solution. *J. Phys. Chem. B* 102 (1998): 2011-2016.
- [106] Wang, Y.J., Bansal, V., Zelikin, A.N., Caruso, F. Templated synthesis of single-component polymer capsules and their application in drug delivery. *Nano Letters* 8 (2008): 1741-1745.
- [107] Cassagneau, T., Caruso, F. Oligosilsesquioxanes as versatile building blocks for the preparation of self-assembled thin films. *J. Amer. Chem. Soc.* 124 (2002): 8172-8180.
- [108] Gan, S.N., Subramaniam, N., Yahya, R. Hydrogenation of natural rubber using nickel 2-ethylhexanoate catalyst in combination with triisobutylaluminum. *J. Appl. Polym. Sci.* 59 (1996): 63-70.
- [109] Bhattacharjee, S., Bhowmick, A.K., Avasthi, B.N. Selective hydrogenation of olefinic bonds in styrene-isoprene-styrene triblock copolymer by palladium acetate catalyst. *Polymer* 49 (1993): 1971-1977.
- [110] Escobar Barrios, V. A., Najera, R.H., Petit, A., Pla, F. Selective hydrogenation of butadiene-styrene copolymers using a Ziegler-Natta type catalyst 2. thermal properties. *Eur. Polym. J.* 39 (2003): 1151-1167.
- [111] Chang, J.R., Huang, S.M. Pd/Al₂O₃ catalysts for selective hydrogenation of polystyrene-*block*-polybutadiene-*block*-polystyrene thermoplastic elastomers. *Ind. Eng. Chem. Res.* 37 (1998): 1220-1227.
- [112] Cassano, G.A., Valles, E.M., Quinzani, L.M. Structure of partially hydrogenated polybutadienes. *Polymer* 39 (1998): 5573-5577.
- [113] Tangthongkul, R., Prasassarakich, P., McManus, N.T., Rempel, G.L. Hydrogenation of *cis*-1,4-Polyisoprene catalyzed by Ru(CH=CH(Ph))Cl(CO)(PCy₃)₂. *J. Appl. Polym. Sci.* 91 (2004): 3259-3273.

- [114] Tangthongkul, R., Prasassarakich, P., Rempel, G.L. Hydrogenation of natural Rubber with $\text{Ru}[\text{CH}=\text{CH}(\text{Ph})]\text{Cl}(\text{CO})(\text{PCy}_3)_2$ as a catalyst. *J. Appl. Polym. Sci.* 97 (2005): 2399-2406.
- [115] Hinchiranan, N., Prasassarakich, P., Rempel, G.L. Hydrogenation of natural rubber in the presence of $\text{OsHCl}(\text{CO})(\text{O}_2)(\text{PCy}_3)_2$: kinetics and mechanism. *J. Appl. Polym. Sci.* 100 (2006): 4499–4514.
- [116] Mahittikul, A., Prasassarakich, P., Rempel, G.L. Hydrogenation of natural rubber latex in the presence of $\text{OsHCl}(\text{CO})(\text{O}_2)(\text{PCy}_3)_2$. *J. Appl. Polym. Sci.* 100 (2006): 640–655.
- [117] Mohammadi, N.A., Rempel, G.L. Homogeneous selective catalytic hydrogenation of $\text{C}=\text{C}$ in acrylonitrile butadiene copolymer. *Macromolecules* 20 (1987): 2362-2368.
- [118] Nikhil, K., Talwar, S.S., Sivaram, S. Solution hydrogenation of chloroprene rubber using a Wilkinson catalyst. *Macromolecules* 27 (1994): 6985-6987.
- [119] Wei, Z., Wu, J., Pan, Q., Rempel, G.L. Direct catalytic hydrogenation of an acrylonitrile-butadiene rubber latex using Wilkinson's catalyst. *Macromol. Rapid Commun.* 26 (2005): 1768–1772.
- [120] Escobar Barrios, V. A., Najera, R.H., Petit, A., Pla, F. Selective hydrogenation of butadiene-styrene copolymers using a Ziegler-Natta type catalyst 1. kinetic study. *Eur. Polym. J.* 36 (2000): 1817-1834.
- [121] Gan, S.N., Subramaniam, N., Yahya, R. Hydrogenation of natural rubber using nickel 2 ethylhexanoate catalyst in combination with triisobutylaluminum. *J. Appl. Polym. Sci.* 59 (1996): 63-70.
- [122] Shinga, N., De, P.P., Sivaram, S. Homogeneous catalytic hydrogenation of natural rubber using $\text{RhCl}(\text{PPh}_3)_3$. *J. Appl. Polym. Sci.* 66 (1997): 1647-1652.
- [123] Bhattacharjee, S., Bhowmick, A.K., Avasthi, B.N. Selective hydrogenation of olefinic bonds in styrene-isoprene-styrene triblock copolymer by palladium acetate catalyst. *Polymer* 34 (1993): 5173-5186.
- [124] Jones, R.V., Moberly, C.W., Reynolds, W.B. Hydrogenated synthetic elastomers. *Ind. Eng. Chem.* 45 (1953): 1117-1122.

- [125] Falk, J.C. Lithium based coordination catalysts for the hydrogenation of diene and vinylaromatic polymers. *Macromol. Chem.* 160 (1972): 291-299.
- [126] Duck, E.W., Locke, J.M. British Patent 1386416, 1975.
- [127] Hattori, Y., Kitagawa, Y. *U.S. Pat.* 302505, 1987.
- [128] Shyr, Y., Bobsein, R.L., Johnson, M.M. *U.S. Pat.* 4,656,230, 1987.
- [129] Wideman, L.G. Process for hydrogenation of carbon-carbon double bonds in an unsaturated polymer in latex form. *U.S. Pat.* 4,452,950; 1984.
- [130] Huitig, S., Miiller, H.R., Thier, W. *Tetrahedron Letters* 1961, 353.
- [131] Corey, E.J., Mock, W.L., Pasto, D.J. *Tetrahedron Letters* 1961, 347.
- [132] Tamelen, E.E., Dewey, R.S., Timmons, R.J. *J. Amer. Chem. Soc.* 83, (1961):3725.
- [133] Tamelen, E.E., Dewey, R.S. *J. Amer. chem. SOC.* 83, (1961): 3729.
- [134] Mahittikul, A., Prasassarakich, P., Rempel, G.L. Nuncatalytic hydrogenation of natural rubber latex. *J. Appl. Polym. Sci.* 103 (2007): 2885-2895.
- [135] Parker, D.K., Ruthenburg, D.M. Process for the preparation of hydrogenated rubber. *U.S. Pat.* 5,424,356 (1995).
- [136] Lin, X., Pan, Q., Rempel, G.L. Gel formation in diimide-hydrogenated polymers. *J. Appl. Polym. Sci.* 96 (2005): 1222-1125.
- [137] Parker, D.K., Roberts, R.F., Schiessl, H.W. A new process for the preparation of highly saturated nitrile rubber in latex form. *Rubber Chem. Tech.* 65 (1992): 245-257.
- [138] He, Y., Daniels, E. S., Klein, A., and El-Aasser, M. S. Hydrogenation of styrene-butadiene rubber latexes. *J. Appl. Polym. Sci.* 64 (1997): 2047-2056.
- [139] Zhou, S., Bai, H., Wang, J. Hydrogenation of acrylonitrile-butadiene rubber latexes. *J. Appl. Polym. Sci.* 91 (2004); 2072-2078.
- [140] De Sarkar, M. De, P.P., Bhowmick, A.K. Diimide reduction of carboxylated styrene-butadiene rubber in latex stage. *Polymer* 41 (2000): 907-915.
- [141] Mahittikul, A., Prasassarakich, P., Rempel, G.L. Diimide hydrogenation of natural rubber latex. *J. Appl. Polym. Sci.* 105 (2007); 1188-1199.

- [142] Simma, K., Rempel, G.L., Prasassarakich, P. Improving thermal and ozone stability of skim natural rubber by diimide reduction. *Polym. Degrad. Stab.* 94 (2009): 1914-1923.
- [143] Xie, H.Q., Li, X.D., Guo, J.S. Hydrogenation of nitrile-butadiene rubber latex to form thermoplastic elastomer with excellent thermooxidation resistance. *J. Appl. Polym. Sci.* 90, (2003): 1026–1031.
- [144] Lin, X., Pan, Q., Rempel, G.L. Hydrogenation of nitrile-butadiene rubber latex with diimide. *J. Appl. Cat. A: General* 276 (2004); 123–128.
- [145] Mammeri, F., Rozes, L., Bourhis, E.L., Sanchez, C. Elaboration and mechanical characterization of nanocomposites thin films Part II. correlation between structure and mechan: 267–272.
- [146] Rattanasom, N., Saowapark, T., Deeprasertkul, C. Reinforcement of natural rubber with silica/carbon black hybrid filler. *Polym. Test.* 26 (2007): 369–377.
- [147] Gauthier, C.E., Vassoille, R.R., Ladouce-Stelandre, L. Analysis of the non-linear viscoelastic behaviour of silica filled styrene butadiene rubber. *Polymer* 45 (2004): 2761–2771.
- [148] Chuayjuljit, S., Boonmahitthisuda, A. Natural rubber nanocomposites using polystyrene-encapsulated nanosilica prepared by differential microemulsion polymerization. *Appl. Surf. Sci.* 256 (2010): 7211-7216.
- [149] Liu, X., Zhao, S. Measurement of the condensation temperature of nanosilica powder organically modified by a silane coupling agent and its effect evaluation. *J. Appl. Poly. Sci.* 108 (2008): 3038–3045.
- [150] Thammathadanukul, V., O'Haver, J.H., Harwell, J.H., Osuwan, S., Na-Ranong, N., Waddell, W.H. Comparison of rubber reinforcement using various surface modified silica. *J. Appl. Polym. Sci.* 59 (1996): 1741–1750.
- [151] Pongprayoon, T., Yooprasert, N., Suwanmala, P., Hemvichian, K. Rubber products prepared from silica modified by radiation-induced admicellar polymerization. *Rad.Phys. Chem.* 81 (2012): 541–546.

- [152] Younan, A.F., Ismail, M.N., Khalaf, A.I. Thermal stability of natural rubber-polyester short fiber composites. *Polym. Degrad. Stab.* 48 (1995): 103-109.
- [153] Park, S.J., Cho, K.S. Filler–elastomer interactions: influence of silane coupling agent on crosslink density and thermal stability of silica/rubber composites. *J. Colloid Interf. Sci.* 267 (2003): 86–91.
- [154] Le Gac, P.Y., Le Saux, V., Paris, M., Marco, Y. Ageing mechanism and mechanical degradation behaviour of polychloroprene rubber in a marine environment: Comparison of accelerated ageing and long term exposure. *Polym. Degrad. Stab.* 97 (2012): 288-296.
- [155] Ha-Anh, T., Vu-Khanh, T. Prediction of mechanical properties of polychloroprene during thermo-oxidative aging. *Polym. Test.* 24 (2005): 775-780.
- [156] Delor, F., Lacoste, J., Lemaire, J., Barrois-Oudin, N., Cardinet, C. Photo- and thermal ageing of polychloroprene: effect of carbon black and crosslinking. *Polym. Degrad. Stab.* 53 (1996): 361-369.
- [157] Rattanasom, N., Kueseng, P., Deeprasertkul, C. Improvement of the mechanical and thermal properties of silica-filled polychloroprene vulcanizates prepared from latex system. *J. Appl. Polym. Sci.* 124 (2012): 2657–2668.
- [158] Mora-Barrantes, I., Rodríguez, A., Ibarra, L., González, L., Valentín, J.L. Overcoming the disadvantages of fumed silica as filler in elastomer composites. *J. Mater. Chem.* 21 (2011): 7381–7392.
- [159] Rattanasom, N., Saowapark, T., Deeprasertkul, C. Reinforcement of natural rubber with silica/carbon black hybrid filler. *Polym. Test.* 26 (2007): 369–377.
- [160] Peng, H., Liu, L., Luo, Y., Wang, X., Jia, D. Effect of 3-propionylthio-1-propyltrimethoxysilane on structure, mechanical, and dynamic mechanical properties of NR/silica composites. *Polym. Compos.* 30 (2009): 955–961.
- [161] Thongsang, S., Sombatsompop, N., Ansarifard, A. Effect of fly ash silica and precipitated silica fillers on the viscosity, cure, and viscoelastic

- properties of natural rubber. *Polym. Adv. Technol.* 19 (2008): 1296–1304.
- [162] Suphadon, N., Busfield, J.J.C. The dynamic properties of fumed silica filled SBR as function of pre-strain. *Polym. Test.* 30 (2011): 779–783.
- [163] Brinke, J.W., Debnath, S.C., Reuvekamp, L.A.E., Noordermeer, J.W.M. Mechanistic aspects of the role of coupling agents in silica-rubber composites, *Compos. Sci. Technol.* 63 (2003): 1165–1174.
- [164] Stephen, R., Jose, S., Joseph, K., Thomas, S., Oommen, Z. Thermal stability and ageing properties of sulphur and gamma radiation vulcanized natural rubber (NR) and carboxylated styrene butadiene rubber (XSBR) latices and their blends. *Polym. Degrad. Stab.* 91 (2006): 1717–1725.
- [165] De Sarkar, M., De, P.P., Bhowmick, A.K. Thermoplastic elastomeric hydrogenated styrene-butadiene elastomer: optimization of reaction conditions, thermodynamics and kinetics. *J. Appl. Polym. Sci.* 66 (1997); 1151-1162.
- [166] Lin, X., Pan, Q., Rempel, G.L. Modeling and simulation of diimide hydrogenation of nitrile butadiene rubber latex. *Ind. Eng. Chem. Res.* 45 (2006); 1300-1306.
- [167] Kamenka, N., Burgaud, I., Zana, R., Lindman, B. *J. Phys. Chem.* 98 (1994); 6785-6792.
- [168] Kiatkamjornwong, S., Apiwattananon, S., Rikukawa, M., Ogata, N. Super-fine particles of poly(styrene-co-methylmethacrylate) by dispersion copolymerization. *Colloid Surf. A: Phys. Chem. Eng. Aspects* 153 (1999); 229-240.
- [169] Jang, J., Park, H. In situ sol-gel process of polystyrene/silica hybrid materials: effect of silane coupling agents. *J. Appl. Polym. Sci.* 85 (2002); 2074-2083.
- [170] Sondi, I., Fedynyshyn, T.H., Sinta, R., Matijevic, E. Encapsulation of nanosized silica by in situ polymerization of *tert*-butyl acrylate monomer. *Langmuir* 16 (2000); 9031-9034.

- [171] Jeon, B.J., Hah, H.J., Koo, S.M. Surface modification of silica particles with organoalkoxysilanes through two-step (acid-base) process in aqueous solution. *J. Ceram. Process. Res.* 3 (2002); 216-221.
- [172] Suppaibulsuk, B., Prasassarakich, P., Rempel, G.L. Factorial design of nanosized polyisoprene synthesis via differential microemulsion polymerization. *Polym. Adv. Technol.* 21 (2010); 467-475.
- [173] Norakankorn, C., Pan, Q., Rempel, G.L., Kiatkamjornwong, S. Synthesis of poly(methyl methacrylate) nanoparticles initiated by azobisisobutyronitrile using a differential microemulsion polymerization technique. *J. Appl. Polym. Sci.* 113 (2009); 375-382.
- [174] Suppaibulsuk, B., Prasassarakich, P., Rempel, G.L. Synthesis of styrene-g-polyisoprene nanoparticles by emulsion polymerization and its effect on properties of polyisoprene composites. *Polym. Adv. Technol.* (2011).
- [175] Liu, J., Pan, Q. Synthesis of nanosized poly(ethyl acrylate) particles via differential emulsion polymerization. *J. Appl. Polym. Sci.* 102 (2006); 1609-1614.
- [176] Norakankorn, C., Pan, Q., Rempel, G.L., Kiatkamjornwong, S. Synthesis of core/shell structure of glycidyl-functionalized poly(methyl methacrylate) latex nanoparticles via differential microemulsion polymerization. *Eur. Polym. J.* 45 (2009) 2977-2986.
- [177] Lopez-Diaz, D., Velazquez, M.M. Variation of the critical micelle concentration with surfactant structure: a simple method to analyze the role of attractive-repulsive forces on micellar association. *Chem. Educator* 12 (2007) 327-330.
- [178] Kongsinlark, A., Prasassarakich, P., Rempel, G.L. Synthesis of monodispersed polyisoprene-silica nanoparticles via differential microemulsion polymerization and mechanical properties of polyisoprene nanocomposite. *Chem. Eng. J.* 193-194 (2012); 215-226.
- [179] Lin, X., Pan, Q., Rempel, G.L. Cupric ion catalyzed diimide production from the reaction between hydrazine and hydrogen peroxide. *Appl. Catal. A* 263 (2004); 27-32.

- [180] Esthappan, S.K., Kuttappan, S.K., Joseph, R. Effect of titanium dioxide on the thermal ageing of polypropylene. *Polym. Degrad. Stab.* 97 (2012); 615-620.
- [181] Yang, F., Yngard, R.I., Nelson, G.L. Flammability of polymer–clay and polymer–silica nanocomposites. *J. Fire. Sci.* 23 (2005); 209-226.
- [182] Nontasorn, P., Chavadej, S., Rangsunvigit, P., O’Haver, J.H., Chaisirimahamorakot, S., Na-Ranong, N. Admicellar polymerization modified silica via a continuous stirred-tank reactor system: Comparative properties of rubber compounding, *Chem. Eng. J.* 108 (2005); 213-218.
- [183] Yooprasert, M., Pongprayoon, T., Suwanmala, P., Hemvichian, K., Tumcharern, G. Radiation-induced admicellar polymerization of isoprene on silica: Effects of surfactant’s chain length. *Chem. Eng. J.* 156 (2010); 193-199.
- [184] Ono, S., Kiuchi, Y., Sawanobori, J., Ito, M. Structure development in silica-filled rubber composites. *Polym. Int.* 48 (1999); 1035-1041.
- [185] Botros, S.H. Preparation and characteristics of NR/EPDM rubber blends. *Polym. Plast. Technol Eng.* 41 (2002); 341-359.
- [186] Peng, Z., Kong, L.X., Li, S.D., Chen, Y., Huang, M.F. Self-assembled natural rubber/silica nanocomposites: its preparation and characterization. *Composite Sci. Technol.* 67 (2007); 3130-3139.
- [187] Ismail, H., Freakley, P.K., Sutherland, I., Sheng, E. Effects of multifunctional additive on mechanical properties of silica filled natural rubber compound, *Eur. Polym. J.* 31 (1995); 1109-1117.
- [188] Wang, Q.Y., Luo, C., Feng, Z., Yi, Q., Qiu, L.X., Kong, Z., Peng, Z. Reinforcement of natural rubber with core-shell structure silica-poly(methyl methacrylate) nanoparticles. *J. Nanomaterials* 2012 (2011); 1-9.
- [189] Zhu, A., Shi, Z., Cai, A., Zhao, F., Liao, T. Synthesis of core–shell PMMA–SiO₂ nanoparticles with suspension–dispersion–polymerization in an aqueous system and its effect on mechanical properties of PVC composites. *Polym. Test.* 27 (2008); 540-547.

- [190] Radhakrishnan, C.K., Rosamma, A., Unnikrishnan, G. Thermal, ozone and gamma ageing of styrene butadiene rubber and poly(ethylene-co-vinyl acetate) blends. *Polym. Degrad. Stab.* 91 (2006); 902-910.

APPENDICES

APPENDIX A

Raw Data of Mechanical Properties of NR/PIP-SiO₂**Table A-1** Mechanical properties of NR filled with PIP-SiO₂ nanocomposites before and after ageing

Rubber sample	NR/PIP-SiO ₂ ^a	SiO ₂ con ^b	Tensile strength (MPa)			Modulus at 300% strain (MPa)			Elongation at break (%)		
			Be ^c ageing	Af ^d ageing	%Re ^e	Be ^c ageing	Af ^d ageing	%Re ^e	Be ^c ageing	Af ^d ageing	%Re ^e
NR	-	-	21.8	11.5	52.8	3.9	1.8	45.0	861	788.7	91.6
NR/SiO ₂ ^f	90/10	10	28.8	20.5	71.1	4.6	2.3	50.0	799	649.6	81.3
NR/PIP-VTS-SiO ₂	95/5	0.5	25.8	22.6	87.5	4.6	3.6	78.9	845	821.3	97.2
	90/10	1	29.7	26.9	90.5	4.9	4.1	84.0	839	782.8	93.3
	80/20	2	34.6	31.1	89.9	5.7	5.1	89.1	805	759.1	94.3
	70/30	3	29.6	23.7	80	4.8	4.2	87.9	794	741.6	93.4
NR/PIP-MPS-SiO ₂	95/5	0.5	25.7	23.5	91.5	4.0	3.7	93.1	829	836.5	100.9
	90/10	1	29.9	27.9	93.4	5.2	3.9	75.2	803	787.7	98.1
	80/20	2	32.1	29.1	90.7	5.7	4.7	81.7	801	757.7	94.6
	70/30	3	25.0	23.3	93.2	4.7	4.1	88.0	780	738.7	94.7

^a NR/PIP-SiO₂, ratio of NR to PIP-SiO₂^b Silica content based on total rubber^c Properties before thermal ageing^d Properties after thermal ageing^e %Retention= (Properties after ageing/Properties before ageing) x 100^f direct mixing of untreated SiO₂ with NRL

Table A-2 Tensile strength of NR filled with PIP-SiO₂ nanocomposite

Rubber sample	NR/ PIP-SiO ₂	Tensile strength (MPa) before ageing					Tensile strength (MPa) after ageing				
		1	2	3	Mean	SD	1	2	3	Mean	SD
NR	-	22.1	21	22.3	21.8	0.7	11.2	10.9	12.4	11.5	0.8
NR/ PIP-VTS-SiO ₂	95/5	25.9	26.4	25.1	25.8	0.7	22.8	23.1	21.8	22.6	0.7
	90/10	29.7	29.7	29.8	29.7	0.1	27.4	26.1	27.1	26.9	0.7
	80/20	35.5	34.1	34.2	34.6	0.8	32.1	31.6	29.6	31.1	1.3
	70/30	28.6	30.1	30.1	29.6	0.9	24.7	23.8	22.5	23.7	1.1
NR/ PIP-MPS-SiO ₂	95/5	25.2	25.8	26.1	25.7	0.5	24.8	23.5	22.2	23.5	1.3
	90/10	29.9	29.3	30.5	29.9	0.6	26.9	27.2	29.7	27.9	1.5
	80/20	31.5	33.1	31.7	32.1	0.9	28.7	30.1	28.5	29.1	0.9
	70/30	25.6	24.8	24.6	25.0	0.5	27.7	22.3	19.9	23.3	4.0

Table A-3 Modulus at 300% elongation of NR filled with PIP-SiO₂ nanocomposite

Rubber sample	NR/ PIP-SiO ₂	Modulus (MPa) before ageing					Modulus (MPa) after ageing				
		1	2	3	Mean	SD	1	2	3	Mean	SD
NR	-	3.6	4.0	4.1	3.9	0.3	1.8	1.9	1.5	1.8	0.2
NR/PIP-VTS-SiO ₂	95/5	4.6	4.6	4.6	4.6	0	3.8	3.3	3.8	3.6	0.3
	90/10	5.1	4.4	5.2	4.9	0.4	4.2	4.8	3.3	4.1	0.7
	80/20	5.2	5.3	6.6	5.7	0.8	5.4	6.1	3.7	5.1	1.2
	70/30	4.1	5.7	4.6	4.8	0.8	4.4	4.3	4	4.2	0.2
NR/PIP-MPS-SiO ₂	95/5	4.3	4.1	3.6	4	0.4	3.3	3.2	4.7	3.7	0.8
	90/10	5.1	5.2	5.3	5.2	0.1	4.1	3.6	4	3.9	0.3
	80/20	5.2	5.5	6.4	5.7	0.6	4.6	4.8	4.6	4.7	0.1
	70/30	4.3	4.2	5.6	4.7	0.8	3.6	4.3	4.5	4.1	0.5

Table A-4 Elongation at break of NR filled with PIP-SiO₂ nanocomposite

Rubber sample	NR/ PIP- SiO ₂	Elongation at break (%) before ageing					Elongation at break (%) after ageing				
		1	2	3	Mean	SD	1	2	3	Mean	SD
		NR	-	864	863	856	861	4.4	799	790	777
NR/ PIP-VTS- SiO ₂	95/5	852	862	821	845	21.4	831	829	804	821	15.0
	90/10	845	833	839	839	6.0	785	789	774	783	7.6
	80/20	814	814	787	805	15.6	755	761	761	759	3.6
	70/30	799	811	772	794	20.0	730	739	756	742	13.1
NR/ PIP- MPS- SiO ₂	95/5	830	830	827	829	1.7	833	851	825	836	13.2
	90/10	814	801	794	803	10.1	772	779	812	788	21.5
	80/20	812	778	813	801	19.9	755	756	762	758	3.9
	70/30	762	771	807	780	23.8	749	737	730	739	9.6

APPENDIX B

Raw Data of Mechanical Properties of NR/HPIP-SiO₂**Table B-1** Mechanical properties of NR filled with HPIP-SiO₂ nanocomposites before and after ageing

Rubber sample	NR/PIP-SiO ₂ ^a	SiO ₂ con ^b	Tensile strength (MPa)			Modulus at 300% strain (MPa)			Elongation at break (%)		
			Be ^c age	Af ^d age	%Re ^e	Be ^c age	Af ^d age	%Re ^e	Be ^c age	Af ^d age	%Re ^e
NR	-	0	21.8	11.5	52.8	3.9	1.8	46.4	861	789.4	91.7
NR/PIP-VTS-SiO ₂	80/20	2	28.9	24.6	85.2	5.3	4.0	76.3	805	759	94.3
NR/HPIP-VTS-SiO ₂ ^f	80/20	2	29.6	25.6	86.2	5.6	4.1	73.9	805	786.5	97.7
NR/HPIP-VTS-SiO ₂ ^g	90/10	1	27.0	23.4	86.7	4.6	3.6	78.5	791	766.5	96.9
	80/20	2	31.4	29.1	92.5	7.2	6.8	94.8	718	711.1	99.0
	70/30	3	36.6	34.1	93.2	8.1	7.8	96.1	656	646.9	98.6
	60/40	4	25.4	25.0	98.3	5.0	4.3	85.4	727.4	704.2	96.8

^a NR/PIP-SiO₂, ratio of NR to PIP-SiO₂^b Silica content based on total rubber^c Properties before thermal ageing^d Properties after thermal ageing^e %Retention= (Properties after ageing/Properties before ageing) x 100^f HPIP-SiO₂ at degree of hydrogenation 64 %^g HPIP-SiO₂ at degree of hydrogenation 98 %

Table B-2 Tensile strength of NR filled with HPIP-SiO₂ nanocomposite

Rubber sample	NR/ HPIP- SiO ₂	Tensile strength (MPa) before ageing					Tensile strength (MPa) after ageing				
		1	2	3	Mean	SD	1	2	3	Mean	SD
NR	-	22.1	21.0	22.3	21.8	0.7	11.2	10.9	12.4	11.5	0.8
NR/PIP-VTS-SiO ₂	80/20	27.1	30.9	28.7	28.9	1.9	24.9	26.5	22.4	24.6	2.1
NR/HPIP-VTS-SiO ₂ ^f	80/20	28.9	30.1	29.8	29.6	0.6	25.5	25.9	25.4	25.6	0.3
NR/HPIP-VTS-SiO ₂ ^g	90/10	27.0	27.9	26.1	27.0	0.9	23.9	23.1	23.2	23.4	0.4
	80/20	30.9	30.5	32.8	31.4	1.2	29.9	29.0	28.4	29.1	0.8
	70/30	36.8	37.1	35.9	36.6	0.6	33.9	34.5	33.9	34.1	0.3
	60/40	24.3	26.8	25.1	25.4	1.3	25.0	24.5	25.5	25.0	0.5

Table B-3 Modulus at 300% elongation of NR filled with HPIP-SiO₂ nanocomposite

Rubber sample	NR/ HPIP- SiO ₂	Modulus (MPa) before ageing					Modulus (MPa) after ageing				
		1	2	3	Mean	SD	1	2	3	Mean	SD
NR	-	3.8	3.9	4.0	3.9	0.1	1.7	1.9	1.8	1.8	0.1
NR/PIP-VTS-SiO ₂	80/20	5.1	5.6	5.2	5.3	0.3	4.5	5.0	2.5	4.0	1.3
NR/HPIP-VTS-SiO ₂ ^f	80/20	5.4	5.8	5.6	5.6	0.2	4.9	4.1	3.3	4.1	0.8
NR/HPIP-VTS-SiO ₂ ^g	90/10	4.3	4.7	4.8	4.6	0.3	3.5	3.7	3.6	3.6	0.1
	80/20	7.0	7.3	7.3	7.2	0.2	6.9	6.1	7.4	6.8	0.7
	70/30	8.3	8.8	7.2	8.1	0.8	7.1	8.1	8.2	7.8	0.6
	60/40	5.1	6.0	3.9	5.0	1.1	4.1	3.7	5.1	4.3	0.7

Table B-4 Elongation at break of NR filled with HPIP-SiO₂ nanocomposite

Rubber sample	NR/ HPIP- SiO ₂	Elongation at break (%)before ageing					Elongation at break (%)after ageing				
		1	2	3	Mean	SD	1	2	3	Mean	SD
NR	-	870	857	856	861	7.8	783	790	795	789.4	6.2
NR/PIP-VTS- SiO ₂	80/20	817	809	789	805	14.4	749	761	767	759	9.2
NR/HPIP-VTS- SiO ₂ ^f	80/20	814	816	785	805	17.3	791	782	787	786.5	4.5
NR/HPIP-VTS- SiO ₂ ^g	90/10	785	794	794	791	5.2	762	773	765	766.5	5.8
	80/20	711	729	714	718	9.6	709	715	709	711	3.5
	70/30	669	650	649	656	11.3	645	653	643	646.9	5.4
	60/40	737	742	702	727	21.8	691	715	707	704.2	12.2

APPENDIX C

Raw Data of PIP-SiO₂ Synthesis**Table C-1** Raw data of influence of monomer/water on PIP-SiO₂ synthesis

M/H ₂ O	Exp Run	particle size (nm)	average particle size (nm)	conversion (%)	average conversion (%)	% GE	average %GE
0.1	1	21.8		48.1		28.3	
0.1	2	19.6	20.7	54.7	51.4	30.1	29.2
0.2	3	30.8		70.3		62.9	
0.2	4	26.2	28.5	68.1	69.2	61.7	62.3
0.3	5	34.7		89.1		76.7	
0.3	6	35.3	35.5	85.4	87.0	80.4	78.0
0.3	7	36.5		86.5		77.0	
0.4	8	41.6		71.9		74.0	
0.4	9	42.4	42.6	78.3	76.2	75.8	73.6
0.4	10	43.8		78.4		71.0	
0.5	11	55.7	55.7	69.1	69.1	69.5	69.5

Condition: SPS = 1 %wt, SDS = 3 %wt, VTS-SiO₂ = 10 %wt based on monomer.

Table C-2 Raw data of influence of initiator concentration on PIP-SiO₂

% Initiator	Exp. Run	particle size (nm)	average particle size (nm)	conversion (%)	average conversion (%)	% GE	average % GE
0.5	1	20.6	22.2	54.9	56.7	80.2	81.4
0.5	2	23.8		58.5		82.6	
1.0	3	35.5	35.5	87	87.0	78	78.0
2.0	4	31.2	32.6	90.3	89.0	67.9	69.0
2.0	5	33.7		88.1		69.5	
2.0	6	32.9		88.6		69.6	
3.0	7	36.8	35.5	88.4	87	71.1	70.4
3.0	8	34.2		85.6		69.7	
4.0	9	31.2	31.2	85	85	56.2	56.2
5.0	10	28.9	28.9	86	86	50.9	50.9

Condition: M/H₂O = 0.3, SDS = 3 %wt, VTS-SiO₂ = 10 %wt based on monomer.

Table C-3 Raw data of influence of SDS concentration on PIP-SiO₂

% SDS	Exp. Run	particle size (nm)	average particle size (nm)	conversion (%)	average conversion (%)	% GE	average % GE
0.5	1	49.3	49	60.2	59.5	51.4	50.4
0.5	2	48.7		58.8		49.4	
1.0	3	39.9	40.3	67.9	68.1	55.7	54.3
1.0	4	40.7		68.3		52.9	
3.0	5	35.7	33.6	87.0	85.0	78.1	80.4
3.0	6	34.9		83.0		84.1	
3.0	7	30.2		85.0		79	
5.0	8	29.1	28.5	88.6	87	76.9	78.5
5.0	9	27.9		85.4		80.1	
7.0	10	22.5	21.5	89.7	89	71.4	72.7
7.0	11	20.5		88.3		74.0	
9.0	12	21.0	21.0	90.0	90	60.0	60.0
10.0	13	20.0	20.0	90.0	90	45.4	45.4

Condition: M/H₂O = 0.3, SPS = 1 %wt, VTS-SiO₂ = 10 %wt based on monomer.

Table C-4 Raw data of influence of silica loading on PIP-SiO₂

%SiO ₂	Exp. Run	particle size (nm)	average particle size (nm)	conversion (%)	average conversion (%)	% GE	average % GE
2.5	1	27.1		90.2		93.1	
2.5	2	29.7	28.4	93.8	92	90.9	92
5.0	3	30.2		89.7		85.2	
5.0	4	39.1	34.6	86.9	90	86.8	86
5.0	5	34.5		93.4		86	
7.5	5	41.1	38.5	86.5	87	87.4	87
7.5	6	35.9		87.5		86.6	
10.0	7	41.9	39.5	88.9	87	84.8	85
10.0	8	37.1		85.1		85.2	
15.0	9	44.5	43	74.7	75.7	73.9	74
15.0	10	41.5		76.7		74.1	
20.0	11	57	57	68.2	68.2	63	63

Condition: M/H₂O = 0.3, SPS = 1 %wt, SDS = 3 %wt based on monomer.

APPENDIX D**Calculation of Polyisoprene Composition**

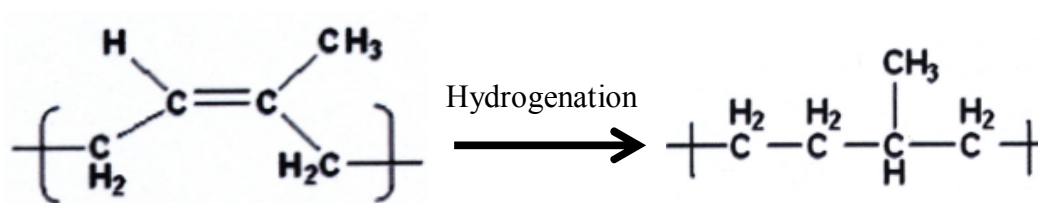
$$\begin{aligned} \%1,4 \text{ polyisoprene} &= \frac{\text{The integrated peak area at 5.15 ppm}}{\text{Peak area at 5.15 ppm} + \text{peak area at 5.7 ppm} + \text{peak area at 4.6-4.8 ppm}} \\ &= \frac{13.00}{13.00+0.83+0.52} \times 100 \\ &= 90.6\% \end{aligned}$$

$$\begin{aligned} \%1,2 \text{ polyisoprene} &= \frac{\text{The integrated peak area at 5.7 ppm}}{\text{Peak area at 5.15 ppm} + \text{Peak area at 5.7 ppm} + \text{peak area at 4.6-4.8 ppm}} \\ &= \frac{0.52}{13.00+0.83+0.52} \times 100 \\ &= 3.6\% \end{aligned}$$

$$\begin{aligned} \%3,4 \text{ polyisoprene} &= \frac{\text{The integrated peak area at 4.8 ppm}}{\text{Peak area at 5.15 ppm} + \text{Peak area at 5.7 ppm} + \text{Peak area at 4.6-4.8 ppm}} \\ &= \frac{0.83}{13.00+0.83+0.52} \times 100 \\ &= 5.7\% \end{aligned}$$

APPENDIX E

Calculation of % Hydrogenation

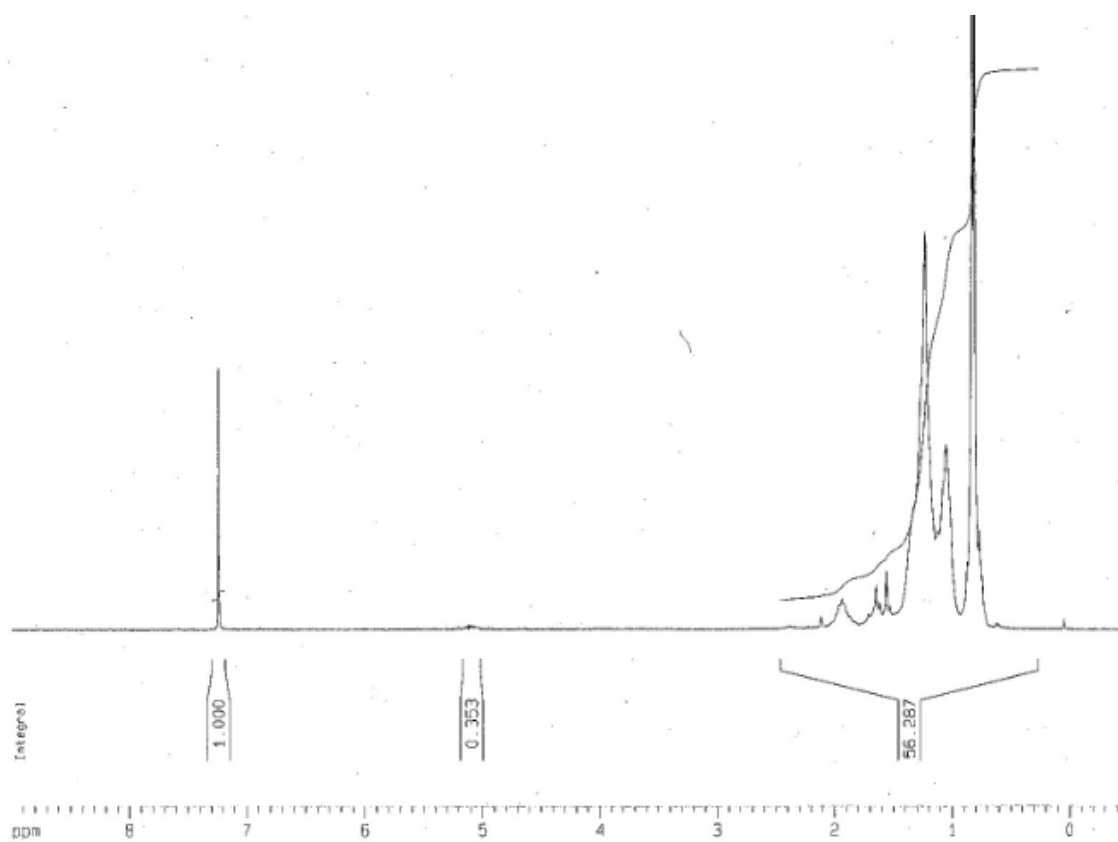


cis-1,4- polyisoprene (Species 1)

Hydrogenated polyisoprene (Species 2)

Proton of repeating unit except =CH in Species 1 = 7 protons

Proton of repeating unit in Species 2 = 10 protons



where A = Peak area except at 5.2 ppm

B = Peak area at 5.2 ppm

C = Peak area of saturated $-\text{CH}_2-$ and $-\text{CH}_3$

$$A = 10C + 7B$$

$$C = (A - 7B)/10$$

Total peak area = Peak area of saturated $-\text{CH}_2-$ and $-\text{CH}_3$ + Peak area at 5.2 ppm

$$= [(A - 7B)/10] + B$$

$$= (A - 3B)/10$$

%Hydrogenation = [(Peak area of saturated $-\text{CH}_2$ and $-\text{CH}_3$)/(Total peak area)] $\times 100$

$$= \frac{(A-7B)/10}{(A+3B)/10} \times 100$$

$$= [(A-7B)/(A+3B)] \times 100$$

For example: A = 24.84 and B = 1.00

$$\% \text{ Hydrogenation} = [56.287-7(0.353)]/[56.287+3(0.353)] \times 100$$

$$= 93.84\%$$

APPENDIX F

**Raw Data of Diimide Hydrogenation of Nanosized Polyisoprene
and Polyisoprene-SiO₂**

Table F-1 Raw data of diimide hydrogenation of nanosized PIP

Exp. Run	Time (s)	%HD at 50°C	%HD at 60°C	%HD at 70°C
1	0	0	0	0
2	600	5	10	16
3	1200	12	20	23
4	1800	20	29	34
5	2460	28	41	47
6	3000	35	48	51
7	3600	41	50	57
8	4800	49	61	65
9	6000	51	69	75
10	7680	56	72	79
11	9600	59	73	81
12	11820	62	74	82
13	13200	62	74	85
14	15420	63	74	88
15	18000	61	76	90
16	19560	63	76	93
17	21300	62	76	94

Condition: [N₂H₄] = 5 mol/L, [H₂O₂] = 7.5 mol/L, [C=C] = 1 mol/L, [H₃BO₃] = 0.15 mol/L, [H₂O] = 10 mol/L.

Table F-2 Raw data of diimide hydrogenation of nanosized PIP-SiO₂

Exp. Run	Time (s)	%HD at 50°C	%HD at 60°C	%HD at 70°C
1	0	0	0	0
2	600	13	19	24
3	1200	20	25	35
4	1800	27	30	41
5	2460	32	35	50
6	3000	40	45	59
7	3600	49	53	69
8	4800	57	62	75
9	6000	64	71	82
10	7680	71	78	89
11	9600	74	80	91
12	11820	76	85	91
13	13200	75	89	94
14	15420	76	91	97
15	18000	77	91	98
16	19560	77	91	98
17	21300	77	92	98

Condition: [N₂H₄] = 5 mol/L, [H₂O₂] = 7.5 mol/L, [C=C] = 1 mol/L, [H₃BO₃] = 0.15 mol/L,
[H₂O] = 10 mol/L.

Table F-3 Raw data for kinetic study of nanosized HPIP

Time (s)	%HD at 50°C	x	1-x	ln 1-x	%HD at 60°C	x	1-x	ln 1-x	%HD at 70°C	x	1-x	ln 1-x
0	0	0.0	1.0	0.00	0	0.0	1.0	0.00	0	0.0	1.0	0.00
600	5	0.1	1.0	-0.05	10	0.1	0.9	-0.11	20	0.2	0.8	-0.22
1200	12	0.1	0.9	-0.13	20	0.2	0.8	-0.22	28	0.3	0.7	-0.33
1800	20	0.2	0.8	-0.22	29	0.3	0.7	-0.34	39	0.4	0.6	-0.49
2460	28	0.3	0.7	-0.33	41	0.4	0.6	-0.53	53	0.5	0.5	-0.76
3000	35	0.4	0.7	-0.43	48	0.5	0.5	-0.65	56	0.6	0.4	-0.82
3600	41	0.4	0.6	-0.53	50	0.5	0.5	-0.69	66	0.7	0.3	-1.08
4800	49	0.5	0.5	-0.67	61	0.6	0.4	-0.94	72	0.7	0.3	-1.27
6000	51	0.5	0.5	-0.71	69	0.7	0.3	-1.17	79	0.8	0.2	-1.56
7680	56	0.6	0.4	-0.82	72	0.7	0.3	-1.27	83	0.8	0.2	-1.77
9600	59	0.6	0.4	-0.89	73	0.7	0.3	-1.31	87	0.9	0.1	-2.04
11820	62	0.6	0.4	-0.97	74	0.7	0.3	-1.35	90	0.9	0.1	-2.30
13200	62	0.6	0.4	-0.97	74	0.7	0.3	-1.36	91	0.9	0.1	-2.41

Table F-4 Raw data for kinetic study of nanosized HPIP-SiO₂

Time (s)	%HD at 50°C	x	1-x	ln 1-x	%HD at 60°C	x	1-x	ln 1-x	%HD at 70°C	x	1-x	ln 1-x
0	0	0.00	1.00	0	0	0.00	1.00	0.00	0	0.00	1.00	0.00
600	5	0.05	0.95	-0.05	10	0.10	0.90	-0.11	20	0.20	0.80	-0.22
1200	12	0.12	0.88	-0.13	20	0.20	0.80	-0.22	28	0.28	0.72	-0.33
1800	20	0.20	0.80	-0.22	29	0.29	0.71	-0.34	39	0.39	0.61	-0.49
2460	28	0.28	0.72	-0.33	41	0.41	0.59	-0.53	53	0.53	0.47	-0.76
3000	35	0.35	0.65	-0.43	48	0.48	0.52	-0.65	56	0.56	0.44	-0.82
3600	41	0.41	0.59	-0.53	50	0.50	0.50	-0.69	66	0.66	0.34	-1.08
4800	49	0.49	0.51	-0.67	61	0.61	0.39	-0.94	72	0.72	0.28	-1.27
6000	51	0.51	0.49	-0.71	69	0.69	0.31	-1.17	79	0.79	0.21	-1.56
7680	56	0.56	0.44	-0.82	72	0.72	0.28	-1.27	83	0.83	0.17	-1.77
9600	59	0.59	0.41	-0.89	73	0.73	0.27	-1.31	87	0.87	0.13	-2.04
11820	62	0.62	0.38	-0.97	74	0.74	0.26	-1.35	90	0.90	0.10	-2.30
13200	62	0.62	0.38	-0.97	74.3	0.74	0.26	-1.36	91	0.91	0.09	-2.41

X : fractional hydrogenation conversion

VITA

The author who is responsible for this dissertation is Miss Anong Kongsinlark. She was born on June 23rd, 1985 in Surin, Thailand. She received the Bachelor's degree with the First class honors degree from the department of Chemistry, Thammasat University. She has received the King Scholarship in 2006. She was admitted to Doctoral Degree in Petrochemistry and Polymer Science, Chulalongkorn University in 2008 and completed the program in 2012. She has received the Royal Golden Jubilee Scholarship from Thailand Research Fund for her Ph.D. study. Anong also served as a teaching assistant for undergraduate courses "Physicochemical Measurements II". She did the research for 1 year (2010-2011) at "Advanced Rubber Technology and Applied Catalysis Laboratory" in Chemical Engineering, University of Waterloo, ON, Canada.

Journal Publication:

1. A. Kongsinlark, G.L. Rempel, P. Prasassarakich. Synthesis of monodispersed polyisoprene-silica nanoparticles via differential microemulsion polymerization and mechanical properties of polyisoprene nanocomposite. *Chemical Engineering Journal* 193-194 (2012); 215-226.
2. A. Kongsinlark, G.L. Rempel, P. Prasassarakich. Synthesis of Nanosized Ethylene-Propylene Rubber Latex via Polyisoprene Hydrogenation. *Journal of Applied Polymer Science* (2012), DOI: 10.1002/APP.37883.

Conference Presentation:

1. A. Kongsinlark, G.L. Rempel, P. Prasassarakich, (2012) "Synthesis of Hydrogenated Polyisoprene-Silica Nanoparticle via Diimide Reduction" oral presentation conference on 7th International Conference on Nanostructured Polymers and Nanocomposites, April 24-27, 2012 in Prague, Czech Republic.
2. A. Kongsinlark, G.L. Rempel, P. Prasassarakich, (2012) "Synthesis of Monodispersed Polyisoprene/Silica Nanoparticles via Differential Microemulsion" oral presentation conference on RGJ-Ph.D Congress XIII, April 6-8, 2012 in Pattaya, Thailand.